ÇUKUROVA UNIVERSITY
INSTITUTE OF NATURAL AND APPLIED SCIENCES

PhD THESIS

Nehir TOKGÖZ

INVESTIGATION OF FLOW CHARACTERISTICS AND HEAT TRANSFER ENHANCEMENT OF VARIOUS DUCT GEOMETRIES

DEPARTMENT OF MECHANICAL ENGINEERING

ADANA, 2014

ÇUKUROVA UNIVERSITY
INSTITUTE OF NATURAL AND APPLIED SCIENCES

INVESTIGATION OF FLOW CHARACTERISTICS AND HEAT TRANSFER ENHANCEMENT OF VARIOUS DUCT GEOMETRIES

Nehir TOKGÖZ

PhD THESIS

DEPARTMENT OF MECHANICAL ENGINEERING

We certify that the thesis titled above was reviewed and approved for the award of degree of the Doctor of Philosophy by the board of jury on 20/08/2014.

....	....	....
Prof. Dr. Beşir ŞAHİN	Prof. Dr. Hüseyin AKILLI	Prof. Dr. Tahsin ENGİN
SUPERVISOR	MEMBER	MEMBER

....	....
Prof. Dr. Galip SEÇKİN	Assoc. Prof. Dr. M. Sami AKÖZ
MEMBER	MEMBER

This PhD Thesis was prepared in Mechanical Engineering Department of the Institute of Natural and Applied Sciences of Çukurova University.
Registration Number:

Prof. Dr. Mustafa GÖK
Director
Institute of Natural and Applied Sciences

This thesis was supported by the Scientific Research Project Office of Çukurova University
Contract no: MMF 2012D17

ABSTRACT

PhD THESIS

INVESTIGATION OF FLOW CHARACTERISTICS AND HEAT TRANSFER ENHANCEMENT OF VARIOUS DUCT GEOMETRIES

Nehir TOKGÖZ

ÇUKUROVA UNIVERSITY
INSTITUTE OF NATURAL AND APPLIED SCIENCES
DEPARTMENT OF MECHANICAL ENGINEERING

Supervisor : Prof. Dr. Beşir ŞAHİN
Year: 2014, Pages: 180
Jury : Prof. Dr. Beşir ŞAHİN
: Prof. Dr. Hüseyin AKILLI
: Prof. Dr. Tahsin ENGİN
: Prof. Dr. Galip SEÇKİN
: Assoc. Prof. Dr. M. Sami AKÖZ

The aim of this study is to determine the flow characteristics and thermal efficiency in various ducts geometries numerically and experimentally. The whole study has been conducted for Reynolds numbers in the range of $3000 \leq Re \leq 6000$. Firstly, the effect of aspect ratio, s/H on heat transfer enhancement and on flow structures was aimed to be examined. Therefore, the corrugated duct geometries were designed for three different aspect ratios such as s/H=0.1, 0.2, 0.3 and various phase shift angles, φ of corrugated channels. Thermal efficiency of these geometries were examined numerically in order to optimize the aspect ratio, s/H. Afterwards, experimental studies were conducted in order to identify hydrodynamic structures and verify findings of numerical solution using Particle Image velocimetry (PIV). Throughout the study, three different phase angles, $\varphi=0°$, $90°$ and $180°$, were utilized. Velocity distributions, patterns of streamline and corresponding turbulent statistics were determined experimentally and numerically in order to reveal hydrodynamics and thermal efficiency of the corrugated channel flow. In numerical calculations, standard k-ε turbulent model was utilized. As a result of numerical studies, Nusselt number, Nu friction factor, f and efficiency index, η were calculated for different corrugated channel geometries. Consequently, it was observed that numerical and experimental results were extremely compatible with each other.

Key Words: Corrugated channel, heat transfer enhancement, phase angle, PIV

ÖZ

DOKTORA TEZİ

ÇEŞİTLİ KANAL GEOMETRİLERİNDE AKIŞ KARAKTERİSTİKLERİNİN VE ISI TRANFERİ İYİLEŞTİRİLMESİNİN İNCELENMESİ

Nehir TOKGÖZ

ÇUKUROVA ÜNİVERSİTESİ
FEN BİLİMLERİ ENSTİTÜSÜ
MAKİNA MÜHENDİSLİĞİ ANABİLİM DALI

Danışman : Prof. Dr. Beşir ŞAHİN
Yıl: 2014, Sayfa: 180
Juri : Prof. Dr. Beşir ŞAHİN
: Prof. Dr. Hüseyin AKILLI
: Prof. Dr. Tahsin ENGİN
: Prof. Dr. Galip SEÇKİN
: Doç. Dr. M. Sami AKÖZ

Bu çalışmanın amacı çeşitli kanal geometrilerindeki akış karakteristiklerini belirlemek ve ısı transferinin iyileştirilmesine kanal geometrilerinin etkisini sayısal ve deneysel olarak araştırmaktır. Çalışmanın tamamı Reynolds $3000 \leq Re \leq 6000$ aralığında yapılmıştır. İlk aşamada, oluk yüksekliğinin kanal yüksekliğine oranının, s/H ısı transferini iyileştirme ve akış yapısı üzerindeki etkisi incelenmiştir. Bu amaçla üç farklı yükseklik, s/H=0.1, 0.2, 0.3 oranlarında oluklu kanal geometrileri tasarlanarak sayısal çalışmalar gerçekleştirilmiştir. Yapılan çalışma sonucunda ısı transferinin en fazla iyileştirildiği oran belirlenmiştir. Daha sonra, hidrodinamik yapının incelenmesi ve sayısal çözüm bulgularının doğrulanması için deneysel çalışmalar Parçacık görüntülemeli hız ölçüm (PIV) yöntemi ile yapılmıştır. Çalışmalarda üç farklı faz, $\varphi=180^\circ, 90^\circ, 0^\circ$ açısı kullanılmıştır. Oyuklu kanal akışının yapısını ve ısıl verimi belirlemek için hız dağılımları, akım çizgileri, türbülans verileri deneysel ve sayısal olarak incelenmiştir. Sayısal hesaplamalarda standart k-ε türbülans modeli kullanılmıştır. Sayısal çalışmalar sonucunda farklı kanal geometrileri için Nusselt sayısı, Nu sürtünme faktörü, f ve verimlilik indeksi, η hesaplanmıştır. Isı transferinin iyileştirildiği geometri belirlenmiştir. Sonuç olarak deneysel ve sayısal sonuçların birbirleriyle son derece uyumlu olduğu görülmüştür.

Anahtar Kelimeler : Oluklu kanal, PIV, faz açısı, Isı tranferinin iyileştirilmesi

ACKNOWLEDGEMENTS

This list would certainly be endless if I attempted to thank all the people that made this work possible. I firstly would like to thank my advisor Prof. Dr. Beşir ŞAHİN for his great support, guidance and encouragement. He has been a great source of motivation, both personally and professionally. His generous advices, encouragements, immense knowledge and constant faith have provided me a very challenging and rewarding experience from the beginning to the end of this demanding process.

I sincerely thank Prof. Dr. Hüseyin AKILLI for his continuous and effective insights to improve myself.

My heartiest thanks and gratitude should go to Muhammed Murat AKSOY and his family. It was my luck to have such a great friend. Also, I would like to thank my friend Ferhan KARABUĞA and his husband Şemistan KARABUĞA. They always have made me feel that they were with me throughout the study. Without their encouragement, patience and support, it would be so difficult to finish this investigation.

I would like to express my special thanks to Feti YAMAN and all the technical staff of The Faculty of Engineering and Architecture's workshop at Çukurova University for their supports and encouragements.

I am thankful to all my close friends; especially, my housemate Demet KAYRETLİ. I would like to thank all the academic staff of Energy Systems Engineering Department at Osmaniye Korkut Ata University. In addition, I would like to thank Engin PINAR, Göktürk M. ÖZKAN, Tahir DURHASAN, Erhan FIRAT and Veli ÖZBOLAT for their continuous friendship, geniality and support.

Last but not least, I would like to thank my father Süleyman TOKGÖZ, my mother Nejla TOKGÖZ, my elder sister Derya BİLGİR, her housband Turan BİLGİR and their little son Emir BİLGİR, my sister Zeynep TOKGÖZ and my little sister R.Reyhan TOKGÖZ who have tremendously encouraged me throughout my academic career as well as my whole life.

Before all and after all, many thanks to the Almighty ALLAH.

CONTENTS **PAGE**

LIST OF FIGURES **PAGE**

ABBREVIATONS

x	: Streamwise direction
y	: Transverse direction
u	: Velocity in x direction
v	: Velocity in y direction
U_∞	: Free-stream velocity
μ	: Dynamic viscosity
ν	: Kinematic viscosity
u'	: Streamwise velocity fluctuation
v'	: Transverse velocity fluctuation
$<u>$	: Time-averaged velocity components in x direction
$<V>$	: Time-averaged velocity fields
$<Y>$	: Time-averaged streamline
$<w>$	: Time-averaged vorticity
$u'u'$	: Streamwise Reynolds normal stress
$v'v'$	: Transverse Reynolds normal stress
$<u'v'>$	: Time-averaged Reynolds shear stress correlations
$<TKE>$	: Time-averaged turbulent kinetic energy
u_{rms}	: RMS value of the streamwise velocity fluctuations
v_{rms}	: RMS value of the vertical velocity fluctuations
Re	: Reynolds number
Nu	: Nusselt number
f	: Friction factor
s	: Height of the corrugations
H	: Height of the channel
L	: Length of corrugations
φ	: Phase Angle
s/H	: Aspect ratio
η	: Heat transfer performance

TI	: Turbulence intensity

1. INTRODUCTION

Energy crises which were experienced in the past and expected to be experienced in near future have stimulated countries to create policies in order to use energy more efficiently. Within this framework, the studies related to energy saving and energy efficiency have been of great importance in industrial business and local managements. Because of the fact that these studies focus on optimum efficiency, the studies on the conditions that will show the highest performance have increasingly gained importance. These investigations can make sense only if accurate studies of design and optimization are carried out. In industrial foundations, on the applications in which recruiting heat transfer is of great importance, carrying out the studies of accurate design and optimization depends upon dealing with interaction between thermal and hydrodynamic areas together and evaluating the results of these interactions extensively.

In this respect, heat transfer has a significant role in a great number of industrial applications from food industry to chemical industry and from metal industry to transportation. For example, in vehicles, heat generated by the motor requires to be removed in a proper operation. Likewise, electronic equipments requires a cooling system to remove heat from the equipments in order to prevent from overheating. Besides, heating, air conditioning and ventilating systems, industrial applications include different heat transfer processes. In most of these cases, heat transfer is realized with the help of some energy equipments such as evaporators, condensers, and heat exchangers. It is essential to improve the heat transfer efficiency of these devices to minimize space occupied by the device and investment cost. Energy conservation and hence material savings encourage the development of heat transfer enhancement techniques and application of these techniques with the aim of heating exchange equipment as well as economic incentives. Additionally, improving heat transfer can reduce associated pumping power requirements.

Heat exchanger are expectedly used for transfer of heat in many processes and a heat exchanger can be described as a complex device providing thermal energy to be transferred between two or more medias at different temperatures and are in thermal contact with each other. Heat exchangers can be used either individually or as components of a large thermal system, in a wide variety of commercial, industrial and domestic applications (i.e. power generation, refrigeration, ventilating and air-conditioning systems, industrial processes, manufacturing, aerospace industries, food technology, electronic chip cooling as well as in environmental engineering). Many researchers have paid attention to the improvements in the performance of the heat exchangers for a long time since they are of great technical, economical, and not the least, ecological importance. Those studies in the literature mainly aim to have a reduction in the size and cost of a proposed heat exchanger to improve the capacity of an existing heat exchanger or to decrease the approach temperature difference for process streams.

1.1. Heat Transfer Enhancement Techniques

In general, reducing the irreversibility resulting from heat transfer at a finite temperature difference and flow friction in a heat transfer process is aimed to be achieved. A great number of techniques related to heat transfer efficiency were developed so far and some of these techniques have been put into use in industrial field. In this regard, Bergles (1983) classifies the enhancement techniques broadly into two categories; passive methods, and active methods requiring external power. The mode of heat transfer determines the effectiveness of these methods. On the other hand, Mahureand et. al., (2012) classifies heat transfer enhancement techniques broadly into three main types; passive heat transfer enhancement techniques, active heat transfer enhancement techniques and compound techniques. The active method necessitates power from an external source for heat transfer enhancement and some examples of active heat transfer techniques can be counted as magnetic fields, cams and plungers to induce pulsation can be seen among the examples of active heat transfer enhancement techniques. The passive heat transfer enhancement methods involve the use of roughened or extended surfaces and many other geometric modifications so as to upgrade convective heat transfer enhancement. However, the compound method of heat transfer enhancement involves a combination of active and passive methods of heat transfer enhancements so as to achieve higher degree of heat transfer efficiency than achieved through use of any of these two methods alone. With the aim of enhancing heat transfer for different applications, passive techniques such as use of ribs, pin fins, vortex generators and dimples have been extensively studied. In this respect, making the thermal boundary layer thinner or even breaking it can help while enhancing the convective heat transfer. This can be achieved through introduction of disturbances in the flow by using the techniques mentioned above.

To give an example, dimples have been used on the golf ball for drag reduction These dimples on the golf balls help while transitioning the boundary layer upstream of the ball from laminar as shown in figure 1.1. (Franke, 2008). Recently, dimples have found their application in heat transfer augmentation techniques and not just for drag reduction. According to Mahmood et al. (Mahmmod, 2001) the use of dimples helps in heat transfer enhancement because it forms vortical flow structures and vortices are shed from each individual dimple and it then advects downstream on the flat surface. Another reason for heat transfer augmentation in the case of dimpled surface is reattachment of the shear layer that forms on top of the dimple. Heat transfer augmentation using techniques such as corrugate, groove and vortex generators result in pressure drop penalties that severely affect the aerodynamic performance as these devices protrude into the flow causing drag force.

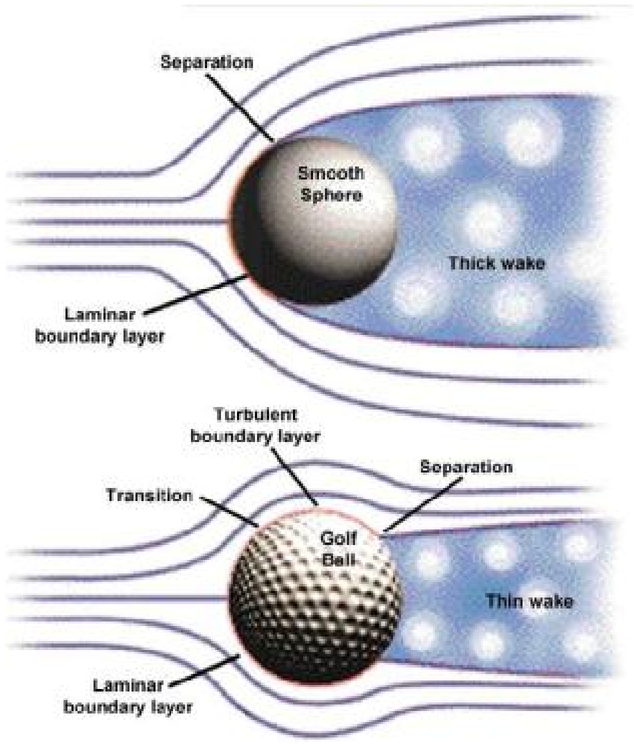

Figure 1.1. Comparison of flow over a smooth sphere and dimpled golf ball (Franke, 2008)

1.1.1. Passive Techniques

The passive controlling methods generally benefit from geometrical modifications of the energy systems which influence the flow characteristics through incorporation of insertions of additional devices such as turbulators, wings and etc. They have the capacity to promote coefficients of heat transfer to a higher value by means of improving or changing the existing flow characteristics which leads to an increase in the pressure drop. In the case of expanded surfaces, effective heat transfer area on the side of the expanded surface is increased. Passive techniques have advantages over the active techniques since they do not necessitate any direct input of additional power. However passive control devises ultimately results in an increase in pressure losses (Gupta, 2012).

1. Treated surfaces refer to the heat transfer surfaces that have a fine scale alteration to their end or coating. Where the roughness is much smaller than what affects single-phase heat transfer, the alteration could be continuous or discontinuous there, and they are used primarily with the aim of boiling and condensing duties.

2. Coated surfaces: This type of technique involves metallic or non metallic coating on surfaces. Those techniques are utilized to enhance the heat transfer in single phase convection or boiling and condensation. Non wetting coating such as teflon is utilized in order to promote drop-wise condensation. Figure 1.2 presents the cross-section of as interred porous metal coating used for nucleate.

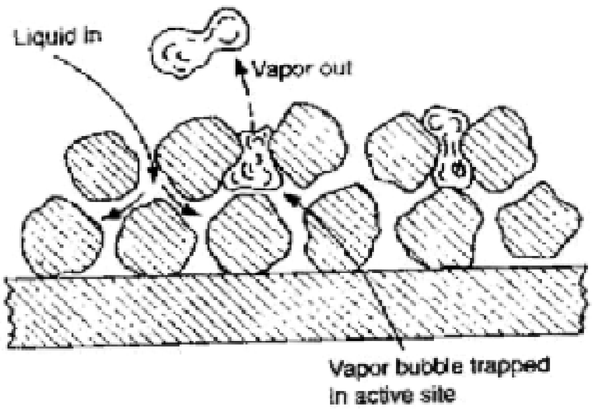

Figure 1.2. Porous metal coating (Webb, 1987)

3. Rough surfaces refer generally to the surface modifications promoting turbulence intensity of the flow field, primarily in single phase flows and they do not lead to an increase the area of heat transfer surfaces. They are either integral (formed by machining) to the base surfaces or are made through placing a roughness surface. The roughness of sand grain type to discrete protuberance configuration is selected in such a way that it promotes the mixing in boundary layer near the surface instead of increasing the heat surface area. The rough surfaces are used in mainly single phase flow. Figure1.3 presents the rough surfaces.

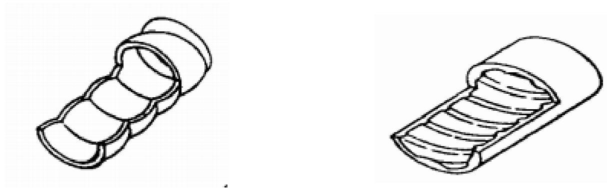

(a)

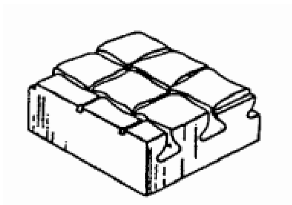

(b)

Figure 1.3. (a)Tube side roughness (b) Rough surface for nucleate boiling (Webb, 1987)

4. Displaced enhancement devices refer to inserts which are used primarily in confined forced convection and could improve energy transport indirectly at the heat exchange surface by means of “displacing” the fluid from the heated or cooled surface of the duct with bulk fluid from the core flow.

5. Extended surfaces known as finned surfaces enable an effective heat transfer surface area enlargement. Many heat exchangers employ the extended surfaces. The enhanced surfaces used on the gas side produces a higher heat transfer coefficients when compared to a plane fin. Figure 1.4 illustrates a variety of enhanced extended surfaces used on the gas side. Extended surfaces can be applied in both single phase and two phase flows.

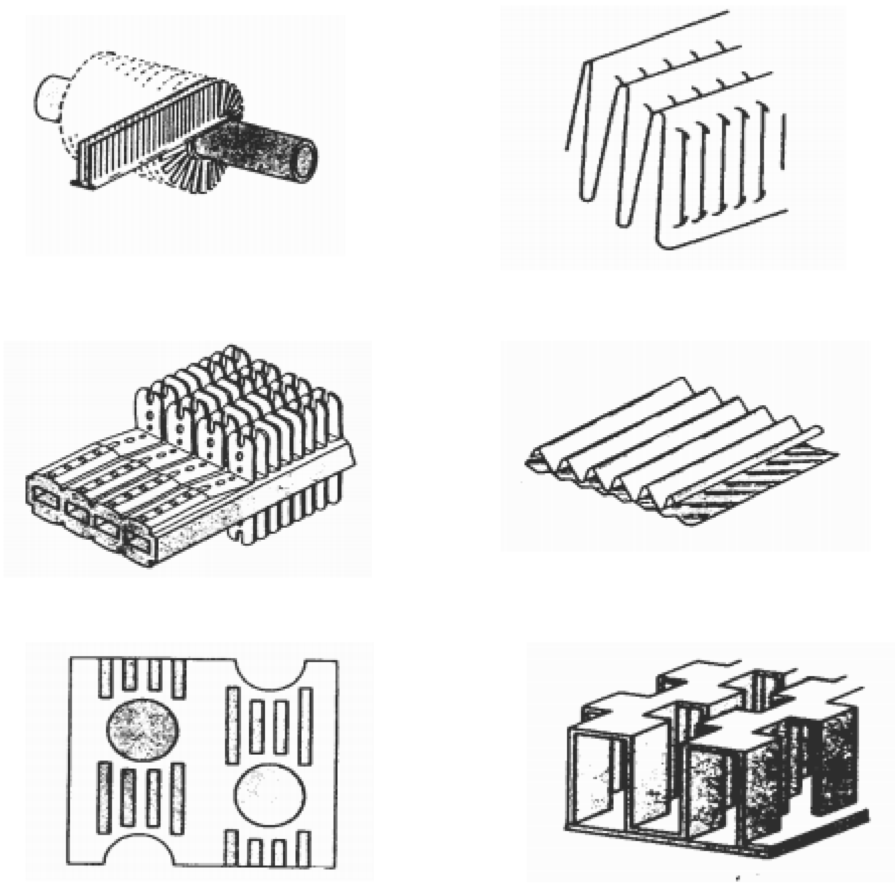

Figure 1.4. Enhanced surfaces for gases (Webb, 1987)

6. Devices of swirl flow introduce secondary recirculation or superimpose swirl on the axial flow in a channel. They involve helical strip or cored screw type tube inserts, twisted ducts and can be utilized for single- phase as well as two-phase flows.

7. Surface tension devices consist of wicking or grooved surfaces directing and improving the flow of liquid to boiling surfaces and from condensing surfaces.

8. Coiled tubes, as the name suggests, result in relatively more compact heat exchangers. The tube curvature produces secondary flows or Dean Vortices as a result of coiling, which promote higher heat transfer coefficients in single phase flows as well as in most regions of boiling.

9. Additives for liquids involve the addition of particles, soluble trace additives, and gas bubbles in single-phase flows, and trace additives, which generally depress the surface tension of the liquid for boiling systems.

10. Additives for gases include liquid droplets or solid particles which are introduced in a single-phase gas flows either in a dilute phase (gas-solid suspensions) or dense phase (fluidized beds).

1.1.2. Active Techniques

Active techniques are more complex in terms of the use and design since the method necessitates some external power input in order to provide the desired flow modification and improvement in the rate of heat transfer. They have limited application as a result of the necessity of external power in many practical applications. When compared to the passive techniques, these techniques have not shown much potential since requiring external power input. In these cases, external power is utilized so as to facilitate the desired flow modification and the concomitant improvement in the rate of heat transfer.

1. Mechanical aids refer to those stirring the fluid by mechanical mean or by means of rotating the surface. Rotating tube heat exchangers and scraped - surface heat and mass exchangers can be given as examples. Figure 1.5 displays types of agitator.

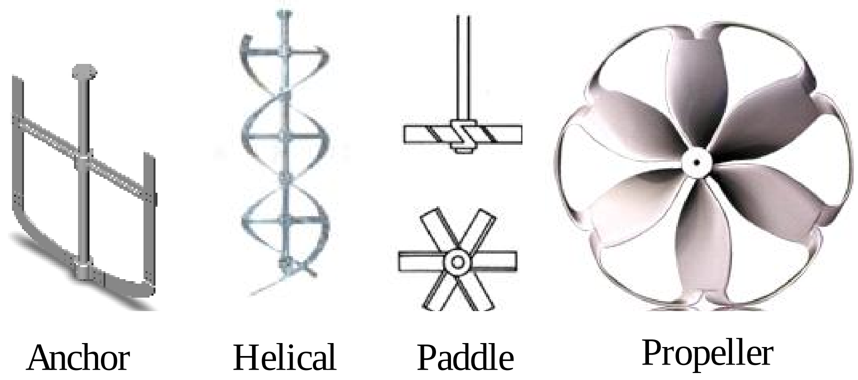

Figure 1.5. Types of agitators

2. Surface vibration has been applied primarily both at low and high frequency, in single-phase flows with the aim of obtaining higher convective heat transfer coefficients.

3. Electrostatic fields could be in the form of electric or magnetic fields or combination of the two from DC or AC sources and can be applied in heat exchange systems including dielectric fluids. The success of the method depends upon the positioning of the electrodes.
4. Injection is used only in a single-phase flow and pertains to the method of injecting the same or a different fluid into the main bulk fluid either via a porous heat transfer interface or via upstream of the heat transfer section.
5. Jet impingement involves directing heating or cooling fluid perpendicularly or obliquely to the heat transfer surface.
6. Fluid vibration or fluid pulsation with vibrations ranging from 1.0 Hz to ultrasound is considered to be the most practical type of vibration enhancement technique used primarily in a single-phase flow.
7. Suction involves either vapor removal through a porous heated surface in nucleate or film boiling, or fluid withdrawal by a porous heated surface in single- phase flow.

1.1.3. Compound Techniques

A compound enhancement technique can be described as the technique in which more than one of the above mentioned techniques is used in combination so as to further improve the thermo-hydraulic performance of a heat exchanger. The term compound enhancement refers to the process in which any two or more of these techniques are employed simultaneously in order to achieve greater enhancement in heat transfer than the one produced when either of them are used individually. Since this passive techniques do not necessitate direct application of external power other than pumping power while active techniques require external power. Among many control techniques employed for enhancement of heat transfer rates inside circular tubes, a wide range of inserts have been benefited when turbulent flow is considered. The inserts studied included:

- ü Coil wire inserts
- ü Brush inserts
- ü Mesh inserts

The heat enhancement techniques have the aim of improving the heat transfer rate, some of which need pumping power as a result of the greater resistance to flow through the heat exchanger. Techniques which do not incur a power penalty are naturally focused on in some cases.

Corrugated surface geometry is one of the many suitable passive techniques which are utilized with the aim of enhancing heat transfer as a result of growing recirculation regions near the corrugated channel and improving the mixing of fluid (Ahmed, 2011). A brief information about categorization of heat exchangers and especially plate heat exchangers in which corrugated surfaces are used commonly has been given at the end of this chapter. While fluid is flowing through the corrugated surfaces, the breaking and destabilizing the thermal boundary in the thermal boundary zone are induced. It is known that the corrugated surfaces are one of the suitable methods to improve the thermal performance of heat transfer devices (Naphon, 2008).

The heat transfer characteristics and hydrodynamics of flow through a corrugated channel are quite different when compared to the case of parallel plate channels. In corrugated channel, the main flow direction is parallel to the channel waviness geometry although the local flow direction is always changed due to channel waviness.

Flow recirculation, separation reattachment periodically interrupts the thermal boundary layer formed on its walls. However, increased pressure drop penalty invariably accompany with the gain of heat transfer.

1.2. Classification of Heat Exchangers

Heat exchangers may be classified according to Shah (2002) studies as seen in figure 1.6.

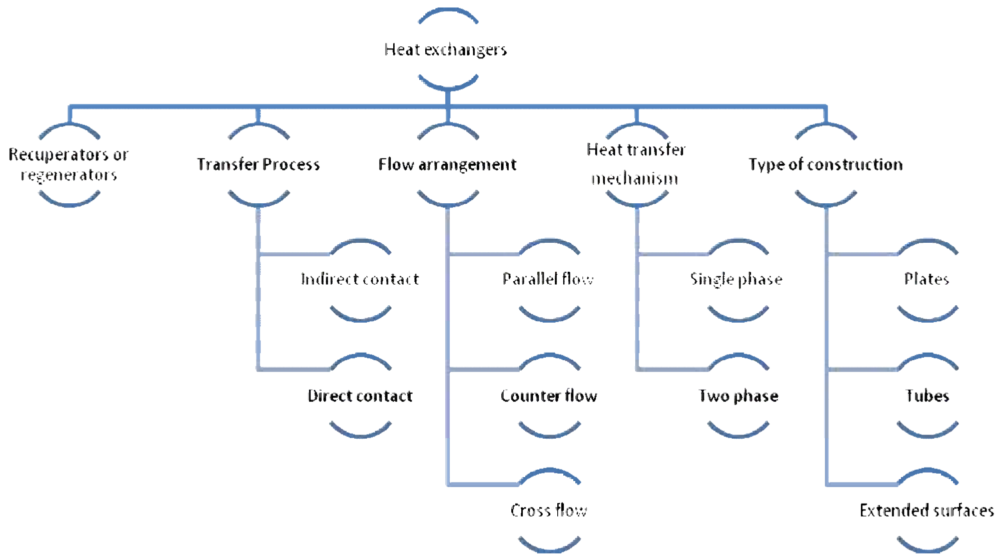

Figure 1.6. Classification of heat exchangers

The plate heat exchanger is widely recognized today as the most economical and efficient type of construction heat exchanger on the market. A flat plate heat exchanger presented in figure 1.8. With its low cost, flexibility, easy maintenance, and high thermal efficiency, it is unmatched by any type of heat exchanger. The key to the plate heat exchanger's efficiency lies in its plates. With corrugation patterns that induce turbulent flows, it not only achieves unmatched efficiency, it also creates a self-cleaning effect thereby reducing fouling. Plate heat exchangers have some advantages such as expandable, high efficiency, less fouling, compact size, easy to remove and clean.

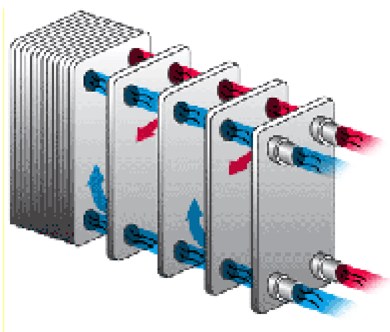

Figure 1.7. A flat plate heat exchanger

To better understand the mechanisms of plate heat exchangers; their flow patterns, swirl flows, namely hydrodynamics and effects on heat transfer and pressure drop, and to translate this into the development of new products, the both experimental study and numerical study of various design parameters is essential.

Several recent previous studies investigations cited above have shown that the corrugated channel flows were examined in terms of heat transfer enhancements, or the flow field hydraulics and turbulence statistics having different corrugate channel geometries either numerically or experimentally. In order to better understand the effect of the corrugated and phase shift channel on the improvement of heat transfer and hydrodynamics of flow, both, the experimental and numerical investigations have been performed in the present work. The main objective of this work was to investigate the flow structure in a straight and corrugated channels with different phase shift and aspect ratio experimentally and numerically in order to observe hydrodynamics of flow and thermal performance of cavities in this corrugated channels for Reynolds numbers in the range of 3000<Re<6000. The main part of the work was experimental studies. PIV measurement and numerical predictions provided hydrodynamics of flow structures, domain of the wake region, locations of the singular points, locations of the peak values of turbulence quantities, for example, the concentration of vorticity, Reynolds stresses, velocity fluctuations and turbulent kinetic energy which are substantially affected by the variation of the Reynolds numbers and phase shift angle of corrugated channels. The presence of a reversed flow in the region of cavities magnifies the level of these flow characteristics when the Reynolds number is increased. Energetic vortices are developed between wake and core flow regions throughout cavities. Heat transfer, friction factor, f, thermal enhancement factor, $((Nu/Nu_s)/(f/f_s)^{1/3})$ and flow characteristics in a periodic corrugated channel were studied numerically. In numerical part of the work, the best aspect ratio of the model, namely, deep of the corrugated channel is divided by height of the channel (s/H=0.3) was examined by studying the enhancement of heat transfer. Here, three different aspect ratio models were studied in order to define best aspect ratio for enhancement of heat transfer. Afterwards, the effect of phase shift, φ was determined for three different phase shifts at previously defined aspect ratios, s/H. Flow characteristics of models in three different phase shifts and at an optimized aspect ratio, s/H=0.3 predicted by the numerical study were measured using the PIV technique. As a result of the studies, it was observed that the numerical and experimental results were in concordance with each other. Finally, it can be concluded that the activation of these flow mechanisms by the existence of energetic vortices increase mass, momentum and heat transfer.

2. PRELIMINARY WORK

In order to minimize the cost, the weight and the size of the heat exchange features, many engineering applications need to improve their systems. For accomplishing this aim, many solutions have been tested. Among them, the most known ones implied the use of materials as rib, groove, helical rib and corrugated wall. These geometries mentioned above were expected to have a certain reaction on the transverse or longitudinal vortices of the mixed combination of flow control elements. Due to their heat transfer capacity to produce self-breaking in suitable thermal conditions, the corrugated surfaces are one of the best thermal control methods for the heat transfer process.

In the related literature, you can find many studies either experimental or numerical on the subject of heat transfer enhancement along with pressure drop through the grooved and corrugated channels.

2.1. Experimental Studies of Heat Transfer Enhancement which are Conducted by Using Ribs or Turbulators

Webb et al. (1971), established a purpose to study the way in which the heat transfer is realized in tubes with transverse ribs. In the same time they were obtained the friction of fluids, by arranging the tubes in relation to a heat flux for fully developed turbulent flow. The result shown a correlation with Stanton number, St and pointed out a certain friction factor, f. Furthermore, Layek et al.(1980), managed to realize in an artificial thermal surrounding, a heat transfer by using rib and groove, adapted to different parameters such as relative roughness pitch, P/e, relative roughness height, e/D_h relative groove position, g/P, chamfer angle, φ and Reynolds number, Re. Han et al. (1989) carried out extensive experiments on the developing and fully developed turbulent flow, heat transfer and friction characteristics of both square and rectangular ducts with rib turbulators on two opposite walls. Also, Martin and Bates (1992) observed velocity field and turbulence structure, using ribbed rectangular ducts, of different heights. In addition, Grosse-Gorgemann et al. (1995)

anticipated the fact that flow became unsteady for the ribbed channel configuration at a Reynolds number, Re larger than 46, while for the plane channel flow, the transition Reynolds number, Re was more than the order of magnitude higher. These unsteady transverse vortices enhance heat transfer by means of ‘Reynolds’ averaged transport. However, for stationary transverse vortices, no substantial increase in global heat transfer has been reported. These unsteady transverse vortices enhance heat transfer by means of ‘Reynolds’ averaged transport. However, for stationary transverse vortices, no substantial increase in global heat transfer has been reported. Lorenz et al (1995) performed the heat transfer coefficients distributions and the pressure drop throughout the wall inside an asymmetrically ribbed channel obtained for both thermally developing and turbulent flow over periodic grooves. Bilen and Yapici (2002) conducted studies about the turbulence promoters of the heat transfer, on a rectangular channel. The results showed that the orientation angle, α with 45^{o} promotes heat transfer to a highest level. Furthermore, Kim et al. (2004) were interested in tube flow where numbers of ribs were mounted on the inner surface of a tube, with different rib angles such as 45˚, 60˚ and 75˚ and 90˚. Tanda (2004) were used to deploy transverse to the main direction of the flow with using the ribs (rectangular or square sections), or V-shaped with an angle of 45 or 60 deg relative to the flow direction. Continuous and broken ribs were also demonstrated the effective results. Yakut and Sahin (2004) conducted experimental work on the rate of heat transfer and friction loss in a coiled wire inserted in tube. In addition, insertion of coiled wire generates vortices which increases mixing of fluid resulting in improving of heat transfer ability of heat exchanger although the rate of entropy generation increases further. Naphon (2006) tried to observe how a coil pitch can influence the heat transfer enhancement and pressure drop through horizontal tubes and he drawn up a conclusion that the coil wires have a certain influence on the heat transfer performance and increasing the Reynolds number, Re tends to increase heat transfer rate. It was shown that the mass flow rates either hot or cold water was directly influenced the heat transfer rate. Experimental studies of San and Huang (2006) reported the heat transfer enhancement of transverse ribs in circular tubes with a length to diameter ratio of 87 for isothermal surface conditions. Here, the rib pitch-to-tube diameter ratio, P/D was varied between 0.304 and 5.72; the rib height-to-tube diameter ratio, H/D was comprised between 0.015 and 0.143; range of Reynolds numbers was taken as $4608 \leq Re \leq 2{,}936$. The mean Nusselt number, Nu and friction factor, f were individually related to the rib pitch-to-tube diameter ratio, P/D with the range of $0.304 \leq P/D \leq 5.72$ and the rib height-to-tube diameter ratio, E/D in the range of $0.015 \leq E/D \leq 0.143$. San and Huang (2006) concentrated their studies especially on the thermal performance of tubes a length-to-diameter ratio, l/D of 87. The rib pitch-to-tube diameter ratio , P/D was varied from 0.304 to 5.72; the rib height-to-tube diameter ratio, E/D was comprised between 0.015 and 0.143; Reynolds numbers (Re) was taken as $4608 \leq Re \leq 12{,}936$. Tijing et al. (2006) studied the effects of star shaped fin on the heat transfer rate and pressure drop in a concentric-tube heat exchanger. The results indicated that the best heat transfer enhancement rate was occurred in the straight-fin configuration of counter flow heat exchanger comparing to the twisted-fin configurations. Heat transfer and friction characteristics in a double pipe heat exchanger fitted with regularly spaced twisted tape elements were experimentally studied by Eiamsa-ard et al. (2006). Their results revealed that the heat transfer coefficient, h were increased with twist ratio, y of tape whereas the increase in the free space ratio, S resulted in improvements both in the heat transfer coefficient, h and in friction factor, f. Chang et al (2007) conducted experimental studies of the heat transfer in a tube having a twisted tape. An empirical correlation allowing the observance above the Nusselt number, Nu and the friction factor, f were developed on a flow region of the smooth and serrated twisted tubes for the purpose of using in engineering applications. The effect of baffle size and orientation on the heat transfer enhancement was studied in detail by Nasiruddin (2007). Their results demonstrated that for the vertical baffle, an increase in the baffle height resulted in a substantial increase in the Nusselt number, Nu but the pressure loss was also very significant. On the other hand the Nusselt number, Nu enhancement was almost independent of the baffle inclination angle, θ. Wang and Sunden (2007) dealt with the heat transfer and friction characteristics in a square duct roughened by various- shaped transverse ribs on one wall. Lin et al. (2007) worked on a corrugated channel experimentally. They reported that local Nusselt, Nu_x was affected primarily by the Reynolds number, Re and corrugated angle, β. Promvonge and Thianpong (2008) observed the heat transfer and the friction loss of the air flow through a constant heat-fluxed channel fitted with different shaped ribs (triangular, wedge and rectangular rib shapes) with in-line and staggered rib arrangements in a turbulent forced convection. They found that the wedge rib pointing downstream yielded the highest increase in the Nusselt number, Nu and the friction factor, f but the staggered triangular rib provided better thermal performance than the others.

Experimental investigation of Kaewkohkiat et al. (2010) was related to the heat transfer and friction features in a rectangular channel with rib-groove turbulators. It was found that the Nusselt number, Nu and friction factor, f increased by the decrease of the pitch ratio. Song et al. (2010) used the inclined discrete ribs in channel to generate longitudinal vortices in order to increase the heat transfer rate. They found that the inclined discrete ribs increase the heat transfer rate substantially comparing to the plain duct. Furthermore, the inclined discrete ribs in channel causes less pressure loss compared with transversal ribs. Naphon (2011) presented the results of the heat transfer characteristics and friction factor, f of horizontal double tubes with twisted wires brush insert. Their study focused on the effect of twisted wires density, inlet fluid temperature, and relevant parameters on heat transfer characteristics and friction factor, f. As a result of the presence of swirl flow, the convective heat transfer obtained from the plain tube with twisted wires brush insert was higher than the plain tube without twisted wires brush insert. Twisted wire brushes inserts have a significant effect on the enhancement of heat transfer with higher pressure drop.

2.2. Numerical Studies of Heat Transfer Enhancement Which are Conducted by Using Ribs or Turbulators

Okamoto and Nakaso (1991) applied their interests on studying the structure of the turbulence having a ribbed plate. They showed that the fluctuation of turbulence were the highest for a pitch-to-height ration of 9.In the same time, between the bottom ribs, the pitch-to-height was 6.6. Stone and Vanka (1999) carried out their study on the heat transfer in forced convection of a channel formed by 14 undulations. The factors of geometrical value kept their condition, but variation of the Reynolds number, Re appeared. The small values of this Reynolds number, Re was found to be 6240 and the channel was considered being stabile, with recirculation appeared at the extreme parts. When the instability of flow is fully developed the rate of heat transfer increase further extend. Saidi and Sunden (2000) dealt with the thermal characteristics in a duct with rib turbulators through use of a simple eddy viscosity model and an explicit algebraic stress model and suggested that the algebraic stress model had some superiority over the eddy viscosity model just as a result of its velocity field structure prediction. Ceylan and Kelbaliyev (2003) proposed a correlation of the factor of friction, f in fully developed flow regime. By using this, new formulas were discovered and used, in order to comprise the heat transfer for the pipes with a roughness of $\varepsilon/D \leq 0.05$. The effectiveness parameter for the heat transfer was studied as a function of the pipe roughness, Reynolds number, Re and Prandtl number, Pr. The effect of fouling on the heat transfer in pipes was briefly discussed, too. Tatsumi et al. (2003) predicted the flow around discrete ribs, obliquely attached to the flow direction in the lower part of a square duct and showed that a strong secondary motion of the flow was obtain in the downstream of the rib and as a result, augmentation of heat transfer enhancement was noticed. Luo et al. (2005) exposed a behavior of fully turbulent flow convections in the horizontal parallel plate channel placed periodic transverse ribs using the standard $k-\varepsilon$ model and a Reynolds stress model, RSM. An anticlockwise vortex was found in the downstream region, even if the length and the strength were substantially different. Chaube et al. (2006) conducted numerical predictions using the shear stress transport, $k-\omega$ turbulence model on the hydrodynamics of flow and heat transfer characteristics of a two dimensional roughened ribs (rectangular/chamfered rib) placed in the rectangular duct with only heating one wall. The objective of numerical studies of Kim and Lee (2007) was to define optimal design of a square channel with V-shaped square ribs and ability of heat transfer rate of heat exchanger using a shear stress transport (SST) model. Korichi and Oufer (2007) constructed simulation model on the heat transfer rate for oscillatory flow in channels which had periodically obstacles upper and lower walls. The flow was found to be stable at lower values of Reynolds numbers, Re comparing to high Reynolds number, Re. Eiamsa-ard and Provonge (2009) studied the convection of a forced thermal transfer and the friction features in a rectangular duct with three types of turbulators (rectangular-rib and triangular-groove, triangular-rib and rectangular-groove and triangular-rib with triangular-groove). They indicated that the turbulators with a low Reynolds number, Re had higher heat transfer enhancement in comparison with the smooth duct, with increments of 80%, 60%, and 46%. The value of the friction factors, f were 6.9, 5.5 and 4.8, respectively. The effects of roughness observed in microtubes were studied by Duan and Muzychka (2010). They solved the Stokes equation in order to better understand the friction factor, f and pressure drops in microtubes. Because of the roughness, there was an important increase of the pressure drop. Bigham et al. (2011) observed the mixed effects of rarefaction, creeping flows and heat transfer in a constant temperature wall of a microchannel. The governing equations in the presence of slip velocity and temperature jump at the solid walls were discretized by a finite volume scheme and solved by using the SIMPLE algorithm in curvilinear coordinate. It was shown that involving the effect of viscous dissipation affects the thermal fluid pattern considerably and also increases the Nusselt number, Nu. It was also found that the Knudsen number, Kn had a declining effect on both the skin friction coefficient, C_f and Nusselt number, Nu. Desruesmak (2012) studied nine geometries consisting of a rectangular channel with transverse rectangular alternated ribs. Nusselt number, Nu and Fanning friction factor, f were numerically investigated for Reynolds numbers, Re varied from 75 to 2000. Further investigation would require comparison between the turbulence model results with DNS of the oscillatory flow. However, massive computational power would be necessary due to the three-dimensional geometry. Thermal enhancement factor was found to be greater than unity for Re $\geq$ 800, but the effective benefit was certainly depended on parameters external to the heat exchanger itself.

2.3. Experimental Studies of Heat Transfer Enhancement Which are Conducted by Using Corrugated, Grooved and Wavy Surfaces

Goldstein and Sparrow (1977) were the first scientists using a naphthalene technique for establishing the heat transfer coefficients of local and average convection in a corrugated channel. They used 30˚ of phase angle; φ for two different corrugations and the comparison of the results with parallel plates were indicated that the enhancement in the average convection heat transfer was increased by a factor of 3 in turbulent flow regimes. In addition to these studied, O'Brian and Sparrow (1982), shown a correlation of the average Nusselt number, Nu in the flow existing between corrugated channels with sharp edged peaks. They proved that the friction factor, f was almost independent of Reynolds number, Re. Even so, the promoted flow separation accompanied with sharp edged corrugations resulted in large pressure drops. Sparrow and Comb (1983) were investigated the effect of corrugated channel height on heat transfer and flow characteristic and showed that the increase of the channel height, H was direct proportionally with the Nusselt number, Nu and the friction factor, f. Moreover, Mendes and Sparrow (1984) conducted an experimental work on the turbulent flow in the converging and divergent tubes. Their main purpose was the analysis of the alteration heat transfer for different aspect ratios, s/H and taper angles, in the entrance region. It was shown that the highest heat and mass transfer were accompanied by a large pressure drop. The researchers affirmed that this result is due to the existing of the circulation zones and the enhancement of the heat transfer related to the converging-diverging channels compared to the straight tubes. Ali and Ramadhyani (1992) underlined the heat transfer occurred in the case of different channels spacing with especially triangular corrugated channel. They stated the fact that effectuation of a larger spacing channel was much better than a smaller one. This experiment reported that the corrugated channels have a higher implication of Nusselt number, Nu comparing to the parallel plate channel. Saniei and Dini (1993) conducted experimental work on a wavy-wall channel and its fluid features, i.e. heat transfer characteristics were analyzed. They discovered that the maximum local Nusselt number, Nu was found in the peak of every wave, while the minimum one had a certain distance related to the same aspects. They revealed that the highest average Nusselt number, Nu was occurred in the second wave and the Nusselt number, Nu remained the same downstream of the third wave as a result of the flow being fully developed periodically. Studies of mass transfers within channels with sinusoidal waves with respect to the different Reynolds number, Re and distances between the plates were performed by Gschwind et al. (1995). The results showed a large variation and series of instabilities for all these aspects being underlined by the small separation values of the plates. Lorenz et al. (1995) measured distributions of the heat transfer coefficient, h and of the pressure drop along the wall inside an asymmetrically grooved rectangular duct for thermally developing and periodic turbulent flow. Stasiek (1998) performed a study about the forced convection heat transfer along heat exchanger surfaces. The most obvious result of his experiment showed that at high inclination (more than 45°), the friction factor, f and the Nusselt number, Nu decreased for corrugated-undulated heat exchanger surfaces. Experimental studies on the wavy channels were also made by Rush et al (1999). Their main purpose was to observe the influence of undulation and of the Reynolds number, Re in the heat transfer of the geometric parameters. They mostly observed mixing and chancing of flow structures in the macroscopic scale which influenced enhancement of heat transfer for both steady and unsteady flow cases. It was observed that mixing of fluid is related to the Reynolds number, Re and to the geometry of the channel. Alteration of flow characteristics occurred near the exit of the channel and along the channel when the Reynolds number, Re was increased to a higher value. In the same time, a macroscopic fluid mixing was observed at a moderate value of the Reynolds number, Re=800. The authors also reported the existence of a transversal velocity component which was also reported when the fluid became macroscopically mixed. The subject was developed by Wang et al. (1999) who delivered studies in order to define the right correlation between wavy plates and tube heat exchangers. Their primary consideration was geometrical parameters. In addition, Kim (2001) performed an experimental study on developing and fully developed flows in a wavy channel which examine the onset of the flow transition and the global fluid mixing. Gradeck et al. (2002) established their main purpose of experimental studies concerning the enhancement of a heat transfer for flows with a single phase, under the effect of laminar and turbulent forced convections. The results of the experiment revealed the fact that the heat transfer coefficient had a higher degree of sensibility on the top of the corrugation, even if the highest disorder was observed at the bottom part of the undulation, with its negligible effects. Ali and Hanaoka (2002) made experiments on the parameters operating with a forced convection of heat transfer for laminar flow of air in a channel having a V-corrugated upper plate heated by radiation. The local Nusselt number, Nu was directly proportional with the inclination angle, β. The mentioned Nusselt number, Nu varied from 33% to 67.3% while the angle was comprised between 0 degree and 60 degree. Islamoglu and Parmaksizoglu (2003) experimentally investigated the effect of channel height on the enhancement of heat transfer characteristics for air flow in a corrugated channel. They discovered that while the channel's height, H and the Nusselt number, Nu increased, the rate of pressure drop decreased. Vicente et al. (2004) organized many experiments regarding the transient, laminar and turbulent flows of different corrugation heights, H and pitches. Their main interest was to define the values of isothermal friction factor, f and the Nusselt number, Nu. It was shown that there was not important changes happened for the laminar flows, but intensive modification were discovered when it came to reveal results about the turbulent flow. They represented this phenomenon as helical corrugation in which roughened surfaces increase flow turbulence and mixes in the near wall flow, which is effective in turbulent flow but not in laminar flow. Wahidi et al. (2005) conducted their study the coefficient of skin-friction, C_f mean velocity, u and turbulence intensity, TI, of turbulent flow over a smooth wall with transverse square grooves using Laser–Doppler Anemometer (LDA). Gradeck et al. (2005) studied the condition of the heat transfer only in a single phase flow and they also observed local temperature distributions at the wall. Jaurker et al. (2006) reported the rate of heat transfer and friction characteristics on a heated wall which had a large aspect ratio, s/H duct and different properties. Layek et al. (2006) observed the pitch ratio on a groove position with a rectangular friction factor, f and a repeated transverse roughness related to the heat transfer. Naphon and Sriromruln (2006) conducted experiments on studies of flow characteristics in the micro-fin tubes. It was shown that an insertion of coil wire can increase the level of thermal performance of the micro-fin tubes. They preformed similar experimental study on horizontal double pipes and their main interest was to investigate the effect of a relative height on the thermal performance of horizontal double pipes. Their collaborations with other scientists showed that the height of corrugation has a big influence on the heat transfer performance. In his research work, Naphon (2007) were interested in the heat transfer characteristics and pressure drop in a channel of different corrugation angle under constant heat flux. The experiments were conducted for laminar and turbulent flow. It was concluded that heat transfer and pressure drop were tremendously enhanced when compared to those of parallel plate channel. They also indicated the promoted recirculation zones and flow separation in corrugated channel flow. Naphon (2007) found in his study that using corrugated plates was a suitable method to increase the thermal performance and higher compactness. Breaking and destabilizing in the thermal boundary layer occurred as a fluid flowing through the corrugated surfaces. The wavy angle and channel height have significant effects on the temperature distribution and flow development. The estimated results obtained from the model were validated with the measured data. There is a reasonable agreement from the comparison between the estimated results and the measured data. It can be observed that the corrugated surface has affected the enhancement of heat transfer and pressure drop significantly. Hasanuzzaman et al. (2007) carried out an experimental study concerning the transfer of the heat in a square of two V-corrugated parallel channels. The results indicated that the peak temperature was higher than the trough in the hot plate although the temperature of the trough was higher than the peak in the cold plate. Elshafei et al. (2008) conducted an experimental study on forced convection heat transfer and pressure drop characteristics of flow in corrugated channels. The results revealed that the coefficient of the heat transfer and the pressure drop increased from 2.6 to 3.2. The average coefficient of heat transfer increased from 1.9 to 2.6 in the channel with parallel plates depending on the spacing and phase shift of parallel plates. Durmus et al. (2009) conducted experiments on the heat transfer and pressure drop with different surface profiles. Their results indicated that the efficiency of the heat exchanger increases by increasing the fluids' contact surface, pressure drop and mass flow rates owing to an enhanced heat transfer to the fluid. Bilen et al. (2009) experimentally studied heat transfer and friction characteristics of a fully developed turbulent air flow in a different grooved tubes (circular, trapezoidal and rectangular) and suggested that heat transfer enhancement was around 63% for a circular groove, 58% for the trapezoidal one and 47% for the rectangular at the highest Reynolds number, Re =38000. Layek et al. (2009) focused upon Nusselt number, Nu and friction factor, f in a chamfered ribbed duct with V-groove having chamfer angles of 5°, 12°, 15°, 18°, 22°and 30°. They found that the performance parameter was directly proportional with the Reynolds number, Re. Overall, the mechanism of heat transfer enhancement by the ribs is based upon the flow separation, reattachment and secondary flow. Kim et al. (2010) carried out an experimental study on the force convection of the cross-flow air in cooled plate heat exchangers. The comparison of double plate heat exchanger with a single wave plate heat exchanger indicates that the double plate heat exchanger causes 30% more pressure drop. Finally, it has been concluded that double plate heat exchanger is needed to be modified in order to keep wider gap between the plates for having less pressure drop. Laohalertdecha and Wongwises (2010) investigated the effect of corrugation pitch on the heat transfer coefficient and pressure drop of R-134a inside a horizontal corrugated tube. The results showed that the corrugation pitch had significant effect on heat transfer heat transfer coefficient and pressure drop augmentations. Petkhool et al. (2011) studied the turbulent heat transfer enhancement in a concentric tube heat exchanger with helically corrugated tube as an inner tube in order to define the effect of three different pitch to diameter ratio, P/D_H and three different heights to diameter ratio, e/D_H on heat transfer and isothermal friction augmentation based on Reynolds numbers, Re in the range of $5500 \leq Re \leq 60000$. Recently, an experimental research work conducted by Faizal and Ahmed (2012) on the heat transfer and the pressure drops using corrugated plate heat exchanger with variables having the water flows by using temperature analysis all over the plate exchanger. The results showed that by increasing the volume flow rate of hot water, the average heat transfer, between two streams increased owing to higher turbulence at higher velocities.

2.4. Numerical Studies of Heat Transfer Enhancement which are Conducted by Using Corrugated Surfaces, Grooved Surfaces and Wavy Surfaces

The first analytical research work dealing with the problem of viscous flow in wavy channels were performed by Burns and Parks (1967) using Fourier series under the Stokes flows. Sparrow et al. (1980) investigated the heat transfer in a circular tube with a slat-like blockage. The heat transfer enhancement was observed to be effective within a distance of 10 tube diameters downstream of the blockage. Asako and Faghri (1987) showed that the heat transfer rate along sinusoidal plates is 40% greater than the flat channel, even if the Reynolds number, Re, pressure drop, pumping power and mass flow were the same. In the numerical simulations, Garg and Maji (1988) investigated phase shift, $\phi = 0^\circ$ sinusoidal wavy channel. They indicated the variation of local Nusselt number, Nu with Reynolds number, Re and the sinusoidal distribution law of the local Nusselt number, Nu along flow direction. Xin and Tao (1988) performed numerical solution related to the flow and the heat transfer in channels with cross-sectional area. It was demonstrated that the Nusselt number, Nu and friction factor, f were influenced by the geometrical parameters and Reynolds number, Re. Most recently, Wang and Vanka (1995), by the help of periodical passages and array, determined the values of the thermal transfer. For the parallel plate channels, the Nusselt number, Nu was just a bit higher than the one for the wavy channel. On the contrary, in a transitional flow process, the rate of heat transfer was around 2.5. Friction factors, f for the wavy channel were about twice those for the parallel-plate channel in the steady-flow region, and remained almost the same in the transitional regime. Fusegi (1997) conducted a numerical study on the fully developed forced-convective heat transfer in a grooved channel with a heated lower plate, and displayed the ability of accurate prediction of sensitive time dependent flows. Blancher et al. (1998) were interested in instabilities of hydrodynamic character in wavy channels, using linear analysis and regulations of the Navier-Stokes energy equations. The result showed a self sustained laminar flow with an unsteady temperature. Sawyers et al. (1998) combined the analytical and the numerical techniques investigated the effects of the three dimensional hydrodynamics in a corrugated channel of the heat transfer. They found that in three-dimensional case, a small mean flow in the transverse direction led to increase heat transfer, while there was a decrease in heat transfer as the transverse flow movement became stronger. Tsal et al. (1999) realized the numerical simulation of flow in the passages formed in the air side of a wavy finned tubes heat exchanger. The objective of modeling was to determine the features of flow that could influence the heat transfer in wavy fins in order to elaborate better design result for the devices used. Lee et al. (1999) performed a numerical study of mass transfer in a wavy channel to investigate pulsating condition having laminar flow. Chaotic regime of flow was observed with a maximal chaoticity response around a certain Strouhal number, St which was approximately equal to the inverse of the wavelength. Excepting the use of turbulence models, Yang (2000) introduces the use of LES (large eddy simulation) in order to observe the turbulent flows in channel which had periodically grooved. Fabbri (2000) investigated the convective heat transfer in a channel composed of smooth and corrugated walls under laminar flow conditions. The velocity and temperature distributions were determined by using the finite element method. It was found that the relative improvements in heat transfer of the optimum corrugated profile increased with the Reynolds number, Re and Prandtl numbers, Pr. Their numerical model was coupled with a genetic algorithm program with the aim of optimizing the corrugated plate profile in terms of heat transfer. The study upon Stokes flow in wavy channel realized by Vasudeviah and Balamurugan (2001) showed that for those conditions of flow, the contractions resisted to fluid flow, and a viscous heat generation existed consequently. Also, they established that by using Stokes flows, the heat transfer rate was lower in wavy channels than in the flat ones. Herman and Kang (2002) studied the temperatures fields, by applying the interferometry technique in rectangular ducts with curved vanes. The curved vanes were added above the downstream end of the heated block so as to redirect the flow from the main duct into the groove. Mahmud et al. (2002) computed a numerical study over the wavy surface flow, by using different geometrical parameters, with sinusoidal function. A critical Reynolds number, Re was observed by establishing patterns of boundary layer separation. Wang and Chen (2002) used a transformation method in their studies about the heat transfer in convergent and divergent sinusoidal channels. While giving different geometrical and Reynolds number, Re values, they showed that the wavy channels increase the heat transfer when the wavelength is also high, as well as the Reynolds number, Re. Comini et al. (2003) conducted numerical studies about the flow and heat transfer in three-dimensional wavy channels. The Nusselt numbers, Nu and friction factors, f have higher values while the aspect ratios were decreased. Numerical investigations of Gut and Pinto (2003) on the forced convection heat transfer with generalized configurations for the plate heat exchangers were studied. Determination of the heat exchanger configuration could be used with assembling algorithm effectively. Furthermore, they concluded that it can be helpful to improve optimization methods for selecting the plate heat exchanger configuration. Metwally and Manglik (2004) numerically studied the periodically developed forced convection in laminar flow through sinusoidal corrugated-plate channels. When the Reynolds number, Re and Prandtl numbers, Pr increase the rate of heat transfer also increases for entrainment of the self sustained vortices. This is shown that a small friction lose appears in the given conditions. Besides, Islamoglu and Kurt (2004) analyzed the transfer in the corrugated channel by using an artificial neural network formulation. It was demonstrated that this can enable successfully the Nusselt number, Nu estimations for the air flow in corrugated channels Yang and Hwang (2004) analyzed the transfer in rectangular ducts using the $k-\varepsilon$ turbulence model numerically. Savino et al. (2004) investigated the pressure drop and heat transfer characteristics of a wavy channel which was nominally two dimensional, but benefited from a three-dimensional numerical simulation for that. They observed that the flow became three dimensional, not due to the action of boundary conditions, but due to the intrinsic fluid flow instabilities. Zhang et al. (2004) performed studies upon the values of the undulation and variation of distances between upper and lower plates of sinusoidal channels. They showed that the enhancement of heat transfer is due to the amplitudes of corrugation which was larger than 0.5. The heat and momentum transfer were studied by Bahaidarah et al.(2005), using finite element methods. They also used sinusoidal and arc-shaped configurations showing an increase of the Reynolds number, Re in both configurations. As a result, they found that the enhancement in heat transfer increased with an increase of the Reynolds number, Re for both channel configurations. Fabbri and Rossi (2005) realized a different study on the heat transfer at entrance region of a similar conditions but comparing the coefficients of heat transfer with the ones of a flat plate channel and observed the changes appeared based on the Reynolds number, Re. Finite element method was used to solve governing equations. The result presented that the effect was direct proportional with the augmentation of Reynolds number, Re. From a numerical point of view, Kanaris et al. (2005) studied the convection of the water flow in a plate heat exchanger having undulated surface and revealed that the best performance was observed when the channel plates were near and with less obtuse corrugations, under the influence of low values of the wider channels. Xiang (2005) conducted research on the effects of a wavy plate spacing on flow characteristic and heat transfer rate for sinusoidal channels with phase shift angle of $\phi = 0^{\circ}$. In additions, similar analyzes were computed for the flow features and heat transfer of different phase angles, ϕ. In the numerical investigation of Naphon and Kornkumjayrit (2007), flow was considered as one dimensional through the channel which has a wavy (V-shaped) shaped lower plate and plane shaped upper plate for the analysis of thermal performance. The k-ε turbulence was used to study related parameters of heat transfer enhancement. In conclusion, breaking and destabilizing the thermal boundary layers are recommended through the corrugated surfaces for improvement of thermal performance. Mohamed et al. (2007) numerically studied the effects of the entrance region of a symmetric wavy-channel on the heat transfer and hydrodynamics. It is concluded that augmentation of the shear stress and the Nusselt number, Nu depends on the Reynolds number, Re and the highest magnitude of Nusselt number, Nu is acquired in the entrance region. Fernandes et al. (2007) were interested in the effects of forced convection of chevron-type heat exchangers. Increases of tortuosity coefficient, τ was observed by varying the aspect ratio, Υ until reaching the chevron angle. Furthermore, Fernandes et al. (2008) conducted a numerical study on natural convection with using cross-corrugated chevron type plate heat exchangers (PHEs). The velocity profiles and the magnitude of the average interstitial velocity affect the flow index according to their predictions. In addition, the value of tortuosity coefficient, τ decreased when the referred index value was reduced. Hong et al (2008) studied the three dimensional microchannel with microstructures using Monte Carlo method. The 3-D microchannel was simulated with the cross-section aspect ratio ranging between 1 and 5. A comparison between 3-D cases and 2-D cases showed that when the aspect ratio, D/H was less than 3, significant effects on the heat transfer rate and flow properties were observed. Cooling and heating features of the microstructure temperature were observed by varying the Knudsen number, Kn. When the aspect ratio, D/H increased, the flow pattern and heat transfer characteristics tended to approach to those of 2-D results. Using finite volume approach, Mohamed et al (2008) solved governing equations for laminar forced convection in the entrance region of a wavy-channel. They revealed effects of the Reynolds number, Re and Prandtl number, Pr as well as amplitudes of wavy channel regarding the flow and the heat transfer. As a result of the increasing Reynolds numbers, Re, Nusselt numbers, Nu and shear stresses has been increased. In the study of Eiamsa-ard et al. (2008), a numerical prediction has been made to predict heat transfer and flow friction behaviors in turbulent channel flows over periodic grooves. Comparison of predicted results using the standard $k-\varepsilon$ turbulence model, the RNG $k-\varepsilon$ turbulence model, the standard $k-\omega$ turbulence model and the SST $k-\omega$ turbulence model with measurements indicated that the RNG $k-\varepsilon$ turbulence model or the $k-\varepsilon$ turbulence model was more proper in predicting heat transfer and fluid channel flow over periodic grooves on one wall. The heat transfer in the channel with periodic grooves can be enhanced although higher pressure loss of the fluid flow is obtained. Thermal enhancement factor of approximately 1.33 is found at the lower Reynolds number, Re for aspect ratio, B/H=0.75. The different values of the flow and heat transfer performances in sinusoidal and triangle channels were studied by Peng (2008) using an unsteady numerical approach for the laminar flow. Self-sustained oscillations appeared at different extreme values of Reynolds numbers, Re and the friction factor, f and heat transfer were higher in the sinusoidal channel. Ismail and Velraj (2009) worked on the fanning friction factor, f using Colburn factors, j for the offset and wavy fins compact plate fin heat exchanger. They developed the Colburn factors, j in the laminar and turbulent regions, by using different models of wavy geometries. Kanaris et al (2009) conducted their studies on the field of forced convection inside compact heat exchangers made of corrugated plates. The simulation results indicated that the comparison of Nusselt number, Nu values for the simplified model shows that the side-channels, besides improving the operability of the heat exchanger by shifting the flooding limit to higher gas velocities when used as reflux condensers, do not have a negative effect on the overall heat transfer enhancement. Furthermore, Turgay and Yazicioglu (2009) elaborated studies searching for the effect of triangular roughness on heat transfer in two parallel plates with constant temperature. They affirmed that the slip velocity and the increase of the temperature had a rarefaction effect. The results indicated that increasing surface roughness reduces heat transfer continuously. When the roughness height is appeared in the slip flow regime the Nusselt number, Nu increases. Assato and de Lemos (2009) numerically studied the evolution of the linear and nonlinear viscosity models, aiming to observe the turbulent flow in a sinusoidal wavy channel. The result showed that the numerical solution using nonlinear models at high Reynolds numbers, Re was stable even with greater relaxation factors and coarser grid sizes. Sui et al. (2010) numerically investigated water flow and heat transfer in wavy microchannels with rectangular cross section. The results indicated that the heat transfer performance of wavy microchannels was much better than that of straight microchannels, however, this performance was accompanied by the increase in pressure drop. The three dimensional of forced convection in conduits with corrugated wall which was encountered in commercial plate heat exchanger were numerically studied by Lin et al. (2010). The predicted results suggested that the initial assumption predicted heat transfer phenomena in a narrow channel with corrugated wall. Numerically studies were performed by Zhang and Che (2011) on the effect of corrugation profile for cross-corrugated plates on the heat and flow characteristics. They considered different corrugation profiles and carried out the numerical simulations using the finite volume method. Results revealed that Nusselt number, Nu and friction factor, f were higher for the trapezoidal channel than for the elliptic channel. Three-dimensional flow and heat transfer between cross corrugated plates have also been numerically investigated by Zhang and Che (2011) using eight turbulence models. They presented and analyzed friction factor, f Colburn factor, j and distributions of local Nusselt number, Nu. Mohammed et al. (2011) investigated laminar water flow and heat transfer characteristics in wavy microchannel heat sink with rectangular cross-section numerically. The governing equations were solved by using finite volume method. It was found that the heat transfer performance of the wavy microchannels was better than the straight microchannels with the same cross-section. The pressure drop penalty of the wavy microchannels, on the other hand, was much smaller than the heat transfer enhancement. Zhang and Che (2011) analyzed the effect of corrugated plates and their flow features numerically. It was proved that the thermal and hydraulic performances were influenced by the corrugations profile. Nusselt number, Nu is higher when it comes about trapezoidal channel comparing to the elliptic one. Han et al. (2012) studied the improvement of realistic applications by the help of nuclear plant design. The obtained values presented that the geometrical parameters maximize the heat transfer rate and minimize the frictional resistance. The alteration of TKE is influenced by the number of corrugations pitches and by the turbulence intensity. Mohammed et al. (2012) studied the characteristics of a 2D corrugated channel. The results indicated different values of the Nusselt numbers, Nu. The average of its value increased with the wavy channel increased. While the pressure drop increases with the wavy channel and angle, it decreases with the channel height. For instance a 17.5 mm channel with wavy angle of 60^{o} saves more energy in comparison with others. Yin et al. (2012) investigated the effects of wave plate phase shift and Reynolds number, Re on the thermal hydraulic performance numerically. The friction factor, f and Nusselt number, Nu decreased as the phase shifts, φ increased. The friction factor, f and goodness factor, G decreased with increasing the Reynolds number, Re while Nusselt number, Nu indicated opposite changes. The thermal-hydraulic performance was closely related to the distributions of streamlines. The more severe the streamlines distort, the greater the resistance loss and the heat transfer rate are. These channels of phase shift 0°to 90° had better overall performance, and the 0°channel had the optimal performance in the region of lower Reynolds numbers, Re.

2.5. Both Numerical and Experimental Studies of Heat Transfer Enhancement Which are Conducted by Using Different Methods

Greiner et al. (1986) investigated grooved and ribbed channel flow experimentally and numerically. It was found that a substantial heat transfer enhancement was observed to occur only when the flow was self fluctuating. The critical Reynolds number for ribbed channel flow was found to be lower than for grooved channel flow. Briefly, the local heat transfer can be enhanced to a larger extent by the use of transverse vortices, but the global heat transfer can be enhanced by flow destabilization owing to the modified velocity profiles leading to large amplitude of self sustained oscillations or turbulence intensification. Nishimura and Mathur (1996) conducted numerical and experimental studies regarding the heat transfer of laminar flow for phase angle ϕ=0˚ in a sinusoidal channel to observe dynamics of vortices. Comparisons of streaklines between phase angle ϕ =0˚ and ϕ=180˚ for sinusoidal channel. It was concluded that a channel with a phase angle of ϕ =180˚ was advised by their numerical results under same flow conditions, and they also reported that various mass transfer rates caused different patterns of streaklines. Besides, Stasiek et al. (1996) carried out numerical and experimental study on forced convective flow and heat transfer for a crossed corrugated geometry, representative of compact heat exchangers including air pre-heaters for fossil-fuelled power plant. It was found that the angle depending of friction factor, f was much larger than that of the Nusselt number, Nu. Experimental and numerical study on a rectangular wavy duct with different angles, φ was conducted by Kwon et al. (2008). It should be mentioned that the highest level was 1.8 for an angle, φ of 100° and the value of the Reynolds number, Re=1000. Naphon (2009) studied the corrugated channels numerically and experimentally. He used a CFD program and his results showed that the corrugated surface influences the pressure drop substantially. Arsenyeva et al. (2011) studied a new corrugation pattern for plate condensers and their results presented that a mathematical model is to be confirmed by a good agreement with calculated results in plate heat exchanger channels. From all the statements analyzed in this work we could observe that there were some scientists interested in the process of heat transfer. One of the most important subjects was the one underlining the fluid friction for a pipe and a channel flow and how they can influence the heat transfer rate. In order to better understand the theoretical issues of the matter, experiments should be conducted for further extends.

3. MATERIAL AND METHOD

3.1. Numerical Study

3.1.1. Pre-Processing

Once the geometry has been created, the next step is discretizing the domain i.e. dividing the domain into a number of elements of same or different nature. The pre-processing step is one of the most important and probably the most time consuming step in the CFD process. The accuracy of the solution heavily depends on the quality of the mesh generated. Generation of mesh can be different in different areas of the solution domain. For example, one may need a finer mesh close to the wall boundaries of the geometry to capture the gradients existing in the boundary layer there. Paranjape (2012) reported that the type of mesh to be generated also depends on the complexity of the geometry available, computer resources, nature of flow and time availability. Structured grids are usually created when the nature and direction of flow is known beforehand and geometry is fairly simple. However recent research in grid generation has given rise to the use of unstructured grids which give a fairly accurate solution and save a lot of time when compared with creation of structured grids. After evaluation of these parameters, the decision to create the type of grid depends on the intuition, experience and skill of the user.

3.1.2. Problem setup

After the grid is generated, it is setup according to the initial and boundary conditions. Precise identification of the boundary and initial conditions and their appropriate numerical application is very important to get a realistic solution. Material selection and implementation of its properties is done in the setup. The solution method or algorithm, appropriate models for the methods and level of accuracy required by defining the residual convergence criteria while solving the flow equations are also decided in this step.

3.1.3. Solution

The solution for the governing equations is then calculated at different grid points or elements using the chosen method. For obtaining a CFD solution, one of finite difference, finite volume or finite element methods is generally used. Use of the finite element method is more popular in structural problems and needs further research and development for solving flow problems. The Finite difference method involves use of a structured grid with uniform or non-uniform spacing and use of numerical methods by marching either in space or time to obtain numerical values at each grid point (Egeregor,2008).The Finite volume method consists of discretizing the domain into several well defined volumes or cells. The volume averaged values of the conserved variables are obtained using this method. The mass, momentum and energy equations are conserved in this method. This method also facilitates the use of an unstructured grid which is useful in case of complex geometries. The finite volume method is therefore popular among fluid dynamicity and engineers in general.

3.1.4. Post processing

The last step of the CFD process is post processing where the results are analyzed using graphs, contour plots, etc. The values of the parameters to be analyzed are extracted. A lot of commercial post-processing packages are available to view results for analysis.

3.1.5. Governing Equation

In CFD, the Navier Stokes equations which govern all problems related to Fluid Mechanics and Heat Transfer are solved numerically. In the present work the Navier Stokes equations are 2D coupled set of partial differential equations. They are derived on the basis of laws of physics dictating conservation of mass, momentum and energy.

Continuity equation: Unsteady state analysis of incompressible flow without considering gravity effects is considered.

$$\frac{\partial u}{\partial x}+\frac{\partial v}{\partial y}+\frac{\partial w}{\partial z}=0$$

Momentum equation: The dimensionless 2D unsteady incompressible momentum equation is given in the following form.

$$\frac{\partial u}{\partial t}+u\frac{\partial u}{\partial x}+v\frac{\partial u}{\partial y}=-\frac{1}{\rho}\frac{\partial p}{\partial x}+v\frac{\partial^2 u}{\partial x^2}+v\frac{\partial^2 u}{\partial y^2}$$

$$\frac{\partial v}{\partial t}+u\frac{\partial u}{\partial x}+v\frac{\partial u}{\partial y}=-\frac{1}{\rho}\frac{\partial p}{\partial y}+v\frac{\partial^2 u}{\partial x^2}+v\frac{\partial^2 u}{\partial y^2}$$

Equations derived from Newton 's second law, where ν is the kinematic viscosity $\nu={}^{\mu}/_{\rho}$ describe the conservation of momentum in the fluid flow and are also known as the Navier-Stokes equations.

Energy equation: Two dimensional energy equation used in the present work is stated as

$$\frac{\partial T}{\partial t}+u\frac{\partial T}{\partial x}+v\frac{\partial T}{\partial y}=\frac{k}{\rho C_p}\frac{\partial^2 T}{\partial x^2}+\frac{k}{\rho C_p}\frac{\partial^2 T}{\partial y^2}$$

3.1.6. The Standard k-ε Model

The simplest "complete models" of turbulence are two-equation models in which the solution of two separate transport equations allows the turbulent velocity and length scales to be independently determined. The standard k- ε model in FLUENT falls within this class of turbulence model and has become the workhorse of practical engineering flow calculations in the time since it was proposed by Launder and Spalding (Fluent 2003). The standard k-ε model is a semi-empirical model based on model transport equations for the turbulence kinetic energy, k and its dissipation rate, ε. The model transport equation for k is derived from the exact equation, while the model transport equation for was obtained using physical reasoning and bears little resemblance to its mathematically exact counterpart. In the derivation of the k- ε model, the assumption is that the flow is fully turbulent, and the effects of molecular viscosity are negligible (Fluent2003).

In the present study numerical solutions made my using the standard k- ε model due to its robustness, computational economy, and reasonable accuracy for a wide variety of turbulent flows. Moreover, in this model the solution of two separate transport equations for k and **ε** allows the turbulent velocity and length scales to be independently determined. According to the Dewan (2011) standard k- ε model one of the simplest complete models of turbulence. Each term of the modeled transport equation for k almost accurately represents the corresponding term in the exact equation. However, the gross effect of several terms in the exact dissipation equation is modeled by few terms, or in other words, there is no one to one correspondence between different terms in the modeled and exact transport equations for dissipation.
The turbulent or eddy viscosity is modeled with respect to applied turbulence model as

$$\mu_t = \rho C_\mu \frac{k^2}{\varepsilon}$$

The turbulent kinetic energy is defined as;

$$\frac{\partial}{\partial x_i}\left(\rho k u_i\right) = \frac{\partial}{\partial x_j}\left[\left(\mu + \frac{\mu_t}{\sigma_k}\right)\frac{\partial k}{\partial x_j}\right] + G_k - \rho\varepsilon$$

The rate of turbulent kinetic energy dissipation is predicted by;

$$\frac{\partial}{\partial x_i}\left(\rho \varepsilon u_i\right)=\frac{\partial}{\partial x_j}\left[\left(\mu+\frac{\mu_t}{\sigma_\varepsilon}\right)\frac{\partial \varepsilon}{\partial x_j}\right]+C_{\varepsilon 1}\frac{\varepsilon}{k}G_k-C_{\varepsilon 2}\rho\frac{\varepsilon^2}{k}$$

Where the rate of turbulent kinetic energy generation is ;

$$G_k=-\rho\,\overline{u_i' u_j'}\frac{\partial u_j}{\partial x_i}$$

The closure coefficients are given by

$$C_{\varepsilon 1}=1.44,\quad C_{\varepsilon 2}=1.92,\quad C_{\mu}=0.09,\quad \sigma_k=1.0,\quad and\quad \sigma_\varepsilon=1.3$$

3.2. Experimental Study

Technological developments, especially in the fields of electric and electronic engineering, have encouraged the development of new measuring techniques. All of the measurement techniques offer some advantages and disadvantages that are directly associated with the specific method. In this respect, it is of great importance not only to measure the mean values at a point in space, but also to measure and characterize turbulent and instantaneous values in the investigated flow field. Particle Image Velocimetry, PIV, refers to a non-intrusive technique utilized so as to measure an instantaneous two dimensional velocity vector field under investigated area. The velocity is determined via measurement of the displacement of particles in a flow field illuminated by a laser sheet.

3.2.1. Water Channel System

Experiments were conducted in an open water channel which was available at the Fluid Mechanics Laboratory the Department of Mechanical Engineering of Çukurova University. The channel test region having 8000mmx1000mmx750 mm was constructed from a 15 mm thick transparent plexiglass sheet as seen figure 3.1. The upstream and downstream fiberglass reservoirs were large enough to avoid swirling. This system was built with the aim of conducting steady flow and unsteady flow experiments. The control of flow speeds was provided by a 15 kW powered water pump with a variable frequency control unit. After the water was pumped into a large reservoir in order to settle the flow and conveyed through a flow straightened section and hence two-to-one channel contraction, before reaching the test chamber. A flow straightened system is located at the entrance of the contraction so as to minimize the free-stream turbulence expected to be less than 1% (Karakuş, 2007). The water channel facility benefits from several devices in order to reduce flow non-uniformities in the test section. Furthermore, a flow straightened section and a two-to-one channel contraction, a horizontal perforated cylinder pipe in the settling chamber permit the water coming from the pump to be dispersed along its entire depth. The temperature of the Fluid Mechanics Laboratory was kept constant of 22° C throughout the experiments. Water was filtered in order to avoid dirts or small solid particles to enter the water flow. Because any small particles may spoil PIV images.

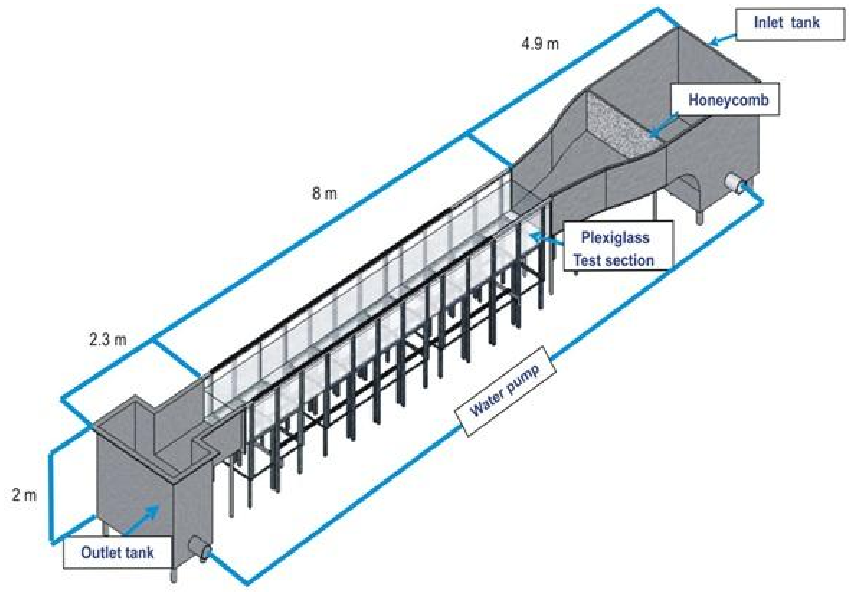

Figure 3.1. Schematic representation of water channel (Aksoy, 2013)

3.2.2. Particle Image Velocimetry (PIV)

The PIV technique allowing instantaneous, non-intrusive and quantitative measurement of two dimensional flow fields is a significant achievement and a well established technique in many areas of modern experimental fluid mechanic applications (Gilliot, 2004). The processes of seeding the water flow field to illuminate the test section under investigation and recording of two images of a specified flow field in rapid succession are involved in this technique. In the present method, seeding the flow field is needed in order to illuminate seeding particles characterizing the flow behaviors. A velocity vector map can be calculated in the flow domain from the movement of the tracer seeding on condition that the time interval between two images is known. The theory of PIV was firstly introduced by Adrian (1988) in the late 1980s. Afterwords experimental implementations were conducted by (Kean et al. 1990 and Kean et al. 1991). At this stage, a single photographic frame was multiply exposed and analyzed through use of an auto-correlation technique owing to hardware limitations. Nevertheless, improved speed of photographic recording soon provided images to be captured on separate frames for analysis via cross-correlation (Kean et al. 1992). The direct recording of particle images was provided with the help of the introduction of digital camera technology to PIV (Willert et al. 1991), at the expense of reduced resolution, which led to the development of digital PIV (Westerweel, 1997). Apart from hardware advances, many new algorithms have been developed in the last decade, which have the potential to increase the accuracy and speed of PIV analysis. PIV technologies have some advantages and disadvantages when compared to other velocimetry techniques (Melling, 1997). Advantages of PIV technique to other velocimetry techniques are; thousands of measurements per image, measurements are simultaneous, few fundamental limitations, non-intrusive and disadvantages are; very expensive, poor temporal resolution, elaborate set-up.

3.2.2.1. Principles of PIV

The Particle Image Velocimetry, PIV method can be described as a measurement technique which aims to obtain instantaneous velocities in a specified two dimensional flow field. Simply, instantaneous velocities can be calculated as, speed =distance / time. In the PIV technique, the property which is measured actually is the distance travelled by particles in the flow field within a known time period. Seeding is very important parameter for this technique. For PIV experiments, different types of seeding particles are utilized depending on the characteristics of the flow. The suitable seeding particles were selected in order to simulate the exact flow behaviors' and detecting the movement particles require illumination using a pulsating laser light sheets.. The technique of PIV consists of two stages; image acquisition and image evaluation. Figure 3.2 presents a typical experimental arrangement designed to carry out PIV measurements.

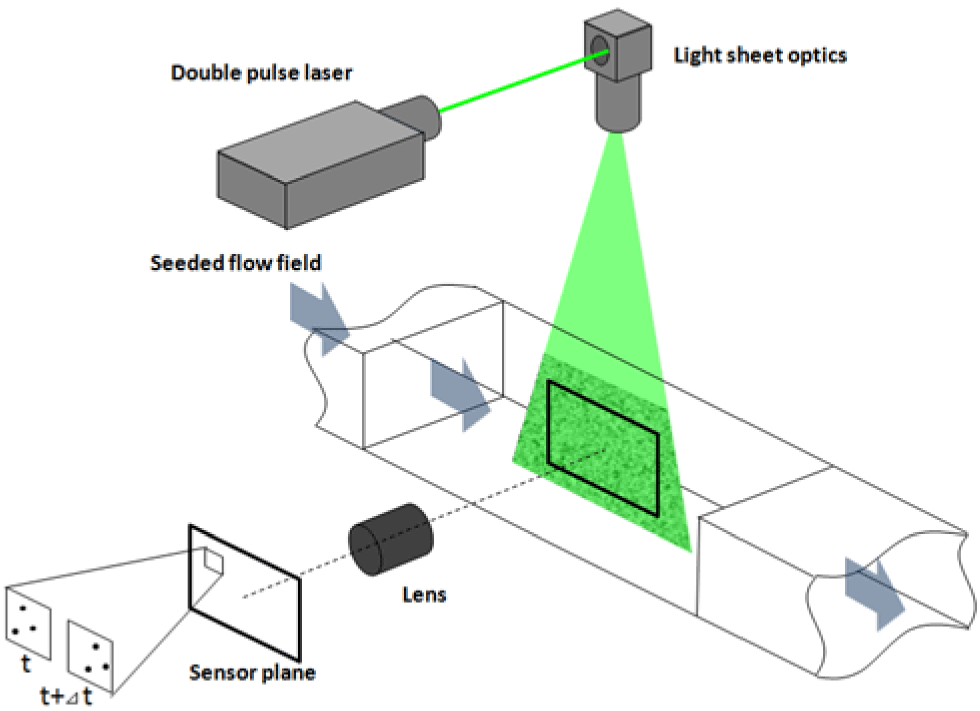

Figure 3.2. A typical PIV experimental set-up

A laser sheet illuminates tracer particles added to the flow under investigation and those images are captured and stored to be analyzed later. The denominator in the equation above is the time between the light pulses. A Charge Coupled Device (CCD) camera is placed at right angles to the laser light-sheet, and particle positions will appear as light specks on a dark background on each image in order to capture the position of the illuminated seeding particles. The pulsing light-sheet and the camera are synchronized so as to make sure that particle locations at the instant of light pulse number 1 are recorded on frame 1 of the camera, and particle positions captured from pulse number 2 are recorded on frame 2. Both the first and the second pulses of the light sheet reflecting locations particles were recorded on the same camera frame since older generations of CCD cameras couldn't switch the frames fast enough.

The camera frames are divided into square regions named as interrogation areas or interrogation regions and the image from the first and the second pulse of the light-sheet are correlated in order to define an average particle displacement vector for each of these interrogation areas. Post-processing is carried out to validate the data and to improve the vector map resolution and accuracy before interrogating the images in this way and generating the vector map. Through use of this vector map, patterns of streamlines, vorticity contours and Reynolds stress correlations can be obtained.

Seeding: Seeding is very important parameter for the PIV technique. If the seeding particles should be chosen as small as possible with similar density, they follow the small scale eddies but on the other hand these seeding particles may not be too small, because then very small particles will not scatter enough light, and hence produce too weak images. Silver-coated particles, Fluorescent, polystyrene, or other highly reflective particles must be used to seed for the water flow. For wind tunnel applications, olive oil or alcohol droplets are generally used to seed the flow field. The choices of seeding particles depend on a number of parameters. Primarily the seeding material should be selected considering the flow that is to be quantitatively observed and the illumination system available. Depending on the nature of the flow, seeding particles used for PIV measurements usually have particle diameters ranging from 0.1 to 50µm. Although measurement using what is naturally present as impurities in the fluid is possible in a few cases, successful seeding can usually necessitate considerable effort and ingenuity. The factors that should be taken into consideration include flow medium (air/water), volume to be seeded, flow velocity, light scattering, particle size, safety considerations (ingestion, risk of explosion). In general, the seeding particles should also be selected in a way that the seeding particles are neutrally buoyant in the fluid flow, but in many flows this is a secondary consideration. Another important parameter is related to stokes number for spherical seeding particle. A measure of the particles' ability to accurately track the flow field is provided by the Stokes number, and limiting that number is also dependent on the flow domain and the existence of significant accelerations or decelerations. Stokes number refers to the ratio of the stopping distance of a particle to a characteristic dimension of the obstacle.

$$St = \frac{\tau_p . U_\infty}{d_{particle}}$$

where τ_p refers the relaxation time of the particle, U_∞ is the free stream fluid velocity of the flow well away from the obstacle and $d_{particle}$ is the diameter of the particle. The particle relaxation time is given by: $\tau_p = \frac{\rho_{particle} d^2_{particle}}{18\rho_{fluid} . \nu_{fluid}}$ with $\rho_{particle}$ and $d_{particle}$ the particle density and particle diameter. For $St >> 1$, particles will go on in a straight line as the fluid turns around the obstacle and as a result affecting the obstacle. For $St << 1$, particles will follow the fluid streamlines closely (Fuchs1989).

3.2.2.2. Correlation and Cross-Correlation Process

Particle Image Velocimetry, PIV enables a complete velocity field in a large number of points for a whole planar region of space. PIV is of great importance for the study of unsteady phenomena because of the fact that it permits capturing the velocity field at a given instant, within a fraction of a millisecond. In some conditions, PIV can be coupled with other methods in order to measure the instantaneous velocity fields and the instantaneous spatial distribution of a scalar quantity simultaneously which allows the determination of velocity-scalar correlations. Alternative analysis algorithms have been developed as well as error correction and post-processing procedures which were designed to improve speed and accuracy of the PIV method since the introduction of the first PIV image evaluation methods. Nonetheless, the classical PIV analysis method is still the most frequently used and forms the basis for many other algorithms (Figure 3.3**).**

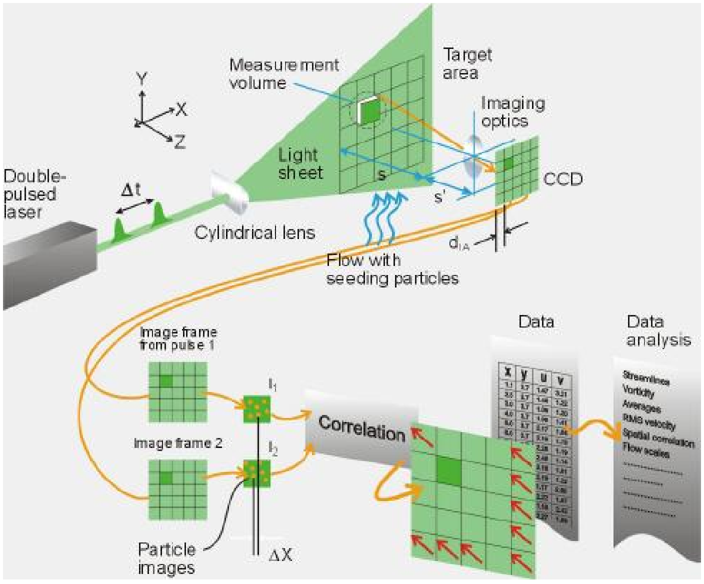

Figure 3.3. Basic PIV analysis process (Schiwietz, Westermann, 2004)

The heart of the PIV analysis refers to the correlation of regions of the input images (known as interrogation areas, figure 3.4) with each other with the aim of determining the displacement vector of the flow in that part. A velocity vector to be calculated from the displacement vector is enabled via knowing the time interval between the images captures. Particle tracking or correlation is the most common methods to determine this distance.

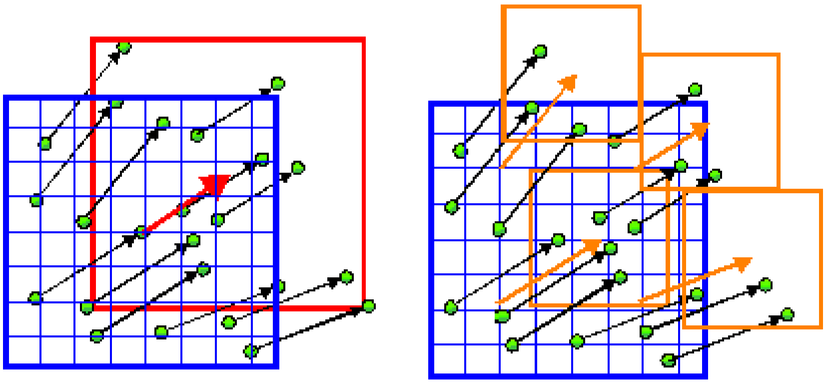

Figure 3.4. Interrogation areas (Dantec Software User's guide, 2007)

These methods involve Autocorrelation, 1-frame Cross-Correlation and 2-Frame Cross-Correlation. The differences in these correlation techniques are related to the image window areas for the first and second particle images. In autocorrelation, both the first and second image window utilizes the same image window. In 1-frame cross-correlation, the second image window is offset from the first image window on the same frame. In two-frame cross, the first image window is on frame 1 and the second image window is on frame 2. Each of these processing techniques provides advantages for some applications (Ozgoren 2000, Ozalp 2006).

Autocorrelation is related to multiple exposure images where the particle motion and image shift together give less than ¼ of the interrogation spot image displacement, which defines the classical PIV processing technique.

One-frame cross-correlation also refers to a multiple exposure technique. It is used when the image shift displacement is large relative to the particle motion displacement. Distance high-resolution measurements can be made by offsetting the second image window from the first via mean particle image displacement. Otherwise, prohibitively large interrogation spot sizes would be required for autocorrelation processing. The interrogation spot size can be reduced by offsetting the second image window via mean particle image displacement, and as a result, fewer lost pairs relative to autocorrelation will occur.

The distances between locations are recorded by two particles which have move between exposures on two image frames. Each of these frames has only one pulse of light. The processing signal-to-noise ratio relative to the single frame techniques is improved by knowing the sequence of the first pulse images and the second pulse images. Zero displacements and reversing flows can be measured by two-frame cross-correlation without image shifting. Two-frame cross-correlation can be utilized with image capture systems with an effective frame rate high enough in order that the particle images on two successive frames provide particle image displacements in the measurable range.

3.2.2.3. Image Post-Processing

Öztürk (2006) reported that the post-processing of the raw velocity field covers vector validation/ removal of spurious vectors, replacement of the removed vectors, and data smoothing and filtering. As soon as the vector fields are determined, time-averaging, phase averaging can be employed. General procedure for the image processing is displayed in Figure 3.5. In the post processing, the vectors are compared against the neighboring vectors. Vectors varying by validation tolerance from the neighborhood average are removed. The left places can be filled in via interpolation of the neighboring vectors in order to get the best estimate of the velocity at that point. The instantaneous velocity field of the flow can be calculated after the vector is validated and missing points are filled in. Following that calculation, other properties of the flows can be calculated from the data of instantaneous velocity field.

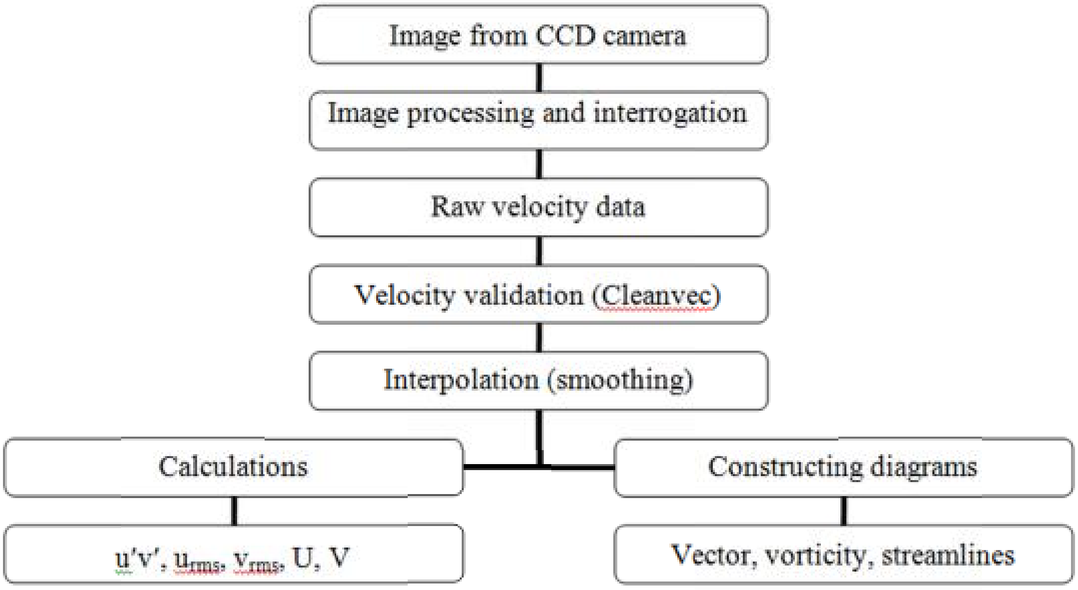

Figure 3.5. General procedure for image processing (Öztürk, 2006)

Due to the mis-matching of particle pairs, Spurious vectors may appear in the velocity vector field of PIV measurements. In this case, accuracy and reliability of measurements deteriorate. Therefore, spurious vectors are detected and removed and replaced the spurious vectors by correct ones before the image processing. Finally, neighborhood averaging technique improve and smoothe the digital images . Vector validation software called CleanVec was utilized in the process of removing bad vector which was incorrect.(CleanVec is a PIV vector validation program written by Ron Adrian's group in Theoretical and Applied Mechanics at the University of Illinois). This software was provided from University of Illinois Urbana-Champing Laboratory of Turbulent and Complex Flows. The software CleanVec contains Fourier statistical filters which were designed for incorrect vector removal:

- Absolute range filter
- RMS tolerance filter
- Magnitude difference filter
- Quality filter

For elimination of incorrect vectors, three of these four filters were used. Following the removal of incorrect vectors, use of CleanVec interpolates between the vectors and areas where incorrect vectors were removed using a bilinear least-square fit technique. Gaussian weighted averaging technique smoothed the interpolated and scaled velocity field based on the work of Landreth and Adrian (1989) in which a smoothing parameter of 1.3 was used. Lastly, the vorticity was calculated via circulation method. The velocity and vorticity data were set to zero in region which contains the bluff body following the smoothing process and vorticity calculation. The contours of constant vorticity were constructed through use of a Spline fit technique with tension factor of 0.13 in the process of smoothing.(Pinar 2013) The sampled-averaged velocity field information was utilized in order to calculate patterns of mean-square velocity and vorticity fluctuations. There are two types of averaging methods. Although one of them is time-averaging, the other one is phase-averaging method.

3.2.3. Experimental Model

Experiments were carried out with three different corrugated channel models which are presented in Figure 3.6.

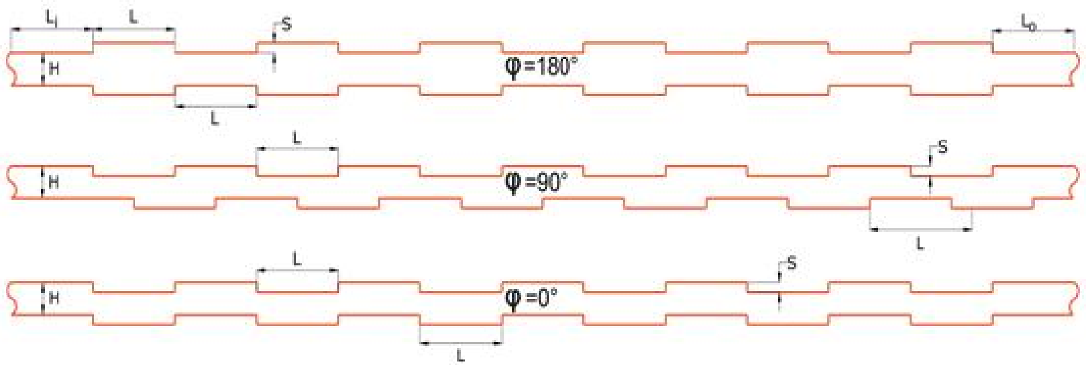

Figure 3.6. Experimental Model Dimension

All of the width of the models is large enough to avoid the effect of the side walls on the observed flow field. All experiments were performed above a platform. The total depth of the water in the channel was adjusted to a 600 mm height from bottom surface of the channel. During all experiments, the water level was (h_w) maintained at the depth of 60 cm. Velocity was U_∞=95.5 mm/s and 63.7 mm/s, corresponding to the Reynolds number of Re=6000 and Re=4000 respectively, which was calculated as Re=(U_∞ D_h /n), based on the hydraulic diameter (4A/S). Here, n refers to the kinematics viscosity, D_h is the hydraulic diameter and U_∞ is the free stream velocity in cavity. Length (L) and depth (S) of corrugated (L) is 100 mm and 10 mm respectively. Inlet length of cavity (I) and outlet length of cavity (O) is 900 mm and 500 mm respectively. 3-D Cavities configuration as seen in Figure 3.7

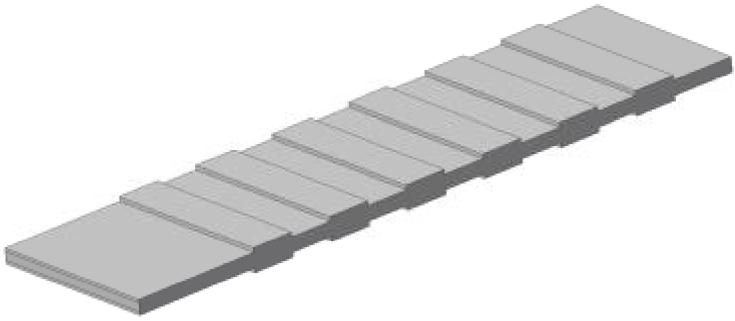

phase angle, φ= 180˚

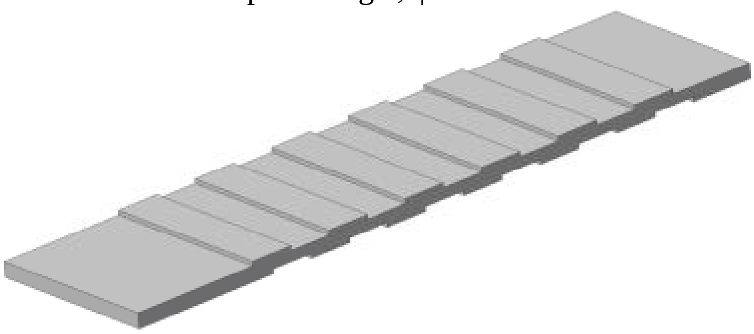

phase angle, φ= 90˚

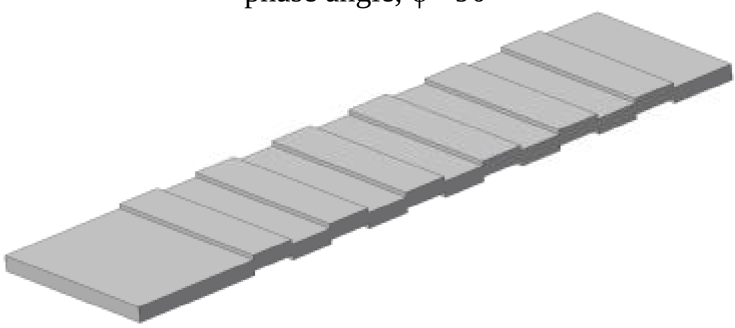

phase angle, φ= 0˚

Figure 3.7. Configurations of Cavity with phase shift (φ)180˚,90˚ and 0˚ respectively

The objective of this study is to search the effects of phase shift, φ and Reynolds number, Re on flow behavior in a corrugated channel. Experimental method is employed in order to determine the flow in channels having rectangular corrugated plates with three different phase shifts, φ (i.e. φ=180°, 90°, 0° and Reynolds number, Re= 4000 and 6000). Total length of cavity was 2.5 m and aspect ratio; s/H was 0.3 for all experimental models. The width of the channel (400 mm) was very large when compared to the height of channel as seen in figure. Experimental models which has different phase angles, φ such as 180˚ , 90˚, 0˚ presented in figure 3.8.

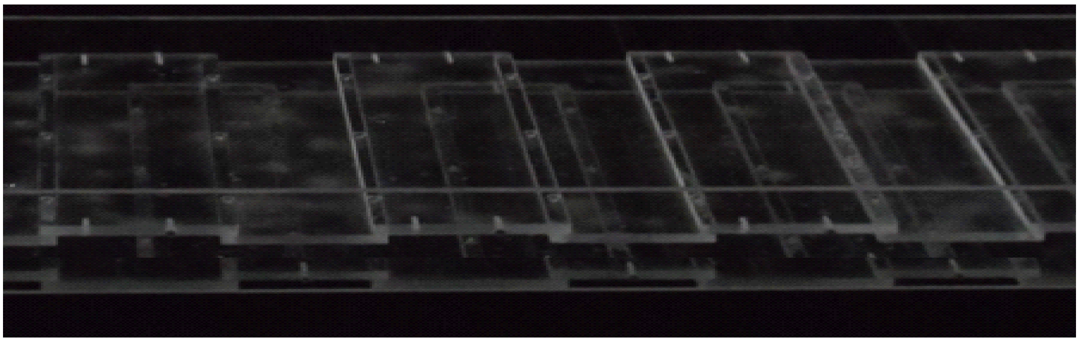

phase angle, φ= 180˚

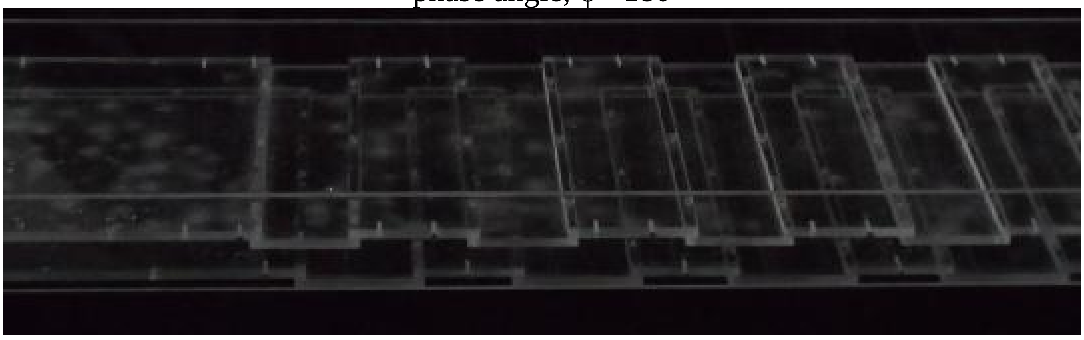

phase angle, φ= 90˚

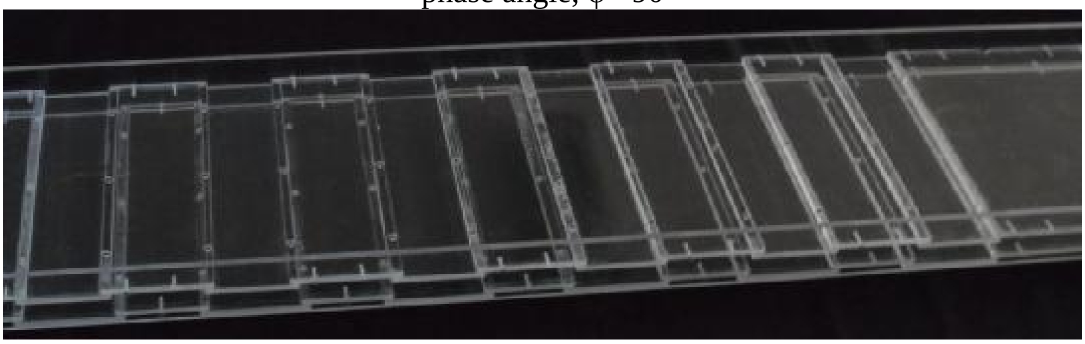

phase angle, φ= 0˚

Figure 3.8. Experimental models

The PIV (Particle Image Velocimetry) technique will be used so as to measure the velocity vector fields. In the modern fluid mechanics and aerodynamics, For the instantaneous velocity measurements in a defined flow field, the PIV technique is one of the most reliable methods. The basic principle of PIV measurements involves capturing images of the flow field which contains seeding particles illuminating in the laser light exposure. By means of a synchronizer, the time between the images to be taken and the laser pulses are synchronized and the velocity vectors of the flow field are measured through comparison of the particle movement between two consequent images (Pinar 2013). The PIV experiments were carried out in one plane called as side-view. An intense and thin laser light sheet illuminated the measurement field by employing a pair of double-pulsed Nd:YAG laser units with maximum energy output of 120 mJ. Dantec Dynamics Processor, at 532 nm wavelength. The laser sheet was positioned vertically to the top surface of the water channel and the experiments were carried out at the midsection of the water height seen as figure 3.9.

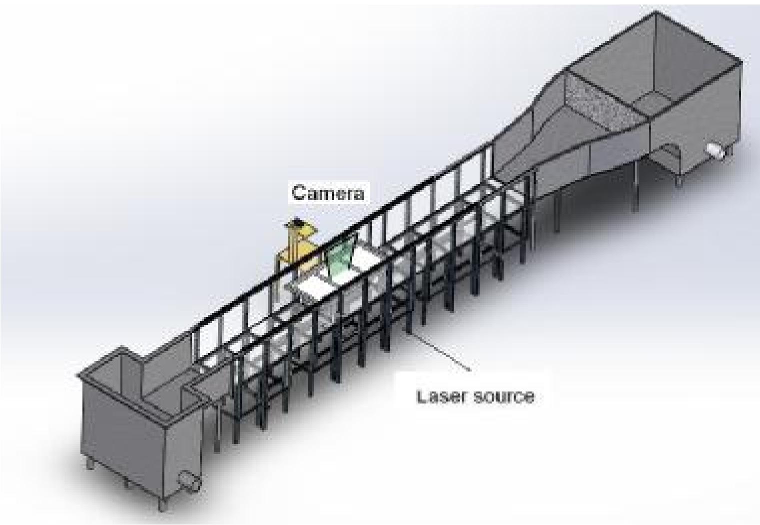

Figure 3.9. Cloosed loop open water channel

The image capturing was performed by a 8-bit cross-correlation charge-coupled device (CCD) camera which had a resolution of 1,600 pixels x 1,200 pixels, equipped with a Nikon AF Micro 60 f/2.8D lens. In the image processing, 32 x 32 pixels rectangular effective interrogation windows were used. The total 7326 (99 x

74) instantaneous velocity vectors were obtained from an instantaneous velocity field at a rate of 15 frames per second. The time interval between pulses was 1750 μs, and the thickness of the laser sheet which illuminated the measuring plane was nearly 2 mm throughout the experiments. Erroneous vectors were removed (less than 2%) and replaced by using interpolation between surrounding vectors in the post-processing step. Velocity vectors of the flow were calculated from this displacement vector field. The vorticity patterns of the wake flow were calculated from the velocity field using a finite difference scheme. Patterns of streamlines and circulation were obtained through post processing of the velocity data. The overall field of view was 117 x 88 mm^2. Patterns of instantaneous particle images (total of 1000 images for a continuous series) were taken at a rate of 15 Hz. An overview of experimental setups for corrugated channel was presented in figures 3.10 and 3.12. The water was seeded with 10 µm-diameter seeding particles. In each test, 1000 instantaneous images were captured, recorded and stored with the aim of obtaining averaged-velocity vectors and other statistical properties of the turbulent flow field. Spurious velocity vectors (less than 2%) were removed through use of the local median-filter technique and replaced through use of a bilinear least square fit technique between surrounding vectors. The velocity vector field was also smoothed in order to avoid dramatic changes in the velocity field by using the Gaussian smoothing technique. A smoothing parameter of 1.3 was chosen so as to minimize distortion of the velocity field.

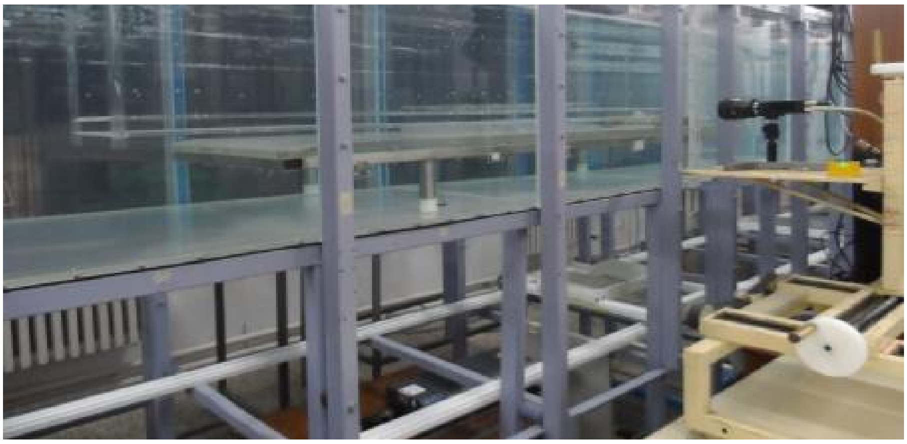

Figure 3.10. The view of immersed test models in the channel

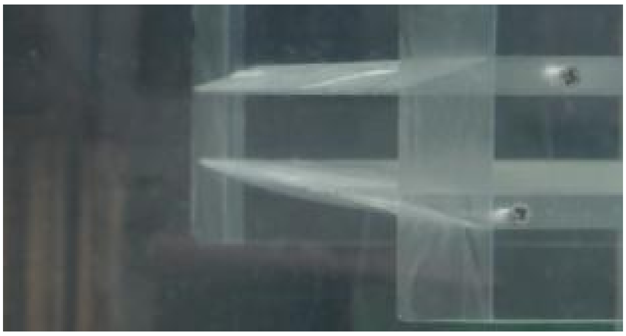

Figure 3.7. Inlet region of test model

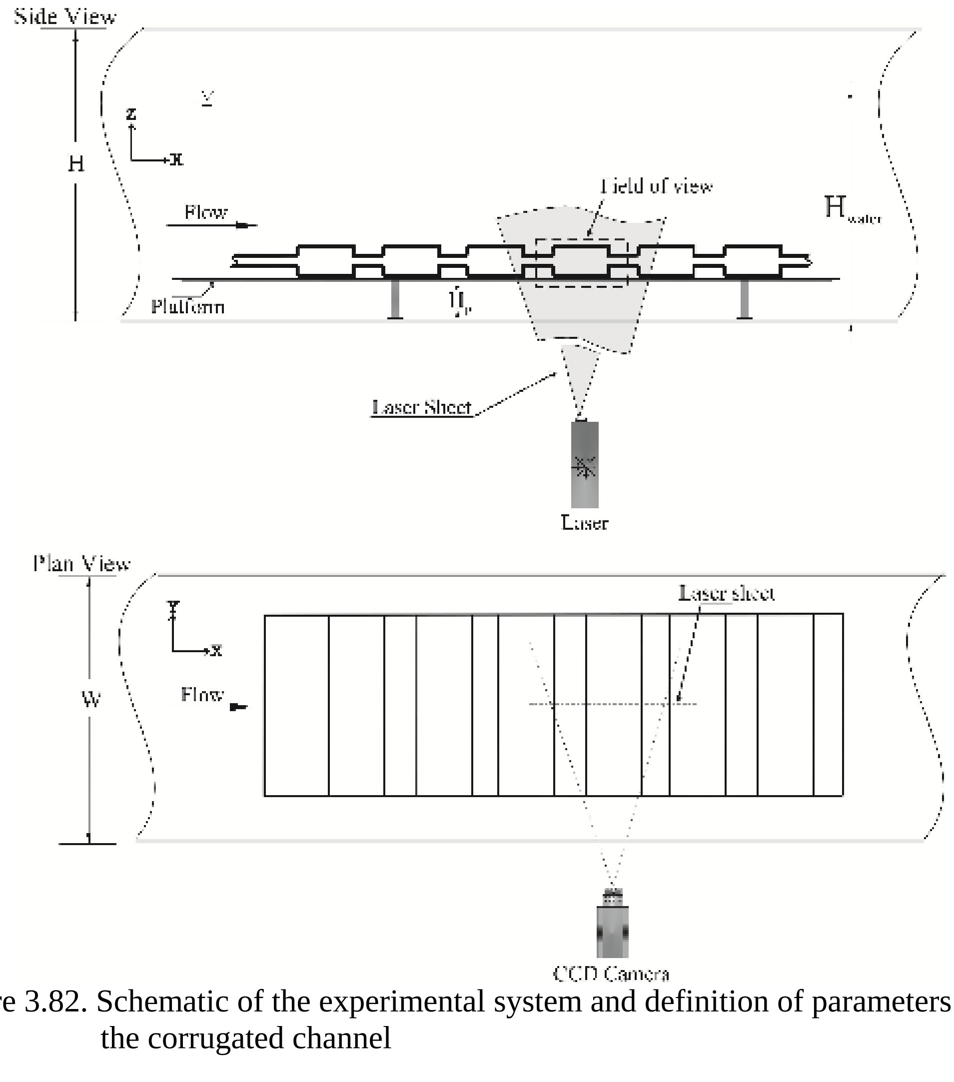

Figure 3.82. Schematic of the experimental system and definition of parameters for the corrugated channel

Comprehensive reviews of PIV techniques were given by Rockwell and Lin (1993), Rockwell et al. (1993), and Adrian (1986, 1991, 2005), Westerweel(1993).

4. RESULTS AND DISCUSSIONS

This section consists of two subsections. The first subsection includes the comparative analysis of experimental and numeric results of the flow field for three different corrugated channels which have varied the phase shift, φ as 0 degree, 90 degree, 180 degree. The second subsection is about the heat transfer enhancement for five different corrugated channels which have varied the aspect ratio ,s/H as 0.1, 0.2, 0.3 and phase shift , φ, as 0 degree, 90 degree, 180 degree

4.1. Experiments Using Particle Image Velocimetry (PIV)

The experiments were conducted using the Particle Image Velocimetry (PIV) technique investigate the flow field in the three different corrugated channels hence to compare the results with numerical prediction studied presently. All channels have the same geometrical parameters as shown in figure 3.6 albeit their phase shift angles, φ is different from each other. A detailed physical knowledge of flow characteristics in the corrugated channels is worthy for objectives of optimization and design. According to available literature, limited research work on the quantitative visualization of flow were done on the turbulent flow characteristics and time dependent development and disappearance of vortices in cavities of corrugated channels by employing the particle image velocimetry (PIV) measuring system. It is obvious that the PIV measuring systems has capability of observing turbulent unsteady flows and provide quantitative numerical data on the spatial characteristics of instantaneous velocity vectors covering defined flow fields. For this reason, the PIV measuring system is used to get instantaneous velocity vectors over a certain flow fields to determine instantaneous and time-mean turbulence statistics in passage of corrugated channels in order to demonstrate local flow structures at a given Reynolds numbers, Re. Information of flow details in the corrugated channels is important in the purpose of optimization and design of corrugated channel as heat exchangers. In order to prove the flow details for designers and other researchers, instantaneous velocity distributions, streamline patterns, $\langle \Upsilon \rangle$, contours of vorticity,

<w>, Reynolds stress correlations, $< u'' >$ and turbulence kinetic energy, <TKE> correlations are presented. Time-averaged flow data are determined by averaging of 1000 PIV images.

4.1.1. Reynolds Number's and Phase Shifts Effects on the Velocity Distribution

In this section, experimental time averaged velocity, <*u*> contours are presented to compare with numerical results for straight channel and channels varying phase shift, φ such as 180 degree,90 degree and 0 degree, respectively.

To determine the time-averaged mean flow structure, 1000 instantaneous velocity fields were measured. Time-averaged parameters which are calculated from PIV images are calculated as follows. Time-averaged streamwise component of velocity;

$$\langle u \rangle = \frac{1}{N}\sum_{n=1}^{N} u_n(x, y)$$

Where N (1000) is the total number of instantaneous images used for the time-averaged values and refers to the instantaneous images.

4.1.1.1. Results of Velocity Contours for Straight Channel

Before starting to measure instantaneous velocity distributions in cavities, it is decided to measure velocities across the plane channel in order to use these data as reference readings to compare with velocity distributions in cavities. The fully developed channel flow can be seen in figure 4.1. In this study, entry length was taken 90 mm for hydrodynamically fully developed flow. In this regard, the entry length is much shorter in turbulent flow, which is in accordance with the expectations, and its dependence on the Reynolds number is weaker. In many channel flows of practical engineering interest, the entrance effects are observed to become insignificant beyond a pipe length of 10 diameters, and the hydrodynamic entry length is approximated as $L_{h,\ turbulent} = 10D_h$ (D_h= 0.0615m). Hydrodynamically fully developed flow region is where the velocity profile is constant along a specified direction in the flow. In the fully developed region of channel flow, local velocity is constant in the axial direction in order that derivatives of velocity are along the central axis zero in the fully developed flow region. The fluid velocity in a channel changes from zero at the surface as a result of the no-slip condition to a maximum at the channel center. At the interface between a fluid and a solid surface, it is required that the fluid velocity and surface velocity is equal. Hence, if the surface is fixed, the fluid is expected to obey the boundary condition that fluid velocity= 0 at the surface.

The left hand side column of figure 4.1 shows the velocity contours of experimental results, for Re=4000, the right hand side column shows the velocity contours of experimental results, for Re=6000. The maximum value of the velocity in the specified region is 0.055 m/s for the Reynolds number of 4000 and similarly the maximum velocity is 0.085 m/s for the Reynolds number of 6000. The incremental value of velocity contour is 0.005 m/s for both Reynolds numbers. At higher Reynolds numbers, Re the inertial forces being proportional to the fluid density and the square of the fluid velocity, are largely relative to the viscous forces, and therefore viscous forces cannot prevent the random and rapid fluctuations of the fluid.

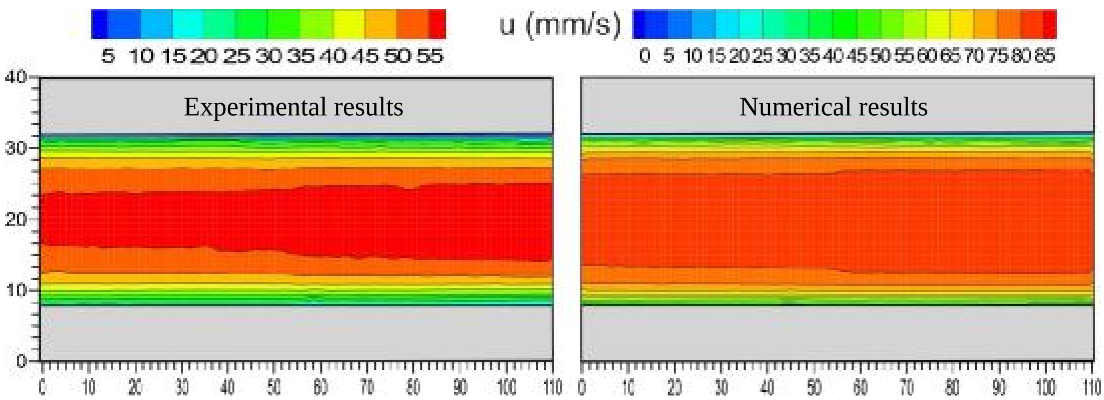

Figure 4.1. Time averaged streamwise velocity, <*u*> contours for straight channel

It is observed that the time averaged streamwise velocity, <*u*> contours in the straight channel denote symmetrical flow structure and fully developed flow for both values of Reynolds numbers, Re. Values of the velocity, <*u*> contours increase with the Reynolds number, Re as expected and quantitative velocity values differ from both Re values despite the fact that velocity profiles make a similar match for both Re values. The flow in a channel is turbulent for Re≥4000, and the swirling eddies transport mass, momentum, and energy to neighbor regions of flow much more rapidly than molecular diffusion, and as a result greatly enhancing mass, momentum, and heat transfer. Consequently, turbulent flow is associated with much higher values of friction, heat transfer, and mass transfer coefficients.

4.1.1.2. Results of Velocity Contours for Corrugated Channels

There were six fields of view for channel with phase shift, φ=180 degree as seen in figure 4.2. Time averaged streamwise velocity, <*u*> contours are shown in figure 4.3 for the case of phase shift, φ with 180 degree in channel and the Reynolds number of 4000. The maximum and incremental values of time averaged streamwise velocity, <*u*> contours are 0.07 m/s and ± 0.01 m/s, respectively.

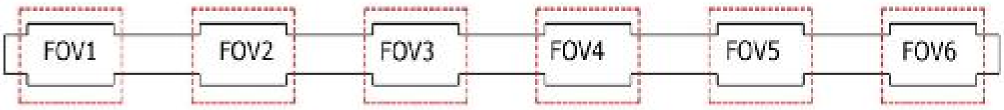

Figure 4.2. Field of view (FOV) for channel with phase shift, φ of 180 degree

In two-dimensional PIV measurements, the value of velocity, <*u*> contours, can be calculated in usual manner from the 1000 instantaneous velocity data for six fields of view (FOV). The left hand side column of figure 4.3 presents measured velocity, <*u*> distributions while the right hand side column shows the velocity, <*u*> contours of numerical results for the Reynolds number of 4000. It is observed that the time averaged streamwise velocity, <*u*> contours of both experimental and numerical results possess symmetrical flow structure in the channel with phase angle, φ of 180 degree and numerical results were confirmed with experimental results for all cavities and especially after the third field of view, the structure of cavities were similar.

Sharp edges of channel with 180 degree phase angle, φ become much clear when compared to straight channel and induces to increase turbulence intensity. Furthermore, time average velocity of channel which has a phase shift, φ of 180 degree is higher than straight channel because of the sharp edges of cavity. Corrugated structure of channel which owns sharp corners leads to manipulate the direction of fluid flow and momentum hereby and tend to augment through the flow direction. Furthermore, increasing momentum causes an increase in turbulence intensity in the corrugated channel which is higher than the case of straight channel.

In this corrugated geometry of channel with 180^{o} phase shift, φ has an abrupt or sudden enlargement of the cross-section as illustrated in figure 4.3. Fluid flow emerging from straight duct with smaller hydraulic diameter is unable to follow the enlargement of the boundary. As a consequence of abrupt deviation in the duct boundary a detachment of flow boundary happens at the corner of sudden enlargement to generate vortices. In general this vortices split into pockets of turbulent eddies just downstream of sharp corners disperse in wake and shear layers. It is worth to mention that this turbulent eddies also causes energy dissipation in the form of heat which is usually stated as pressure losses. For a given Reynolds number, Re velocity profile upstream of sudden expansion or straight duct is sensibly uniform over the cross-section. Downstream of sudden enlargement or entrance of cavities energetic flow mixing between core and wake flow regions caused by frequently shedding vortices. This shedding vortices rotates clockwise or counter clockwise depending on upper or lower side of cavity is taking the central axis as a reference line.

As observed from the cinema of instantaneous velocity vectors distributions, beside shedding vortices, other vortices are also developer in the weak and shear layers either moves further downstream vanishes exterior of the shear layers. After certain distance in the downstream direction attachment of flow boundary occurs, in other words, the separated flow region ends. The point of boundary layer attachment moves forward and backward in random motion downstream of wake region along wall surfaces. Active mixing caused by the vortices guides to even out the velocity profile across the cavity. Beyond entrance of sudden enlargement the velocity on the central axis decreases as the cavity area occupied by through flow which increases in size in order to fill the available cross-section of corrugated channels.

Although high turbulence intensity has a positive advantage for heat transfer enhancement improvement of heat transfer enhancement has to be determined with efficiency index, η due to increasing friction factor, f with increasing turbulence. Briefly, heat transfer enhancement is conceivable for high turbulence intensity; however, it depends not only on turbulence but also on friction losses in channels. This subject will be discussed in the following chapter.

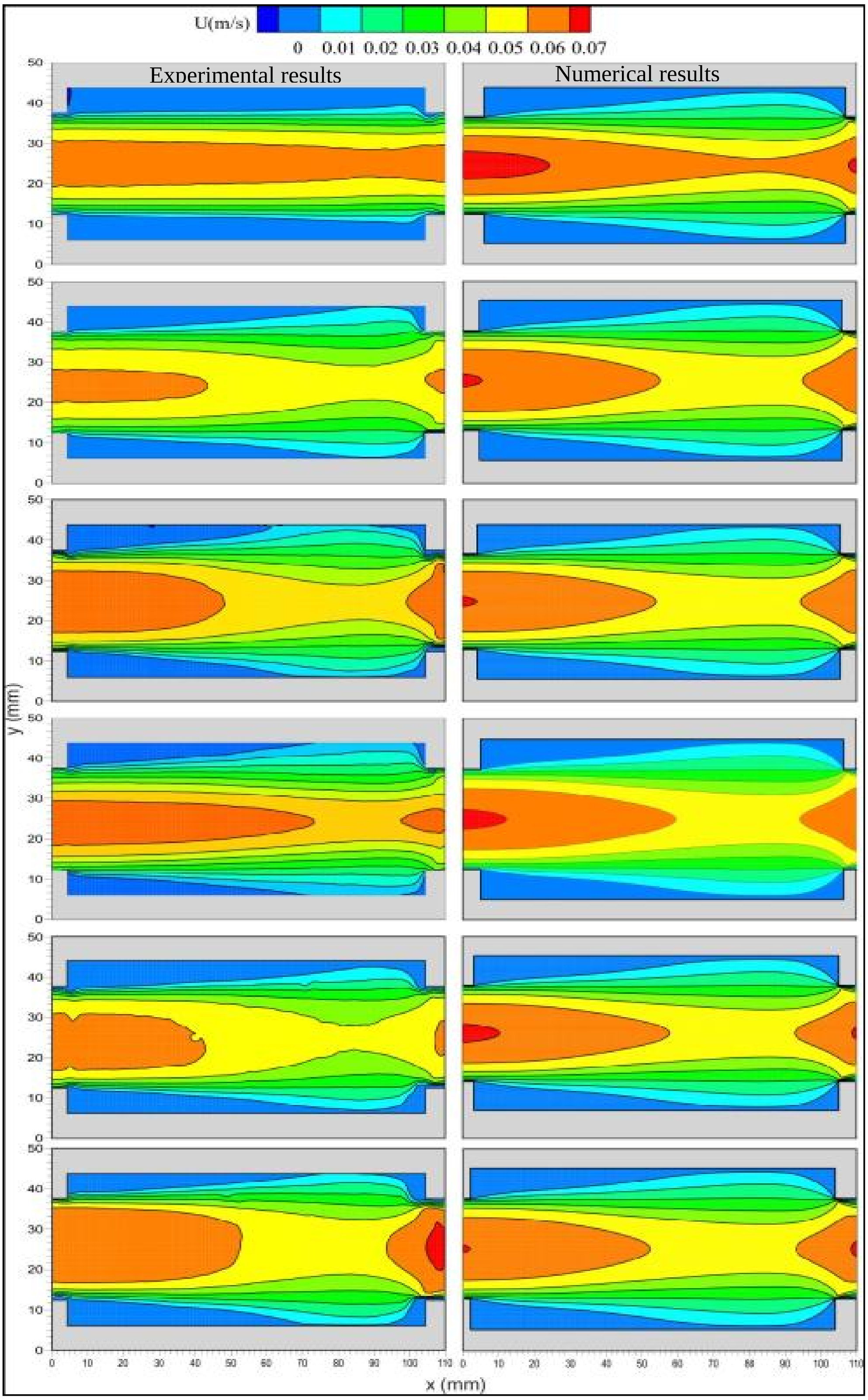

Figure 4.3.Time averaged streamwise velocity, <*u*> contours, for Re=4000, channel with phase angle, φ of 180 degree

Time averaged streamwise velocity, $<u>$ contours are shown in figure 4.4 for the channel with 180 degree phase shift, φ and the Reynolds number, 6000. The maximum and incremental values of time averaged streamwise velocity, $<u>$ contours are 0.1 m/s and 0.01 m/s, respectively. The velocity, $<u>$ contours of experimental results are presented in the left hand side column of figure 4.4 on the other hand the right hand side column shows the velocity, $<u>$ contours of numerical results for the Reynolds number, 6000. Flow structure of time averaged streamwise velocity $<u>$, contours in the channel with 180 degree phase shift, φ were observed to have symmetrical pattern even with the Reynolds number, Re=4000. Increasing the Reynolds number, Re time average velocity, $<u>$ contour values were increased. It can be seen that numerical results comply with experimental results. Periodical flow field is developed after the third cavity (i.e. FOV3).

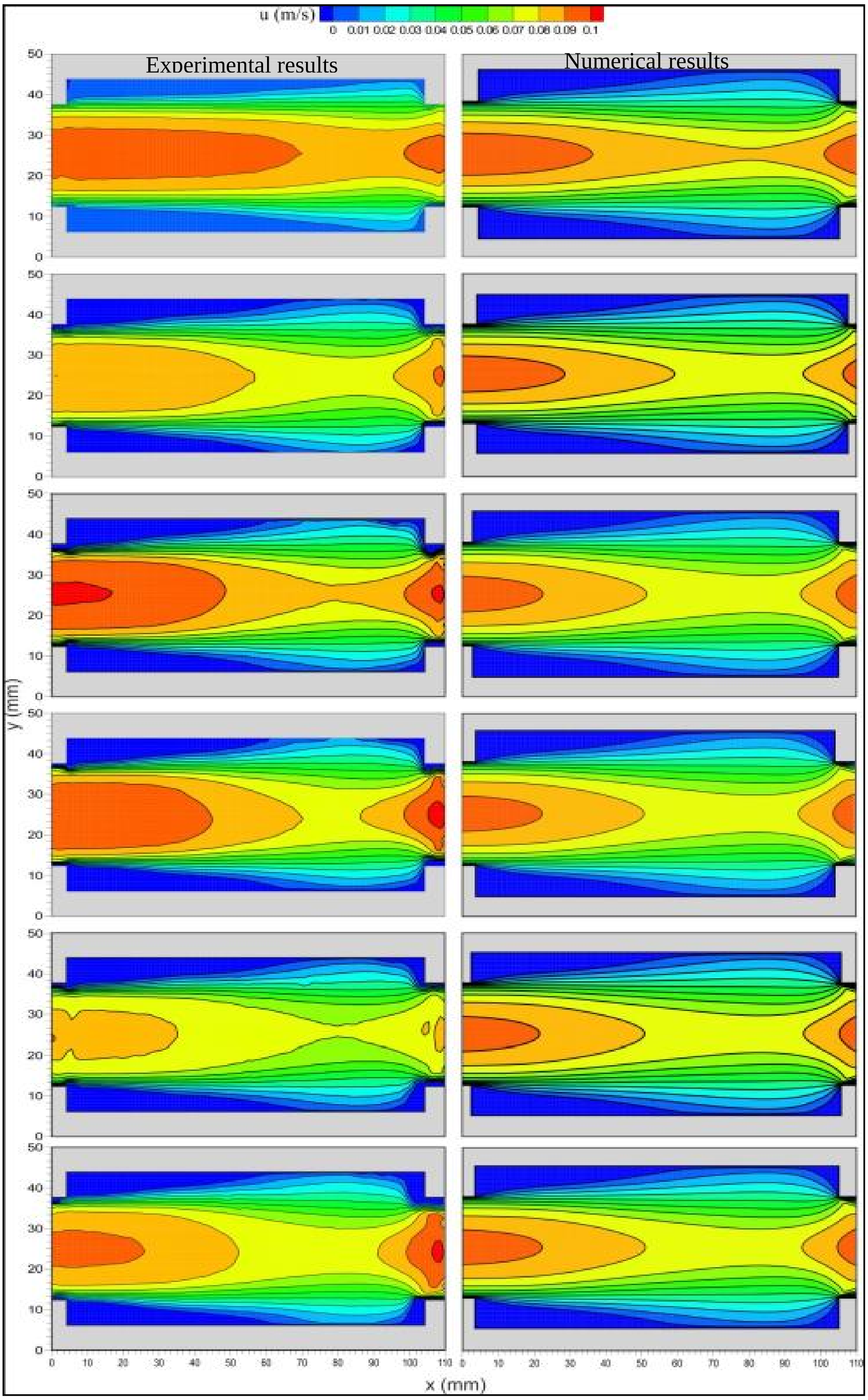

Figure 4.4. Time averaged streamwise velocity, <*u*> contours for Re=6000, channel with phase angle, φ of 180 degree

The time averaged streamwise experiments normalized velocity profiles for Reynolds numbers, 2000 and 6000, with 180 degree phase shift, φ for six field of views (i.e., FOV1,2,3,4,5,6 respectively) are presented in figure 4.5. Here, velocity components are normalized with the free-stream velocity, U_{∞} of straight channel. Figure 4.5 shows the velocity profiles, $<u>/U_{\infty}$ at five different x/L locations (x/L=5, 25, 45, 65, and 85) downstream of the model for six field of views. For the Reynolds number, Re=2000, negative velocity values occurred at the entrance region of the cavity; however, these negative velocity values decreased and diminished at the exit section of the FOV6 at x/L=45. Negative velocities at the upper and lower regions of cavity indicate secondary flow structures for the Reynolds number, Re=2000.

Moreover, the Reynolds number, Re=6000, negative velocity, $<u>$ contours were taken place at the entrance region of all field of views of cavities as it happens for the case of Reynolds numbers, Re. But the magnitude of negative velocities decreased gradually and diminished completely at the exit section of the all of field of views at x/L=25. In other words, the magnitude of negative velocities are much higher at Re=2000 than the Reynolds number, Re=6000. Reducing region of secondary flow structure amalgamate fresh fluid flow by increasing the Reynolds number. At the Reynolds number, Re=2000, velocity profile is parabolic in the cross section of cavity (like as laminar flow), but this parabolic velocity profile becomes more uniform since the flow is fully turbulent in cavities at the Reynolds number, Re=6000.

Figure 4.6 represents the experimental and numerical velocity profiles at the Reynolds number, Re=6000. Experimental and numerical results are agreed well with each other as presented in Figure 4.6 and hence it is conformed that numerical heat transfer results are reliable for various parameters. The percentages of this agreement in velocity profiles across-central plane of cavities are 2 % between numerical and experimental results.

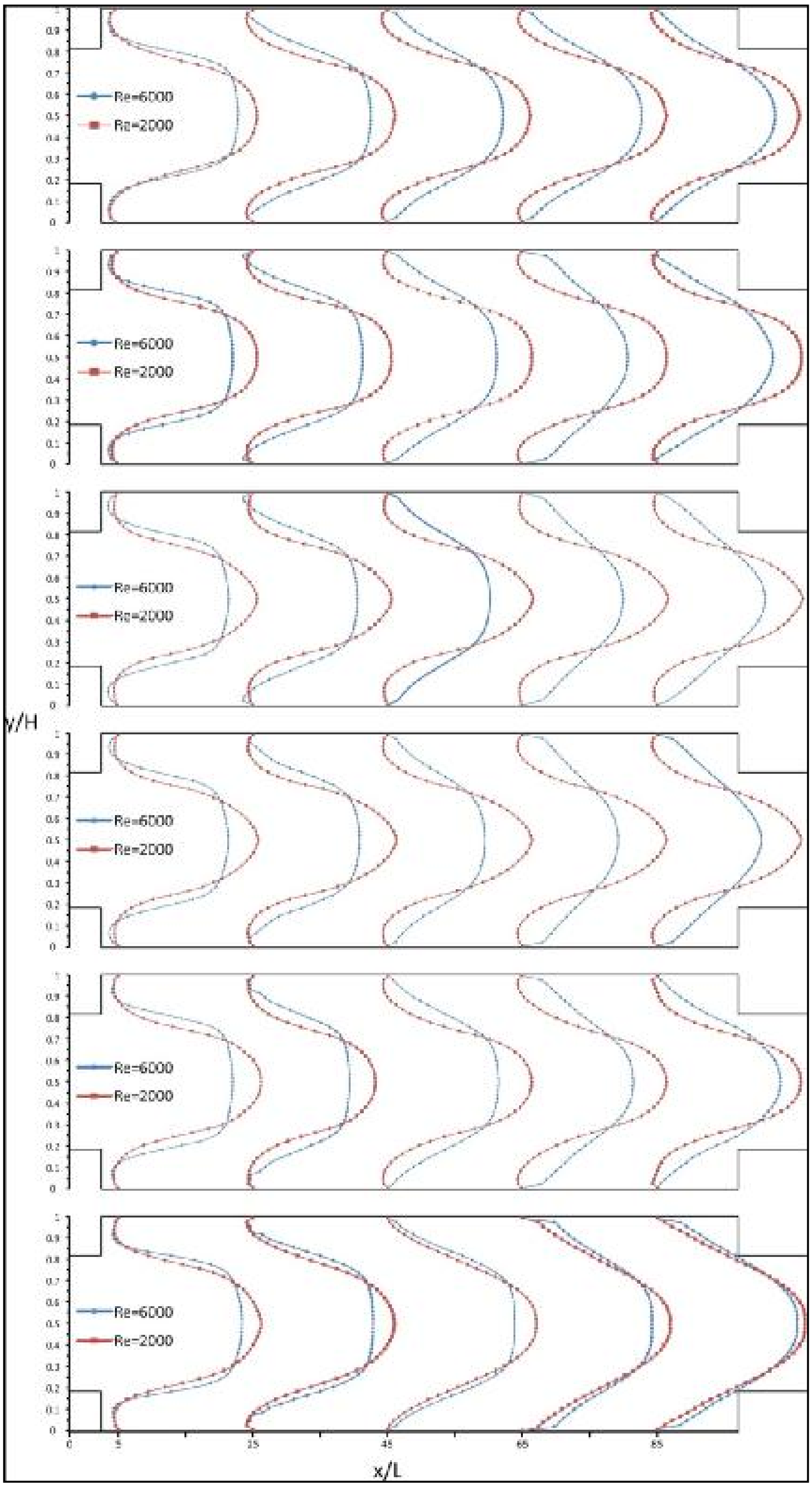

Figure 4.5. Experimental variation of time-averaged streamwise velocity, <*u*> at cross-section of cavities for Re=2000 and Re=6000, channel with phase angle, φ of 180 degree

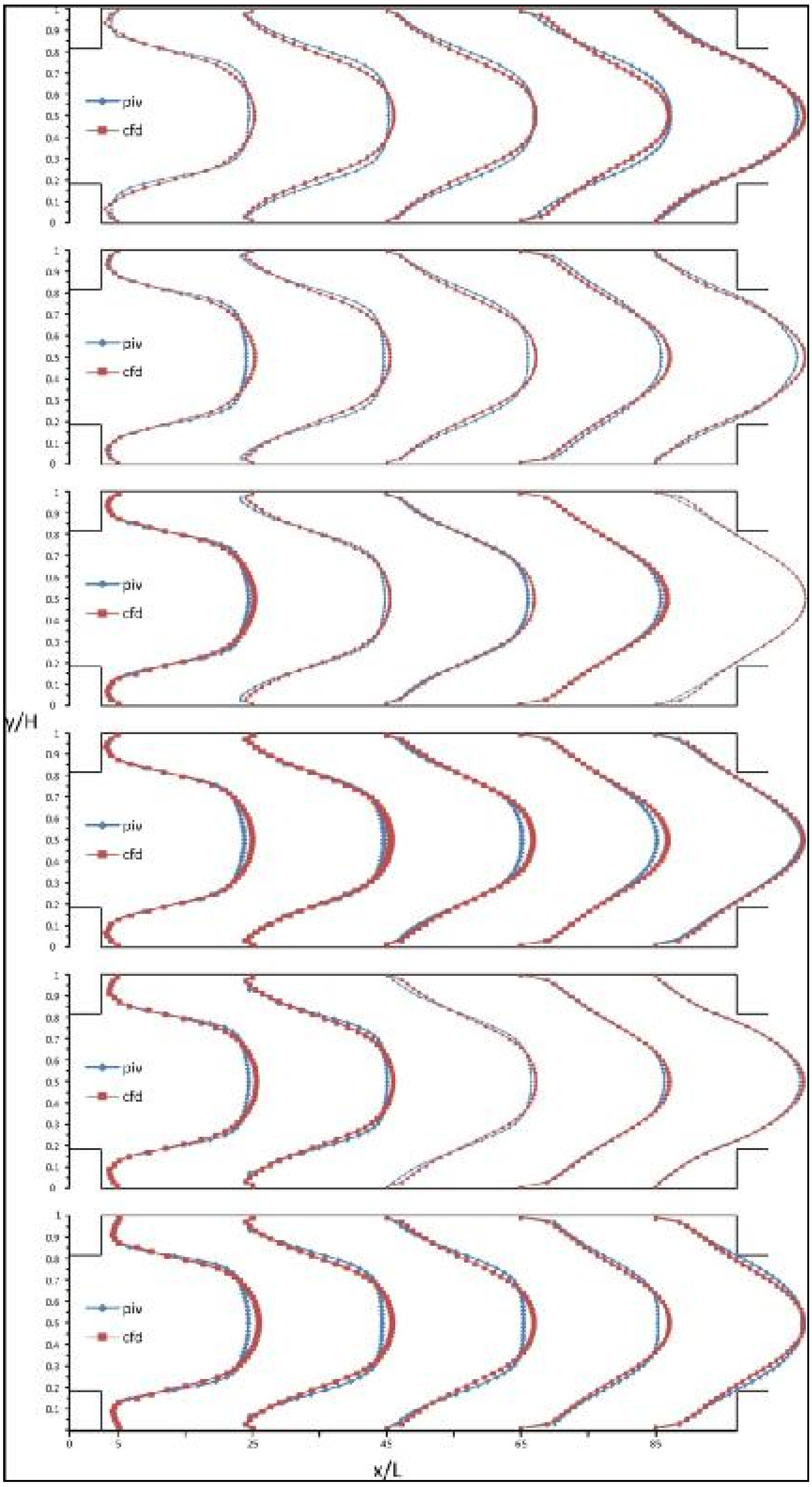

Figure 4 6. Comparisons of time-averaged streamwise velocities, <u> at cross-section of cavities, for Re=6000, channel with phase angle, φ of 180 degree

Figure 4.7 presents the eleven field of views for channel with the phase angle, φ of 90 degreeand red color circles (FOV1, FOV3, FOV5, FOV7, FOV9, FOV11) have the same geometrical parameters and blue color (FOV2, FOV4, FOV6, FOV8, FOV10) have the same geometrical parameters as in the red circles. Time averaged streamwise velocity, <*u*> contours are shown in Figures 4.8 and 4.9 for channel with phase angle, φ of 90 degree and Reynolds numbers is equal to 4000 and 6000, respectively. The maximum and incremental values of time averaged streamwise velocity, <*u*> contours for the Reynolds number, 4000 are 0.09 m/s and 0.01 m/s, respectively. The maximum and incremental values of time averaged streamwise velocity, <*u*> contours for the Reynolds number, 6000 are 0.12 m/s and 0.01 m/s respectively. The time evolution of a wake flow region in cavities of corrugated channels and flow hydrodynamics influencing thermal performances of heat exchangers with corrugated shape were not visualized quantitatively using the PIV technique in previous works. The results obtained in the present work provide more details of flow structures in cavities comparing to the single point velocity measuring devices. From this point of view present experimental work using the PIV technique provides original information about flow of corrugated channels.

Figure 4.7. Field of view (FOV) for channel with phase angle, φ of 90 degree

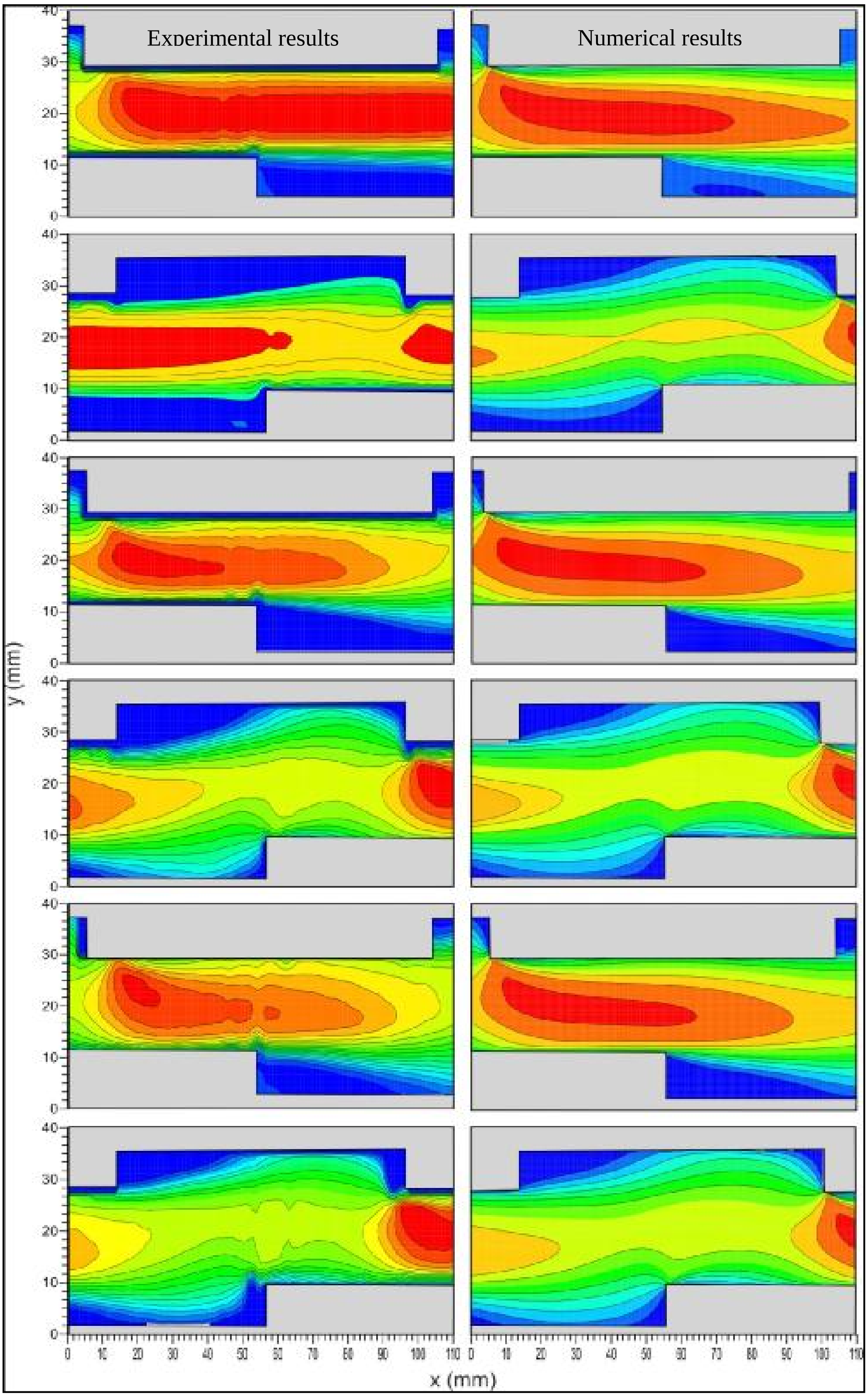

Figure 4.8. Time averaged streamwise velocity, <u> contours for Re=4000, for channel with phase angle, φ of 90 degree

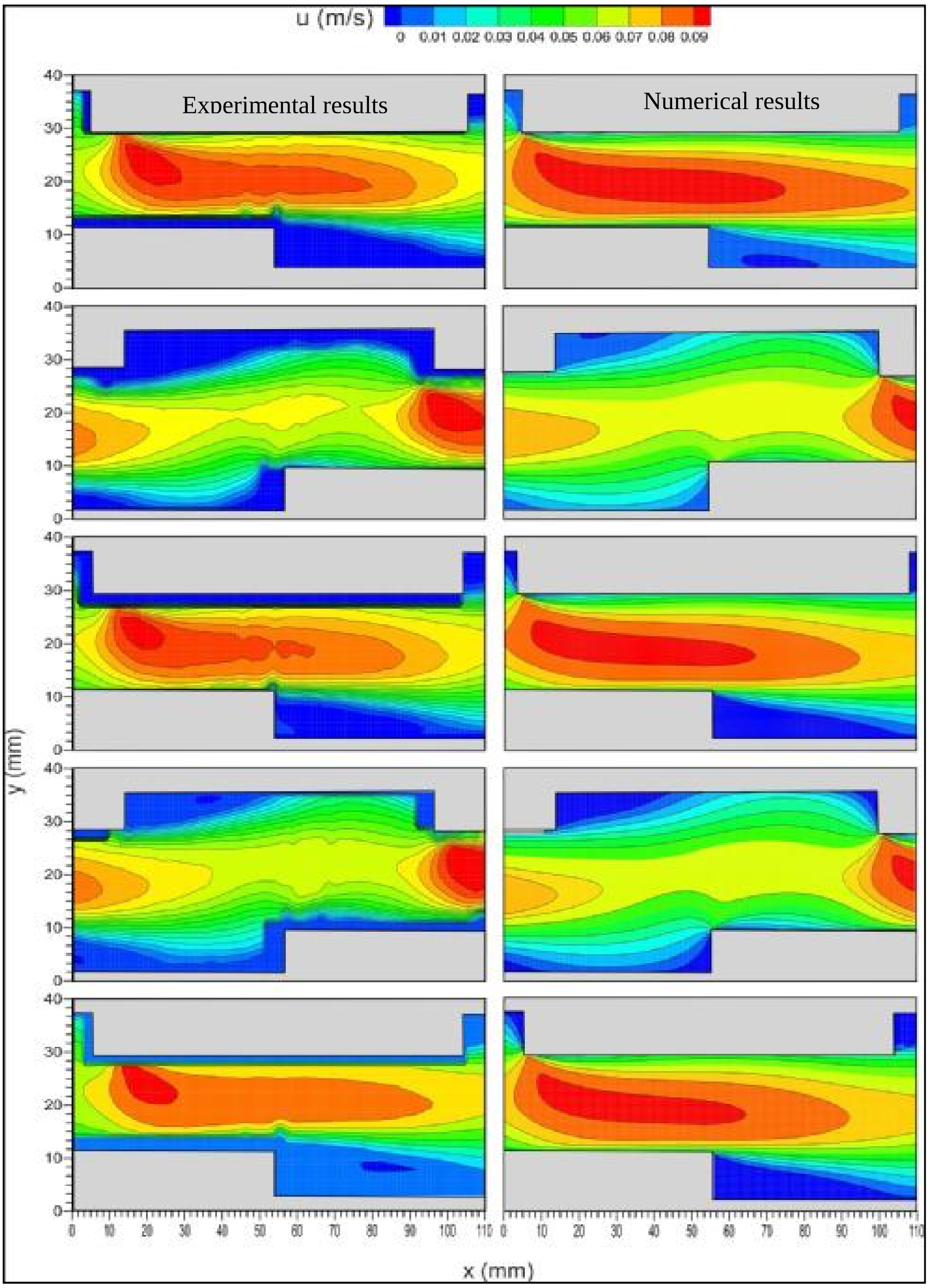

Figure 4.8. Time averaged streamwise velocity, <*u*> contours for Re=4000, for channel with phase angle, φ of 90 degree (continued)

The first column of figures 4.8 and 4.9 presents the streamwise velocity, <*u*> contours of experimental results while the second column presents the streamwise velocity, <*u*> contours of numerical results for Reynolds numbers, 4000 and 6000, respectively. Here, eleven side views of images are presented consecutively between first row and last row of images. It is experimentally observed that asymmetrical time averaged streamwise velocity, <*u*> distributions takes place throughout the corrugated channel with phase angle, φ of 90 degree. As seen in figures 4.8 and 4.9 numerically predicted time averaged velocity distributions agrees well with experimental result. Negative and positive velocity, <*u*> contours are reported in cavities for both Reynolds numbers, Re=4000 and Re=6000. Velocity, <*u*> contours in large cross-sections occurred in a positive manner while negative velocity, <*u*> contours existed in corrugated shapes of cavities due to lack of fresh fluid moving towards the wake region due to narrow cross-sections of the cavity. Flow structures of both Reynolds numbers are similar although turbulence intensity increases as the Reynolds number is increased as expected. Heat transfer enhancement is expected for the reason that increasing turbulence intensity. But, higher turbulence causes more pressure drops which results in extra pumping power.

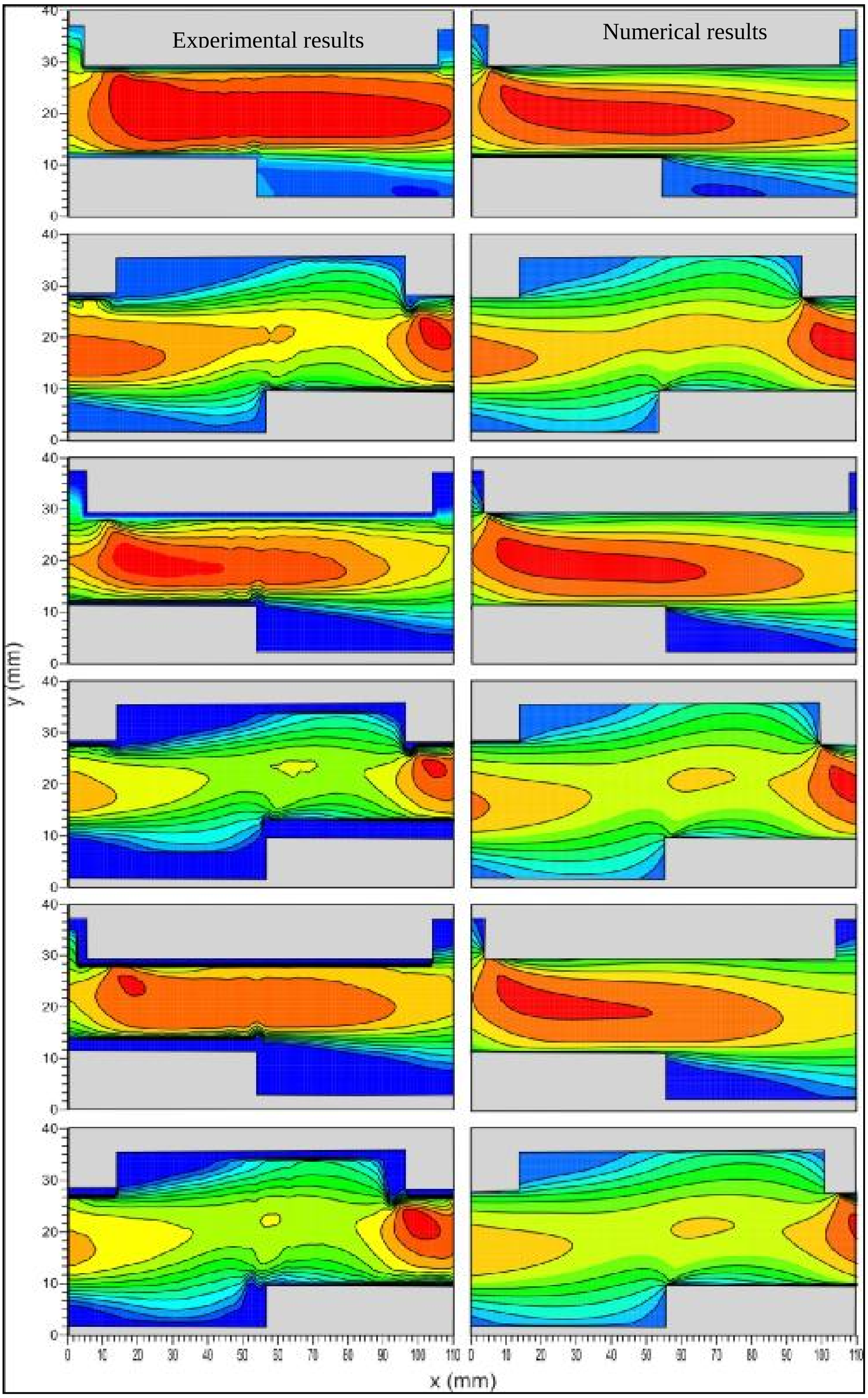

Figure 4.9. Time averaged streamwise velocity, <*u*> contours, for Re=6000, for channel with phase angle, φ of 90 degree

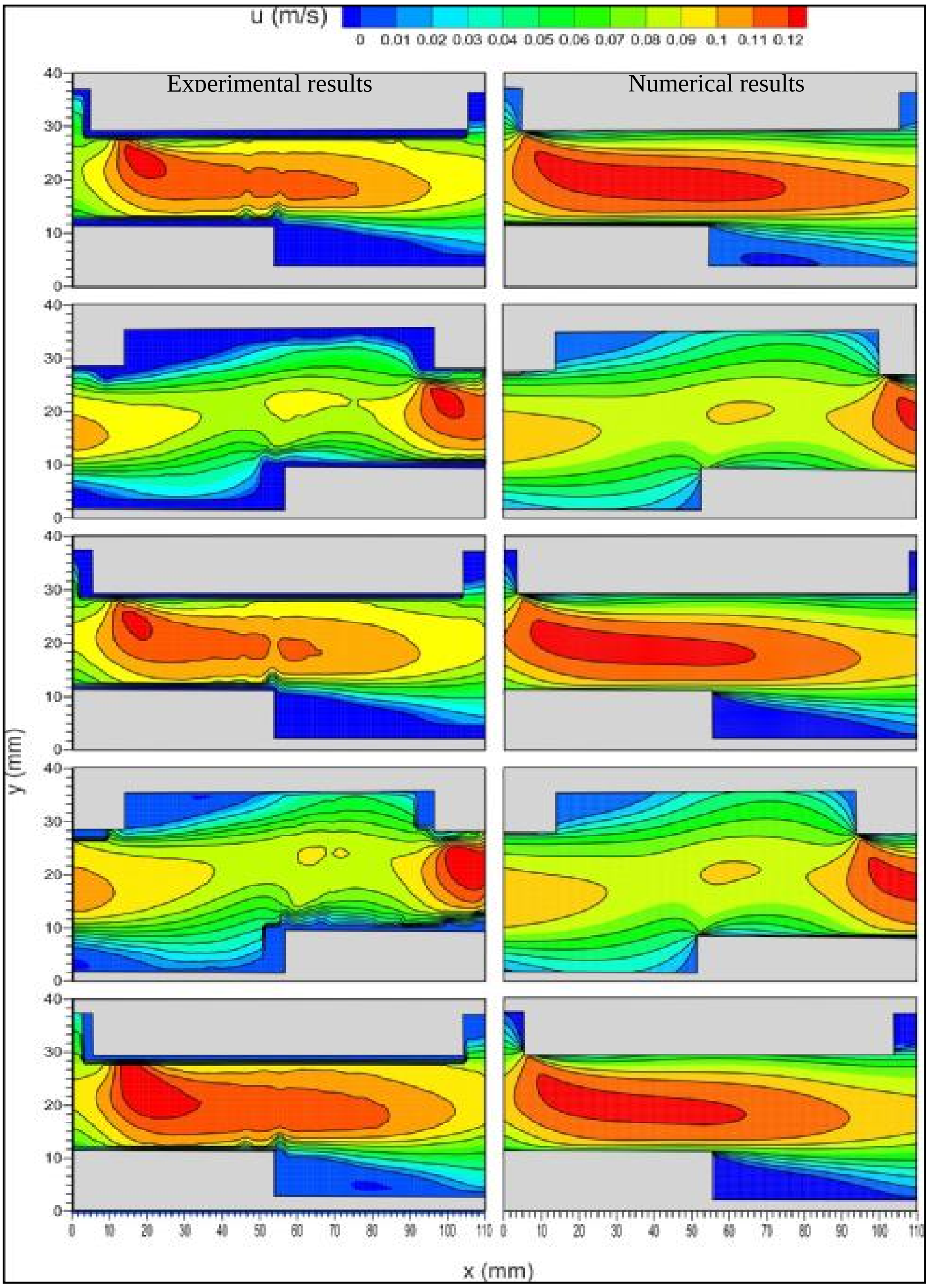

Figure 4.9. Time averaged streamwise velocity, <*u*> contours, for Re=6000, for channel with phase angle, φ of 90 degree (continued)

Patterns of time averaged streamwise velocity, <*u*> through the channel with 90 degree phase shift, φ are more severe when compared the case of channel with 180 degree phase shift, φ since shifting phase angle leads to an increase in the magnitude of secondary flow by virtue of sharp edges. Furthermore, vigorous flow structure is acquired at channel with 90 degree phase shift, φ and it will contribute to the enhancement of heat transfer in response to vigorous flow.

Red (FOV1, FOV3, FOV5, FOV7, FOV9, FOV11) and blue (FOV2, FOV4, FOV6, FOV8, FOV10) circles in figure 4.10 represent the eleven field of view. Red and blue circles have the same geometrical parameters in it. Time averaged streamwise velocity, <*u*> contours are shown in Figure 4.11 for channel with 0 degree phase shift, φ and the Reynolds number, 4000. The maximum and incremental values of time averaged streamwise velocity, <*u*> contours are 0.1 m/s and 0.01 m/s, respectively.

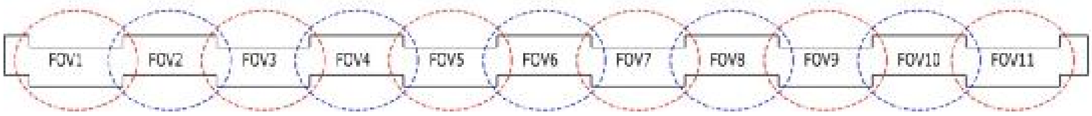

Figure 4.90. Field of view (FOV) for channel with phase angle, φ of 0 degree

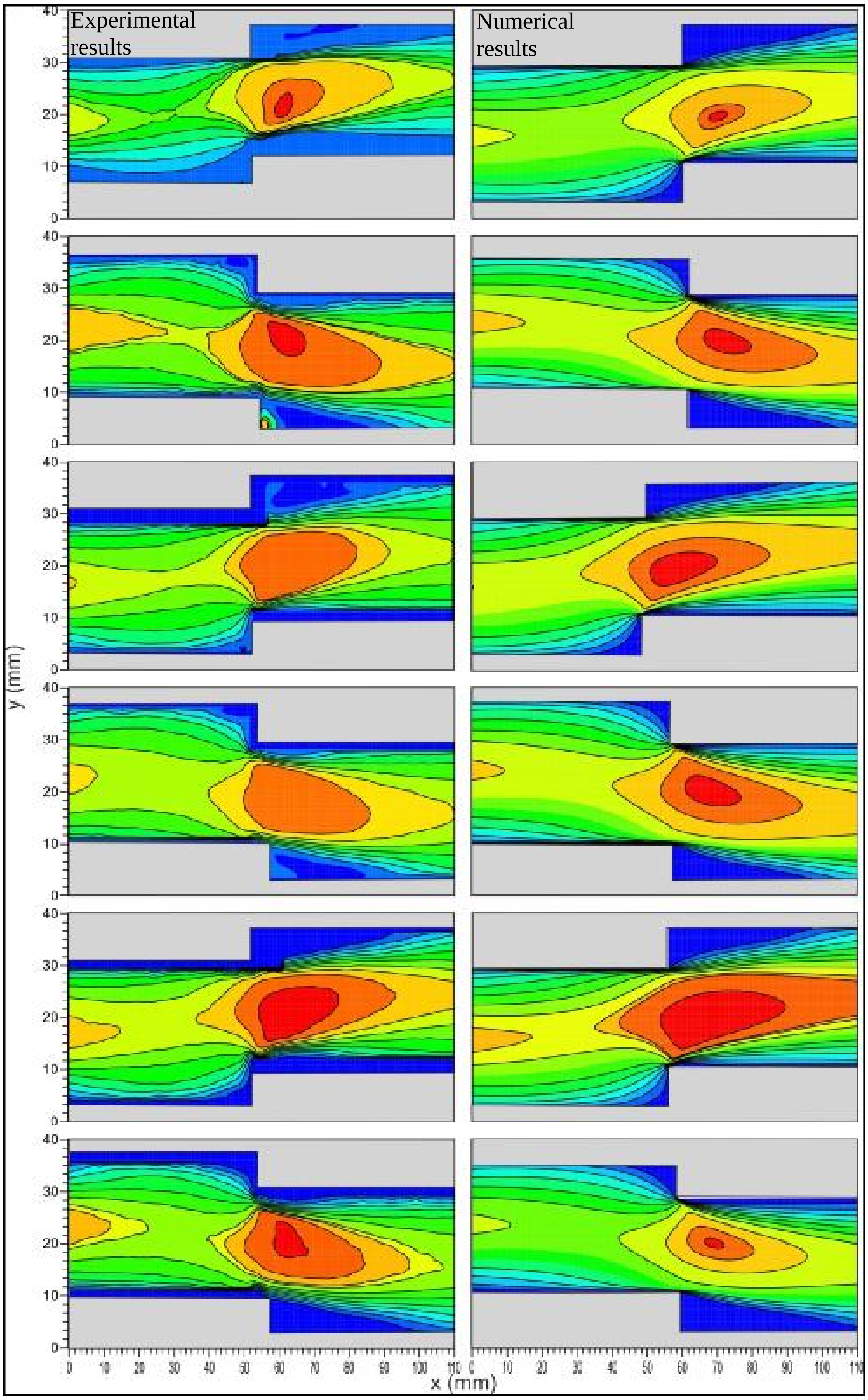

Figure 4.10. Time averaged streamwise velocity, <u> contours for Re=4000 channel with phase angle, φ of 0 degree

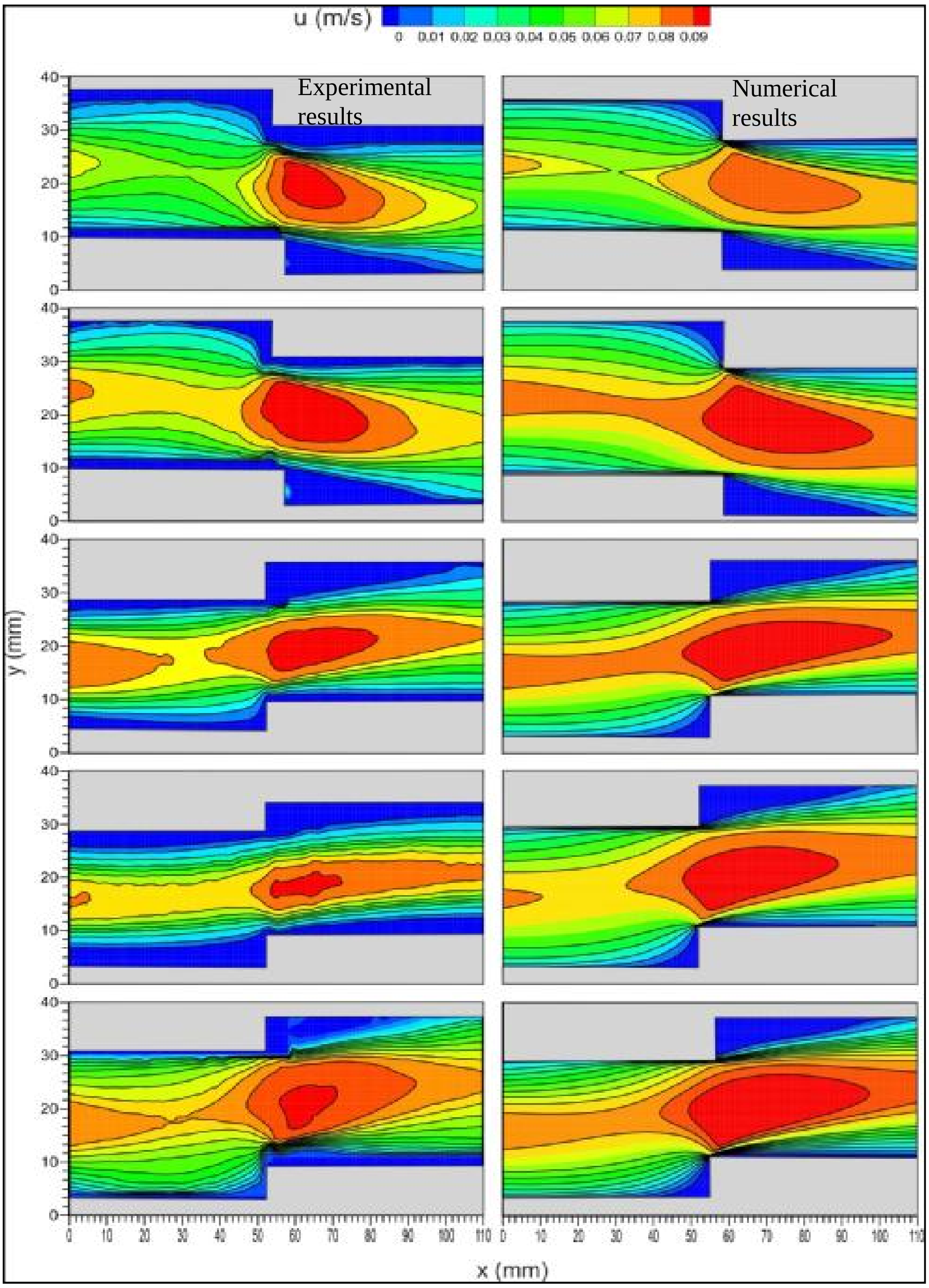

Figure 4.11. Time averaged streamwise velocity, <u> contours for Re=4000 channel with phase angle, φ of 0 degree (continued)

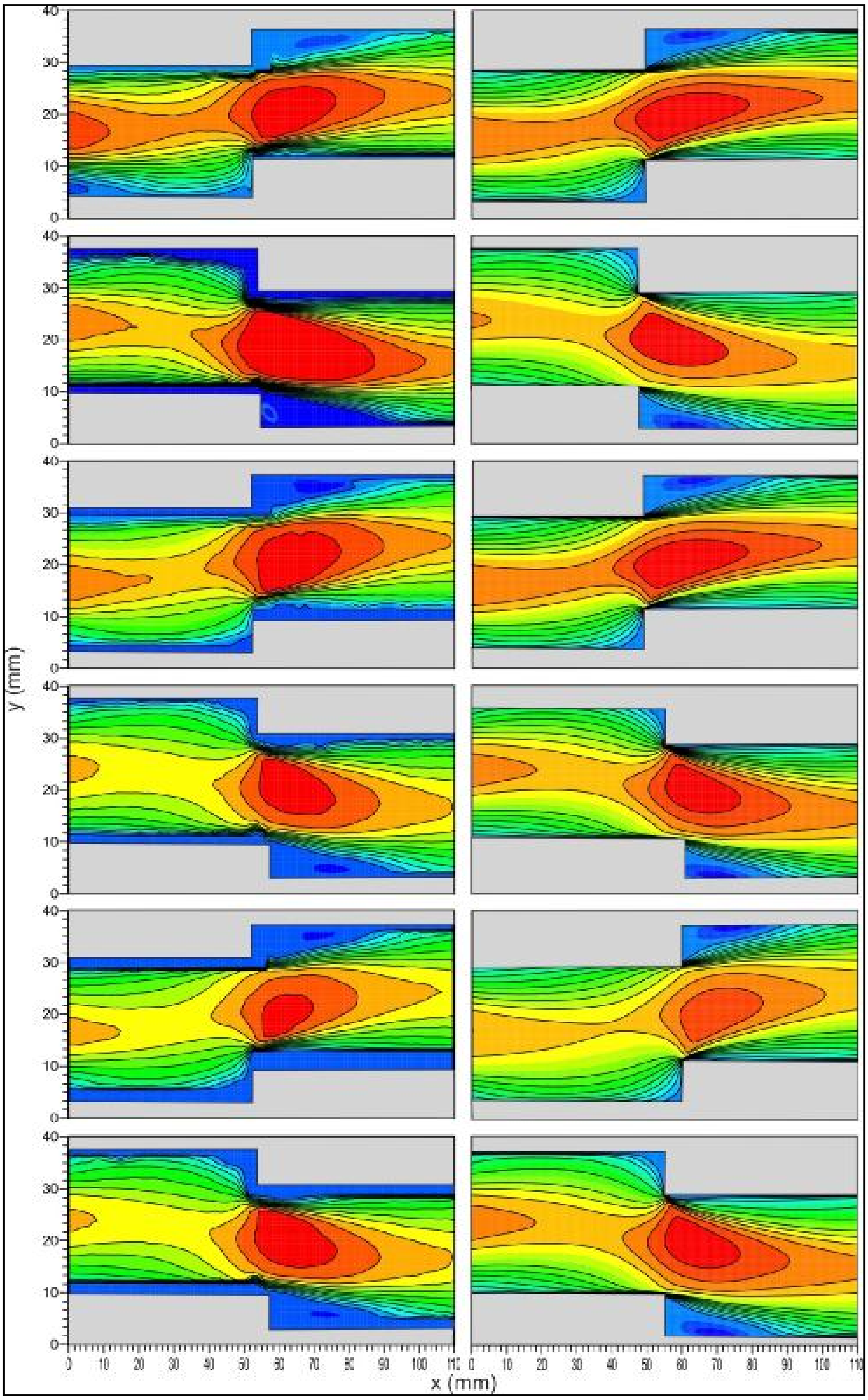

Figure 4.12. Time averaged streamwise velocity, <u> contours for Re=6000, channel with phase angle, φ of 0 degree

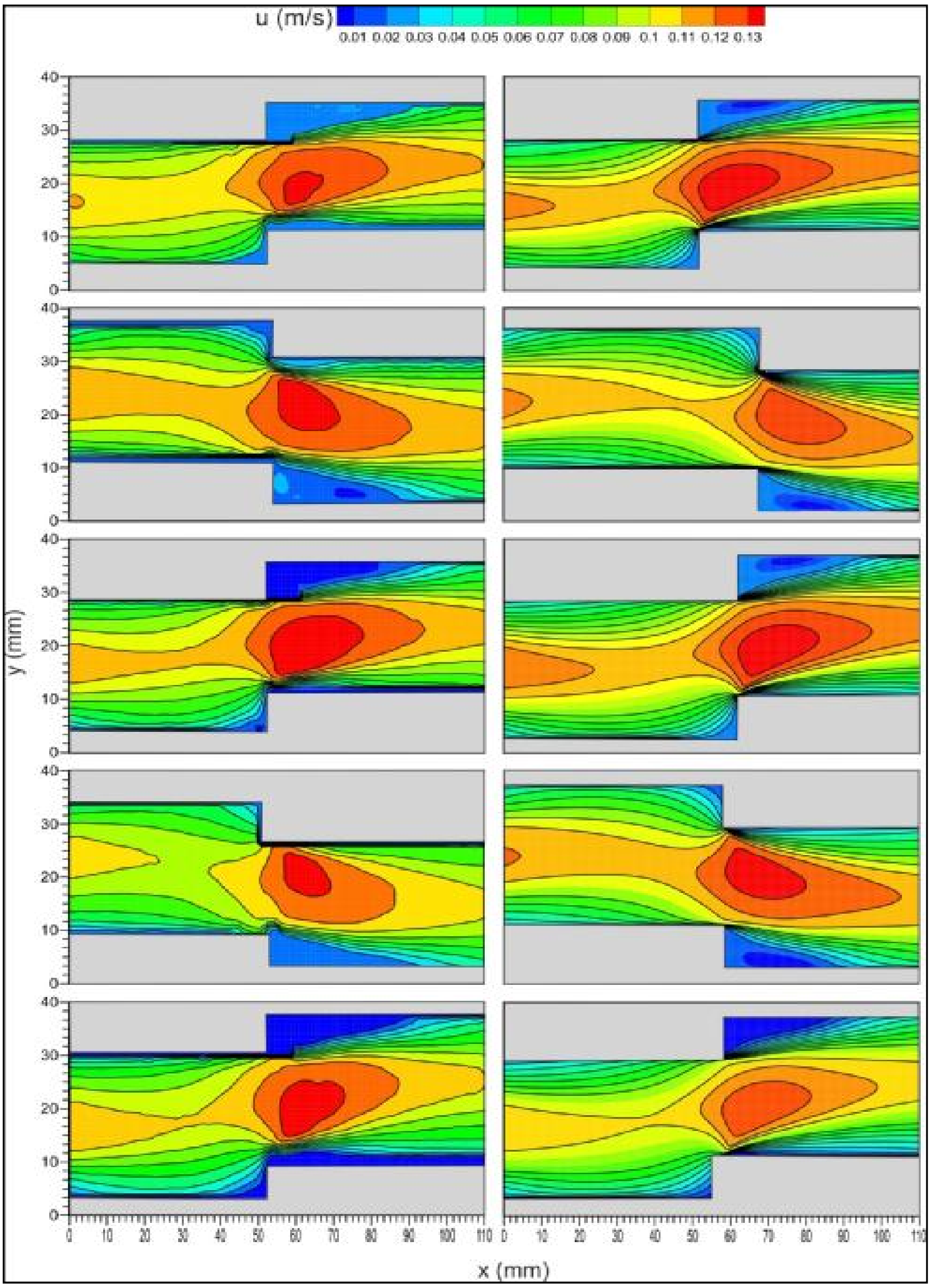

Figure 4.13. Time averaged streamwise velocity, <*u*> contours for Re=6000**,** channel with phase angle, φ of 0 degree (continued)

Figure 4.12 represents time averaged streamwise velocity, <*u*> contours channel with phase angle, φ of 0 degree and the Reynolds number, 6000. The maximum and incremental values of time averaged streamwise velocity, <*u*> contours are 0.13 m/s and 0.01 m/s respectively. First column of figure 4.12 indicates the velocity, <*u*> contours of experimental results while the second column indicates the velocity, <*u*> contours of numerical results for the Reynolds number, 6000. Animations of instantaneous velocity vectors covering whole longitudinal cross-section corrugated channels demonstrated that the vortical flow structures in wake and shear flow regions can be classified as: (i) The steady vortex system, (ii) The periodically oscillatory vortex system, and (iii) The turbulent-like chaotic vortex system for Reynolds numbers, based on the average velocity, varied from 4000 to 6 000.

Maximum velocity value occurred in the channel which was 0 degree phase shift in comparison to 90^o and 180^o channels. Furthermore, the maximum heat transfer enhancement takes place in channel with 0 degree phase angle, φ. It was shown that changing the phase shift of the channel had enormous effect on the flow structure as a result of the experiments.

In conclusion, we infer from experiments that the Reynolds number of flow and phase shift of the channel have a significant effect on the flow structure. Velocity in the corrugated channel was increased due to the increased Reynolds number and effect of the sharp corner of the cavity as a result, heat transfer ratio is expected to enhance when compared to the straight channel. Argument of heat transfer enhancement, hereby, will be discussed to prove that improvement in the next chapter.

4.1.2. Effect of Reynolds Numbers and Phase Shifts on Flow Structures Presented by Streamlines

In this section, streamlines based on experimental results are presented to compare with numerical results for straight channel and channels which have varied the phase shift such as 180 degree, 90 degree and 0 degree, respectively. Streamlines are presented for Reynolds numbers, 4000 and 6000.

Streamlines can be described as a curve that is everywhere tangent to a velocity vector in a fluid velocity field at a fixed instant in time. Therefore, the streamlines reveal the direction of the fluid motions at each point. In a steady flow, streamlines are constant in time and fluid particles move along streamlines. However, in a non steady flow, the streamlines change with time and fluid particles do not move along streamlines.

4.1.2.1. Results of Velocity Fields for Straight Channel

Figure 4.13 presents only experimental results of time-averaged streamline, patterns<Y> for straight channel. The first and second column of figures 4.13 show the patterns of streamlines and distributions of velocity vector, for Reynolds numbers of Re=4000 and Re=6000, respectively.

It is clearly seen from these figures that the results are symmetrical with respect to the centerline of the straight channel.

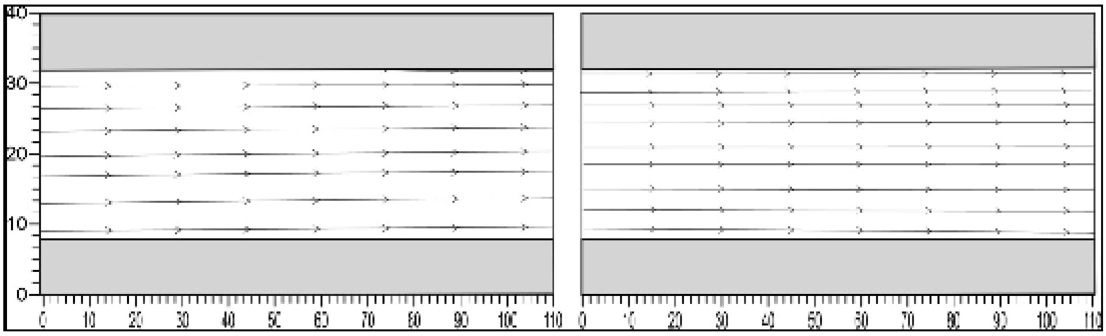

Figure 4.14. The time-averaged streamline topologies, <Y> for straight channel

4.1.2.2. Results of Velocity Fields for Corrugated Channels

The time-averaged patterns of streamlines, <Y> contours can be seen in figures 4.14 and 4.15 for six field of view in corrugated channel with phase shift angle of 180 degree. The first and second column of figures show the velocity field of experimental and numerical results for Reynolds numbers of Re= 4000 and Re=6000, respectively. Field of views is presented consecutively starting from the first row until the last row. It can be seen that from the figures 4.14 and 4.15, for both Reynolds numbers, the patterns of streamlines are symmetric with the centerline through the corrugated channels. It is better to state that the upper and lower walls have similar geometry of corrugation. Nevertheless symmetric recirculation flow regions have been observed from the streamline, $\langle Y \rangle$ contours which appear near the upper and lower corrugated walls. Patterns of streamlines indicate that well defined recirculation flow bubble rotate counter clockwise at the upper cavity and other recirculation flow bubble rotate clockwise at the lower cavity. The size of recirculation flow region gets smaller while the Reynolds numbers, Re increases. This flow behavior conforms that fresh fluid moves close to the cavity walls with higher amount which results in enhancement of heat transfer. In addition the higher velocity gradient increases the kinetic energy of the fluid near the upper and lower walls of cavities. The fluid is able to flow into a large portion of diverging part of the channel with having smaller separation region. It is clearly seen from figures that two well-defined foci are developed and they are almost symmetrical with respect to the centerline of the channel. The center a point of recirculation regions occur close to the lower and upper wall of the cavity at a location approximately 35-40 mm and 30-35mm far from the entry of cavity at Re=4000 and Re=6000, respectively for all field of views except for first field of view at Re=4000.

Figures 4.14 and 4.15 present experimental and numerical results. Although the image of first cavity which present experimental results have a disagreement with numerical results, the rate of discrepancy decreases rapidly while fluid moves further downstream, for example, the size of separated flow regions defined experimentally are similar with the numerical results in third and following cavities for the case of phase shift, φ with 180 degree in channel at the Reynolds number, Re=4000. Several reasons may be suggested for aforementioned differences. But, it is quite difficult to specify reasons of discrepancy between experimental and numerical results studies at inlet of cavity. In additions the size of separated flow regions in both columns gets smaller while fluid moves further downstream through cavities presented experimentally and numerically. It can be conducted that the flow structure starting from third cavity does not change dramatically in corrugated channels. This confirms that geometric parameters used in this study (i.e. six corrugated cavity) are sufficient to have developed the flow in a corrugated channel.

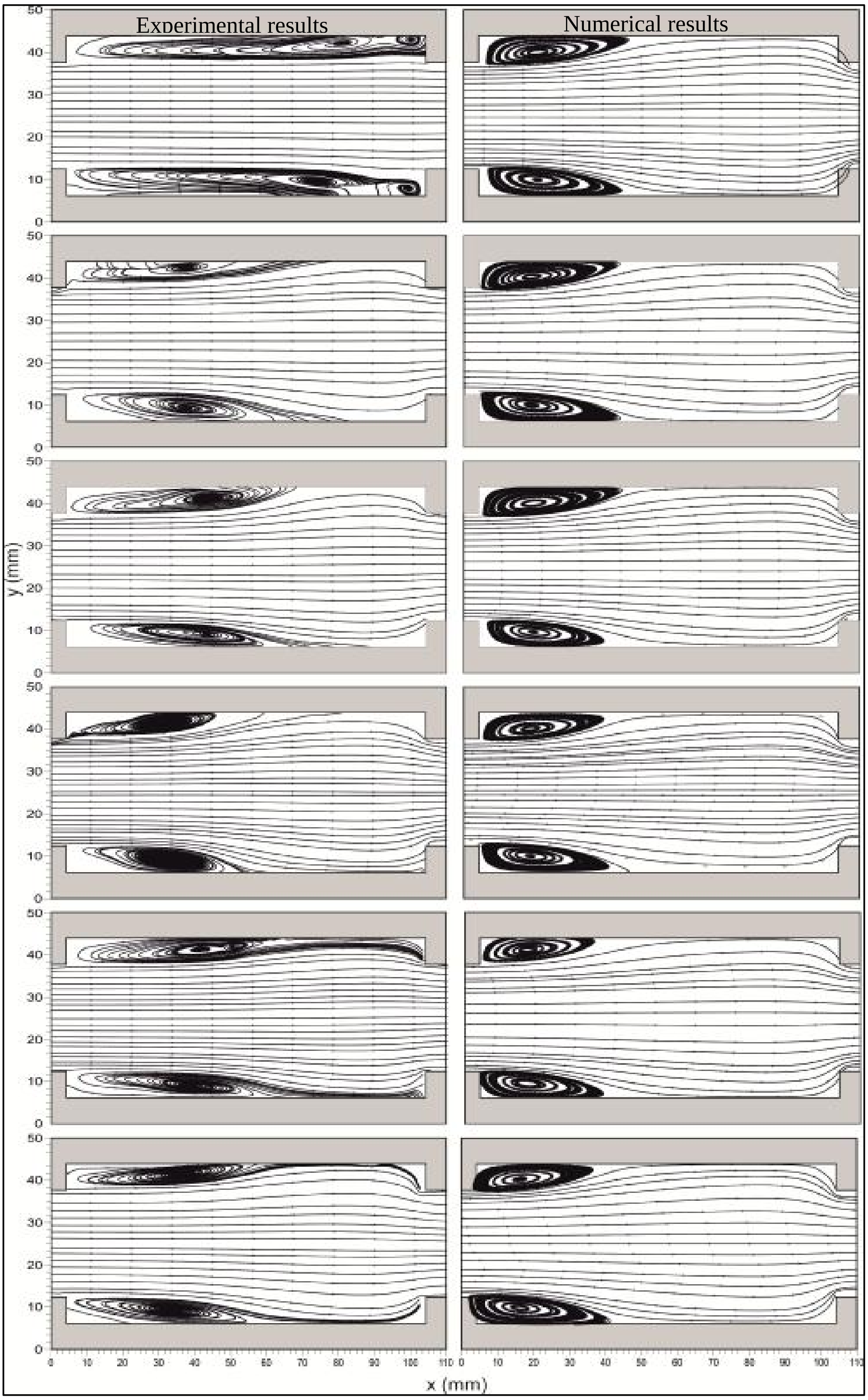

Figure 4.15. The time-averaged streamline topologies, $\langle \Psi \rangle$ for Re=4000**,** channel with phase angle, φ of 180 degree

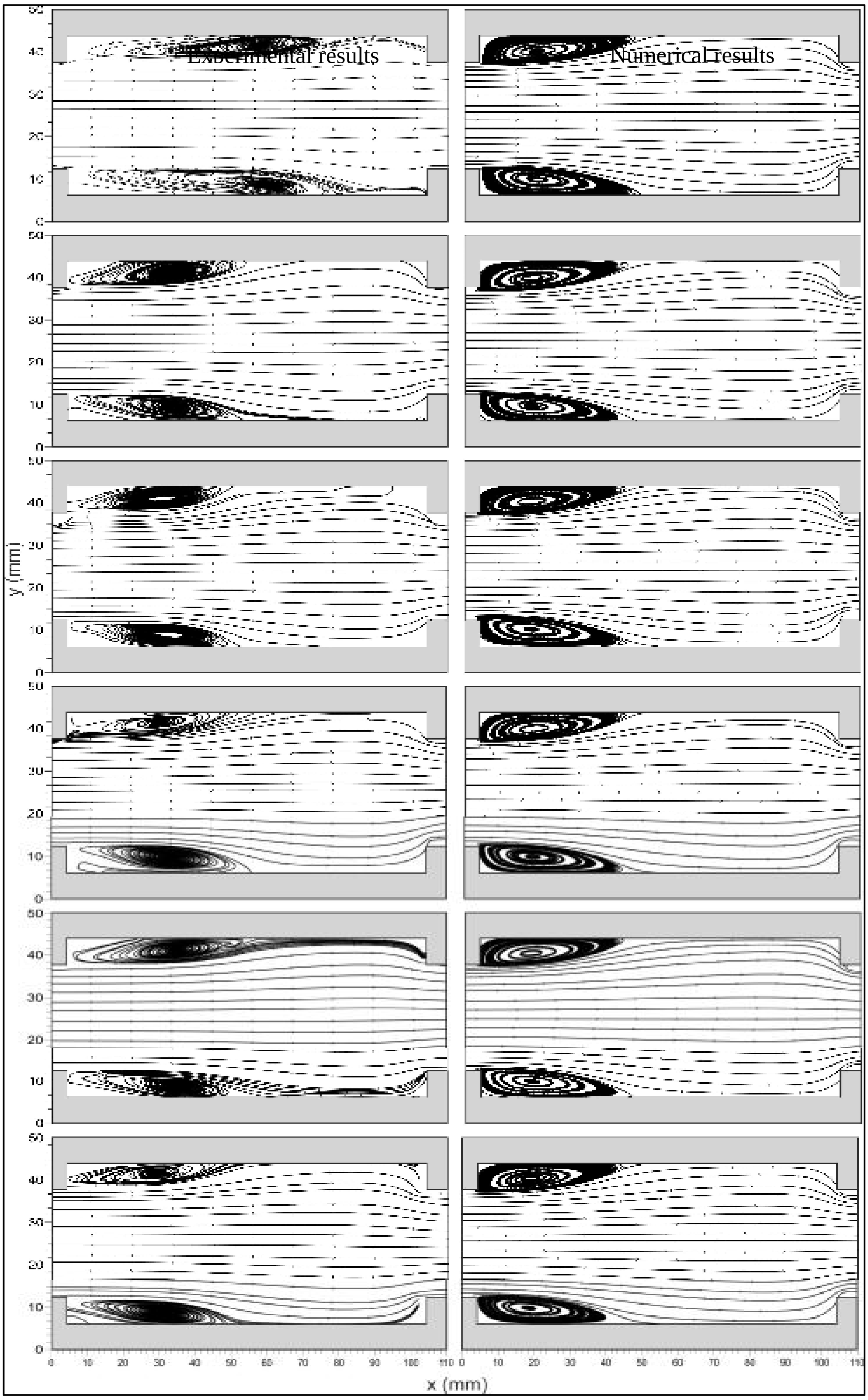

Figure 4.16. The time-averaged streamline topologies, <Ψ> for Re=6000, channel with phase angle, φ of 180 degree

For the case of phase shift with 90 degree in channel, the time-averaged streamline, $<\Psi>$ contour can be seen in figures 4.16 and 4.17 for eleven fields of views or cavities. The first and second column of figures show patterns of time averaged streamlines, $<\Psi>$ obtained experimentally and numerically results for Re= 4000 and Re=6000, respectively. It can be seen from figures 4.16 and 4.17 that for both Reynolds numbers, time averaged streamlines of channel are asymmetric on contrary to channel with 180° phase angle, φ. The upper and lower recirculation rotates counterclockwise and clockwise directions, respectively. The sharp corners of the corrugated walls alter the position of reattachment points, and more active flow mixing occurs between the main flow and recirculation in flow region. A well-defined focus is obvious in figures 4.16 and 4.17. Furthermore, the center of recirculation region occurs downstream and upstream which is located approximately 80-85 mm and 70-75 mm inlet from the cavity, for Re=4000 and Re=6000 respectively throughout the corrugated channel. As seen from figures the flow structures alter as the phase shift angles of corrugated channels are changed and flow parameters are also varied. A comprehensive experiments using PIV covering whole cavities were performed. It was pointed out that a quantitative flow visualization using PIV provide useful information about flow physics for such geometries.

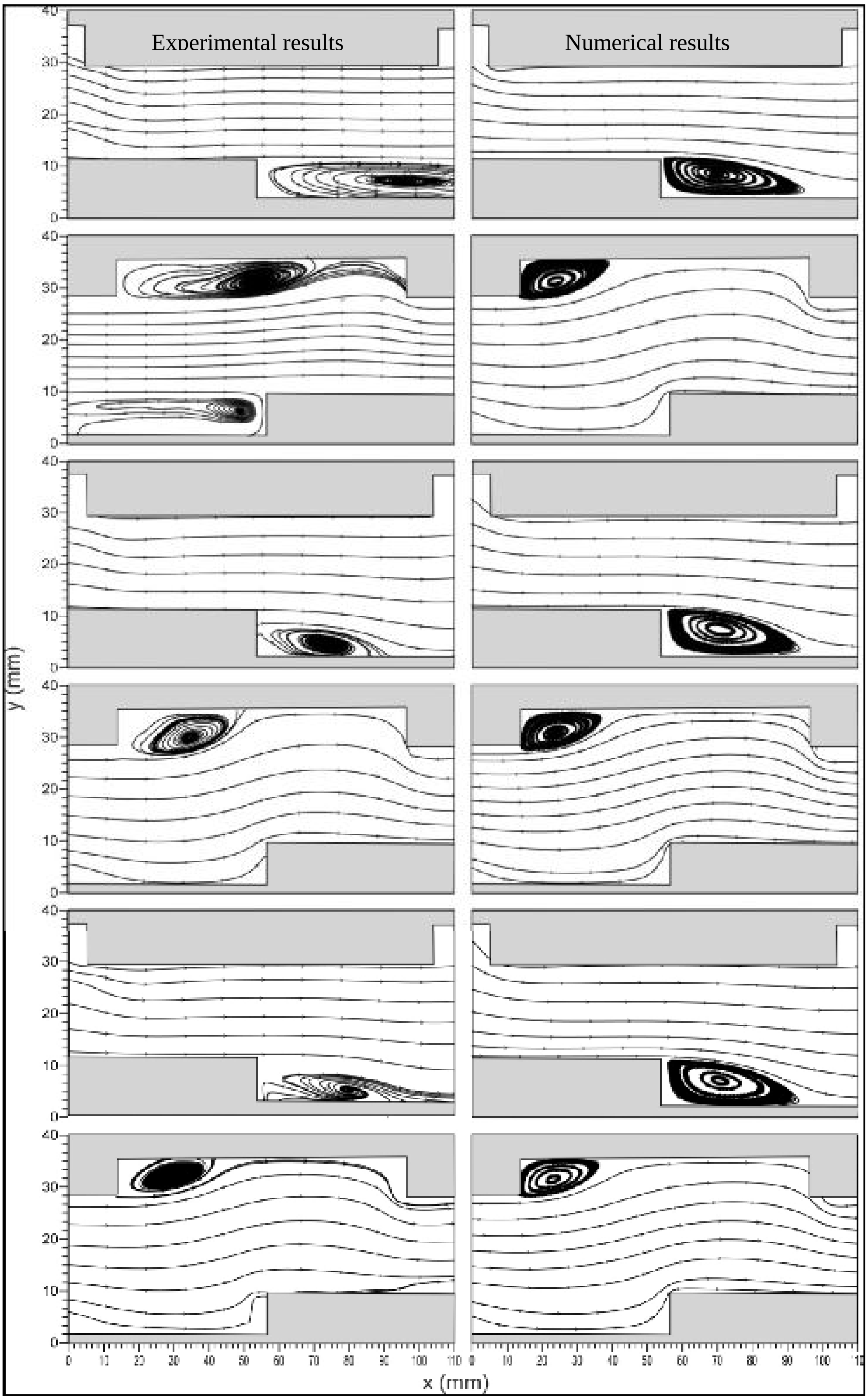

Figure 4.17. The time-averaged streamline topologies, <Y> for Re=4000, channel with phase angle, φ of 90 degree

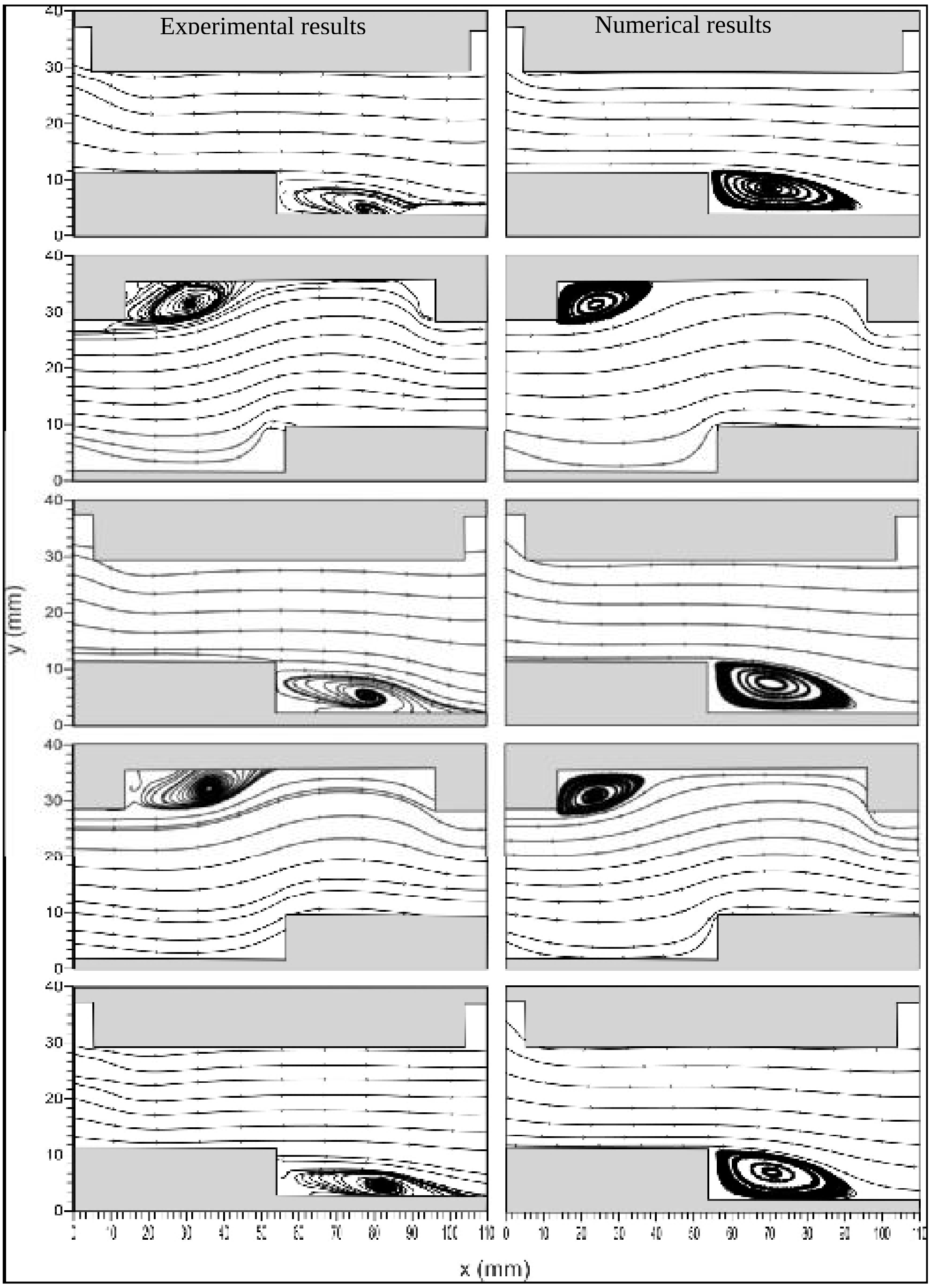

Figure 4.18. The time-averaged streamline topologies, <Ψ> for Re=4000, channel with phase angle, φ of 90 degree (continued)

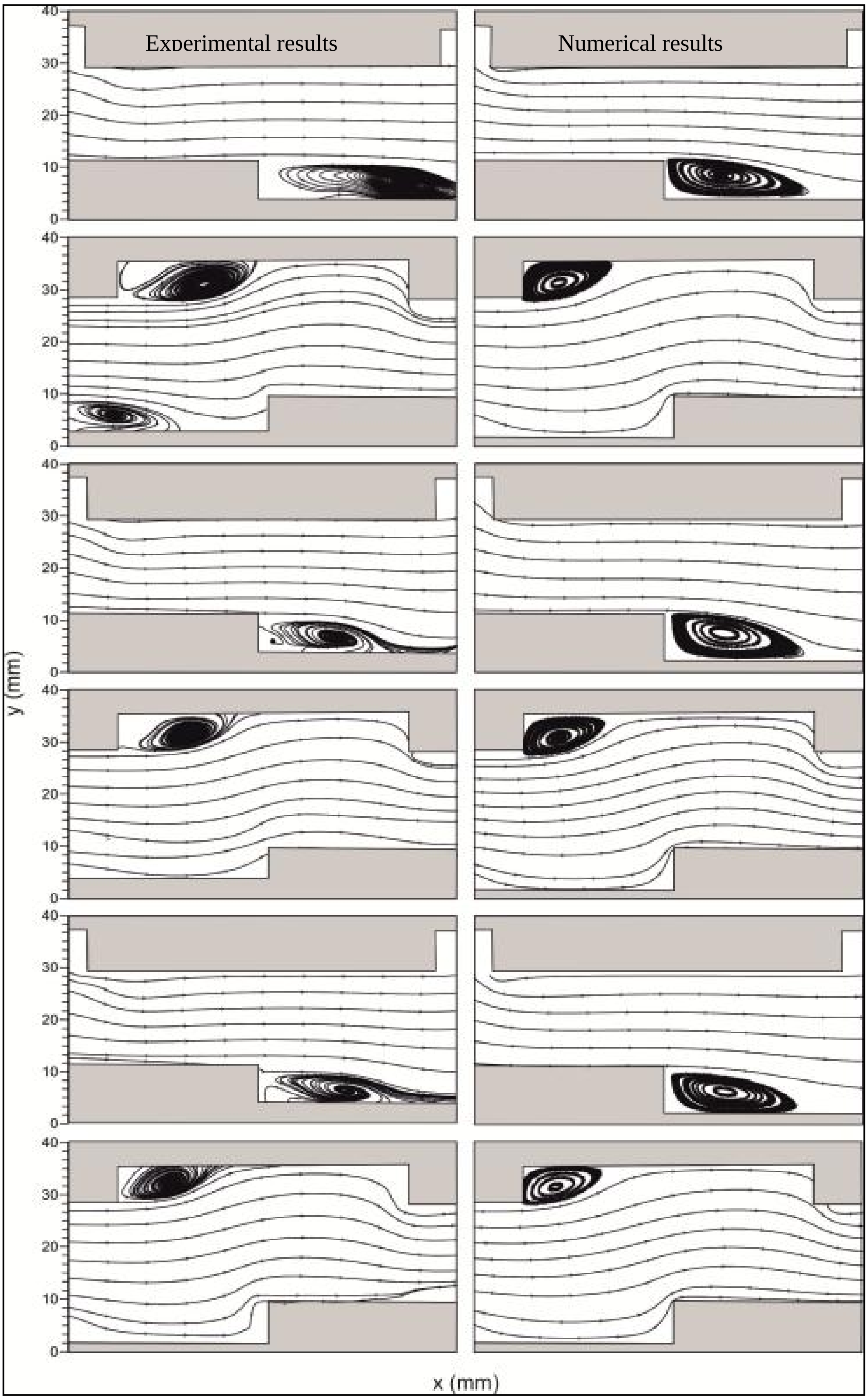

Figure 4.19. The time-averaged streamline topologies, <Ψ> for Re=6000, channel with phase angle, φ of 90 degree

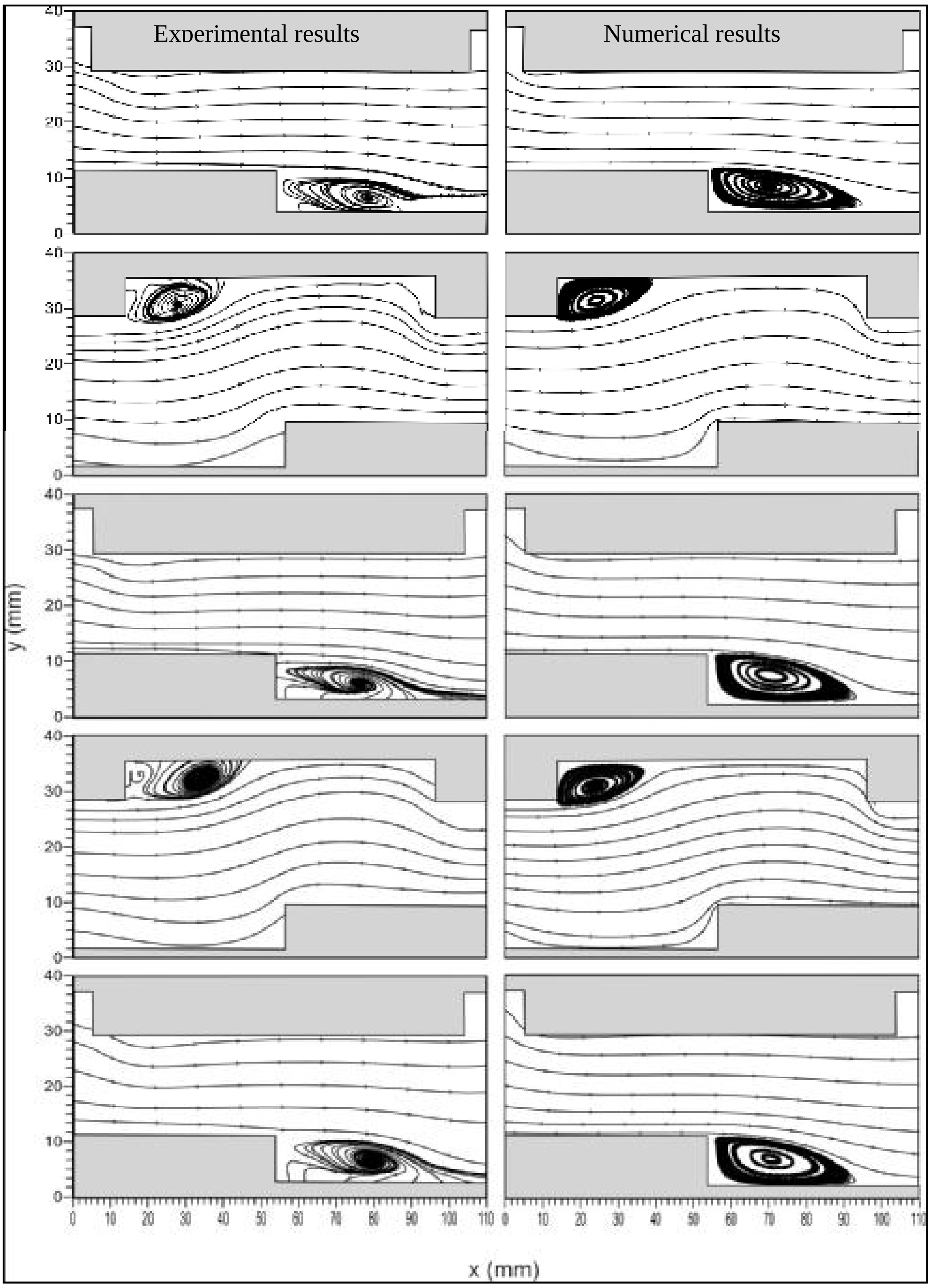

Figure 4.20. The time-averaged streamline topologies, $\langle \Psi \rangle$ for Re=6000, channel with phase angle, φ of 90 degree (continued)

For corrugated channel with the phase shift angle of 0 degree, the time-averaged streamline contour, $\langle \Psi \rangle$ are presented in figures 4.18 and 4.19 for eleven field of views in other words in whole upper and lower wall cavities. The first and second column of figures present patterns of time averaged streamlines for the purpose of comparison between experimental and numerical predictions for Reynolds numbers of Re= 4000 and Re=6000, respectively. Time- averaged patterns of streamlines for both Reynolds numbers indicate asymmetric flow structure in corrugated channel with phase angle, φ of 90 degree. Fresh fluid flow amalgamates significantly with the recirculation flow region more than the other channels as a result of the effect of sharp edge corners which activates recirculation to the further extend hence reattachment occurs earlier. The size of flow circulation bubble is smaller comparing to the other phase shift cases.

Figs, 4.15, 4.17, 4.19 elucidate that axial enlargement of the recirculation region is reduced in comparison to the case of Re=4000. The real flow would show stationary recirculation solely in the area where the calculated streamlines show a remarkable shrinking size of separation bubble. In turbulent flow, the shear layers promote the production of turbulence which causes a reduction in the size of the separation region. In turbulent flow, the heat transfer is strongly affected by the flow field and the turbulence structure. Therefore, it is necessary to discuss in addition to the flow field characteristics of the turbulence further in order to understand the calculated Nusselt numbers, Nu. The Nusselt number, Nu predicted numerically is going to be presented in the following chapter.

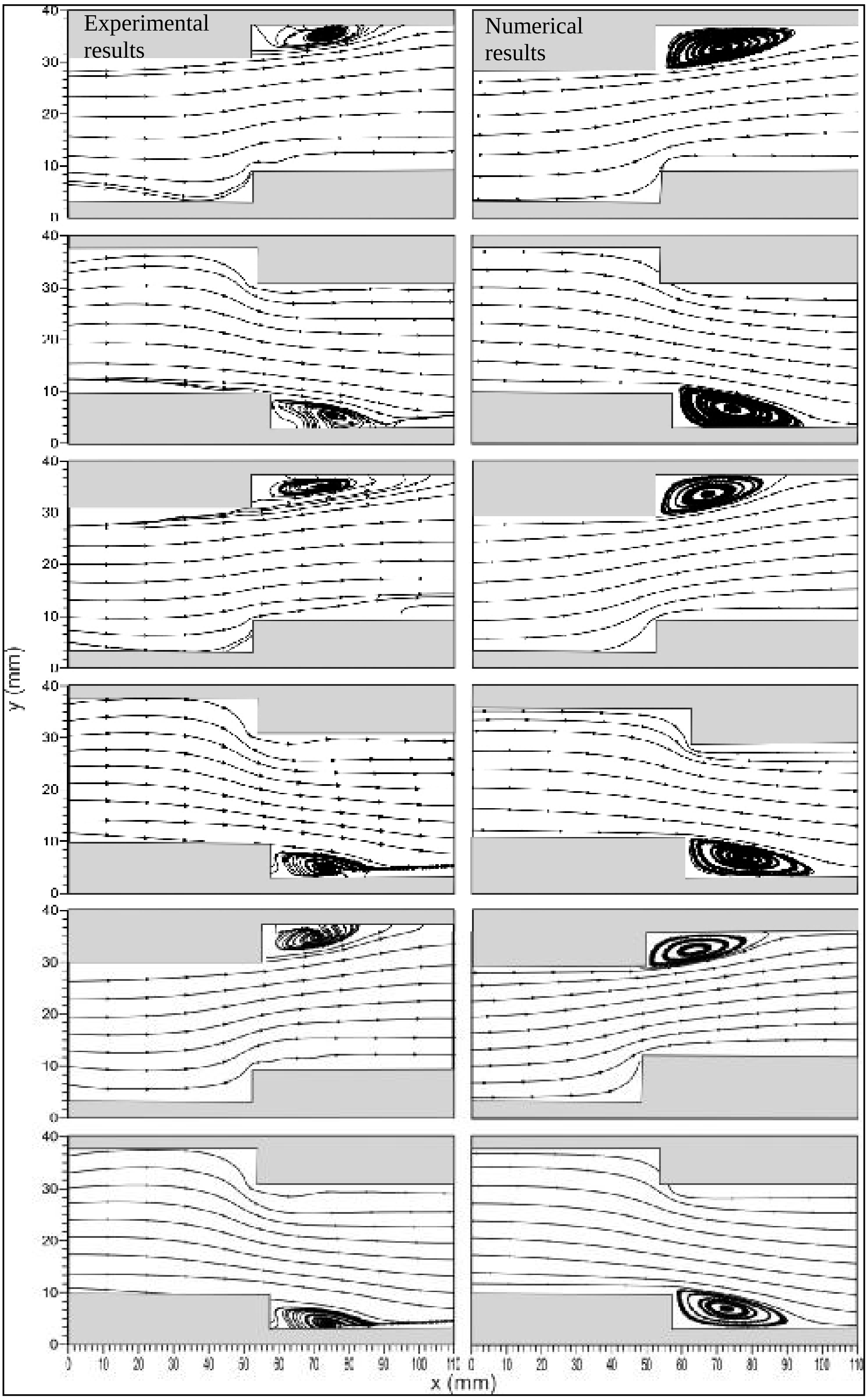

Figure 4.18. The time-averaged streamline topologies, $\langle Y \rangle$ for Re=4000, channel with phase angle, φ of 0 degree

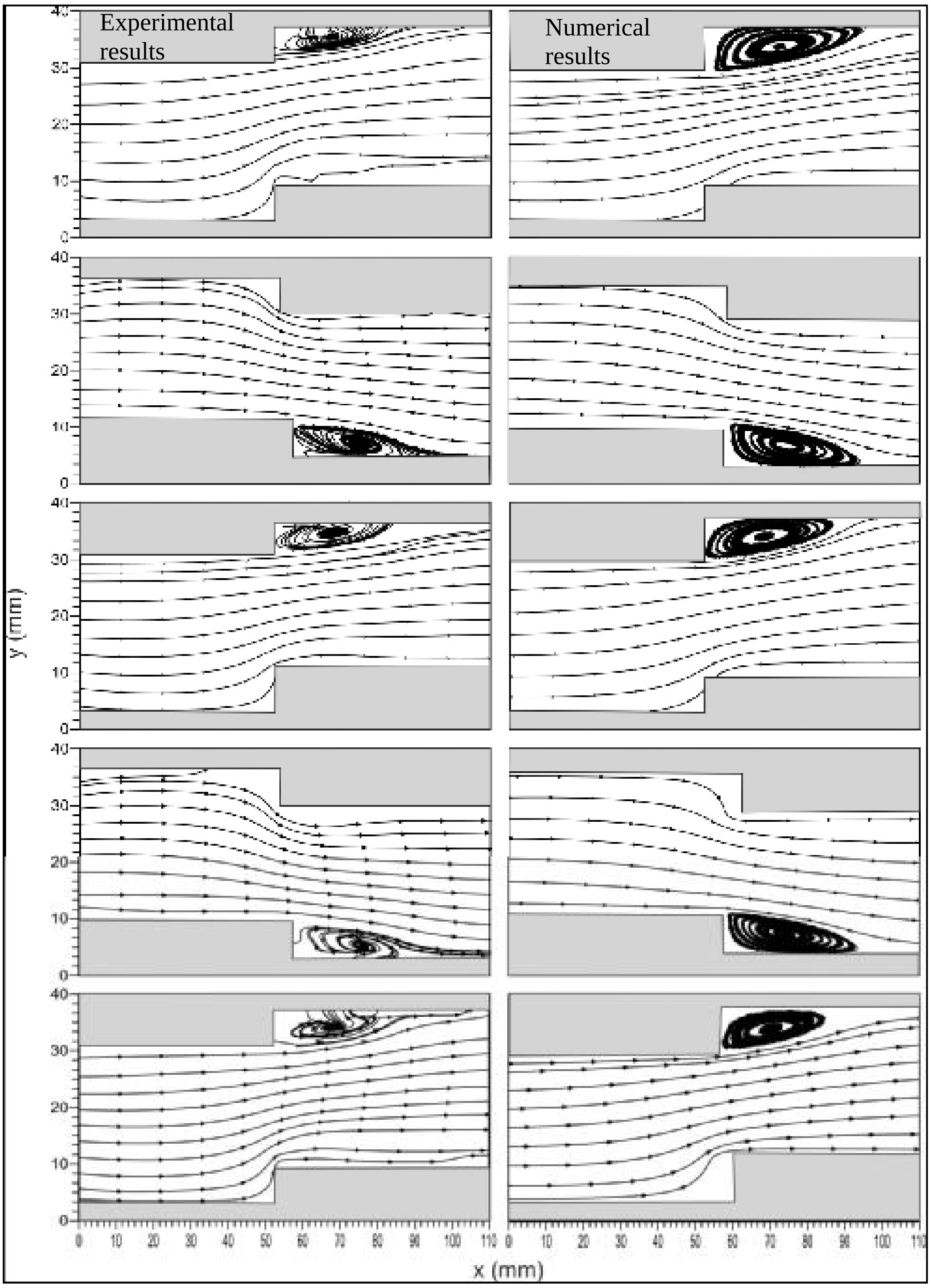

Figure 4.18. The time-averaged streamline topologies, $<\Psi>$ for Re=4000, channel with phase angle, φ of 0 degree (continued)

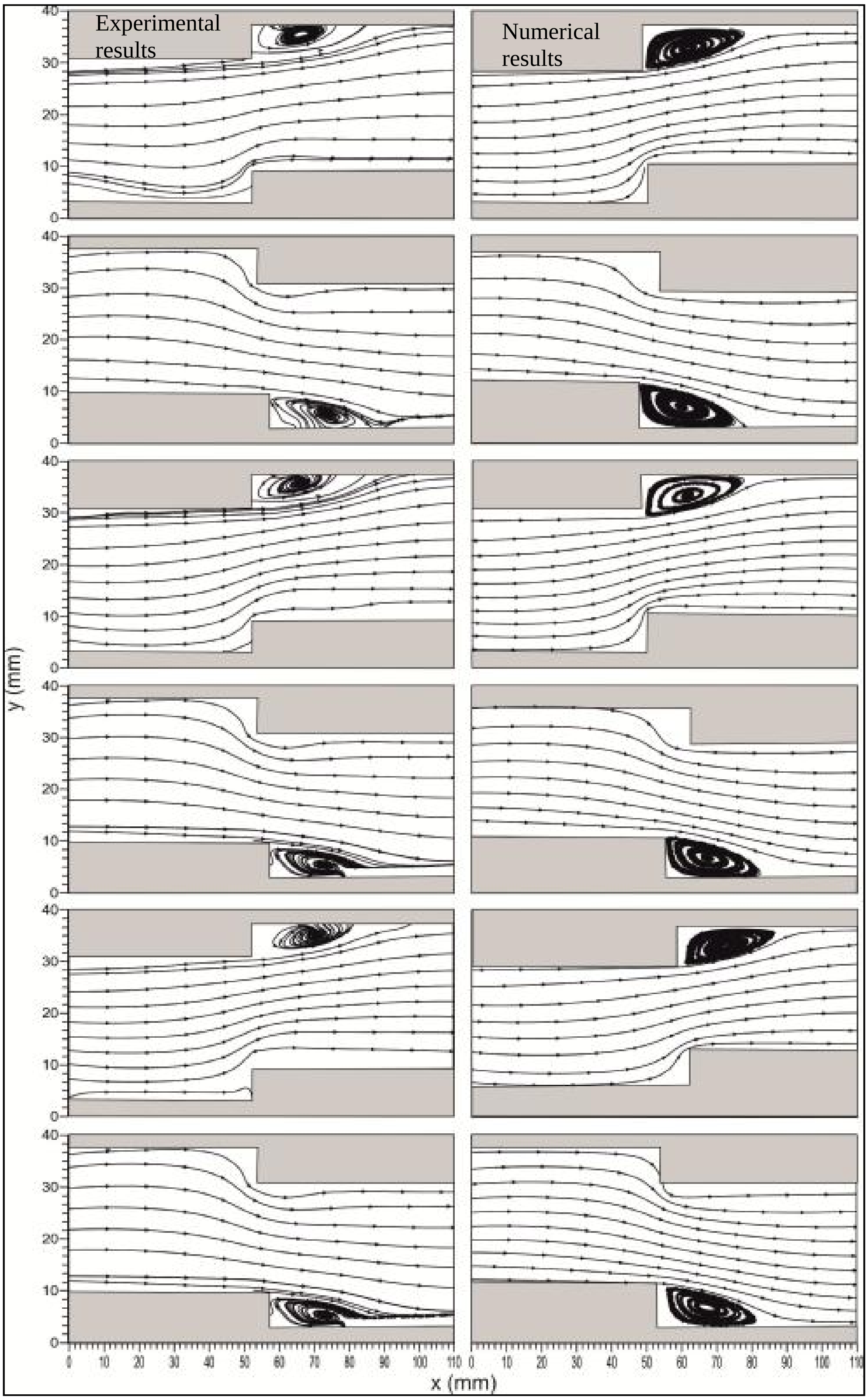

Figure 4.19. The time-averaged streamline topologies, $<\Upsilon>$ for Re=6000, channel with phase angle, φ of 0 degree

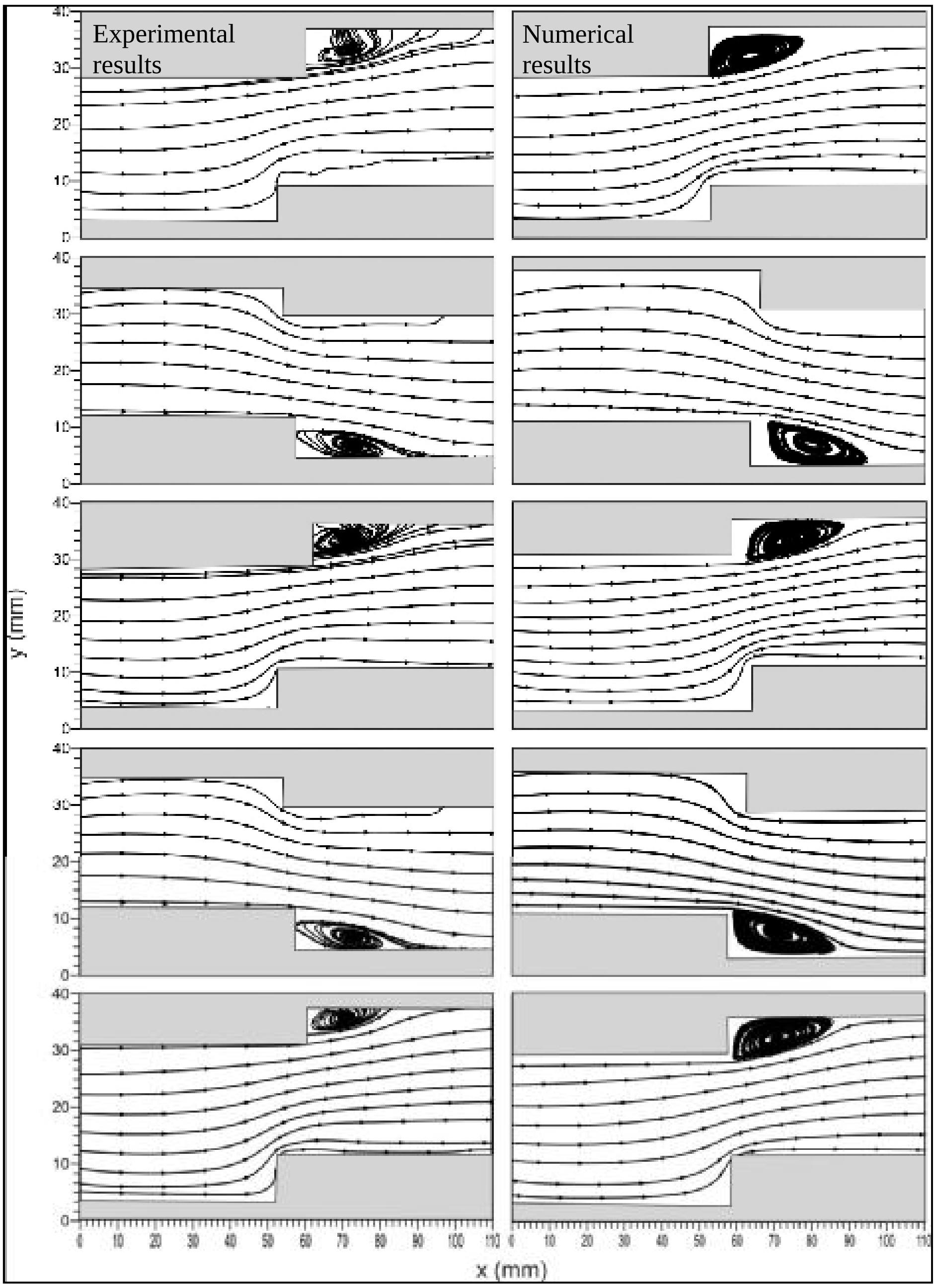

Figure 4.19. The time-averaged streamline topologies, <Y > for Re=6000, channel with phase angle, φ of 0 degree (continued)

Prediction of the flow hydrodynamics thorough the corrugated channels of heat exchangers are necessary for optimizing design parameters. Special channel shapes, such as the corrugated channels which have sharp edge of the cavity, have a significant effect on the enhancement of heat transfer. In consequence of this thermal boundary, layers for corrugated flow became thinner than the case of the straight pipe and secondary vortices inside corrugates contributed to the enhancement of the heat transfer. This allows almost all the fluid elements to affect heat transfer from adjacent channels, which not only produces more turbulence and good fluid mixing than the straight tube but also increases the heat transfer area. Therefore, it is advisable to always prefer corrugated plates over straight plates for plate type heat exchangers.

The influence of phase shift of corrugated channels through quantitative flow visualizations, instantaneous and time-mean flow data revealed that the formation of vortical flow structures in the passages of corrugated channels depends on the phase shift, distances between upper and lower plates and Reynolds numbers, Re. There is vast variety of numerical predictions reporting flow characteristics, for example patters of streamlines, distributions of velocity field, patterns of vorticity and other turbulent statistics. But these data needs validating by experimental data. The present work is very necessary for validating numerical predictions. Numerical results in the present work agree well with experimental results conducted in the present work for all fields of views and both Reynolds numbers as it can be seen in figures clearly.

A few papers have been published to investigate heat transfer and fluid flow characteristics in a turbulent flow with corrugated shapes. Generally, the effect of the corrugated geometry on the enhancement of heat transfer and hydrodynamics of flow for both pipe and channel was investigated, and most of them were studied numerically. So, to have a better understanding of the effect of the corrugated geometry and phase shift on the enhancement of heat transfer and flow characteristics and to compare the results with each other, additional experiments were needed channel configurations for turbulent flows. Numerous studies have reported qualitative flow characteristics of for laminar flow using the smoke technique. However, smoke technique is not able to visualize this behavior, since the smoke diffusion is very intensive in turbulent flow and does not allow for an identification of secondary flow. In this study, velocity field has been investigated with the Particle Image Velocimetry (PIV) technique in order to reveal flow physics in further detail.

4.1.3. Effect of Reynolds Numbers and Phase Shifts on Turbulence Kinetic Energy

In this section, turbulence kinetic energy, TKE contours are discussed in accordance with the results of two dimensional Particle Image Velocimetry (PIV) for straight channel and three different corrugated channels.

In fluid dynamics, turbulent kinetic energy, TKE refers to the mean kinetic energy per unit mass which is associated with eddies in turbulent flow. Turbulent Kinetic Energy, TKE is one of the most significant variables in boundary layer region due to the fact that it is a measure of turbulence intensity. It is directly in relation to the transport of heat, moisture, and momentum through the boundary layer. If turbulent kinetic energy, TKE decreases with time, then it is inevitable for flow in boundary layer to become less turbulent with time; however, if turbulent kinetic energy, TKE increases with time, then boundary layer is observed to become further turbulent with time.

In two-dimensional PIV measurements, the values of streamwise Reynolds normal stress, $<u'u'>$ and transverse Reynolds normal stress, $<v'v'>$ can be calculated in usual manner (for example, by subtracting the mean values of the velocity components from their instantaneous values such as U_∞, u_i and then by averaging the products) from the 1000 instantaneous velocity data obtained by the PIV measuring system. Assuming isotropic flow, the third fluctuating velocity component can be estimated by a 2D approximation (Sheng et al. 2000), namely, the third component has been supposed to be equal to the half of $(<u'u'> + <v'v'>)$, then TKE, which is directly related to the dynamics of the vortices and usually utilized as the measurement of the turbulence mixing (Feng et al. 2010; Benard et al.2008; Schafer et al.2009). It can be calculated with the following expression

$$\text{TKE} = \frac{3}{4}\left(<u'u'> + <v'v'>\right) \tag{1}$$

The rate of momentum transfer and kinetic energy of fluid increases in accordance with the rise of Reynolds number, Re. At large Reynolds numbers, Re the inertia forces that are proportional to the density and the velocity of the fluid are largely relative to the viscous forces, and therefore, the viscous forces can not preclude the random and rapid fluctuations of the fluid. The large Reynolds number, Re is attributed to the higher velocity which can disturb the flow and as a result, the heat transfer is strengthened. As a result of increasing the Reynolds number, Re the Nusselt number, Nu which is an important dimensionless parameter that represents the temperature gradient at a surface where an increase of heat transfer by convection is taken place. On the other hand, this condition causes pressure drop in the corrugated channel. In order to reduce this pressure drop additional consideration is needed.

4.1.3.1. Results of the Turbulence Kinetic Energy Contours for Straight Channel

It is initially necessary to experimentally determine the flow characteristics in the straight channel in order to take these results as a reference data in order to compare with the results of other geometries. Patterns of dimensionless turbulent kinetic energy, <TKE> are presented in figure 4.20. It is notice that the left hand side of figure shows flow data of Re=4000 and the right hand side of figure presents flow data of Re=6000) for the straight channel. Both minimum and incremental values of turbulent kinetic energy, <TKE> contours were taken as 0.002 for Re=4000 and Re=6000. The maximum value of turbulent kinetic energy, <TKE> were taken as 0.032 and 0.044 for Re=4000 and Re=6000, respectively.

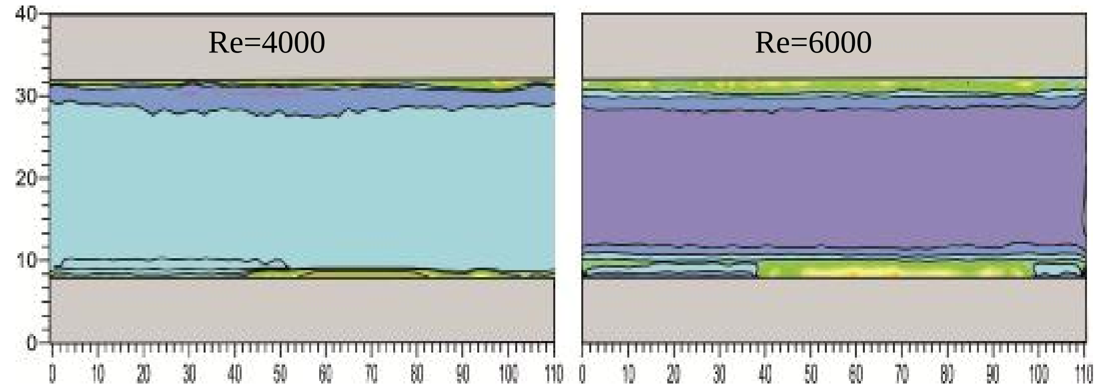

Figure 4.21. Patterns of Turbulent kinetic energy,|< $(TKE)_{min}$>| =0.002, <Δ(TKE)>=0.002 for straight channel

4.1.3.2. Results of the Turbulence Kinetic Energy Contours for Corrugated Channels

The contours of dimensionless turbulent kinetic energy, <TKE> are presented in figures 4.21 and 4.22 for the case of phase shift, φ with 180 degree in channel by the experimental data for both Reynolds numbers (Re=4000 and Re=6000). The first column of the figure shows the dimensionless turbulent kinetic energy, <TKE> contours, the second column of the figure presents streamwise Reynolds normal stress, $< u'u' >$, the third column of the figure reports transverse Reynolds normal stress $< v'v' >$, respectively. Both minimum and incremental values are taken as 0.005.

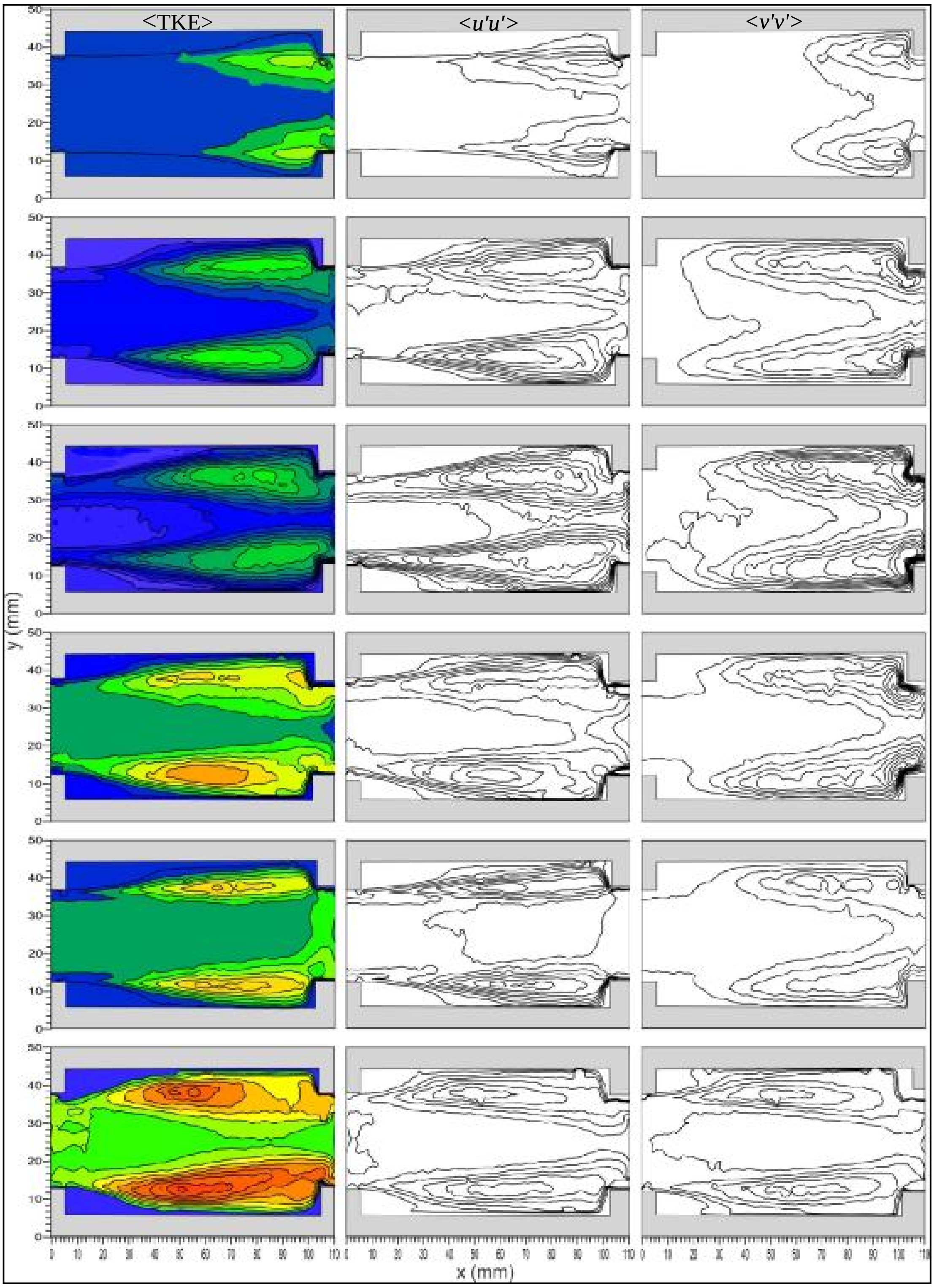

Figure 4.22. Patterns of Turbulent kinetic energy,$|<(TKE)_{min}>|$ =0.005, $<\Delta(TKE)>$=0.005, streamwise Reynolds normal stress, $<u'u'>$, transverse Reynolds normal stress $<v'v'>$, respectively for Re=4000, channel with phase angle, φ of 180 degree

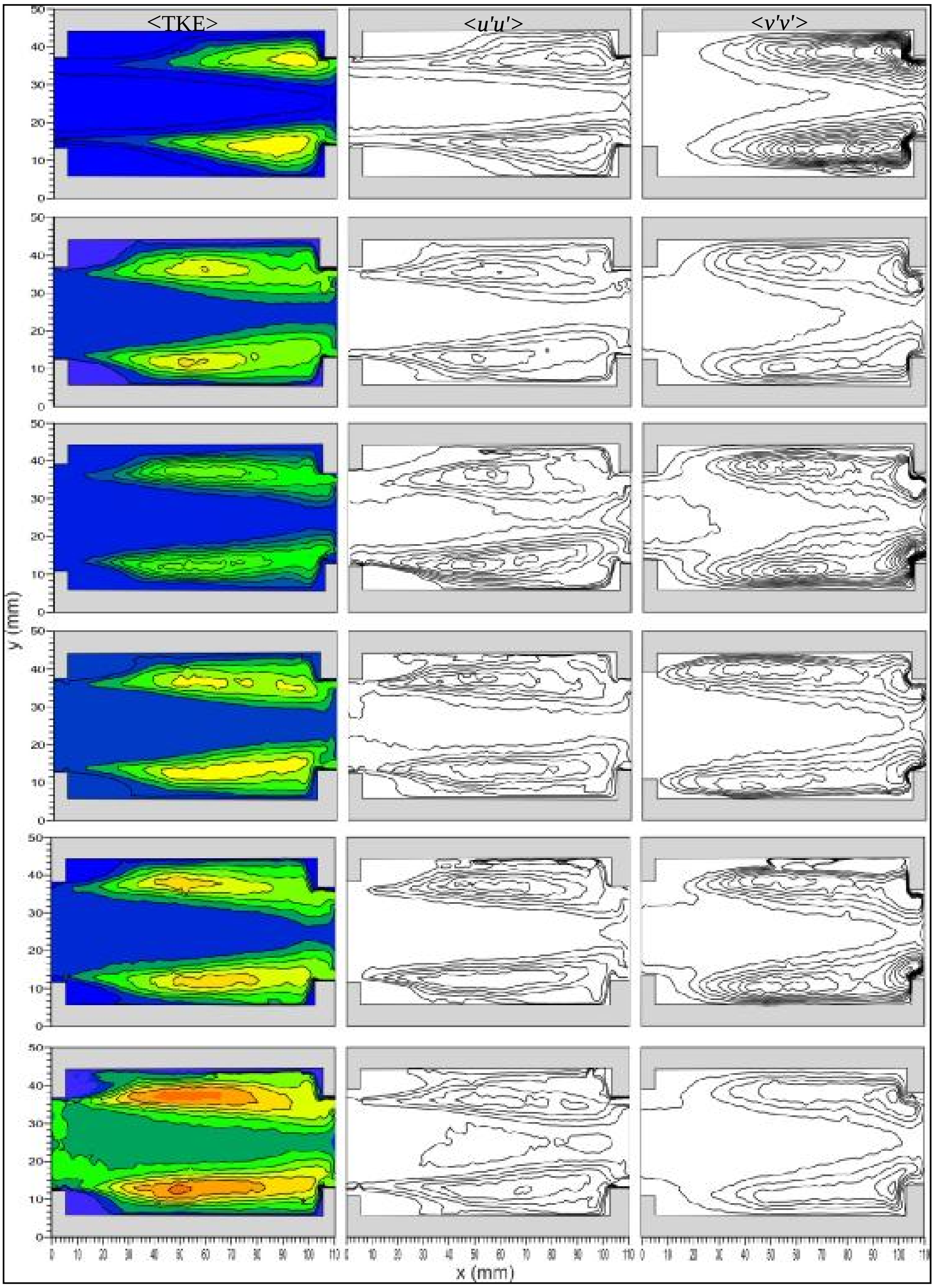

Figure 4.22. Patterns of Turbulent kinetic energy $|<(TKE)_{min}>|$ =0.005, $<\Delta(TKE)>$=0.005, streamwise Reynolds normal stress, $<u'u'>$, transverse Reynolds normal stress $<v'v'>$,for Re=6000, channel with phase angle, φ of 180 degree

The rows of the figures show the patterns of turbulent kinetic energy, <TKE> for field of views (FOV) 1, 2,3,4,5 and 6, respectively. As it can be understood from the formula (1), dimensionless turbulent kinetic energy, <TKE> contours are presented in second and third column of the figures. In both of Reynolds numbers, Re dimensionless turbulent kinetic energy, <TKE> contours is symmetric with taking the central axis as a reference line since the channel has the same corrugated geometries on both upper and lower walls as shown in figure 4.22. Turbulent kinetic energy, <TKE> increases from the first field of view until the last field of view due to effect of square corner of cavities. Furthermore maximum value of the <TKE> in the first cavity plane and last cavity plane are 0.073 and 0.094, respectively for Re=4000. On the other hand, increasing the Reynolds number to the value of Re=6000 causes an increase in the turbulent kinetic energy, <TKE> values. Maximum value of the <TKE> in the first cavity plane and last cavity plane are 0.081 and 0.14, respectively for Re=6000.

The region in which flow is accelerated due to converging of core flow region caused by sharp edges, TKE increases up to have a maximum value along shear layers while the minimum TKE values is taken place in the wake regions. According to the time-averaged flow data entrainments between core and wake flow region are not clear as shown in figures 4.21 and 4.22. In order to demonstrate the entrainment process between these two flow regions it is necessary to observe animation of instantaneous flow data. Animation of 1000 flow images in sequence demonstrate that entertainment between core and wake flow regions simulated by the development of vortices along exterior of shear layers in all cavities causes high rate of mass and momentum transfers as well as velocity fluctuations.

It is observed from figures 4.21 and 4.22 that the reversed region in images which is colored blue (low energy region) nearly disappeared owing to the effects of turbulent kinetic energy, <TKE> between planes of cavities. Dimensionless turbulent kinetic energy, <TKE> contours are symmetrically expanded and influence the flow domain judging successively to the field of views from downstream to upstream direction. These results indicate an increase of the kinetic energy, <TKE> increases in the flow domain.

Turbulent kinetic energy, <TKE> at corrugated channel is greater than the straight channel due to the sharp edges of cavity for all fields of views. This result explains clearly the reason why corrugated channels transfer the heat to a higher level.

The contours of dimensionless turbulent kinetic energy, <TKE> as a result of combination of streamwise Reynolds normal stress, $< u'u' >$ and transverse Reynolds normal stress, $< v'v' >$ which were mentioned above in this chapter. It was observed from figures that streamwise Reynolds normal stress, $< u'u' >$ contours have an effect on the <TKE> distributions much more than the transverse Reynolds normal stress, $< v'v' >$ contours. This conclusion demonstrated that the side walls did not affect the core flow regions especially in streamwise direction at the center of model. To enable that, i.e., to avoid the walls impact on the flow, the channel models were manufactured wide enough. During the experiment, the laser sheet was oriented vertically to the top surface of the water channel and measurements were carried out at the midsection of models.

The contours of dimensionless turbulent kinetic energy, <TKE>, streamwise Reynolds normal stress, $< u'u' >$ and transverse Reynolds normal stress, $< v'v' >$ are presented in figures 4.23 and 4.24 using experimental flow data for the case of phase shift, φ with 90 degree in channel for both Reynolds numbers (Re=4000 and Re=6000). Both minimum and incremental values are taken as 0.005. The rows of the figures present the contours for fields of views (FOV) 1, 2,3,4,5,6,7,8,9,10 and 11 respectively. The peak value of dimensionless turbulent kinetic energy, <TKE> contours for Reynolds numbers, Re=4000 and Re=6000 are determined to be 0.115 and 0.0149, respectively.

It can be seen from figure 4.23 that the first two field of view's contours do not reveal flow behavior clearly. However, after forementioned field of views dimensionless turbulent kinetic energy, <TKE> contours obviously clarify the flow structure much better. After the second cavity, flow structures do not alter significantly. It is expected that dimensionless turbulent kinetic energy, <TKE> contours are directly function of velocity components. As mentioned earlier, at velocity contours, the magnitude of turbulent kinetic energy, <TKE> is much more higher comparing to the case of channel with 180 degree phase angle, φ. As a result, this enhancement of heat transfers in cavity with phase angle, φ of 90 degree is greater than channel with phase angle, φ of 180 degree.

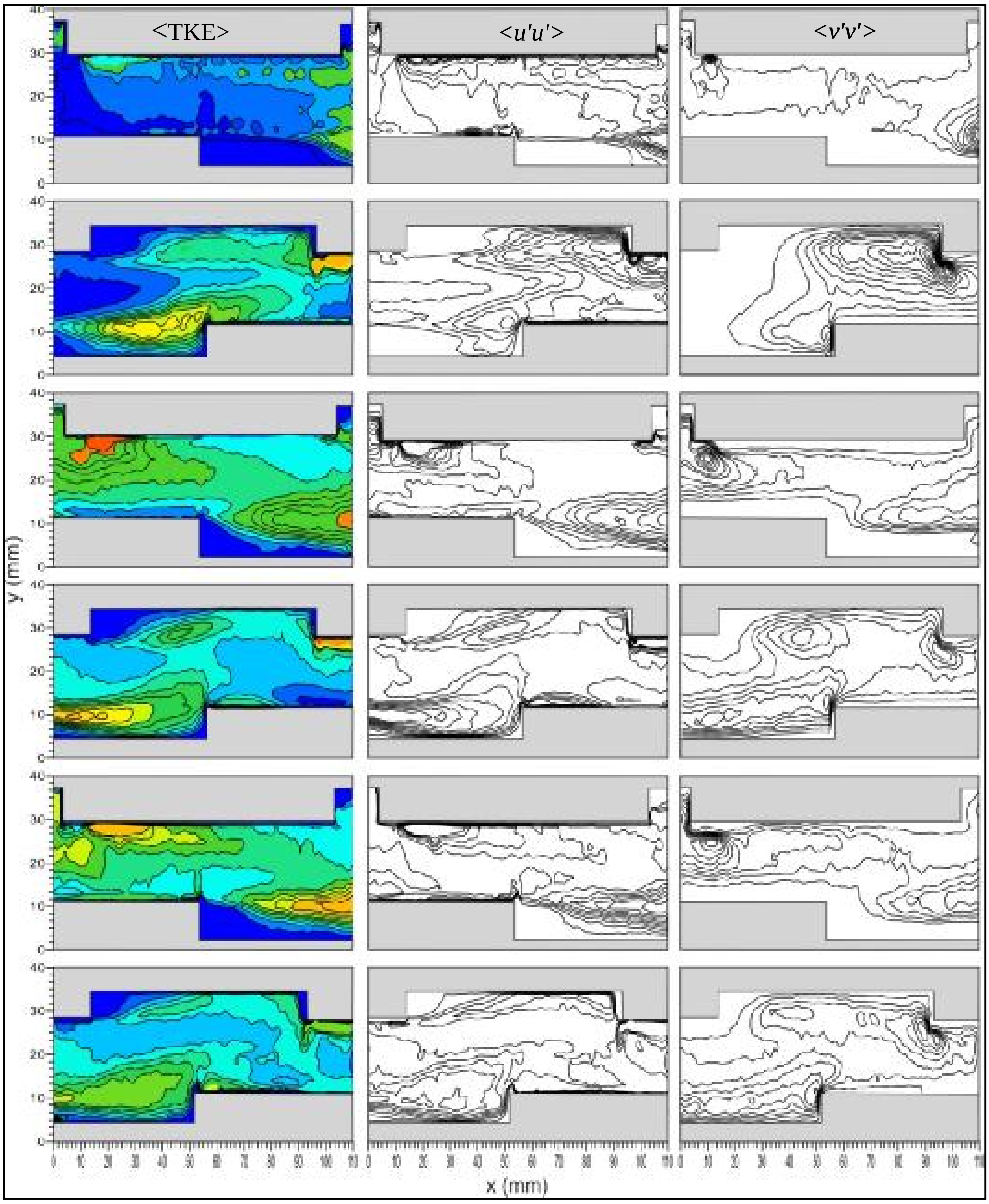

Figure 4.23. Patterns of Turbulent kinetic energy $|<(TKE)_{min}>|$ =0.005, <Δ(TKE)>=0.005, Reynolds streamwise normal stress, $<u'u'>$, Reynolds transverse normal stress $<v'v'>$,for Re=4000, channel with phase angle, φ of 90 degree

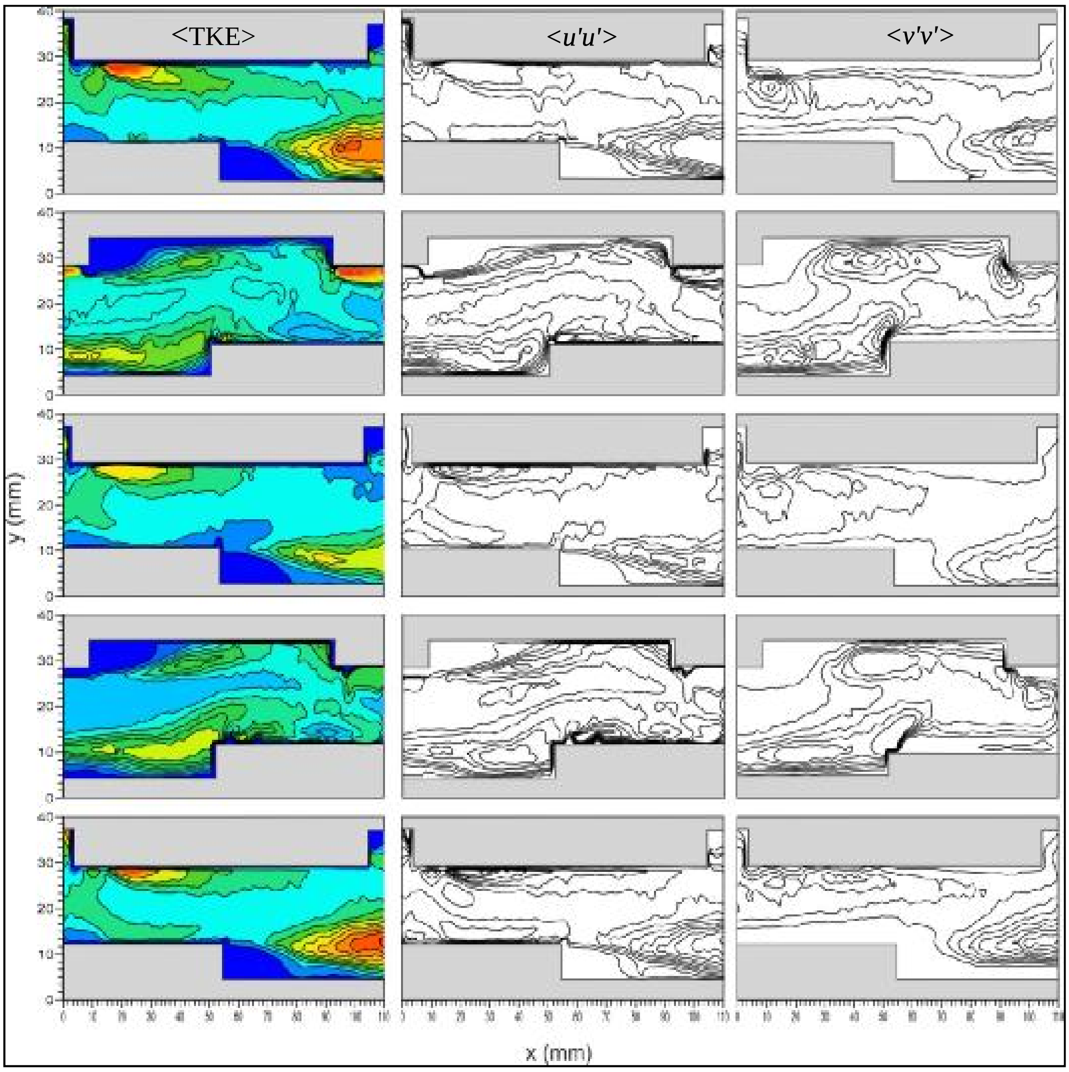

Figure 4.23. Patterns of Turbulent kinetic energy $|<(TKE)_{min}>|$ =0.005, $<\Delta(TKE)>$=0.005, Reynolds streamwise normal stress, $<u'u'>$, Reynolds transverse normal stress $<v'v'>$,for Re=4000, channel with phase angle, φ of 90 degree (continued)

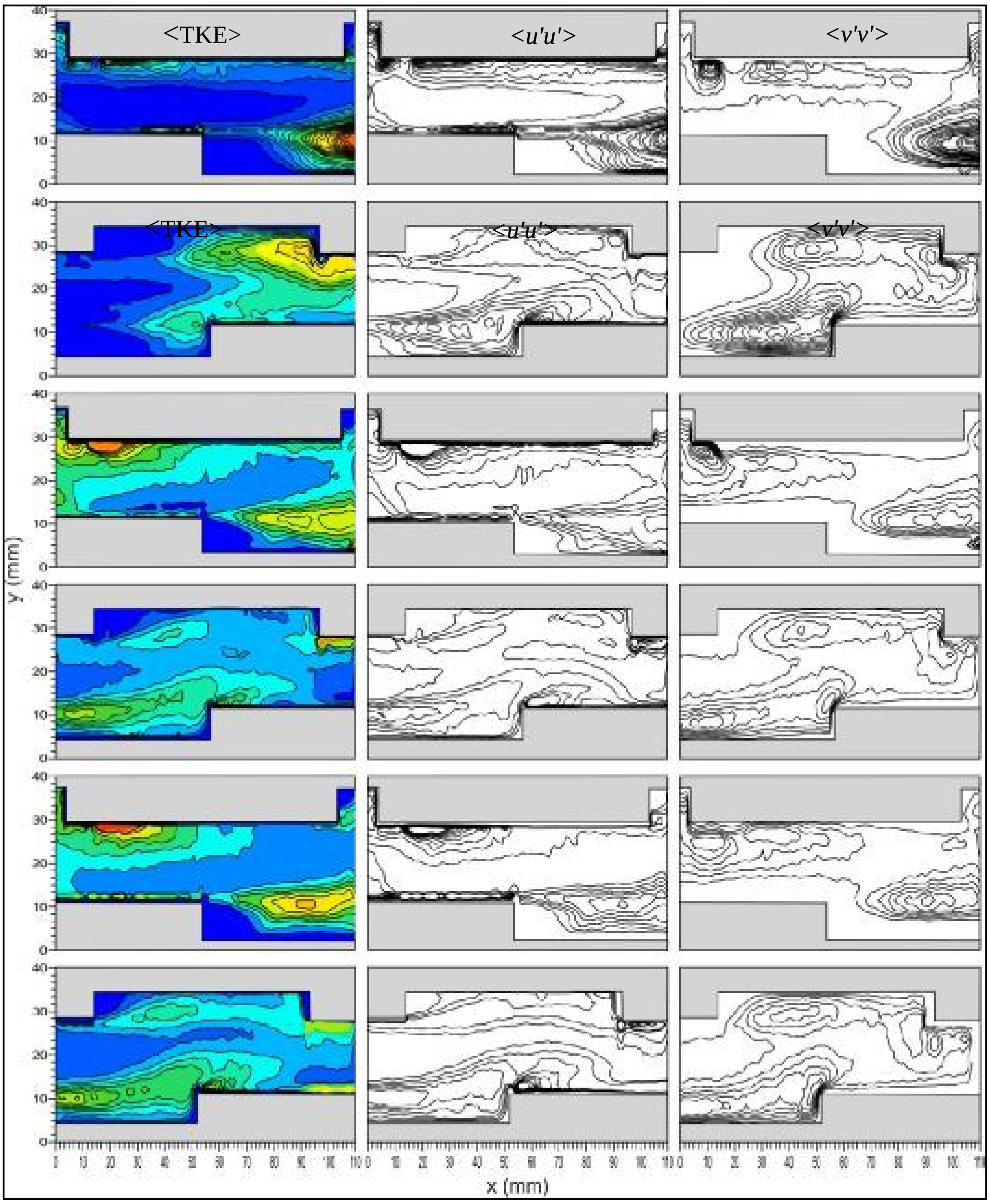

Figure 4.24. Patterns of Turbulent kinetic energy $|<(TKE)_{min}>|$ =0.005, $<\Delta(TKE)>$=0.005, Reynolds streamwise normal stress, $<u'u'>$, Reynolds transverse normal stress $<v'v'>$, for Re=6000, channel with phase angle, φ of 90 degree

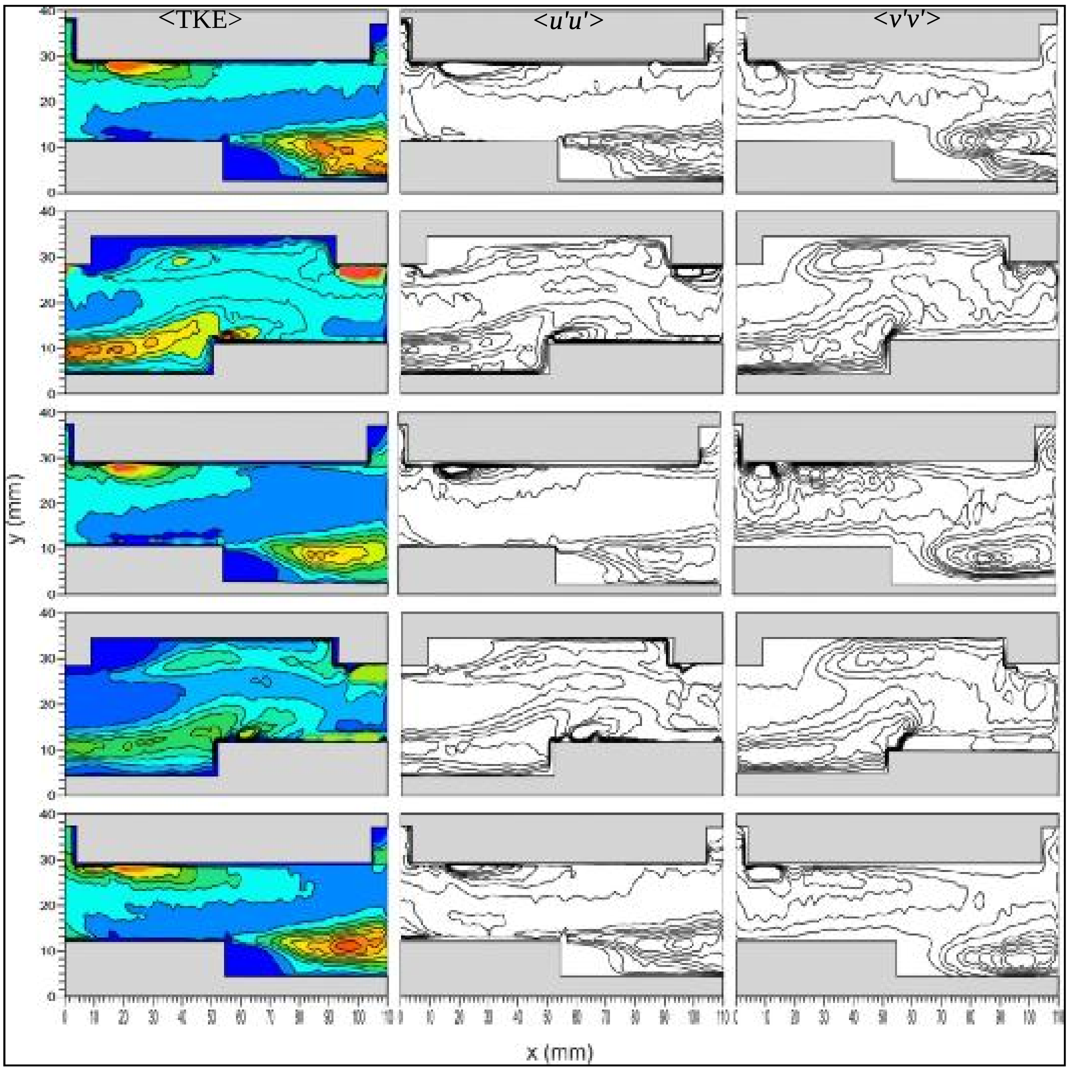

Figure 4.24. Patterns of Turbulent kinetic energy $|<(TKE)_{min}>|$ =0.005, $<\Delta(TKE)>$=0.005, Reynolds streamwise normal stress, $<u'u'>$, Reynolds transverse normal stress $<v'v'>$,for Re=6000, channel with phase angle, φ of 90 degree (continued)

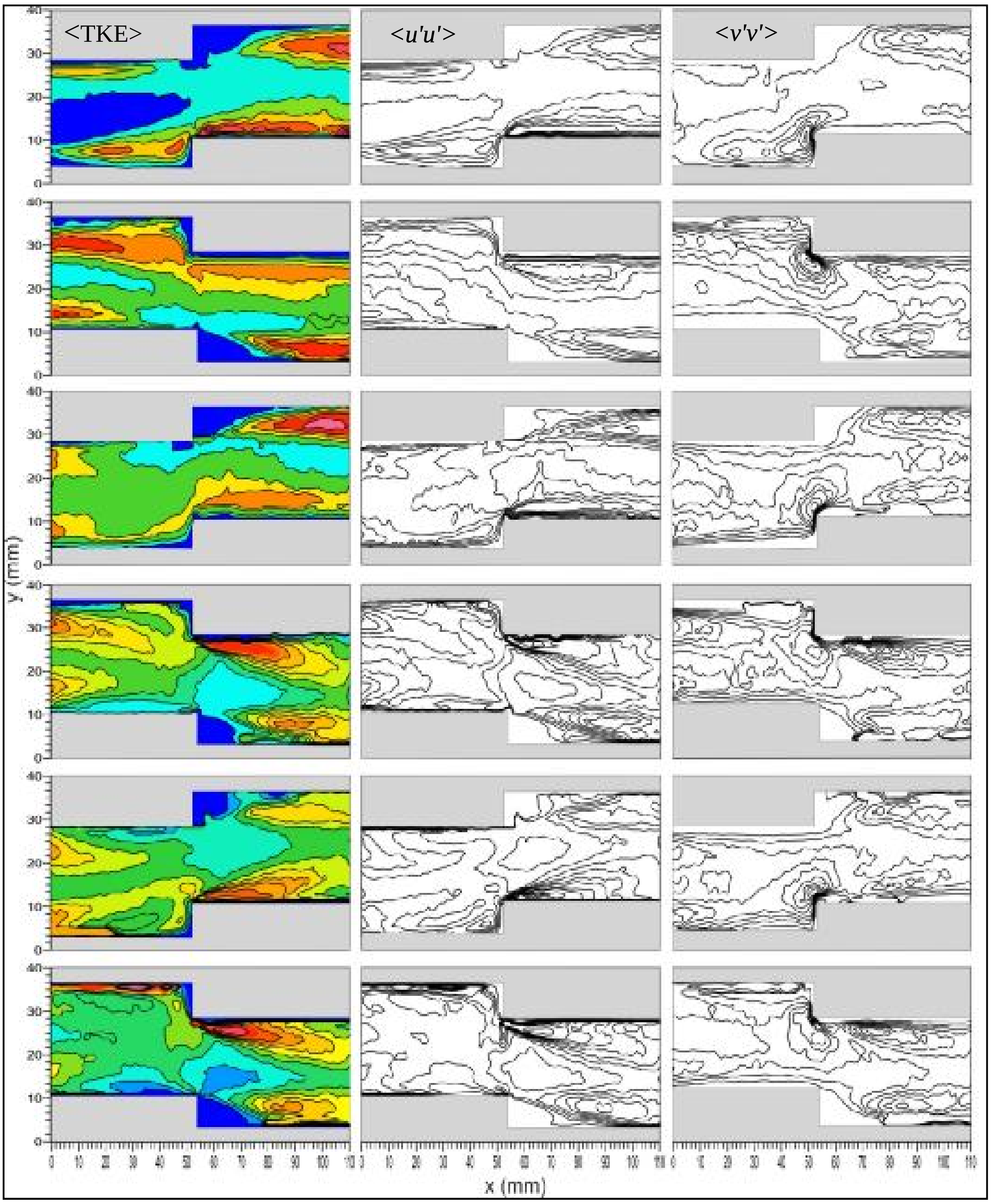

Figure 4.25. Patterns of Turbulent kinetic energy $|<(TKE)_{min}>|$ =0.005, $<\Delta(TKE)>$=0.005, Reynolds streamwise normal stress, $<u'u'>$, Reynolds transverse normal stress $<v'v'>$,for Re=4000**,** channel with phase angle, φ of 0 degree

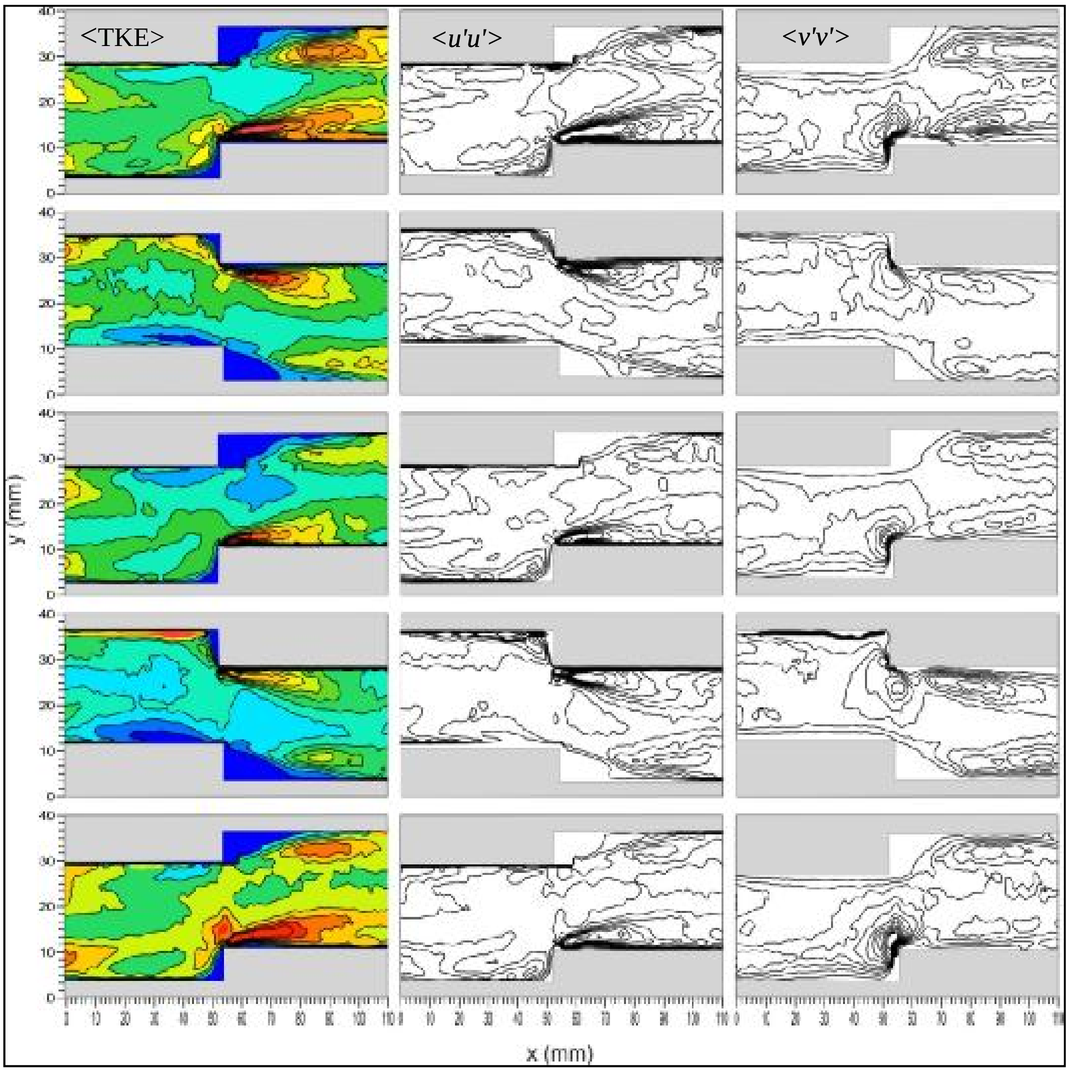

Figure 4.25. Patterns of Turbulent kinetic energy $|<(TKE)_{min}>|$ =0.005, $<\Delta(TKE)>$=0.005, Reynolds streamwise normal stress, $<u'u'>$, Reynolds transverse normal stress $<v'v'>$,for Re=4000, channel with phase angle, φ of 0 degree (continued)

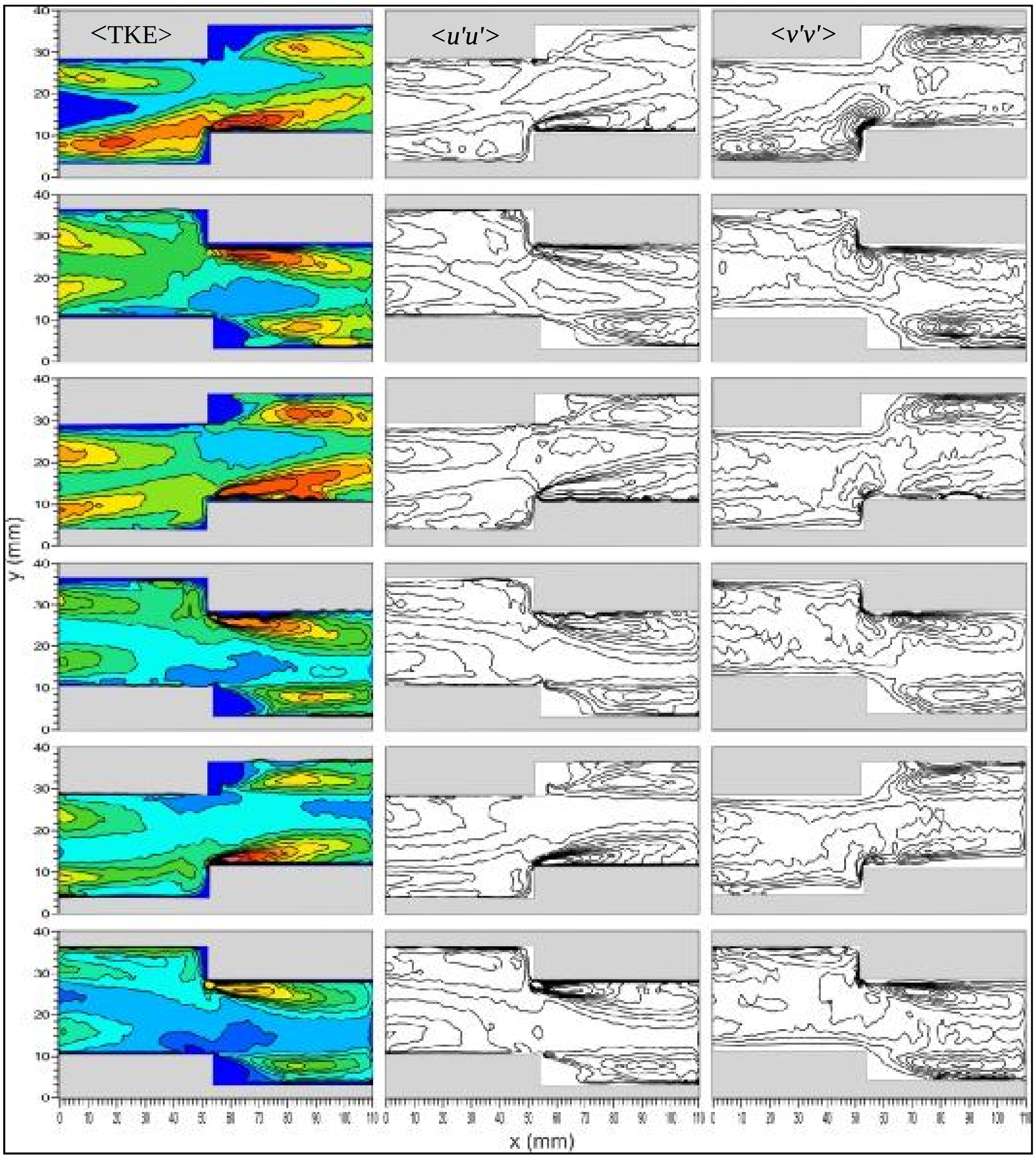

Figure 4.26. Patterns of Turbulent kinetic energy $|<(TKE)_{min}>|$ =0.005, $<\Delta(TKE)>$=0.005, Reynolds streamwise normal stress, $<u'u'>$, Reynolds transverse normal stress $<v'v'>$,for Re=6000, channel with phase angle, φ of 0 degree

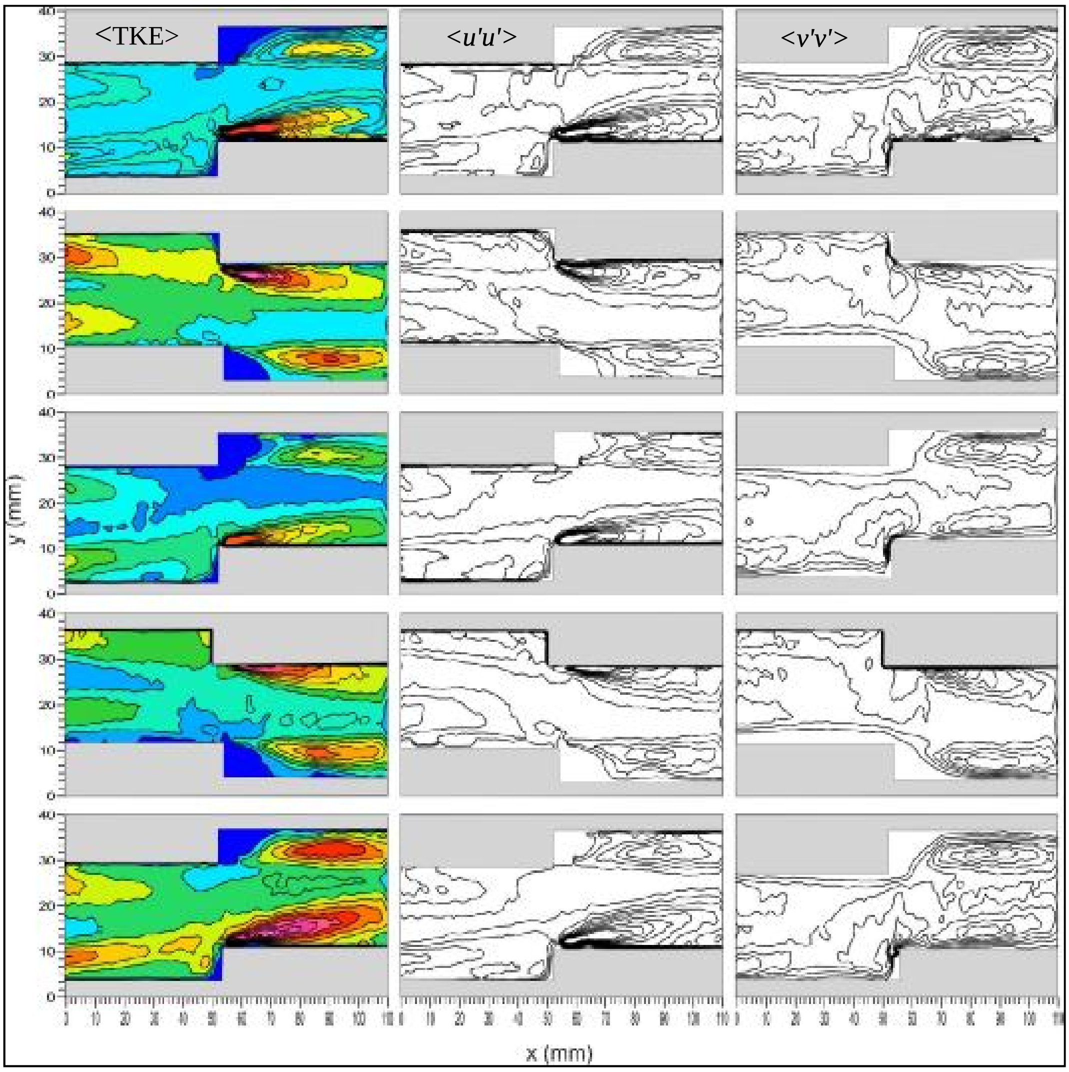

Figure 4.26. Patterns of Turbulent kinetic energy $|<(TKE)_{min}>|$ =0.005, $<\Delta(TKE)>$=0.005, Reynolds streamwise normal stress, $<u'u'>$, Reynolds transverse normal stress $<v'v'>$,for Re=6000**,** channel with phase angle, φ of 0 degree (continued)

The contours of dimensionless turbulent kinetic energy, <TKE> are presented in figures 4. 25 and 4.26 in the channel with phase shift, φ of 0 degree using the PIV data for both Reynolds numbers (Re=4000 and Re=6000). In total of eleven cavities were considered and designated as fields of views (FOV) 1, 2, 3, 4, 5, 6, 7, 8, 9, 10 and 11 respectively as seen in figure. The peak value of dimensionless turbulent kinetic energy, <TKE> contours for Reynolds numbers, Re=4000 and Re=6000 are determined to be 0.134 and 0.0154, as seen in figures 25 and 26.

In the corrugated channel with the phase angle, φ of 0 degree, effect of contours intensity is under the influence of sharp corner of the cavities for all field of views, i.e. it can be understood that kinetic energy of fluid is higher when compared to the other channel with phase angles, φ of 90 degree and 180 degree. High rate of momentum and heat transfer are expected to occur for phase shift, φ of 0 degree. comparing to other cases. Shedding vortices emerging from the sharp corner to increase the dimensionless turbulent kinetic energy, <TKE> for both Reynolds numbers (Re=4000 and Re=6000) along shear layers between core and wake regions. Contours of first field of views are more clear and explicit for the case of phase shift, φ with 90 degree in channel comparison to other channel models (φ=180 degree and 0 degree). It is expected that the rise of heat transfer enhancement is a result of increasing turbulent kinetic energy due to higher rate of shear and velocity fluctuations. The highest turbulent kinetic energy, <TKE> contours values are obviously occurred through the channel with phase angle, φ of 0 degree. It should be remarked additionally that at this point corrugated channel provides that TKE and $< u'u' >$ contours are mostly similar as in all figures including TKE images; furthermore, TKE are much influenced from $< u'u' >$ rather than $< v'v' >$ as mentioned before. An interpretation of these results is that the presence of corrugated shapes in the channel, leading to low level transverse velocity fluctuations $< u'u' >$ which is more dominant on the magnitude of TKE. The intense mixing of the fluid in turbulent flow results in enhancement of heat and momentum transfer between fluid particles as a result of rapid velocity fluctuations, which in turn rises the friction force on the surface as well as the convection heat transfer rate. It also paves the way for the boundary layer to enlarge. Both the friction, f and heat transfer coefficients, h are observed to reach maximum values when the flow is fully turbulent. In this sense, the enhancement in heat transfer in turbulent flow does not come for free. Overcoming the larger friction forces accompanying the higher heat transfer rate may require the use a larger pumping power.

4.1.4. Effect of Reynolds Numbers and Phase Shifts on Contours of the Reynolds Shear Stress

In this section, Reynolds shear stress, $<u'v'/U^2>$ correlations are discussed in terms results taken by two dimensional Particle Image Velocimetry (PIV) for straight channel and three different corrugated channels.

In turbulent flows, velocity components (and other variables) are separated into mean plus fluctuating components. Six new terms appear that are given by fluid density times the averaged product of two velocity components when the equation for mean streamwise velocity component is derived from the Navier– Stokes equation. These new terms are called turbulent stresses or Reynolds stresses since they have the same units as stress (force/area). Reynolds stress tensor with Reynolds normal stress components and Reynolds shear stress components are defined just as viscous stresses can be written as a tensor. Although Reynolds stresses are not true stresses, they have qualitatively similar effects as do viscous stresses, but as a result of the large chaotic vortical motions of turbulence rather than the microscopic molecular motions that underlie viscous stresses (Çengel, 2007).

The root-mean-square calculations of streamwise, $<u_{rms}>$ and transverse, $<v_{rms}>$ components of velocity and Reynolds stress correlation were obtained from PIV data using the following equations:

$$u_{rms} \equiv < u >_{rms} \equiv \left[\frac{1}{N}\sum_{n=1}^{N}[u_n(x,y) - < u(x,y) >]^2\right]^{1/2}$$

$$v_{rms} \equiv < v >_{rms} \equiv \left[\frac{1}{N}\sum_{n=1}^{N}[v_n(x,y) - < v(x,y) >]^2\right]^{1/2}$$

$$< u'v' > = \frac{1}{N}\sum_{n=1}^{N}[u_n(x,y) - < u(x,y) >]\,[v_n(x,y) - < v(x,y) >]$$

Where N (N=1000 in the present study) is the total number of instantaneous images used for the time-averaged data and refers to the instantaneous images.

In order to determine detailed information on the flow by obtaining instantaneous flow field, the PIV technique was employed to capture images of instantaneous velocity vectors. By averaging instantaneous images of velocity, the time-averaged velocity vector field and Reynolds stress correlations and other turbulent statistics were obtained.

Momentum, mass, and energy to other regions of flow have been carried away much more rapidly than molecular diffusion by virtue of the swirling eddies which greatly enhance mass, momentum, and heat transfer. As a result, turbulent flow is associated with much higher values of friction, heat transfer, and mass transfer coefficients (Çengel, 2007). On the other hand experimental studies present that this is not the case, and the shear stress is much larger due to the turbulent fluctuations. Furthermore, it is convenient to think of the turbulent shear stress as consisting of two parts: the laminar component, which accounts for the friction between layers in the flow direction and the turbulent component, which accounts for the friction between the fluctuating fluid particles and the fluid body.

The contours of the Reynolds shear stress, $\langle u'v'/U^2\rangle$ root mean square of streamwise, $\langle u_{rms}\rangle/U$ and transverse velocity components, $\langle v_{rms}\rangle/U$ normalized by free-stream velocity, U in channel are presented in Figure 4.27 and 4.28 for both Reynolds number (Re=4000 and Re=6000). The first, second and third column of the figures demonstrate the dimensionless Reynolds shear stress, $\langle u'v'/U^2\rangle$ contours, normalized streamwise velocity components, $\langle u_{rms}\rangle/U$ and the normalized transverse velocity components, $\langle v_{rms}\rangle/U$, respectively. The minimum and incremental values of dimensionless Reynolds shear stress, $\langle u'v'/U^2\rangle$ contours were taken as ±0.001 and 0.001, respectively. For channel with phase angle, φ of 180 degree, the solid and dashed lines present positive and negative Reynolds shear stress, $\langle u'v'/U^2\rangle$ contours, respectively. It is obvious from the figures 4.27, 4.28 that the negative and positive Reynolds shear stress, $\langle u'v'/U^2\rangle$ contours are symmetrical along the centerline of the channel for both Reynolds numbers. The contours of Reynolds shear stress, $\langle u'v'/U^2\rangle$ are as a result of combination of root mean square of normalized streamwise velocity components, $\langle u_{rms}\rangle/U$ and root mean square of transverse velocity components, $\langle v_{rms}\rangle/U$ which is also mentioned before in this section.

Magnitudes of the dimensionless Reynolds shear stress, $<u'v'/U^2>$ also increases with increasing the Reynolds number. The maximum Reynolds shear stress, $<u'v'/U^2>$ has the value of 0.011 for Reynolds number, Re=4000, but this Reynolds shear stress increases to a value of 0.013 for Reynolds number, Re=6000. As a result of increasing Reynolds number, the rate of fluctuating instantaneous velocities also increase to further level. The peak value of the dimensionless Reynolds shear stress contours, $<u'v'/U^2>$ are withdrawn from the sharp edge of cavities and these peak points move close to the upper and lower walls of cavity similar flow structures occur in all cavities as seen in figures 4.27 and 4.28 clearly. Since the peak values of the normalized streamwise velocity components, $<u_{rms}>/U$ occur apart from the sharp edge. Streamwise velocity components, $<u_{rms}>/U$ is more dominant on the distribution of the dimensionless Reynolds shear stress, $<u'v'/U^2>$ contours. Furthermore, the peak value of transverse velocity components $<v_{rms}>/U$ is developed in the vicinity of the sharp edge of the corner.

The negative and positive dimensionless Reynolds shear stress, $<u'v'/U^2>$ values are symmetrical along the centerline of the cavity for both values of Reynolds numbers because of the geometrical symmetry. It can be seen in figure 4.28 that dimensionless Reynolds shear stress contours, do not change rapidly especially after the third measuring cross-section of cavity as mentioned earlier.

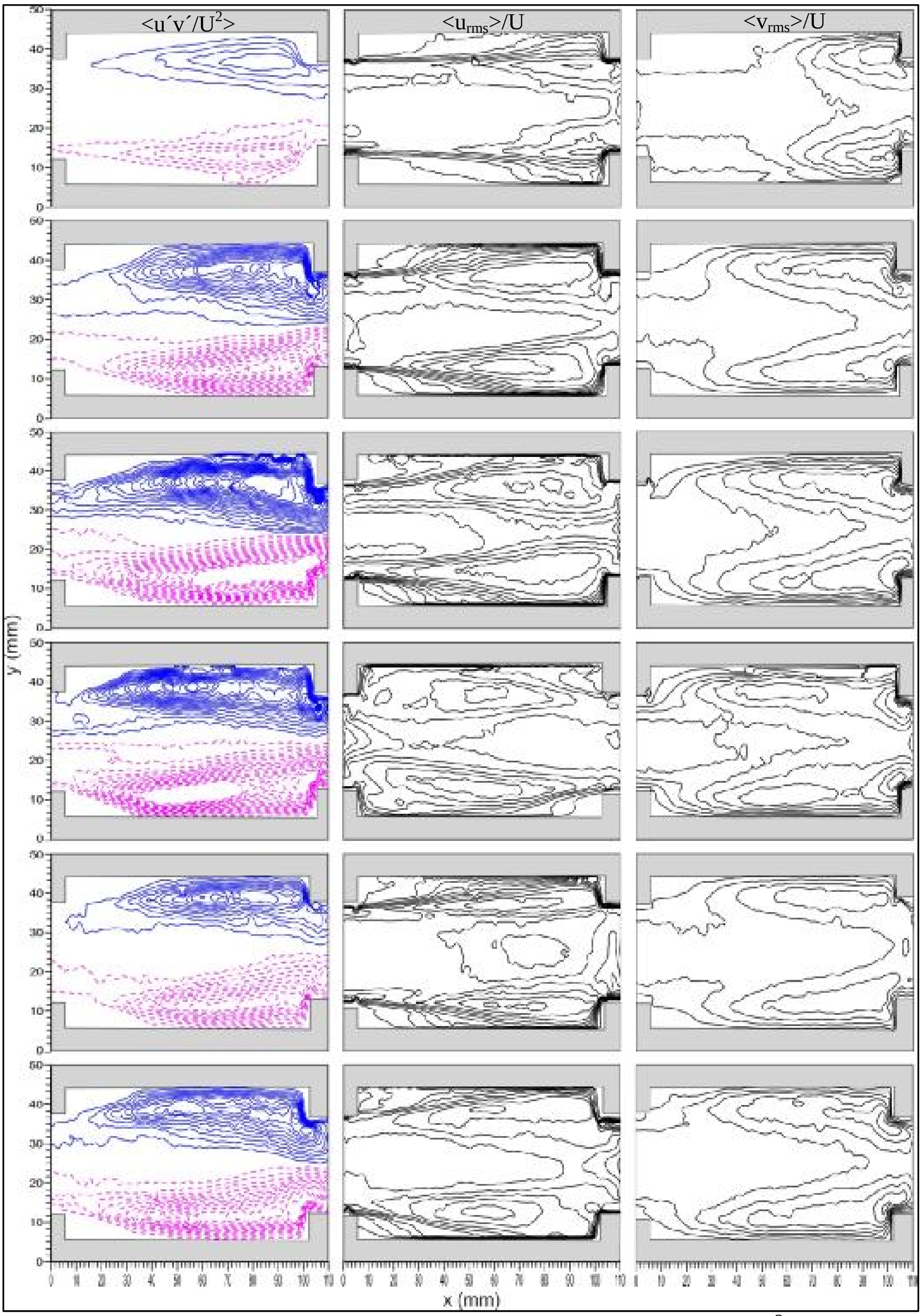

Figure 4.27. Patterns of Reynolds stress correlations, $| < (u´v´/U^2)_{min}>|$ =0.001 $<\Delta(u´v´/U^2)>$=0.001 for Re=4000, channel with phase angle, φ of 180 degree

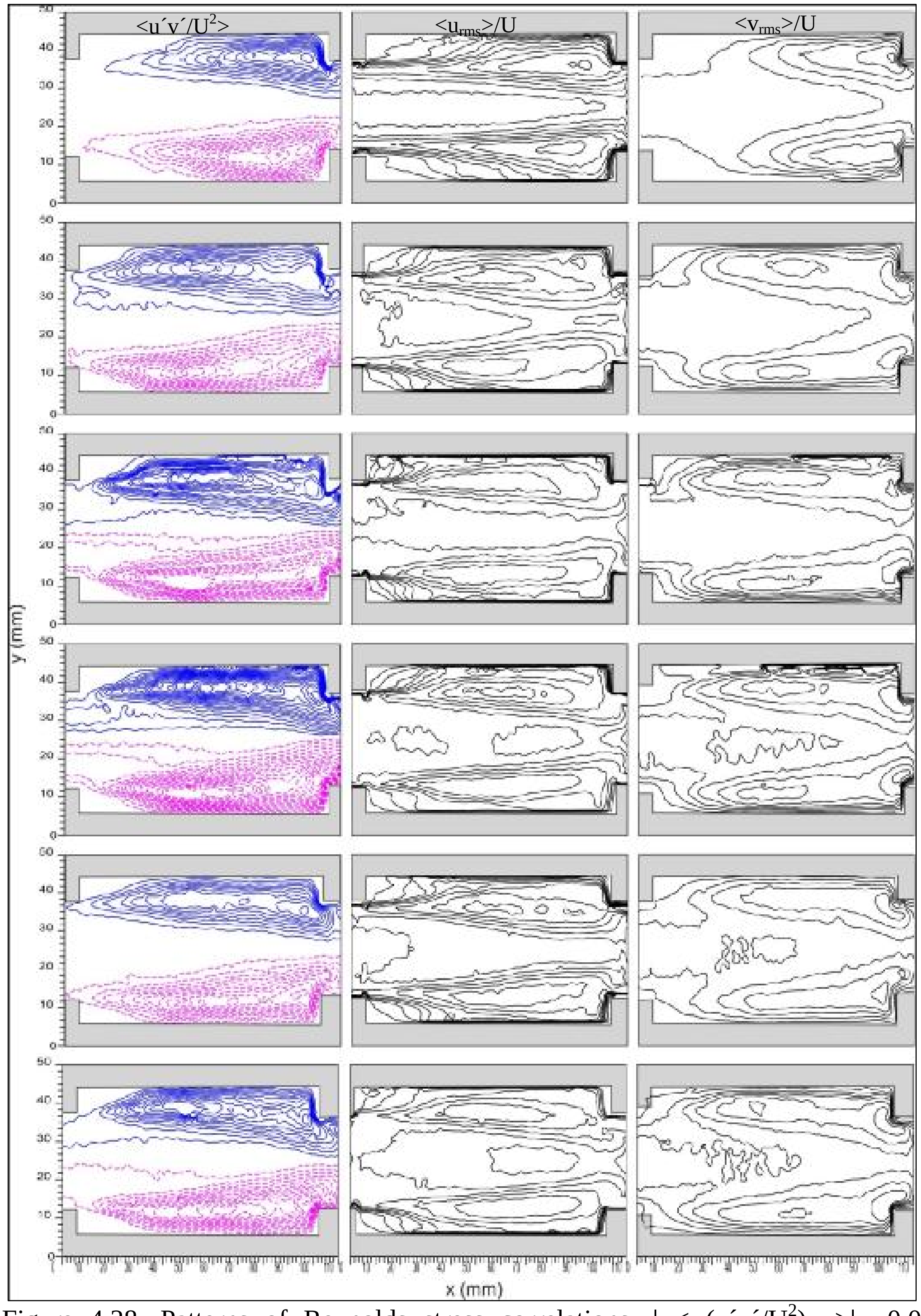

Figure 4.28. Patterns of Reynolds stress correlations, $| < (u´v´/U^2)_{min}>|$ =0.001 $<\Delta(u´v´/U^2)>$=0.001 for Re=6000, channel with phase angle, φ of 180

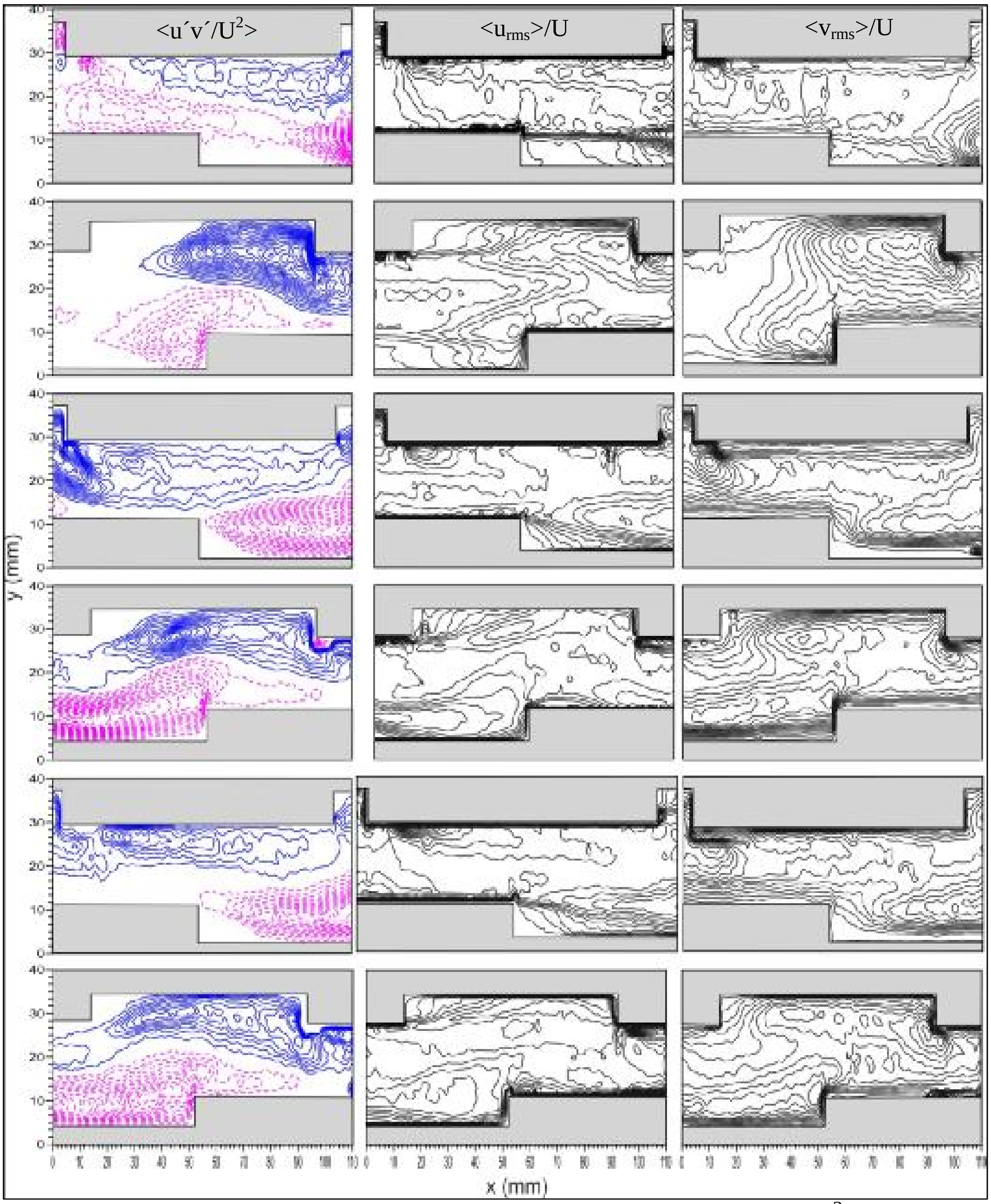

Figure 4.29. Patterns of Reynolds stress correlations, $| <(u'v'/U^2)_{min}>| = 0.001$ $<\Delta(u'v'/U^2)> = 0.001$ for Re=4000, channel with phase angle, φ of 90 degree

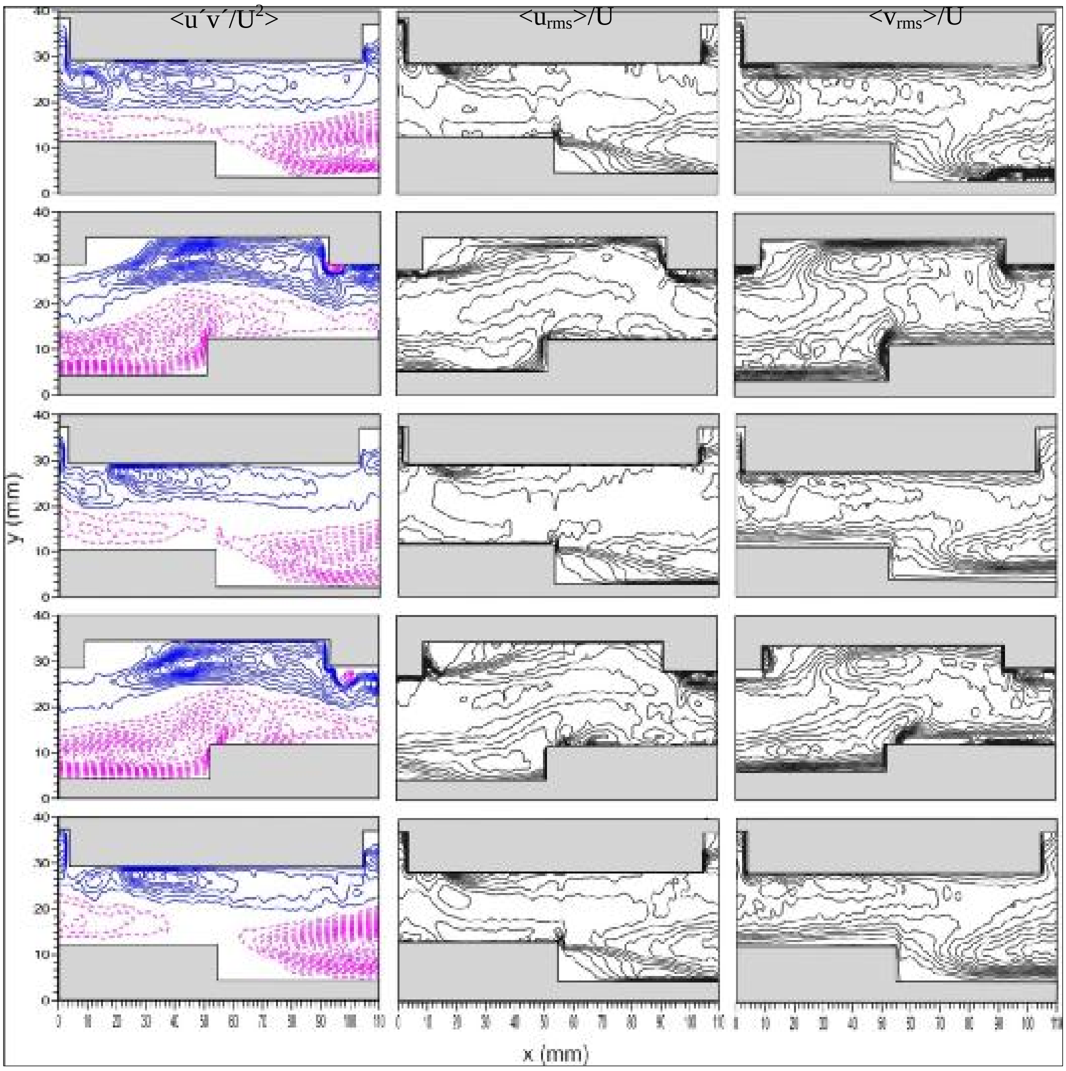

Figure 4.29. Patterns of Reynolds stress correlations, $|<(u'v'/U^2)_{min}>|$ =0.001 $<\Delta(u'v'/U^2)>$=0.001 for Re=4000, channel with phase angle, φ of 90 degree (continued)

Distributions of dimensionless Reynolds shear stress correlations, $<u'v'/U^2>$, root mean square of normalized streamwise and transverse velocity components, $<u_{rms}>/U$ and $<v_{rms}>/U$ are presented in Figures 4.29 and 4.30 for both Reynolds numbers (Re=4000 and Re=6000) for channel with phase angle, φ of 90 degree. The solid and dashed lines dimensionless Reynolds shear stress correlations, $<u'v'/U^2>$ illustrate positive and negative patterns of Reynolds shear stresses, respectively. Minimum positive and negative numerical values of dimensionless Reynolds shear stress correlations, $<u'v'/U^2>$ are taken as ±0.001 and incremental numerical value is taken as 0.001. The first, second and third columns in all figures in this subsection present patterns of the dimensionless Reynolds shear stress correlations, $\langle u'v'/U^2 \rangle$, root mean square of normalized streamwise velocity components $\langle u_{rms} \rangle/U$ and, root mean square of transverse velocity components, $\langle v_{rms} \rangle/U$, respectively. The Reynolds stress concentrations were used to explain the characteristics of the flow such as velocity distributions, corresponding vorticity contours and streamline topology.

Reynolds shear stress correlations, $\langle u'v'/U^2 \rangle$ are magnified further starting from the cavity of entry region (FOV3) as seen in figure 4.30 generally. In addition, intensity of the Reynolds shear stress correlations, $\langle u'v'/U^2 \rangle$ occur in the second half of cavities increase starting from the cavity until the last cavity especially aforementioned region (the onset or left hand side of cavities). This result resemble with distribution of velocities throughout the corrugated channel. For channel with phase angle, φ of 90 degree, as 0.012 and 0.014, the maximum value of Reynolds shear stress correlations, $\langle u'v'/U^2 \rangle$ are determined for both Reynolds numbers, Re=4000 and 6000, respectively. As a result, Reynolds stress contours in the corrugated channels are declaration of energetic core flow compared to the straight channel.

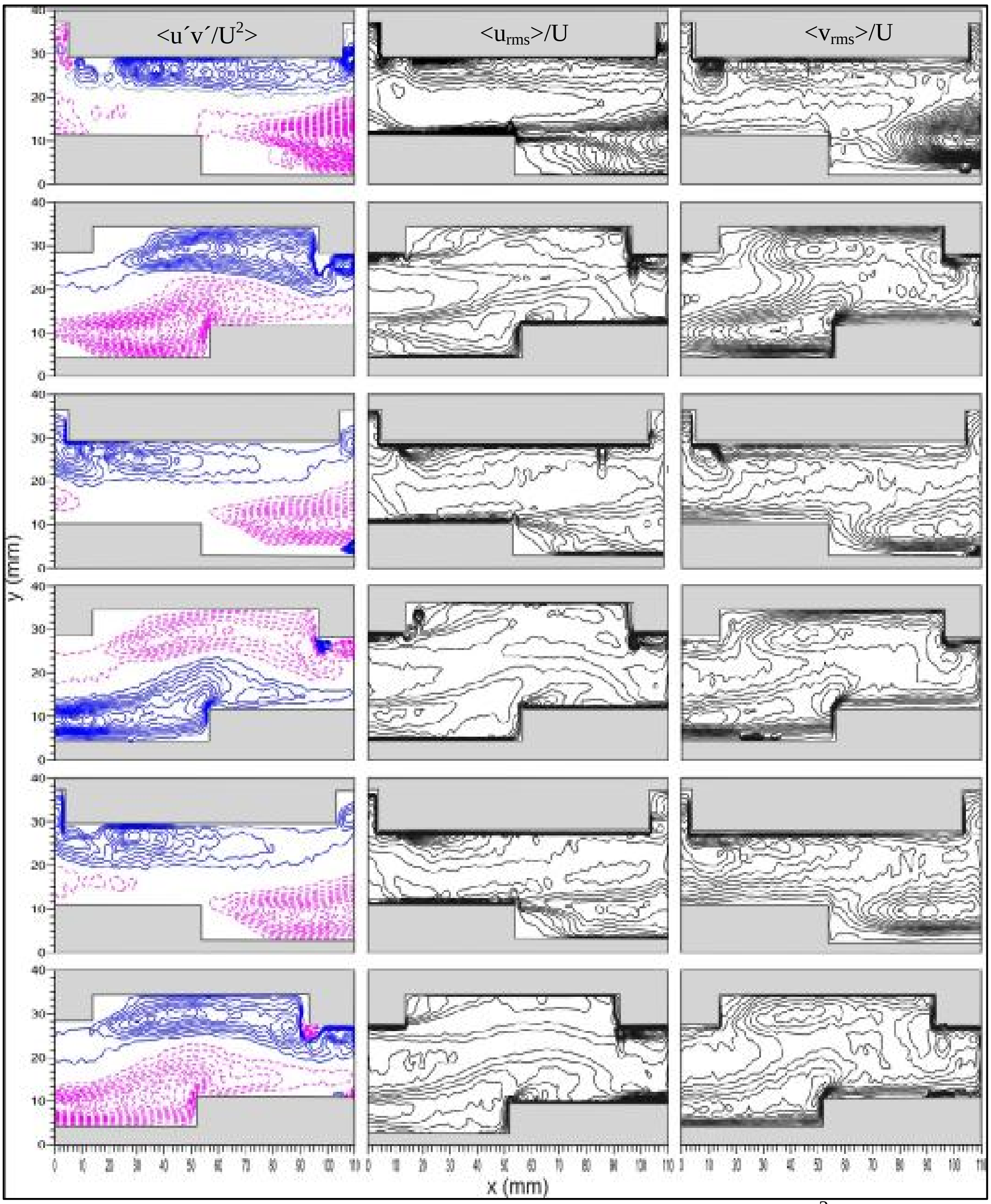

Figure 4.30. Patterns of Reynolds stress correlations, $| < (u'v'/U^2)min>| = 0.001$ $<\Delta(u'v'/U^2)>=0.001$ for Re=6000, channel with phase angle, φ of 90 degree

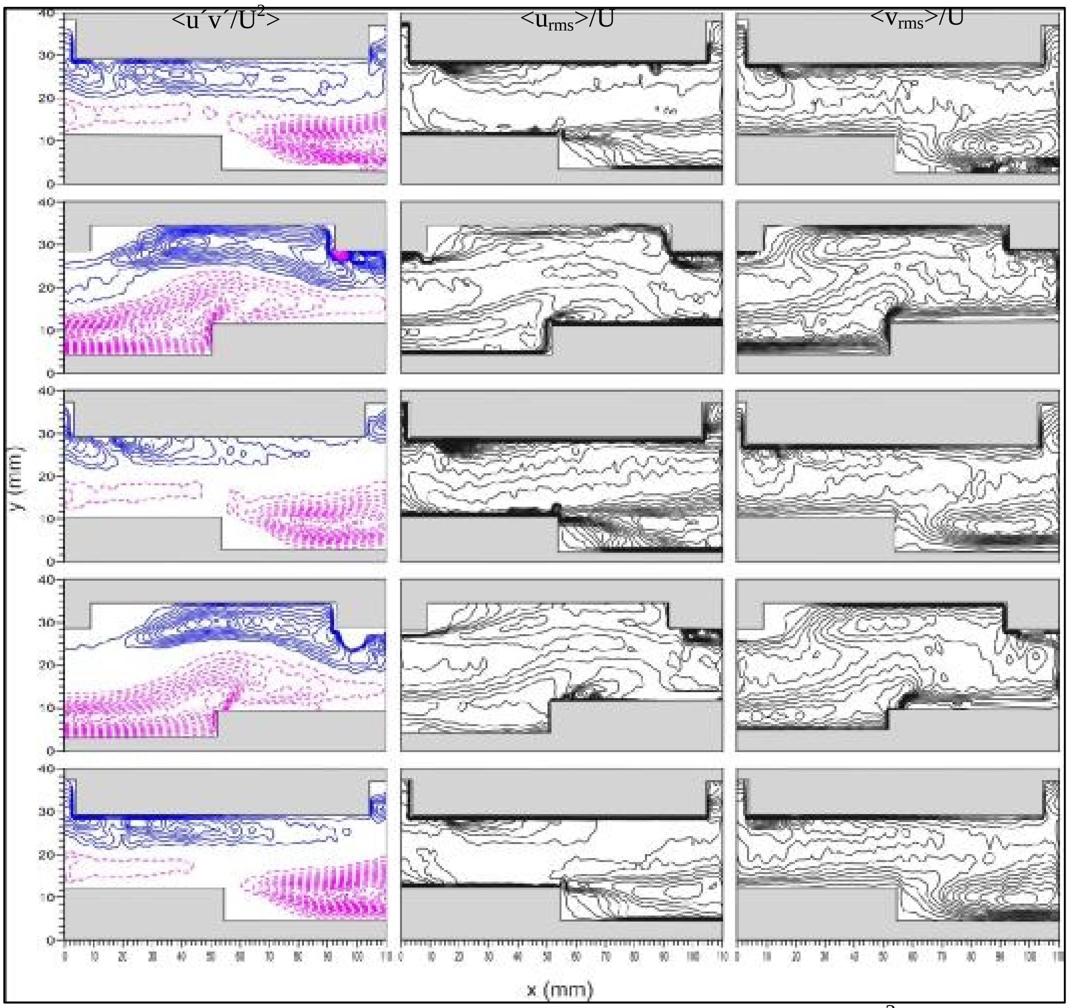

Figure 4.30. Patterns of Reynolds stress correlations, $| <(u'v'/U^2)min>|$ =0.001 $<\Delta(u'v'/U^2)>$=0.001 for Re=6000, channel with phase angle, φ of 90 degree (continue)

Dimensionless Reynolds shear stress correlations, $<u'v'/U^2>$, in successive field of views of the channel with phase angle, φ of 0 degree for Reynolds numbers, Re=4000 and Re=6000 are presented in Figures 4.31 and 4.32. In the first, second and third column of Figures 4.31 and 4.32 the dimensionless Reynolds shear stress correlations, $<u'v'/U^2>$, normalized streamwise velocity components, $<u_{rms}>/U$ and the transverse velocity components, $<v_{rms}>/U$, are presented respectively.

As mentioned before distribution of the negative variables are designated by a dash line and distributions of the positive variables are designated by solid lines. Minimum and incremental values of normalized Reynolds shear stress correlations, $<u'v'/U^2>$ contours, are ±0.0005 and 0.0005, respectively.

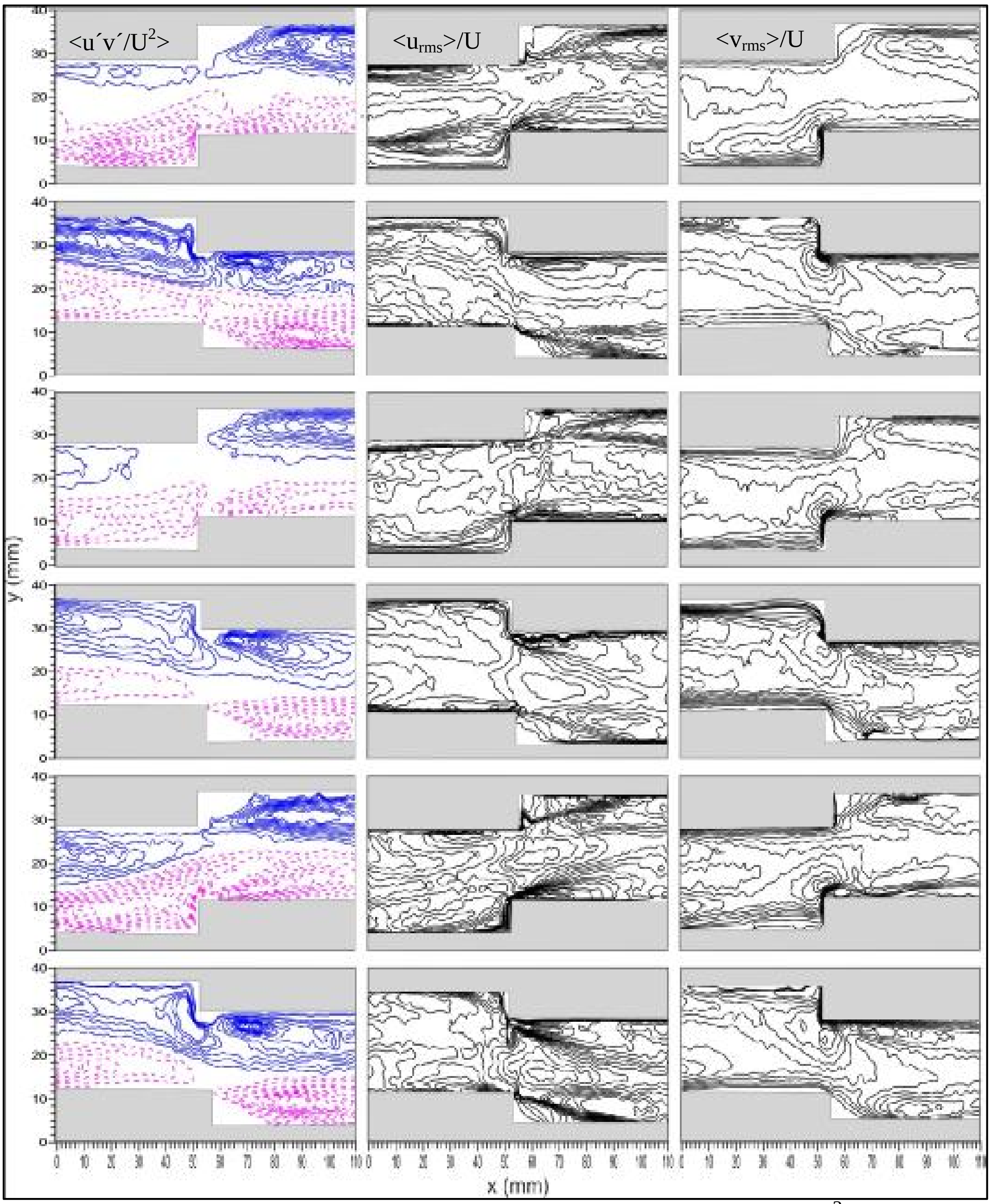

Figure 4.31. Patterns of Reynolds stress correlations, $| < (u'v'/U^2)_{min}>| = 0.001$ $<\Delta(u'v'/U^2)>=0.001$ for Re=4000, channel with phase angle, φ of 0 degree

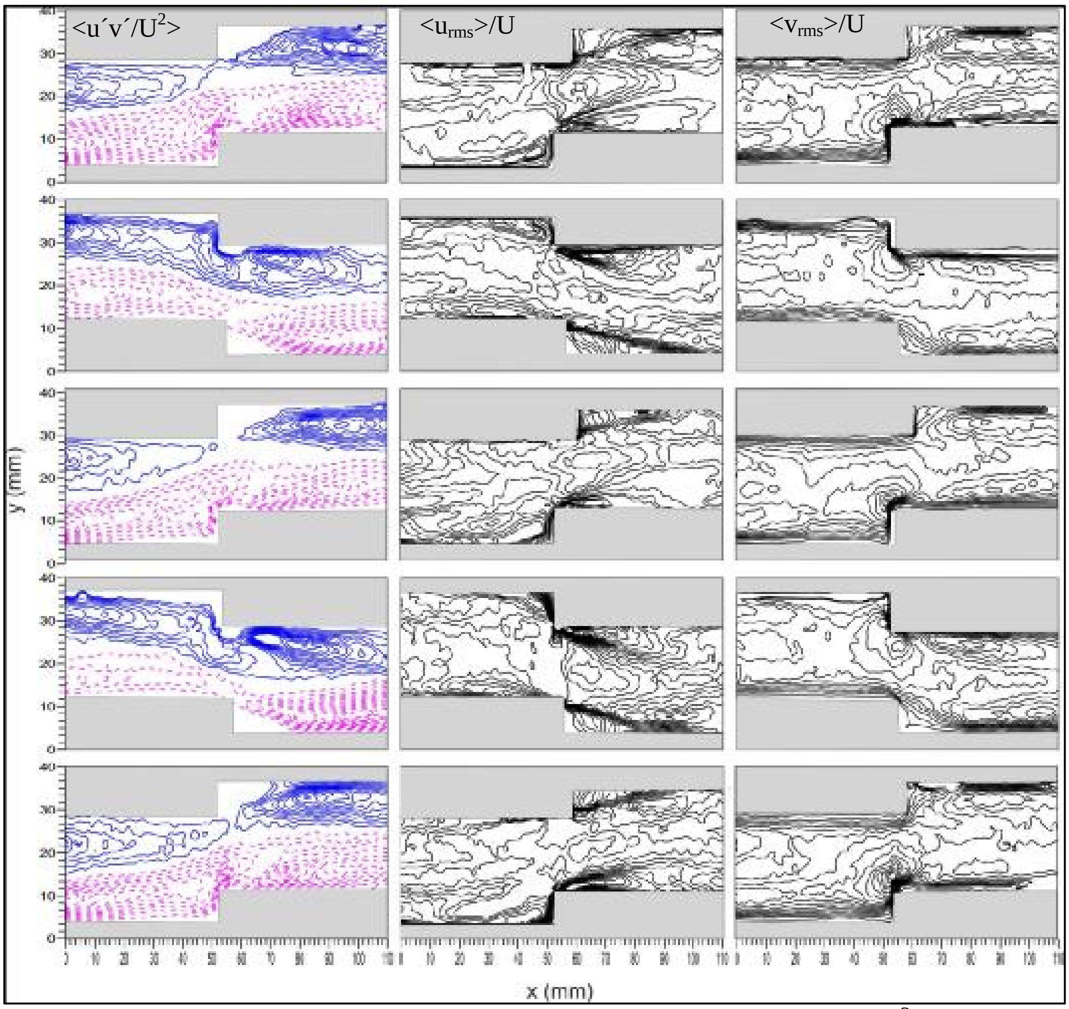

Figure 4.31. Patterns of Reynolds stress correlations, $|<(u'v'/U^2)_{min}>| = 0.001$ $<\Delta(u'v'/U^2)> = 0.001$ for Re=4000, channel with phase angle, φ of 0 degree (continued)

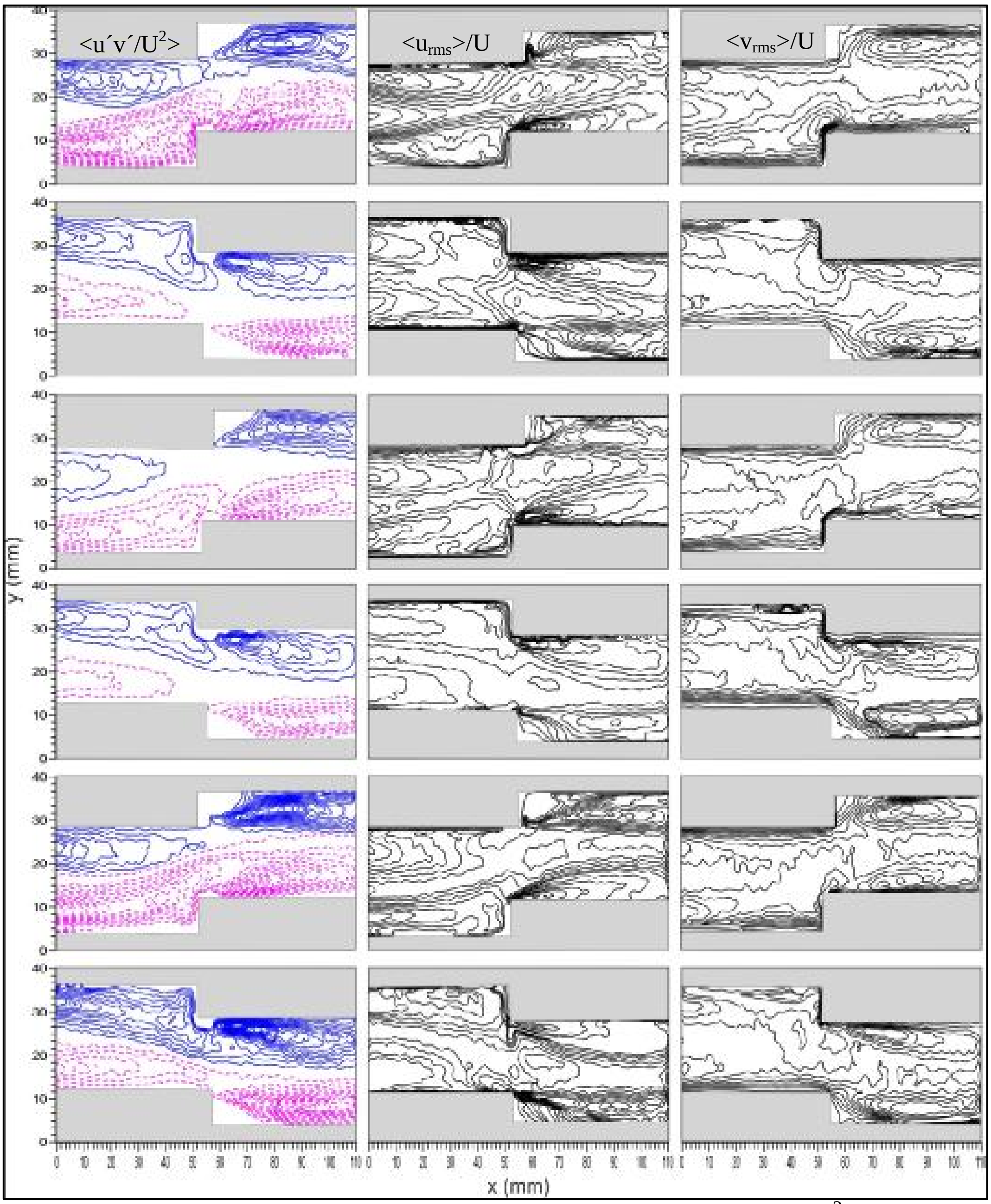

Figure 4.32. Patterns of Reynolds stress correlations, $| < (u'v'/U^2)_{min}>| = 0.001$ $<\Delta(u'v'/U^2)> = 0.001$ for Re=6000, channel with phase angle, φ of 0 degree

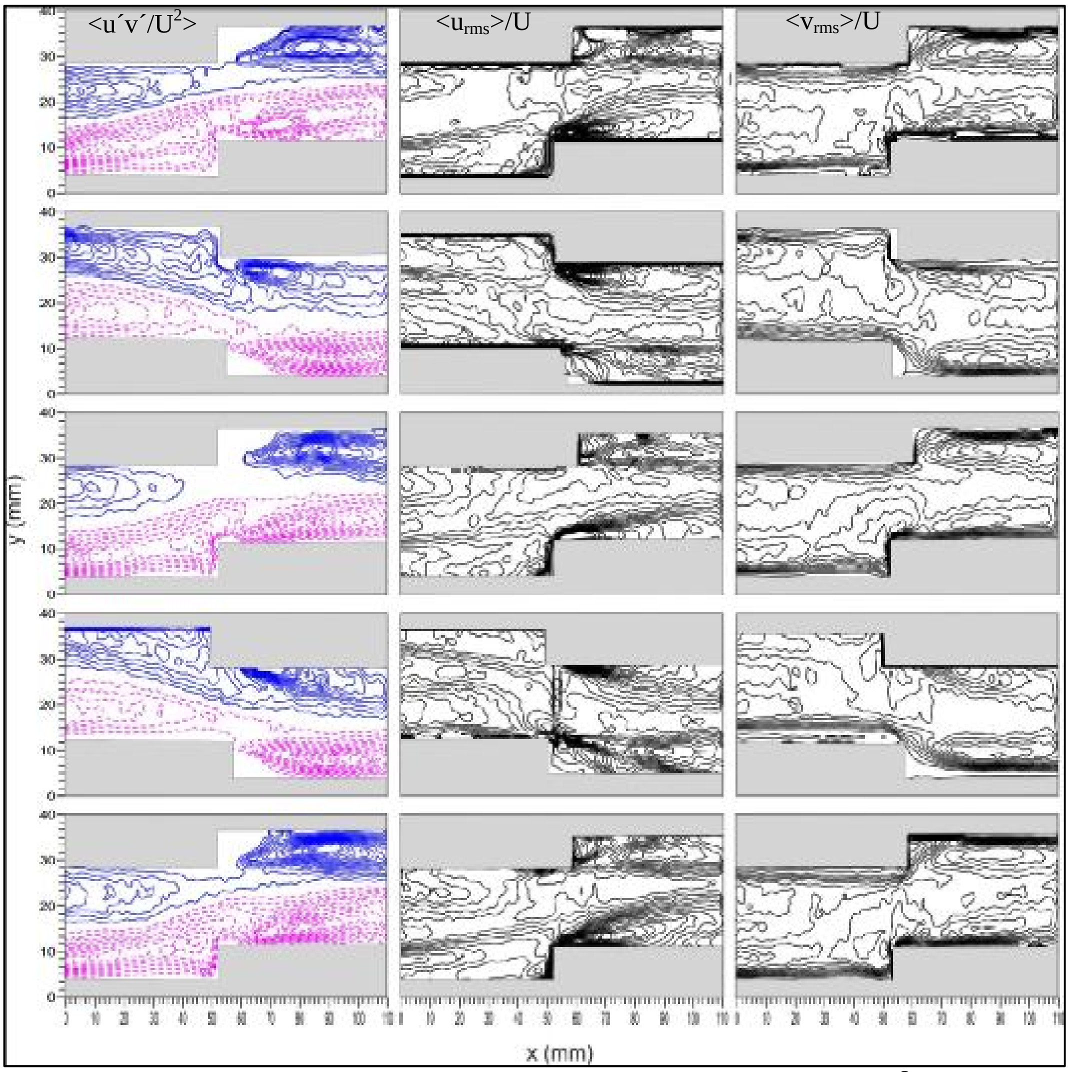

Figure 4.32. Patterns of Reynolds stress correlations, $| <(u'v'/U^2)_{min}>| = 0.001$ $<\Delta(u'v'/U^2)> = 0.001$ for Re=6000, channel with phase angle, φ of 0 degree (continued)

The maximum Reynolds shear stress correlations, $<u'v'/U^2>$ contour has the value of 0.015 for the Reynolds number, Re=4000, but this value increases to a value of 0.017 for the Reynolds number, Re= 6000 for channel with phase angle, φ of 0 degree. As mentioned above dimensionless Reynolds shear stress correlations, $<u'v'/U^2>$ is continuously increased with the Reynolds number proportionally. Reynolds shear stress, $<u'v'/U^2>$ contours get the maximum value where the effects of the sharp corner are available. As a result of the effect of sharp edges, higher velocity gradients take place in the region of cavities.

For both Reynolds numbers, Re=4000 and Re=6000, peak points location of root mean square of normalized streamwise velocity contours, $\langle u_{rms}\rangle/U$ are shifted from the edges of sharp corner close to upper and lower wall. This phenomenon occurs successively beginning from the first cavity until the last cavity. On the other hand, peak points of root mean square of transverse velocity contours, $\langle v_{rms}\rangle/U$ are located at sharp corner edges and close to upper and lower walls for both cases of Reynolds numbers, Re=4000 and Re=6000. Furthermore, peak points of Reynolds shear stress contours, $\langle u'v'/U^2\rangle$ occur at almost the same location for the same field of views but different Reynolds numbers since root mean square of streamwise velocity contours, $\langle u_{rms}\rangle/U$ are more dominant rather than root mean square of transverse velocity, $\langle v_{rms}\rangle/U$ for channel with phase angle, φ of 0 degree. As a result of the effect of edges of sharp corners, higher velocity gradients take place in the region of cavities.

It can be concluded that the Reynolds shear stress, $\langle u'v'/U^2\rangle$ distributions that both normalized streamwise, $\langle u_{rms}\rangle/U$ and transverse, $\langle v_{rms}\rangle/U$ velocity fluctuations are reduced by increasing phase shift. Furthermore, it should also be implied that the Reynolds shear stress, $\langle u'v'/U^2\rangle$ values are low for corrugated channel with phase angle of 180 degree compared to the channel with the phase angle of 90 degree likewise the Reynolds shear stress, $\langle u'v'/U^2\rangle$ values are low for the channel with the phase angle of 90 degree compared to the corrugated channel with phase angle of 0 degree. It was noticed from figures that dimensionless Reynolds shear stress, $\langle u'v'/U^2\rangle$ and normalized streamwise velocity components, $\langle u_{rms}\rangle/U$ contours are mostly similar, furthermore dimensionless Reynolds shear stress, $\langle u'v'/U^2\rangle$ are mostly affected from normalized streamwise velocity components, $\langle u_{rms}\rangle/U$ rather than transverse velocity components, $\langle v_{rms}\rangle/U$ as emphasized previously. As a conclusion, flow in corrugated channel is especially in streamwise direction, i.e. the side walls impact do not affect the flow structure along the centre of model due to high distance between side walls.

4.1.5. Effect of Reynolds Numbers and Phase Shifts on Contours of Vorticity

In this section, the time-averaged vorticity, $<\omega>$ contours are discussed in accordance with the results of two dimensional Particle Image Velocimetry (PIV) for straight channel and three different corrugated channels. In order to determine detailed information on the flow by obtaining instantaneous flow patterns of vorticity, $<\omega>$ the PIV technique was employed.

Time-averaged vorticity;

$$< \omega > = \frac{1}{N} \sum_{n=1}^{N} \omega_n \, (x, y)$$

Where N is the total number of instantaneous images (N=1000 for the present study) used for the time-averaged values and refers to the instantaneous images.

Measurement of unsteady flow fields, for instance, in shear flows or wake region, is one of the most complicated problems in the area of fluid dynamics. The objective of the present study is to investigate the hydrodynamics of vortical flow in the region boundary layer coming very close to the surface of cavities including sharp corners. To get the details of the flow mechanisms in wake and shear flow regions can provide worthy of knowledge for establishing the method to control the flow in order to improve the thermal performance of heat exchangers with corrugated channels. The dynamics of vortices along shear layers between core and wake regions stimulate the transverse exchange of mass, momentum as well as heat. Verifications of the structure of turbulent flow along the shear layers were done using data which composed of time series of streamwise velocity distributions.

Time averaged vorticity, $<\omega>$ contours for channel with phase angles, φ of 180 degree, 90 degree and 0 degree are shown in figures 4.33,4.34 and 4.35 respectively. The positive (counterclockwise) vorticity layers and the negative (clockwise) vorticity layers are drawn as a solid and dashed line, respectively. For all corrugated channels, the minimum and the incremental values of the vorticity are $\omega=\pm0.3s^{-1}$ and $\Delta\omega=0.3s^{-1}$, respectively.

The first column represents time averaged vorticity, $<\omega>$ contours for the Reynolds number 4000 and the second column shows represents time averaged vorticity, $<\omega>$ contours for the Reynolds number 6000 for all corrugated channels (i.e. for phase shifts, φ=180 degree, 90 degree, and 0 degree).

As can be seen from figure 4.33, time averaged vorticity, $<\omega>$ contours do not dramatically change with respect to different field of views (i.e. from FOV1 to FOV6 with phase angle, φ of 180 degree) or it can be said that they resemble each other at the same Reynolds number. It is observed that the vorticity layers are symmetric with each other according to the plane of symmetry of the cavity for channel with phase angle, φ of 180 degree. However time averaged vorticity, $<\omega>$ contours are asymmetry for other cases owing to the geometrical parameters. It is clearly seen that the vorticity layers beginning from the sharp corner edge of the cavities expand in the flow direction along the shear layer. A high level of vortices, $<\omega>$ developed on the sharp corner edges of the cavity due to the interaction between shear layer and wall for all corrugated channels which have been studied within the scope of the present study. Furthermore, it can be seen from figures 4.5 alteration of velocity profiles along transverse direction causes higher vorticity, $<\omega>$ values in the region closed to the shear layers.

In order to understand the effect of the Reynolds number on the flow structure in detail, it is better to compare columns of the figures which show the time averaged vorticity, $<\omega>$ contours with reference to foregoing Reynolds numbers. When the vorticity, $<\omega>$ contours are investigated, the peak magnitude of vorticity, $<\omega>$ increases with increasing the Reynolds number, Re. In the case of the corrugated heat exchangers, development of energetic vortices in cavities results in better flow mixing between wake and main flow regions and hence heat transfer increase in the junction region.

For all phase angles, φ positive (counter-clockwise) and negative (clockwise) vorticity, $<\omega>$ contours are lied along upper and lower walls in cavities, respectively. Because direction of vorticity, $<\omega>$ do not changes due to insufficient cavity dept from leading to trailing corner as opposed of lid driven cavities. Furthermore, jet-like flow is not occurred at phase angle, φ of 180 degree. However, jet-like flow is expected to reveal for higher Reynolds numbers, Re as seen in figures 4.34 and 4.35 although jet-like flow is not clearly existed with phase angles, φ of 90 degree and 0 degree in the present study.

For the case of phase angle, φ with 90 degree in channel both clockwise and counter clockwise vortices, $<\omega>$ developed at the regions close to the lower wall of the cavity with increasing the Reynolds number, Re as seen in field of views such as FOV1, FOV3, FOV5, FOV7, FOV9, and FOV11. Similarly, anticlockwise vortices, $<\omega>$ are emanated close to the upper wall regions of cavity for field of views, FOV2, FOV4, FOV6, FOV8, and FOV10.

The energy and momentum interaction with the shear layer at the leading edge is amplified as it is transported to the trailing corner of the cavity as results better enhancement of heat transfer for phase angles, φ of 90 degree and 0 degree.

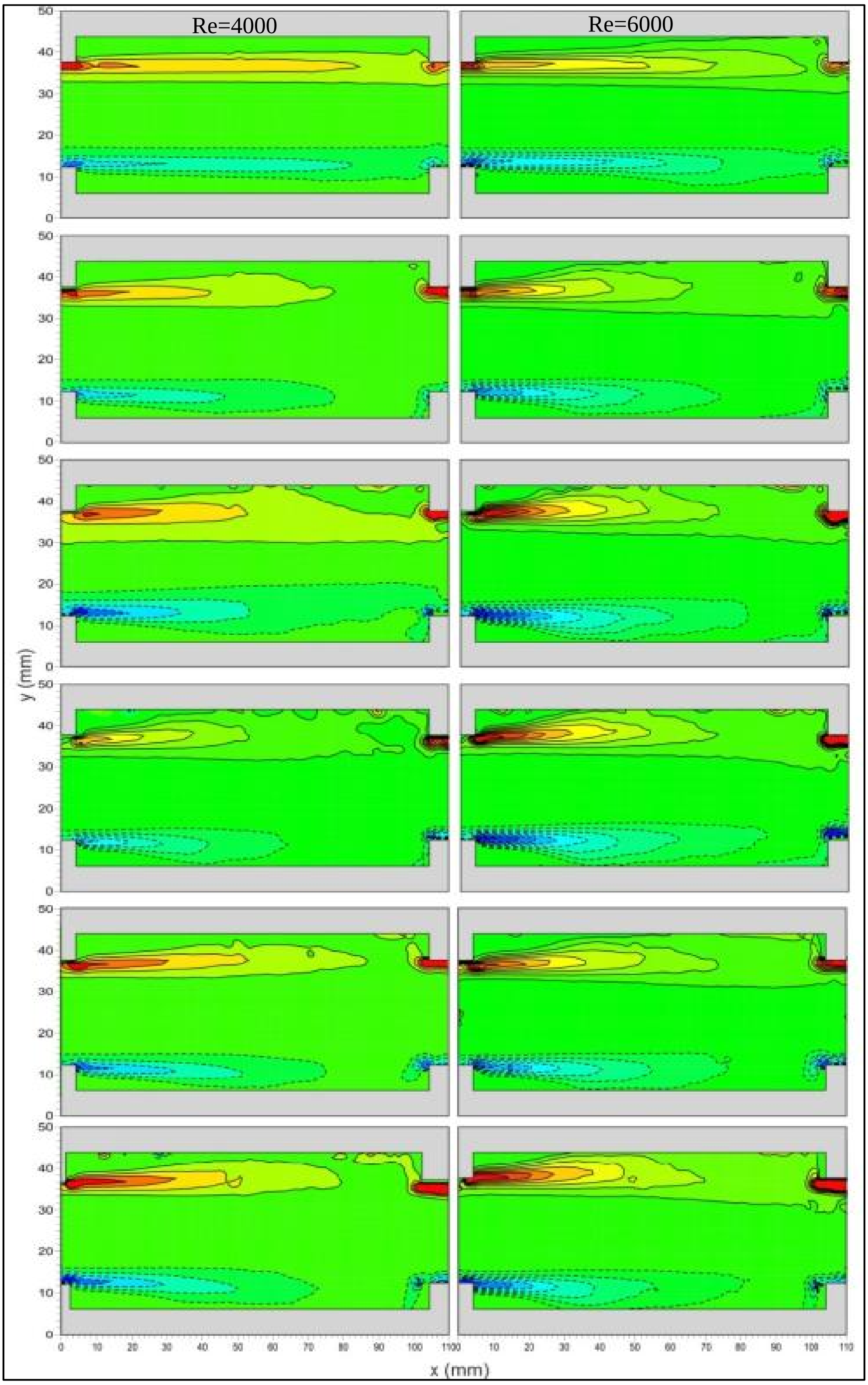

Figure 4.33. Patterns of time-averaged vorticity, $|<\omega_{min}>|= 0.3$, $<D\omega>=0.3$ for channel with phase angle, φ of 180 degree

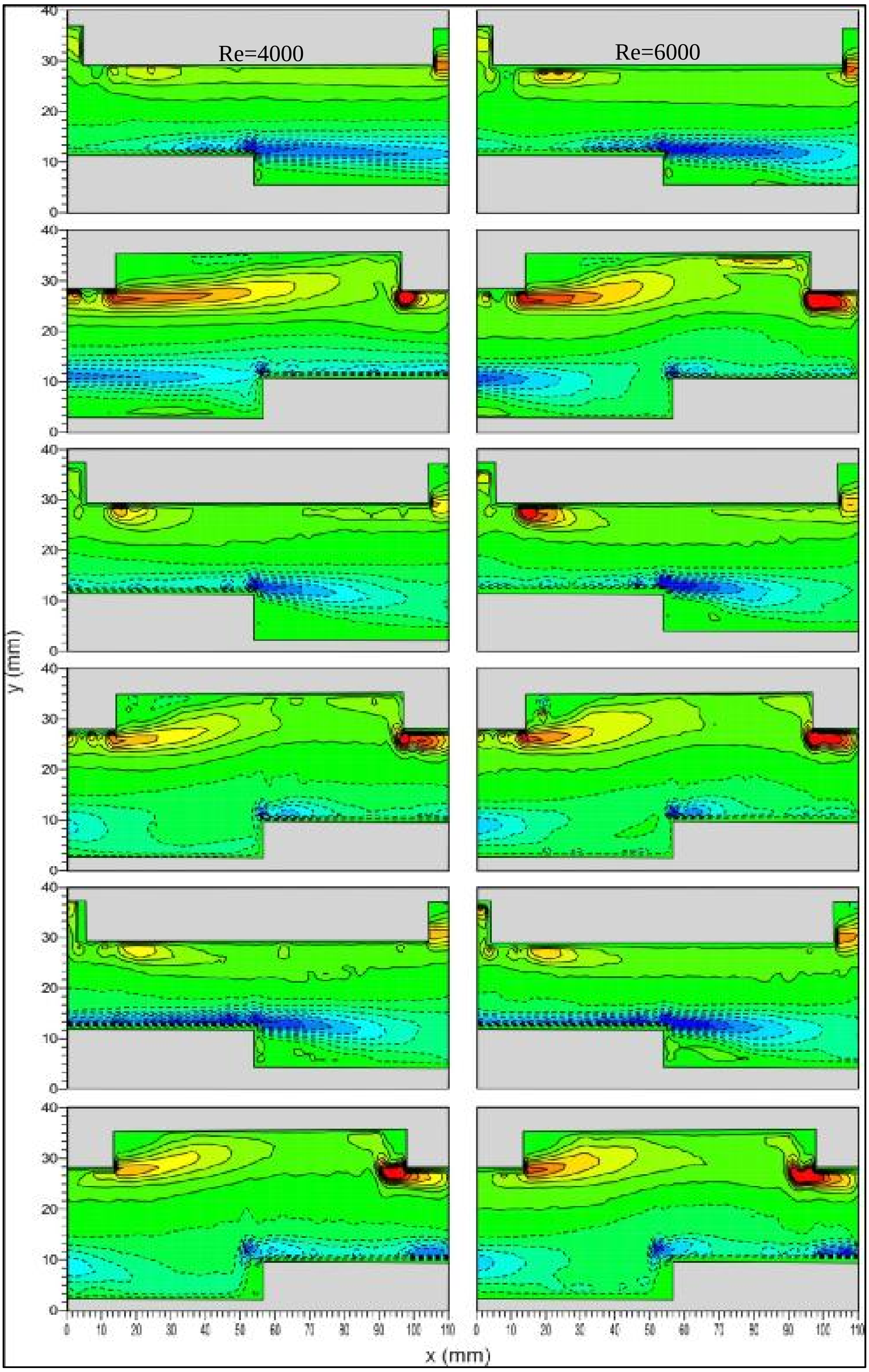

Figure 4.34. Patterns of time-averaged vorticity, $|\langle w_{min} \rangle| = 0.3$, $\langle Dw \rangle = 0.3$ for channel with phase angle, φ of 90 degree

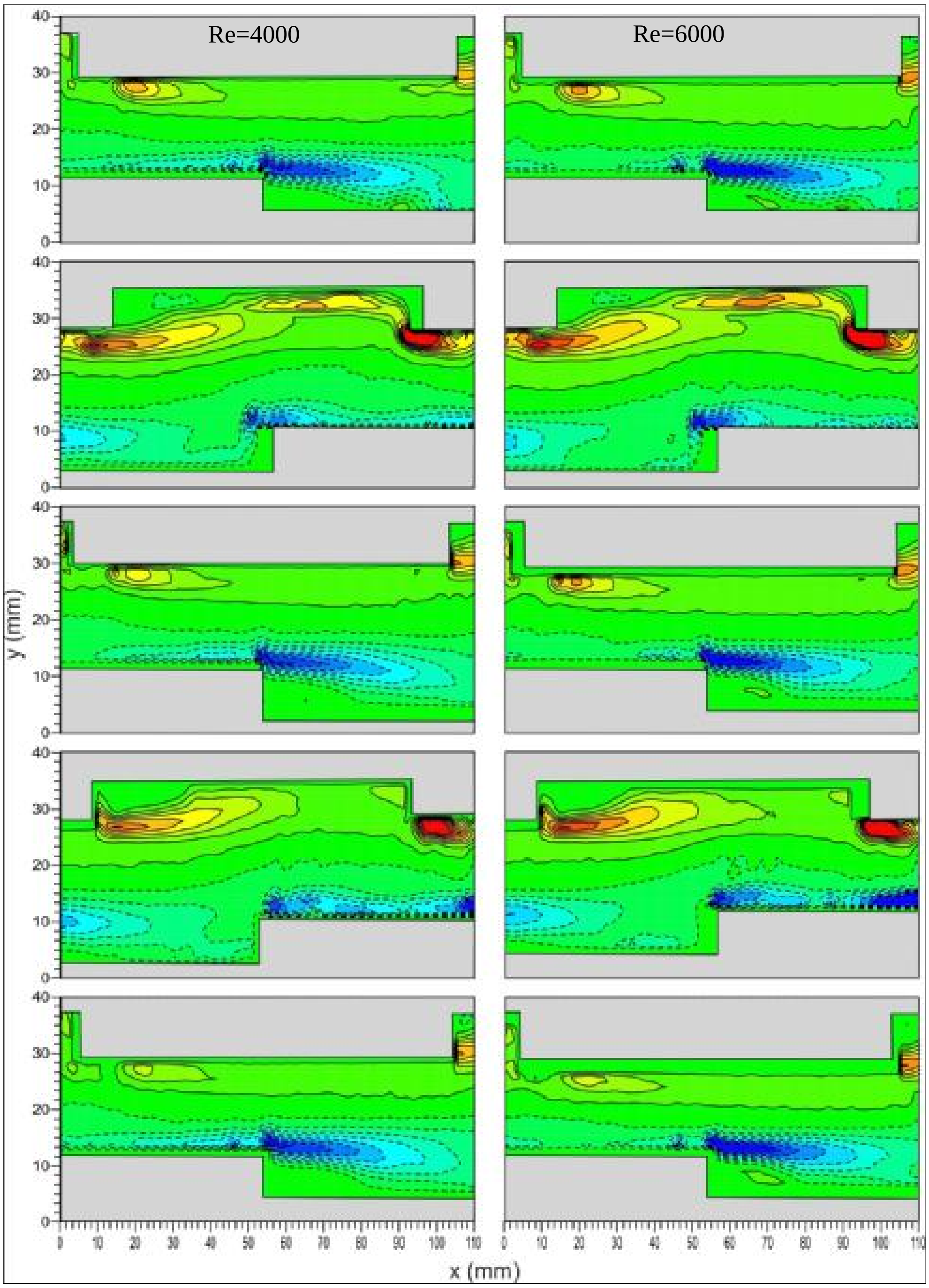

Figure 4.34. Patterns of time-averaged vorticity, $|<\omega_{min}>|= 0.3$, $<D\omega>=0.3$ for channel with phase angle, φ of 90 degree (continued)

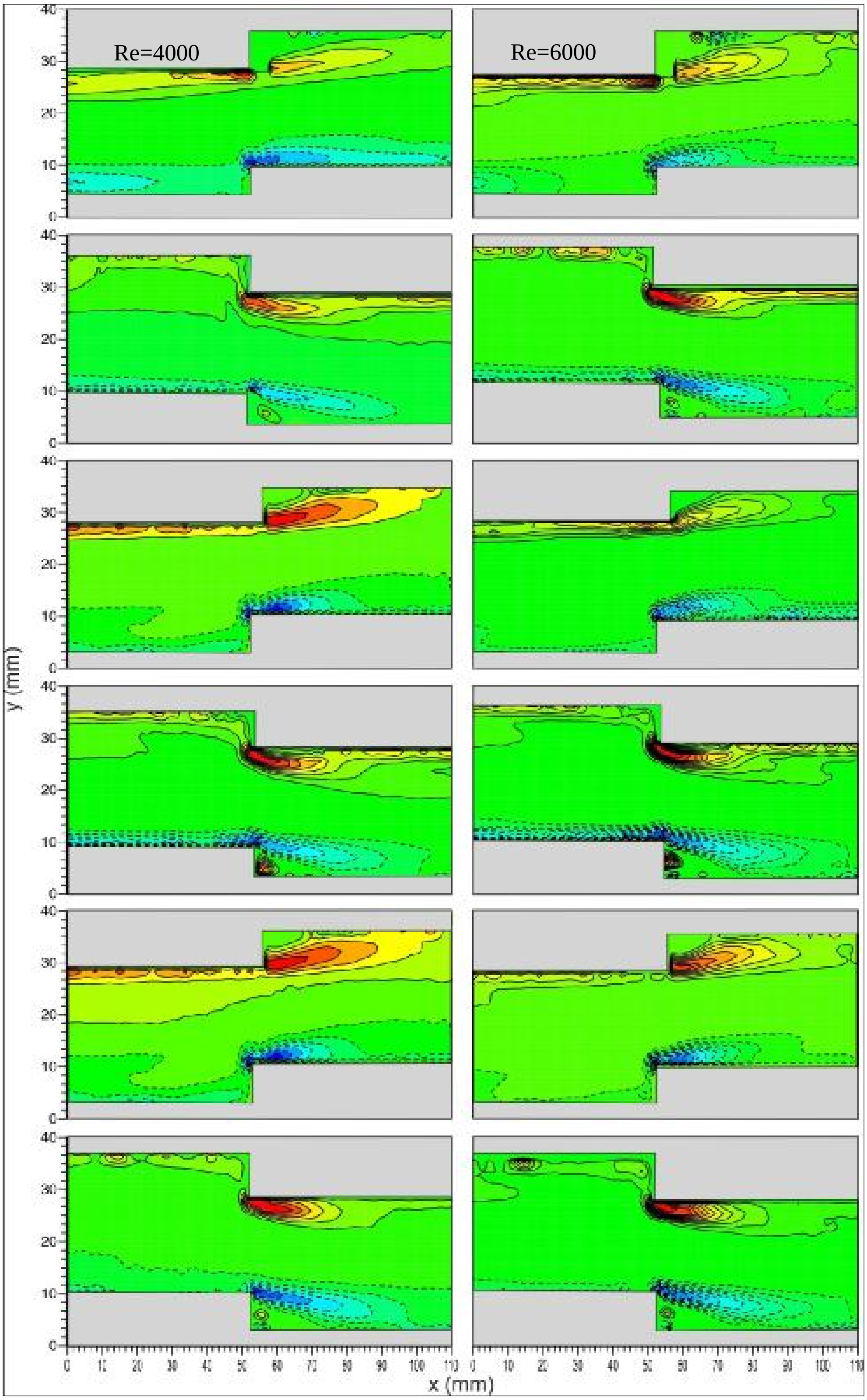

Figure 4.35. Patterns of time-averaged vorticity, $|\langle w_{min}\rangle| = 0.3$, $\langle Dw\rangle=0.3$ for channel with phase angle, φ of 0 degree

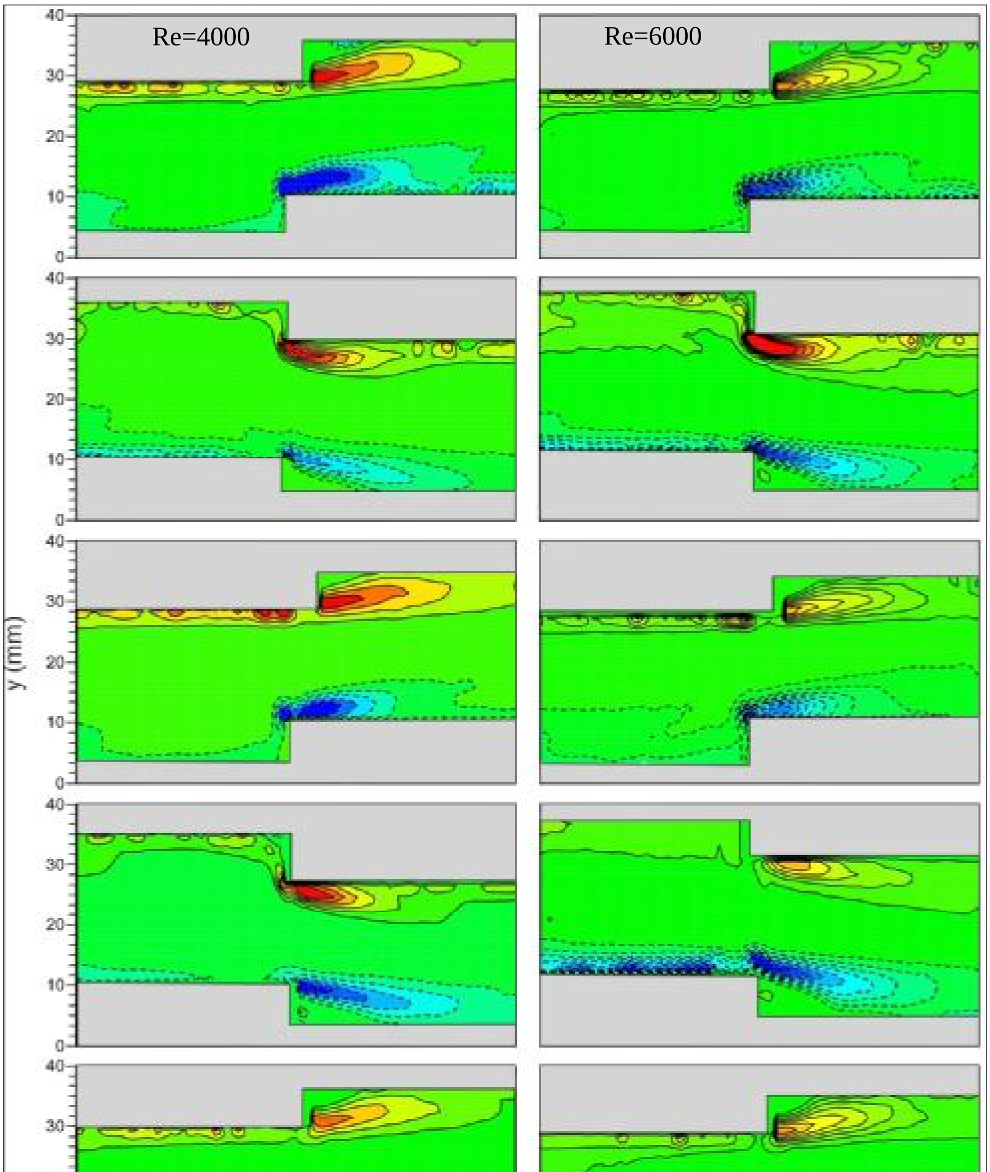

Figure 4.35. Patterns of time-averaged vorticity, $|\langle w_{min} \rangle|= 0.3$, $\langle Dw \rangle=0.3$ for channel with phase angle, φ of 0 degree (continued)

4.1.6. Validation of Three Set Datum

Figure 4.36 presents the time-averaged streamwise velocity profiles, u/U_∞ on the horizontal xy-plane at an elevation of x/L = 0.34 in the last field of view for corrugated channel with phase angle, φ of 180 degree and Reynolds number, 4000. Three sets of data were obtained at different period of time owing to appointed of discrepancy among these sets of data. The total numbers of data was 1000 for these three sets of data. The reverse flow region occurs resulting in a negative streamwise velocity, u beginning from the deep of the corrugated surface of the model on both upper and lower walls. The flow characteristics are almost symmetric along both sides of the centerline of the model. Dimensionless velocity components show that maximum velocity occurs at the central axis of the present field of view. Comparisons of three sets of data indicate that all results velocity profile comply with each other for the time-averaged velocity profiles in the vertical plane at x/L = 0.34 crossing the central axis. Finally, it can be concluded that total numbers of instantaneous velocity data are sufficient.

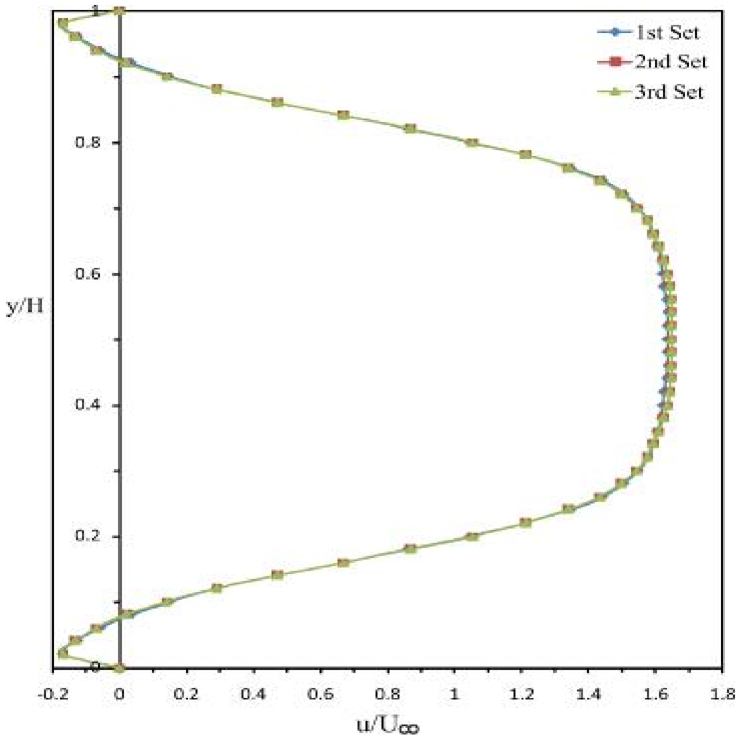

Figure 4.36. Dimensionless streamwise velocity component, u/U_∞

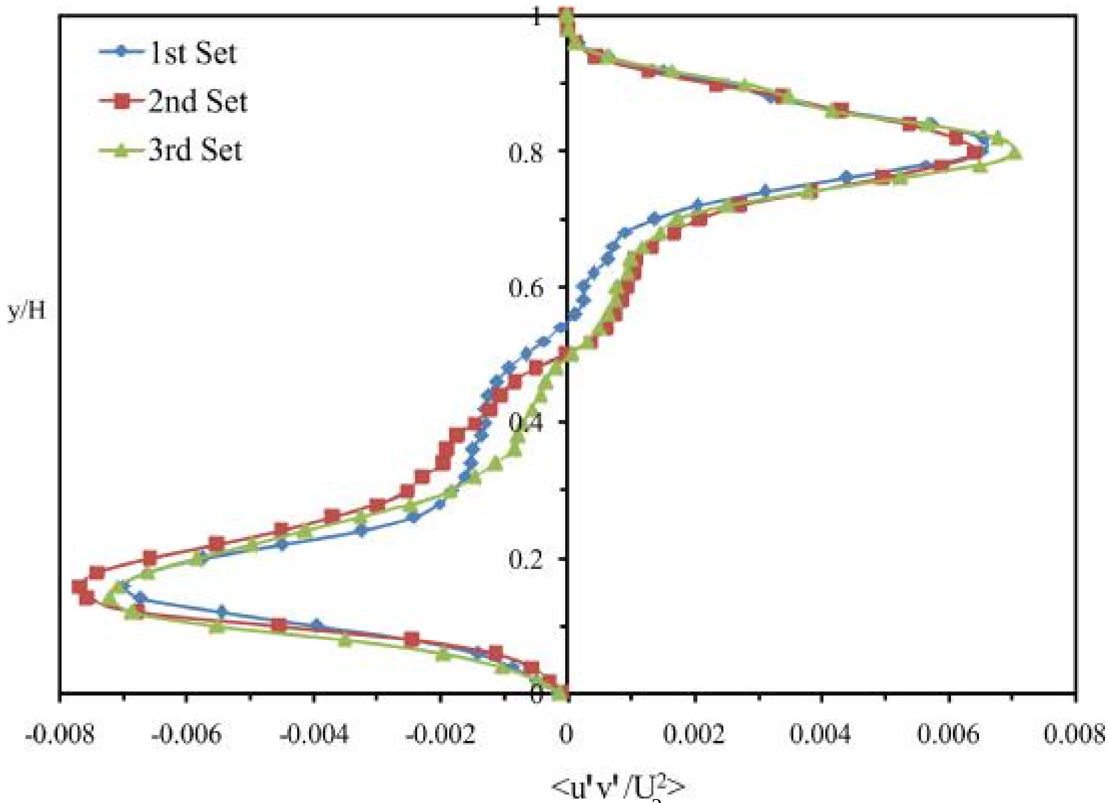

Figure 4. 37. Reynolds stress correlations, $<u'v'/U^2>$

Figure 4.37 shows profiles of three sets of the corresponding Reynolds stress correlations, $<u'v'/U^2>$ in the central plane of the duct at a location x/L=0.34. Figure 4.37 indicates that the peak values of the Reynolds stress correlations, $<u'v'/U^2>$ occur at the sharp edge of the cavity from the both sides of the corrugated channel axis. All sets of data follow the same trend and it can be concluded that a low rate of discrepancy occurs between data sets. In summary reliability of experimental data is very high.

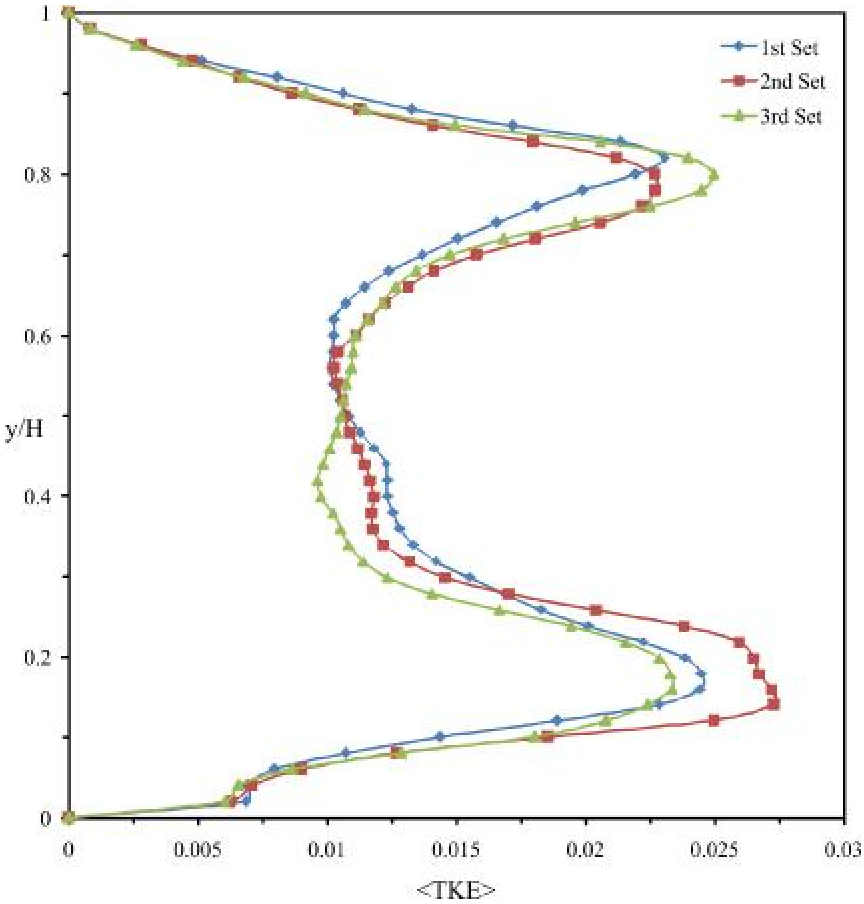

Figure 4.38. Dimensionless Turbulent Kinetic energy, <TKE>

The dimensionless Turbulent Kinetic energy, <TKE> shown in Figure 4.38 for three sets of data. Turbulent Kinetic energy, <TKE> distributions at y/H=0.5 are minimum values while Reynolds shear stress, $<u'v'/U^2>$ contours approximately at the same line, y/H=0.5 are transformed from positive to negative values. Whole values of three sets have been converged with each other.

Streamwise velocity, u/U_∞ values of three sets coincide much better with each other rather than the Reynolds stress correlations, $<u'v'/U^2>$ and the dimensionless Turbulent Kinetic energy, <TKE> values, respectively. Because in these turbulent statistics, <TKE> and $<u'v'/U^2>$ fluctuating velocity components are taken into account.

Total numbers of instantaneous datum were 1000 for each set in the present study and Gurlek at all. (2012) agreed that more than 350 datum were needed for attenuation of divergency. Furthermore, it was affirmed that divergence of the values are lower in the present study.

4.2. Numerical Results

In this section, the effect of aspect ratio, s/H and the effect of phase shift, φ on the heat transfer enhancement of corrugated channel are discussed as based upon the numerical study (CFD) for straight channel and five different corrugated channels. The advantage of Computational Fluid Dynamics (CFD) is well known in the field of Fluid Mechanics by researchers and engineers. The advantage of simulating fluid mechanics problems using CFD comparing to experiments is cheaper. But, for the validation of the numerical predictions, experimental data are substantially important.

The best aspect ratio model was determined with the help of studying the enhancement of heat transfer on three different aspect ratio models. Following that, the effect of phase shift on enhancement of heat transfer was determined by means of analyzing three different phase shifts, φ at aspect ratio, s/H that was previously determined. Besides, heat transfer, Nu, friction factor ,f , thermal enhancement factor, η and flow characteristics in a periodic corrugated channel have been determined.

4.2.1. Solution Procedure for Numerical Study

4.2.1.1. Definition of Physical Domain

The applied corrugations were rectangular shaped cavities with a constant cavity length. Figure 4.39 and figure 4.40 indicate the applied corrugated geometries in the present study. They consist of two symmetric corrugated walls for channel with phase angle, φ, 180 degree and two asymmetric corrugated walls for channel with phase angles, φ, of 90 degree and 0 degree and their height difference between upper and lower corrugated wall is H=20 mm.

Three different cases such as case one (C_1), case two (C_2), case three (C_3) are investigated. All the aforementioned cases (C_1, C_2, C_3) have similar rectangular cavity shapes and widths of the corrugations, s are different among the C_1, C_2, C_3 cases. In other words, C_1, C_2, and C_3 correspond to three different dimensionless corrugation widths of s/H=0.1, 0.2, and 0.3, respectively as seen in Figure 4.39.

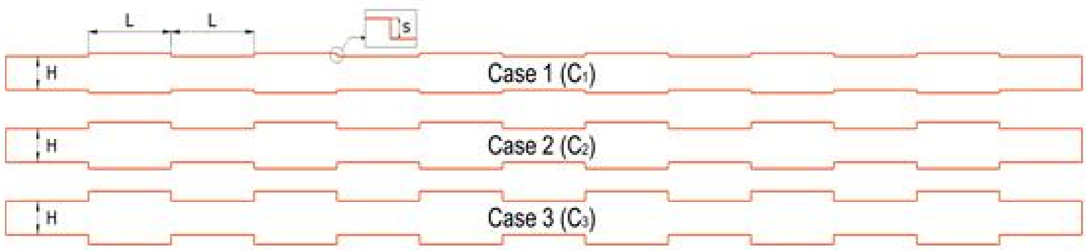

Figure 4.39. Corrugated channel geometries with different aspect ratios, s/H=0.1, 0.2, and 0.3

There are six symmetric cavities along the upper and lower walls of channels. The axial length of corrugated (L) is 100 mm and total length of corrugated channel is 1300 mm. The flow in this type of channel is two dimensional at the central cross-section. For this reason, flow domain is assumed to be two-dimensional, incompressible and Newtonian. The upper half of the channel is merely used as the computational domain in numerical solution to save computational time by virtue of symmetry boundary condition that is applied at the center of the channel for case 1, case 2 and case 3.

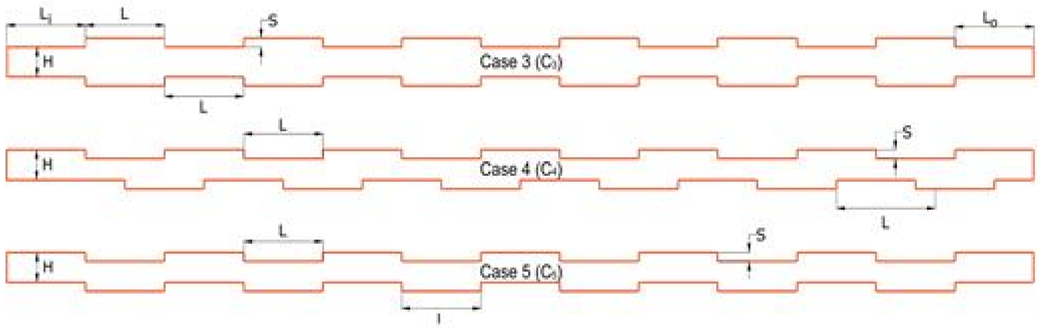

Figure 4.40. Corrugated channel geometries with different phase shift, φ=180 degree, 90 degree and 0 degree, respectively in the present study

On the other hand, case 3(C_3), case 4 (C_4) and case 5(C_5) have the same aspect ratios but different phase shifts as shown in Figure 4.40. The phase shifts of the corrugated channel are taken as 180 degree, 90 degree, 0 degree for C_3, C_4, and C_5 respectively. Computations were carried out for Reynolds numbers in the range of 3000≤Re≤6000. However, asymmetry boundary condition is applied for case 4 and case 5 due to phase shift, φ.

4.2.1.2 Geometry creation and mesh generation

As mentioned earlier, the analysis was carried out using Gambit as the pre-processor for the geometry creation and mesh generation. There were five geometries created with Gambit programme. The minimum element size near the walls of the corrugated channel is the same for all cases and equal to λ/H=0.0005. The total grid numbers are 126681, 135741, 144801, 409195, and 414160 for C_1, C_2, C_3, C_4 and C_5, respectively.

For each individual case, a non-conformal multi-block grid system is defined as shown in figure 4.41. In order to define the multi-block grid system firstly, specified geometries are divided into different blocks and following that, the non-conformal grid systems are defined for each case.

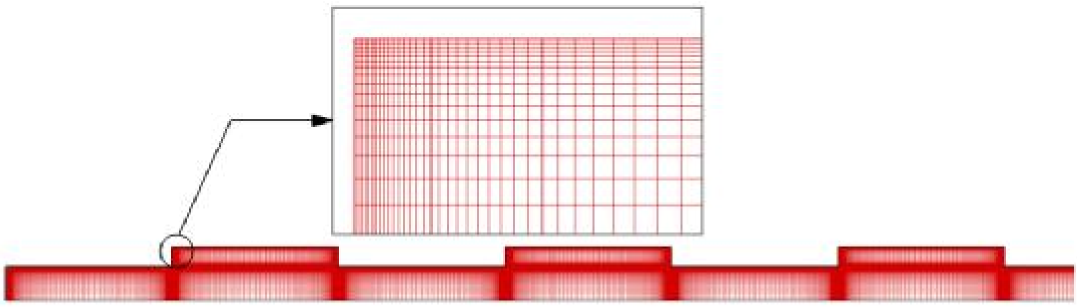

Figure 4.41.Grid system for cases

4.2.1.3 Boundary Conditions

Symmetry boundary condition applied at the centre of the corrugated channels which have different aspect ratios is presented in figure 4.42. Specific temperature and no-slip condition are defined on the wall of the channel. In addition the flow before the corrugated channel is in fully developed condition in most cases. For this reason, in order to avoid extra computational efforts, higher upstream length for development of the fully developed velocity profile is defined at the inlet section of the corrugated channel. Different fluid velocities enter the geometry and they vary to ensure that Reynolds numbers are kept in the range of 3000-6000. For incoming flow, a uniform temperature is also defined.

Figure 4.42. Applied boundary conditions

The mathematical descriptions of the boundary conditions are shown below.
For incoming flow

$$u_i = 6\bar{u}\left[0.25 - \left(\frac{y}{H}\right)^2\right] \quad and \quad T = T_i$$

On the walls of the channel

$$u = v = w = 0 \quad and \quad T = T_w$$

On the axis of channel

$$\frac{\partial \bar{u}}{\partial y} = \frac{\partial \bar{v}}{\partial y} = \frac{\partial \bar{w}}{\partial y} = \frac{\partial \bar{T}}{\partial y}$$

The value of the mean velocity is obtained based on the Reynolds number which is defined as

$$\mathrm{Re} = \frac{\rho_f \bar{u} D_h}{\mu_f}$$

Where

$$D_h = 2H$$

In the present study, the problems are computed using the aforementioned governing equations under unsteady flow condition. The standard *k-ε* is carried out for prediction of the turbulence characteristics. The computations are performed by means of an advanced finite volume code. In this regard, for discretization of the momentum and energy equations, a second order upwind scheme is used. Whereas, for the other transport equations, a first order upwind scheme is implemented. Furthermore, the SIMPLE algorithm proposed by Patankar (1980) is adopted for pressure-velocity coupling. In this algorithm, firstly, the velocity field is obtained with the momentum equation using a primary guessed pressure. Thereafter, the guessed value for pressure is updated using the continuity equation. This iterative approach is continued until the convergence of the numerical solution which is being envisioned situation is established. The convergence criteria for all flow data is set to 10^{-8}.

The surface heat transfer coefficient is estimated by using the following equation

$$h(x) = \frac{q''(x)}{T_s - T_m}$$

where T_m, is bulk temperature which can be determined as Incropera, (2011)

$$T_m = \frac{\int_0^{H/2} uTdA}{\int_0^{H/2} udA}$$

In addition, the value of the local Nusselt number, Nu is computed by using the following correlation

$$Nu = \frac{hD_h}{k}$$

Furthermore, the value of the mean Nusselt number, Nu is obtained by integration of equation over the corrugated channel surface as

$$\overline{Nu} = \frac{1}{\xi}\int_0^{\xi} Nu\,dx$$

Where

$$\xi = \sum_{i=0}^{i=n} (p_i + S_i)$$

Finally, the friction factor, f is obtained by

$$f = \Delta p \frac{2D_h}{L\left(\rho\,\bar{u}^2\right)}$$

In comparison to the straight channel heat transfer element, enhancement of heat transfer (increase of Nu at the same Reynolds number) accompanies with a penalty of flow resistance elevation (increase of f at the same Reynolds number) in general when a corrugated channel are used as a heat exchanger. Hence, it is required to set up an assessment criterion in order to evaluate the improvement of overall heat transfer performance of the corrugated channel to be investigated. The function of overall heat transfer performance is adopted as follows:

$$\eta = \frac{\frac{Nu}{Nu_S}}{\left(\frac{f}{f_S}\right)^{1/3}}$$

The overall heat transfer efficiency index η > 1 reveals that the corrugated channel is superior to the straight channel.

4.2.1.4. Grid size independence study

In order to study the grid size independence of the results, two different grid sizes are examined for C_1, C_2, and C_3. The first grid system (present grid system) has the minimum element size of λ/H=0.0005 and the finer grid system has the minimum element size of λ/H=0.0004 near the corrugated channel walls. Details of two applied grid systems are indicated in Table 1. In this regard, figure 4.43 shows the grid size independence study results for water flow in all three corrugated duct. As seen, values of mean Nusselt number are not altered using the finer element size.

Table 1: Two applied grid system

Case title	Channel No.	Minimum element size	Grid number
Present case	C1	0.0005	126681
	C2	0.0005	135741
	C3	0.0005	144801
Finer grid case	C1	0.0004	155251
	C2	0.0004	164311
	C3	0.0004	173371

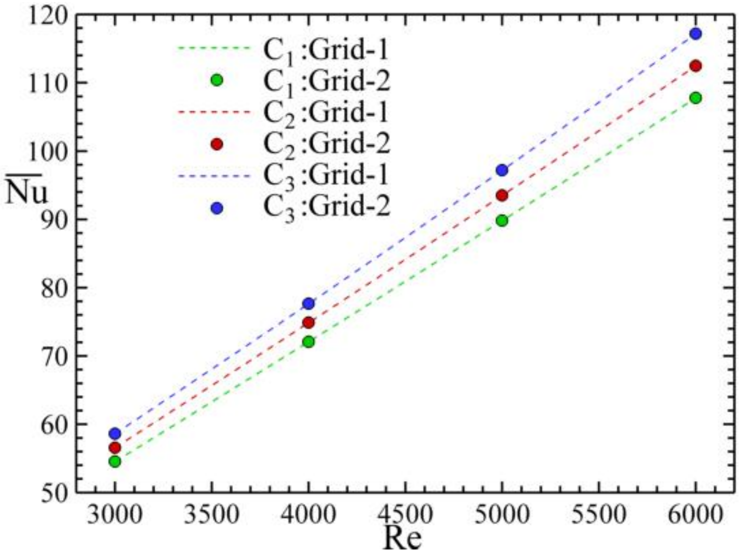

Figure 4.43. Grid size independence study

4.2.2. The Effect of the Aspect Ratio on the Heat transfer Enhancement of Corrugated Channel

Since effects of the corrugated channel are considered in the present study, it is useful to discuss the obtained results in terms of the corrugation effects distinctly. In this subsection, effects of the corrugated channels, C_1, C_2, and C_3 are studied for water flow and the obtained results are compared with that of the straight channel in order to find out the effects of the corrugation width on the thermal-hydraulic characteristics. It is worth mentioning that the presented results in this subsection are compared with those of the straight channel only for water flow. First of all, effects of three defined geometries such as C_1, C_2, and C_3 on the hydrodynamic characteristics of the water flow are presented in Figure 4.44. The left hand side column of Figure 4.44 illustrates the streamwise velocity distributions on the axis of the corrugated channel for different geometries under consideration of different Reynolds numbers in the range of $3000 \leq Re \leq 6000$. In addition, the right hand side column of Figure 4.44 shows the turbulence intensity over the central cross-section. It is observable that using very small rectangular shaped corrugations on the plates of the parallel channel lead to increase turbulence intensity through the corrugated channel. The rate of turbulence intensity varies as a function of the corrugation width. In other words, by increasing the corrugation width, the rate of turbulence intensity through the corrugated channel increases as might be expected. Increasing the Reynolds number for each individual case such as C_1, C_2, or C_3 leads to augment the rate of the turbulence intensity along the shear layer on both side central axis. Increasing the flow mixing and turbulence intensity improve the thermal transport through the corrugated channel. However, this condition results in an increase the pressure drop through the channel which requires additional consideration. Examination of the streamwise velocity distribution on the axis of the corrugated channel reveals that using the rectangular shaped corrugation on the plates of the parallel channel develops a harmonic velocity distribution on the axis. The amplitude of the velocity variation on the axis depends on the corrugation width and the Reynolds number. The amplitude of the streamwise velocity on the axis is small for low Reynolds number such as Re=3000. However, this amplitude increases at higher Reynolds numbers and higher corrugation widths as illustrated in Figure 4.44.

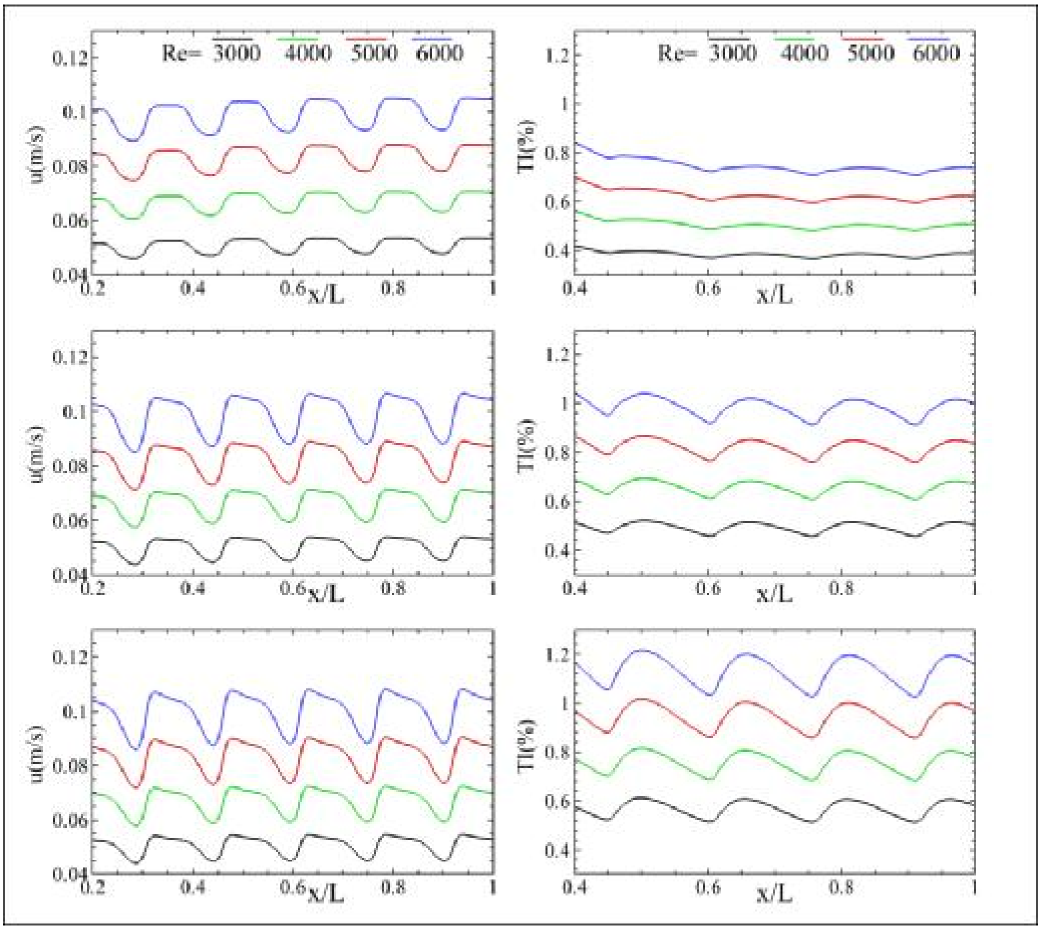

Figure 4.44. Distribution of streamwise velocity (left column) and turbulence intensity (right column) along the channel axis

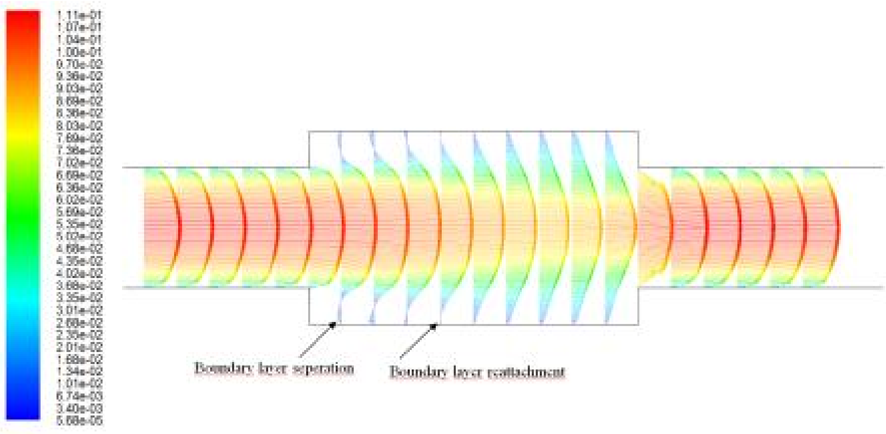

Figure 4.45. Distributions of time-averaged velocity vectors

As the flow passes through the entrance of cavities the flow separates away from the sharp corner to form a jet-like flow. Between this free jet-like flow and boundary of cavity a reversing flow region is formed. This broad feature of the flow structures occurs in all cavities of corrugated channels. Due to the large velocity difference between the jet and the core flow, a thin shear layer is created and it is highly unstable as seen in figure 4.45.The shear layer is subjected to flow instabilities that eventually lead to the generation of strong turbulent fluctuations and the shear layer continuously grows in the downstream direction. This highly turbulent shear flow entrains core flow into the jet and enhances the flow mixing. Consequently, the shear layers and the jet spreads laterally outward and the jet velocity decreases downstream. A well-defined separating streamline acts as a boundary between the core flow and the wake flow regions between the cavity entry and sudden contraction, as it is know that the cross-section of free-jet gradually decreases so as to pressure gradient along the central axis also decreases. Downstream from the sudden contraction, this free-jet expands and well defined identity of core-flow and wake flow are rapidly deteriorated in a region where turbulent mixing is increased further and adverse pressure gradient dominates this area. There is a higher entrainment rate between core flow and wake flow in the mixing region activating the circulatory motion to further extend within the wake region. An amount of mass flow rate which leaves core flow region and enter into the wake region. On one hand, an amount of fluid leaves the core flow region enters into wake flow region. On the other hand same amount of fluid leave the wake flow regions and enter into core flow region ensuring that the continuity condition is satisfied. Eventually, core flow reattaches to the cavity wall. In this type of geometry the level of contraction of the free-jet is intimately depends on the aspect ratio, s/H. Behaviors of these flow characteristics were observed in the animations of 1000 images of instantaneous flow data. For example animation instantaneous of velocity vectors, patterns of streamlines and vorticity demonstrate similar flow behaviors stated above.

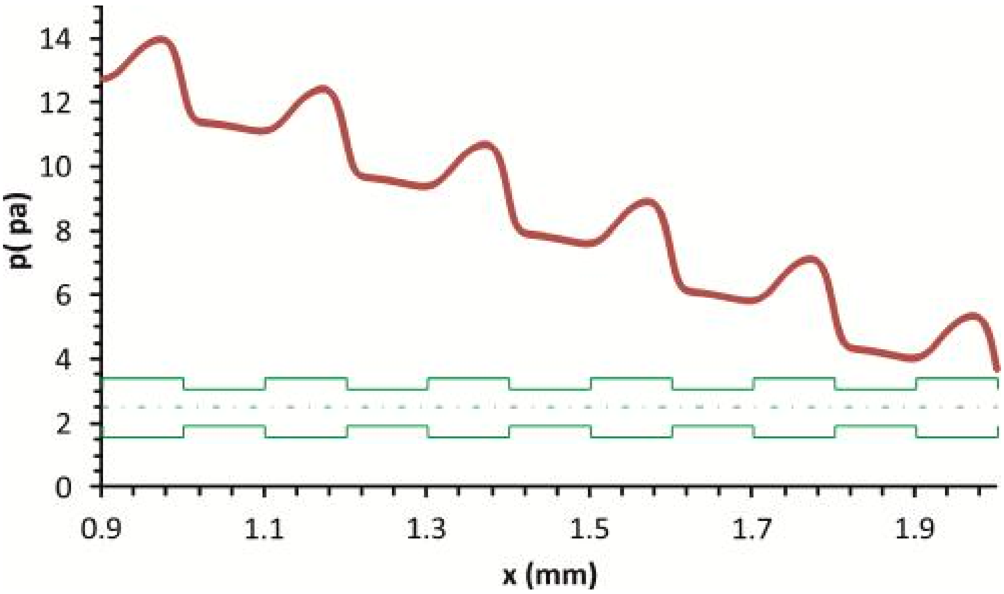

Figure 4.46. Axial statistic pressure distributions along the central axis of corrugated channel with phase shift angle, φ of 180 degree Reynolds number, Re=6000

As the flow progresses from the separation point or entry of sudden contraction a rapid pressure drop happens in the flow direction due to the construction of core flow regions, but, beyond the entry of sudden expansions there is a rapid pressure rise for a certain distance because of expansion of core flow region as seen in Figure 4.46. As the flow separates from the sharp corners or entry of sudden expansion because of adverse pressure gradient and flow reverses along the exterior (on the wake flow side) of the shear layers rotates either counterclockwise close the upper wall or clockwise close to the lower wall of the corrugated channel. Periodic changes of pressure gradients occur throughout the corrugated channel due to the periodic geometrical changes. Namely, this behavior of pressure gradient repeats itself for the other corrugation. When the momentum of the fluid layers near the surface is not sufficiently high to overcome the pressure recovery (Adverse pressure), the velocity gradient at the surface becomes zero and hence the boundary layer of the flow detaches from the surface of the corrugated channel. When the expansion of core flow region is completed conversion of kinetic energy into the adverse pressure is ended. Hence, the momentum of the fluid layers near the surface is sufficiently high to overcome the pressure recovery (adverse pressure), the boundary layer of the flow attaches to the surface of the corrugated channel.

Effects of the rectangular shaped corrugated channel on the Nusselt number, Nu as a main thermal characteristic of the flow are demonstrated in first row of figure 4.47 for water flow as a function of the Reynolds number. It can be seen that as the Reynolds number increases, the average Nusselt number also increases. The heat transfer rate also increases with the rise of the aspect ratio and shows a maximum value at s/H =0.3 that corresponds to the highest aspect ratio, s/H. Namely, it can be explained by a strong turbulence intensity of the presence of corrugation leading to rapid mixing between the core and wall flow especially at highest aspect ratio.

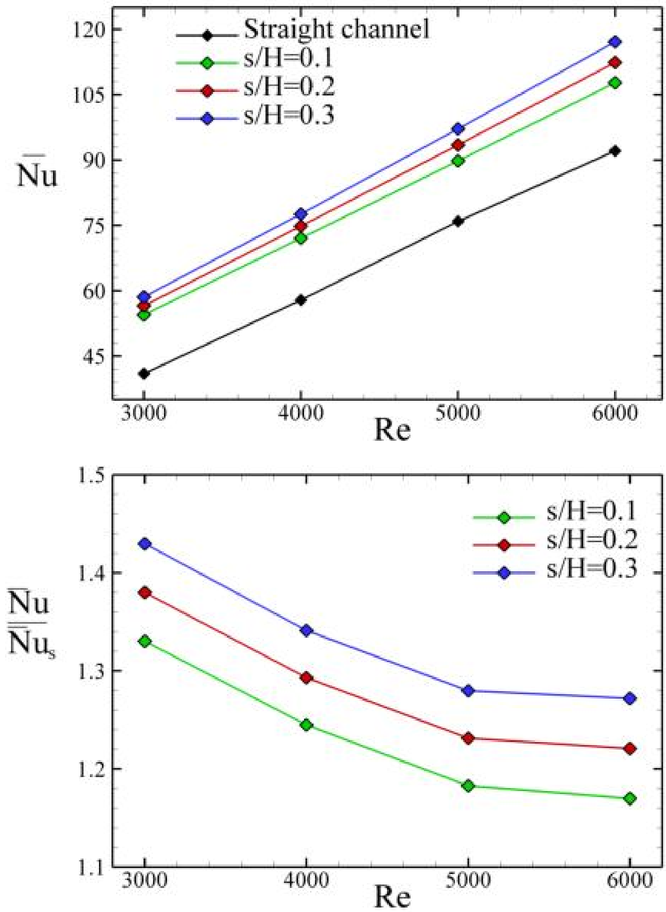

Figure 4.47. Variation of the Nusselt number, Nu with the Reynolds number, Re for all cases such as C_1, C_2, and C_3 and comparison with straight channel data

As mentioned before, since the rate of flow mixing changes as a function of the corrugation width, it is expectable that the rate of heat transport and consequently the thermal efficiency become higher for corrugated channels. It is observed that the aspect ratio, s/H=0.3 has the best heat transfer when compared to other aspect ratios, s/H=0.1 and s/H=0.2 mm, respectively. The increment of heat transfer for high aspect ratio can be explained by a strong turbulence intensity generated by aspect ratio, leading to a rapid mixing of the flow especially at the higher Reynolds number. The enhancement on the heat transfer is proportional to the corrugation width and the Reynolds number as shown in second row of figure 4.47. In generally, as fluid flow through the corrugated surface, the fluid re-circulation or/and the swirl flows are generated in the corrugation troughs. The onset and growth of recirculation zones promote the mixing of fluid in the boundary layer and as a result enhance the heat transfer. So as to compare the performance between corrugated channels and straight channel, ratio of Nu in the corrugated channel to that in the straight channel (Nu/Nu_s) is adopted in order to reveal the heat transfer enhancement. It is clearly seen in figure 4.47 that minimum ratios of the Nusselt number for corrugated channel on that of the straight channel are 1.17, 1.22, and 1.27 for C_1, C_2, and C_3, respectively. However, these ratios reach to their maximum values at Re=3000 to the levels of 1.33, 1.38, 1.43 for C_1, C_2, and C_3, respectively. From the second row of figure 4.47, it can be inferred that the effect of corrugations on heat transfer rate is more efficient at a lower Reynolds number. This situation can be related to the thickness of the thermal boundary layer, since the thermal boundary layer becomes thicker at the lower Reynolds number and therefore, the outcome of the disruption of the thermal boundary layer becomes more appreciable.

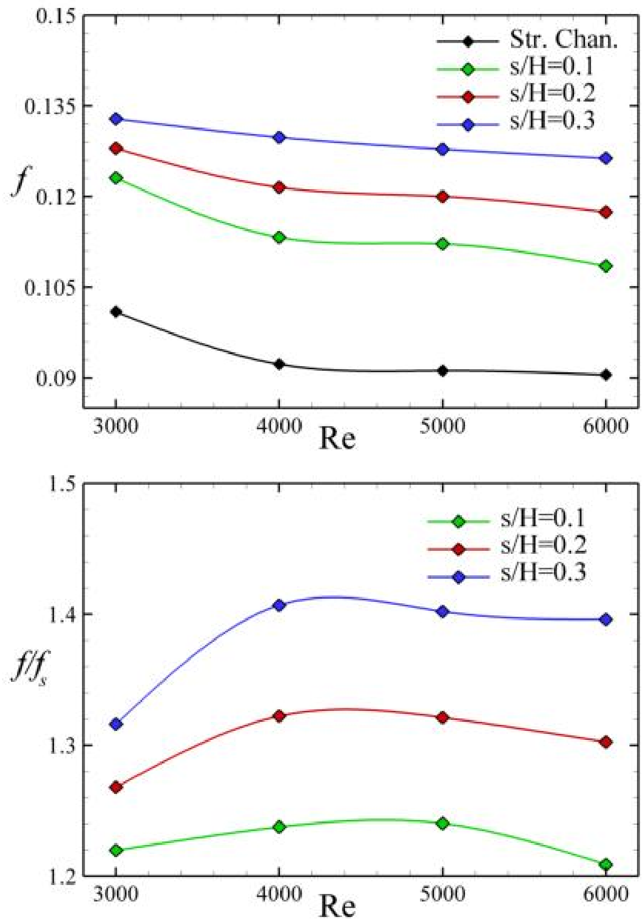

Figure 4.48. Variation of friction factor, f with the Reynolds number, Re for all cases such as C_1, C_2, and $C_3$and comparison with straight channel data

Development of the turbulent flow in the corrugated channels influences the friction factor, f as a main hydraulic characteristic of the flow. The variation of the friction factor, f as a function of the Reynolds number, Re for different corrugated channels such as C_1, C_2, and C_3 is presented in Figure 4.48. The friction factor varies with the variation of the aspect ratio in all cases as expected because of the suppression of viscous sub-layer and the introduction of the corrugated surface yields to higher friction factor, f in comparison to that of the straight channel surface as presented in seen figure 4.48 clearly. It is obvious that the friction factor decreases gradually for all configurations as a result of the increase of Reynolds number, Re. It can be seen that the aspect ratio, s/H = 0.3 has the highest friction factor, f and it is followed by s/H = 0.2, 0.1 mm, respectively and using the larger corrugation widths develops higher friction factors in the channels when compared to straight channel.

The augmentation on the friction factor, f for corrugated channel in comparison to straight channel is very small in lower Reynolds number, Re. However, increasing the Reynolds number, Re increases the friction factor, f in the corrugated channel. On the other hand, it can be found from figure 4.48 that using the higher corrugation widths increases the friction factor, f to a higher level.

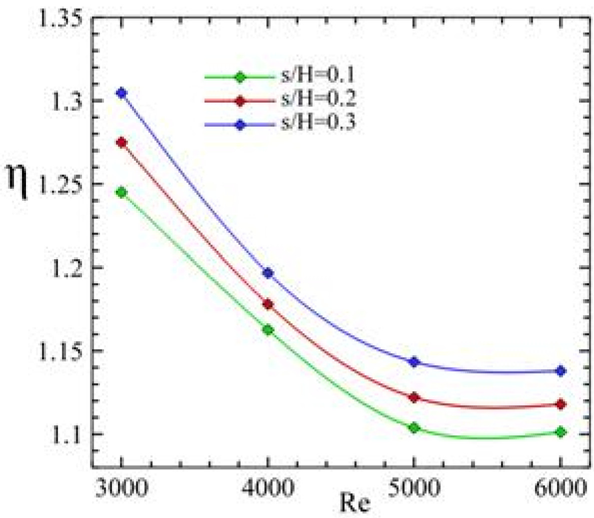

Figure 4. 49. Variations of efficiency indices, η with the Reynolds number, Re for all corrugated cases such as C_1, C_2, and C_3

Either friction factor, f or Nusselt number, Nu increases in virtue of application of corrugated in channels. Furthermore, the efficiency index, η (which is dependent on friction factor, f and Nusselt number, Nu as mentioned above) of the flow should be computed in terms of the Reynolds number, Re in order to find and optimum case of the corrugated ducts. The efficiency index, η is considered under the equal pumping power condition. Figure 4.49 depicts the efficiency index, η calculated by using the computed Nusselt numbers, Nu and friction factors, f. The result indicates that for each case the values of efficiency index, η have quite similar trend in the considered range of Reynolds numbers, Re. In this regard, Figure 4.49 illustrates variations of the efficiency indices, η with the Reynolds number for each individual case such as C_1 (s/H=0.1), C_2(s/H=0.2), and C_3(s/H=0.3). It seems that the enhancement on the efficiency index, η is higher for the case of C_3 when compared to other cases. Additionally, as the Reynolds number increases, the rate of enhancement of the efficiency indices decreases for each corrugated duct. The maximum enhancements of the efficiency index, η are 24%, 27%, and 30 % at Re=3000 for C_1, C_2, and C_3, respectively. It is concluded that using an aspect ratio of s/H=0.3 would lead to achieve a better heat transfer augmentation.

4.2.3 The Effect of the Phase Shift on the Heat Transfer Enhancement of Corrugated Channel

In this section, to find out the effect of different phase shifts (C_3, C_4, C_5) on the thermal-hydraulic characteristics, water flow in three geometries are studied and obtained results are compared with straight channel. Figure 4.50 shows the effects of channel phase shift on the variation of streamwise velocity distributions and turbulence intensity along the axis for Reynolds number, Re ranging from 3000 to 6000 for phase shift (φ) 180 degree, 90 degree, 0 degree. It is observable that using rectangular corrugated plates develops harmonic velocity distribution on the axis of the channel. The amplitude of the velocity distribution depends on the phase angle, φ and the Reynolds number, Re and amplitude of the streamwise velocity distribution increases with increasing Reynolds number, Re. In addition, highest amplitude occurs at phase shift, φ=180°. Turbulence intensity rate varies with the Reynolds number and phase angle while corrugated plates lead turbulence along the axis of the channel. For all the geometric configurations, the rate of turbulence intensity increases with the Reynolds number as it can be seen from right hand side of the figure 4.50.

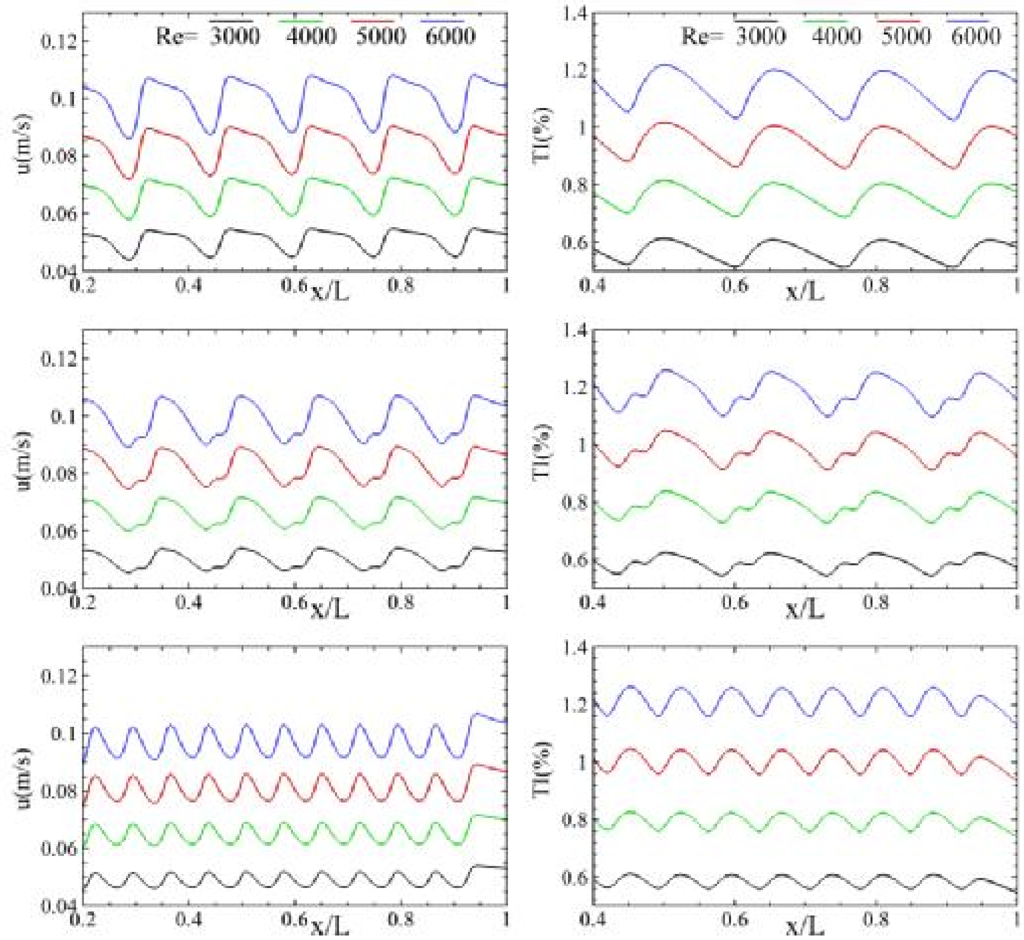

Figure 4.50. Distribution of streamwise velocity (left hand side) and turbulence intensity (right hand side) along the channel axis

The variation of the computed average Nusselt number with Reynolds numbers for various phase shifts, φ is presented in first row of figure 4.51. The large Reynolds number is attributed to the higher velocity which in turn can result in disturbance of the flow and thus, the heat transfer is strengthened. In all cases, the corrugated channel flows gave higher values of Nusselt number than straight channel flow owing to the induction of high disturbance, thin boundary layer and the flow separation or reversing flow in the corrugated channels, which paved the way for higher temperature gradients. It can be clearly seen from figure that the Nusselt numbers, Nu at higher phase shifts, φ are higher than those at lower ones. Increasing phase shifts, φ leads to decrease Nusselt number, Nu since small phase shift results in larger region recirculation a larger region or/and higher swirl flows intensity in the corrugation trough and furthermore, all Nusselt values are larger than those of straight channel.

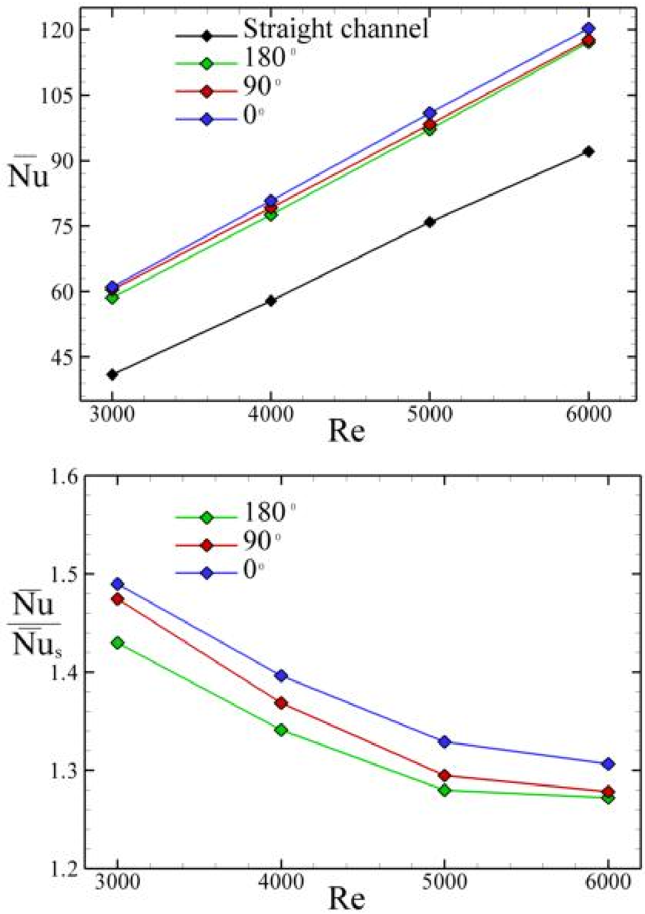

Figure 4.51. Variation of the Nusselt number, Nu with the Reynolds number, Re for all cases such as C_3, C_4, and C_5 and comparison with plain duct data

The rate of heat transfer and the thermal efficiency for three cases are higher than those of the straight channel due to the fact that the flow mixing increases with using plate corrugations. The heat transfer enhancement increases with the Reynolds number, Re and phase angle, φ. It is accurately revealed the results that the corrugated channel with phase shift, φ=0 degree has the highest average Nusselt number, Nu at all Reynolds seen as a second row of figure 4.51 clearly.

The second row of figure 4.51 shows the ratio of Nu in the corrugated channel in comparison to that in the straight channel (Nu/Nu_s), which has a different phase angle. It is found that minimum Nusselt number, Nu enhancements for corrugated channels over the straight channel are 1.27, 1.28, and 1.30 for C_3, C_4, and C_5 respectively. However, these ratios reach to their maximum values such as 1.43, 1.47, 1.49 for at Re=3000 C_3, C_4, and C_5, respectively. From figure 4.51, we can note that the effect of corrugated channel on the heat transfer rate is more efficient at a lower Reynolds number, Re. This situation can be related to the thickness of the thermal boundary layer, as the thermal boundary layer becomes thicker at the lower Reynolds number, thus the outcome of the disruption of the thermal boundary layer becomes more appreciable.

Increasing the flow mixing improves the thermal transport although increase in flow mixing causes more pressure drop. The friction factor, f by using the corrugated channel is observed to be higher than that from the straight channel for all cases studied as expected due to the suppression of viscous sub-layer Figure 4.52 also exhibits the variation between friction factor, f and Reynolds number, Re for different phase shift, φ arrangements. The friction factor, f of the present straight duct is also included for comparison.

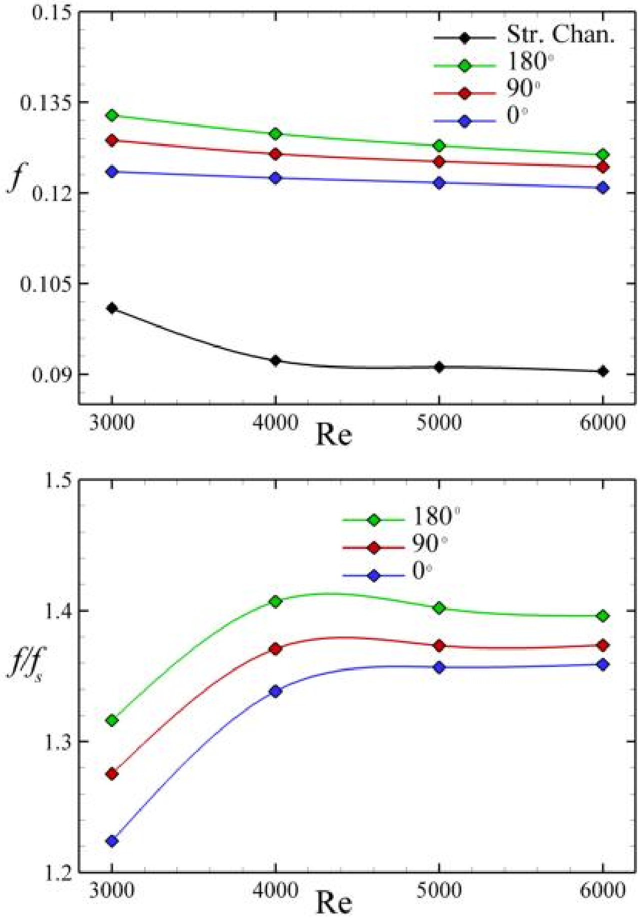

Figure 4.52. Variation of friction factor, f with the Reynolds number, Re for all cases such as C_3 (φ=180 degree), C_4 (φ=90 degree), C_5 (φ=0 degree) and comparison with straight channel data

It can be seen in figure 4.52 clearly that friction factor, f decreases with increase in Reynolds number, Re for all the configurations as expected because friction factor has been inversely proportional changing with square of the velocity. Velocity increases as Reynolds number, Re is rised and as a result of this, friction factor, f decreases. In addition, using corrugated channel produces more friction when compared to the straight channel. The value of friction factor for phase shift, φ= 180° is the highest when compared to other configurations while the lowest value is related to phase shift, φ = 0°. In other words, the friction factor, f increases with phase angle, η and case3 (φ = 180°) has highest friction factor values for all Reynolds numbers, Re.

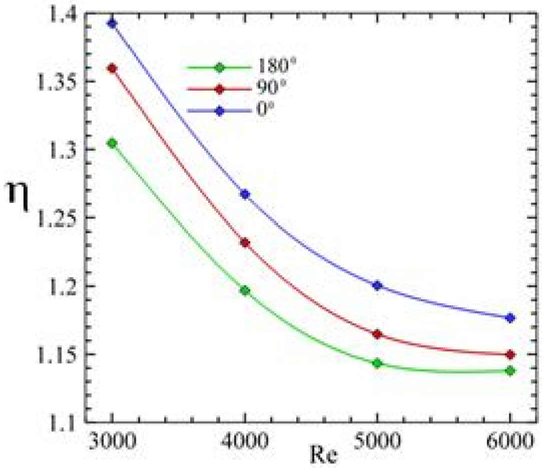

Figure 4.53. Variations of efficiency indices, η with the Reynolds number, Re for all corrugated channel cases such as C_3 (φ=180 degree), C_4, (φ=90 degree), and C_5(φ=0 degree)

Corrugated channels also result in a significant pressure drop as well, in comparison with the straight channel as expected. The increase in the Nusselt number, Nu leads to an increase in friction factor, f because of the fact that the corrugated channel disturbs the entire flow field and causes more friction as presented in figure 4.52. Evaluating the net enhancement obtained in the corrugated channel is necessary due to the fact that improvements in heat transfer are also accompanied by an increase in the frictional losses. There are various evaluation criteria in accordance with heat exchanger design purposes. Here, the relative thermal-hydraulic performance enhancement is evaluated by enhancement index, η. Figure 4.53 illustrates the efficiency index, η variation with Reynolds number for different phase angles. It can be seen in figure 4.53 that the value of the enhancement index decreases when Reynolds number for all phase shifts is increased. It is seen that efficiency index, η increases in accordance with the decrease in phase shift. Among all cases, efficiency index, η of C_5 has the highest value. The maximum efficiency index, η enhancements are 30%, 35%, and 39% for C_3, C_4, and C_5, respectively at Reynolds number, Re=3000. The thermal enhancement index for the phase angle, φ=0 degree is achieved and it is better than that for the other cases. The use of corrugated channel at lower the Reynolds number gives higher enhancement index than that at higher one.

For better enhancement index, for the channel zero phase angel, φ with aspect ratio, s/H=0.3 should be preferred.

5. CONCLUSIONS

The main purpose of the present study is to provide details of flow structures and heat transfer enhancement of the corrugated channels which have different aspect ratios such as s/H=0.1, 0.2, 0.3 and phase shift angels of φ=180˚, 90˚, 0˚ numerically and experimentally. Numerical study was performed to investigate the thermal and hydraulic characteristics of forced convection in corrugated channels for turbulent regime with Reynolds numbers in the range of $3000<Re<6000$. The experiments were performed using the Particle Image Velocimetry (PIV) technique that can be used to understand the time-averaged and instantaneous structures of the fluid flow in the field of view. Heat transfer augmentation was emphasized as a conclusion of different factors which included different phase shifts between the upper and lower walls, different aspect ratios and different Reynolds numbers. Heat transfer enhancement of the corrugated channel was studied numerically using FLUENT software to produce numerical results in order to decide upon numbers of parameters for experimental studies. The CFD predictions were compared with experimental results and found to be in reasonably good agreement.

Firstly, experimental time-averaged velocity contours are presented in order to compare with numerical results for straight channel and corrugated channels having phase angles of 180˚, 90˚, and 0˚, respectively. In summary, different geometries give different results at different flow conditions. Maximum local velocity value occurs close to the wall in the corrugated channel with 0˚ phase shift in comparison to 90˚ and 180˚ channels. Augmentation of the Reynolds number leads to an increase in velocity due to the sharp corner edges of cavity and as a result, heat transfer ratio is expected to enhance when compared to the straight channel. Thermal boundary layers for corrugated flow become thinner than the case of the straight channel and activation of vortices inside cavities improve the enhancement of the heat transfer.

Turbulence Kinetic Energy, <TKE> and Reynolds Shear Stress<u´v´/U^2>, contours are briefly discussed in accordance with the results of two dimensional Particle Image Velocimetry (PIV) for straight channel and three different corrugated channels. Dimensionless turbulent kinetic energy, <TKE> contours indicate that the magnitude of turbulent kinetic energy, <TKE> increases as a result of sharp corner edges of the cavities. High rate of momentum and heat transfer are expected to occur at the phase angle, φ of 0˚due to an increase of turbulence. Normalized the Reynolds shear stress, $<u'v'/U^2>$ values are maximum for channel with phase angel, φ of 0˚ that is indication of the high streamwise velocity components in the corrugated channel. Patterns of dimensionless Reynolds shear stress, $<u'v'/U^2>$, dimensionless turbulent kinetic energy, <TKE> and streamwise velocity components, contours are mostly similar. Additionally, aforementioned are mostly affected from streamwise velocity components rather than transverse velocity components.

The effect of aspect ratio, s/H and the effect of phase shift, φ on the heat transfer enhancement of corrugated channel were analyzed using numerical predictions for straight channel as well as five different corrugated channel geometries and four different Reynolds numbers, Re=3000, 4000, 5000 and 6000. Enhancements of heat transfer in the corrugated channel are promoted due to increase of turbulence intensity with the penalty of pressure drop. By increasing the corrugation height, the rate of turbulence intensity on the axis of corrugated channel increases as expected. Increasing the Reynolds number for each individual case such as C_1 (s/H=0.1), C_2(s/H=0.2), or C_3 (s/H=0.3) results in an increase in the rate of the turbulence intensity along the axis. In addition, the amplitude of the velocity distribution depends on the phase angle, φ and the Reynolds number and amplitude of the streamwise velocity distribution increases with the Reynolds number.

Heat transfer rate increases with the rise of the aspect ratio, s/H and shows a maximum value at s/H =0.3 that corresponds to the highest aspect ratio. Besides, the corrugated channel with phase shift, φ of 0˚ has the highest average Nusselt number, Nu. The advantage is that the corrugated channel has a sharp corner leading edge which helps in the early generation of vortices to promote entrainment between core and wake flow regions resulting in the higher average Nusselt number, Nu than the straight channel.

The friction factor, f in corrugated channels, also depends on the phase shift, φ and, aspect ratio, s/H. That is to say, sharp corner edges of cavities cause higher pressure losses. The highest friction factor, f occurs in the corrugated channel with aspect ratio of s/H=0.3 and it is followed by s/H = 0.2, and 0.1, respectively. A larger corrugation width develops higher friction factors, f compared to the straight channel. The friction factor, f increases with phase angle, φ of 180° and hence case three, C_3 (s/H=0.3) has highest friction factor, f values for all Reynolds numbers that were examined in the present study.

Nusselt number, Nu and friction factor, f of corrugated channel are dependent on the geometry. Since this is the case, the question now lies in 'the choice of suitable channel geometry'. Furthermore, the efficiency index (which is dependent on friction factor, f and Nusselt number, Nu as mentioned before) of the flow should be computed in terms of the Reynolds number, Re in order to find an optimized geometry of the corrugated channel. The maximum enhancements of the efficiency index are 24%, 27%, and 30% at Re=3000 for C_1, C_2, and C_3, respectively. It is also concluded that using an aspect ratio of s/H=0.3 would lead to achieve better heat transfer augmentation. The maximum efficiency index enhancements are 30%, 35%, and 39% for C_3, C_4, and C_5, respectively at Reynolds number, Re=3000. The thermal enhancement index for the phase angle, φ=0˚ is achieved and it is better than that for other cases. The use of corrugated channel at the lower Reynolds number provides higher enhancement index than that of higher one. For better enhancement index, the channel 0˚ with aspect ratio, s/H=0.3 should be preferred.

Phase shift of corrugated channels, cavity depth and height of channels and Reynolds numbers influence flow hydrodynamics and thermal performance when compared to the straight channel geometry. That is to say, the turbulent flow structures, domain of the wake, positions of singular points, velocity fluctuations, locations and magnitude of the peak values of turbulence quantities, such as vorticity concentrations, correlations of Reynolds stress are highly affected by the geometrical change of corrugated channels and Reynolds numbers. Flow characteristics and turbulent statistics were examined in terms of instantaneous and time-averaged flow data for Reynolds numbers in the range of 3000<Re<6000. The grade of flow structures are magnified further when the phase shift angle becomes 0˚ degree which results in enhancement of heat transfer. Furthermore, creating cavities on the opposite surfaces of straight walls of channels activate flow mechanisms to further extend magnifying mass, and momentum transfers as well as heat transfer. Thermal performance can be conveniently increased by using corrugated channel. Significant effect on the temperature distribution and flow development exist with the influence of phase angle, φ and aspect ratio, s/H. The numerical results acquired from the model are validated with the experimental data. Good agreement has been observed from the comparison between numerical and experimental results and it can be concluded that the corrugated walls have substantial effect on the enhancement of heat transfer and partially pressure drop.

REFERENCES

AHMED, M.A., SHUAIB, N.H., YUSOFF, M.Z., AL-FALAHI, A.H., 2011. Numerical investigations of flow and heat transfer enhancement in a corrugated channel using nanofluid. International Communications in Heat and Mass Transfer, 38: 1368–1375.

AKSOY, M.M, 2013. Passive Flow Control Downstream a Circular Cylinder Usıng Perforated Cırcular Cylınder In Deep Water. Çukurova University Institute of Natural and Applied Sciences, Turkey, MSc Thesis.

ALI, H.H., HANAOKA, Y., 2002. Experimental Study On Laminar Flow Forced-Convection In A Channel With Upper V-Corrugated Plate Heated By Radiation, International Journal of Heat and Mass Transfer, 45: 2107–2117.

ALI, M., RAMADHYANI S., 1992. Experiments On Convective Heat Transfer In Corrugated Channels. Experimental Heat Transfer, 5.175–93.

ARSENYEVA, O., TOVAZHNYANSKY, L., KAPUSTENKO, O., KHAVIN, G., 2011. Investigation of The New Corrugation Pattern For Low Pressure Plate Condensers. Applied Thermal Engineering, 31: 2146–2152.

ASAKO, Y., FAGHRI, M., 1987. Finite Volume Solutions For Laminar Flow An Heat Transfer İn A Corrugated Duct. Journal of Heat Transfer, 109: 627–634.

ASSATO, M., LEMOS, M.J.S., 2009. Turbulent Flow In Wavy Channels Simulated With Nonlinear Models And A New Implicit Formulation. Numerical Heat Transfer, Part A, 56: 301–324.

BAHAIDARAH, H.M.S., ANAND, N.K., CHEN, H.C., 2005. Numerical Study Of Heat And Momentum Transfer In Channels With Wavy Walls. Numerical Heat Transfer, Part A, 47: 417–439.

BERGLES, A.E., 1983. Augmentation of Heat Transfer. Heat Exchanger Design Handbook. Hemisphere Publishing Co., Washington DC.

BIGHAM, S., SHOKOUHMAND, H., ISFAHANI, R.N., YAZDANI, S., 2011. Fluid Flow And Heat Transfer Simulation In A Constricted Microchannel: Effects Of Rarefaction, Geometry, And Viscous Dissipation. Numerical Heat Transfer, Part A, 59: 209–230.

BILEN, K., CETIN, M., GUL, H., BALTA, T., 2009. The Investigation Of Groove Geometry Effect On Heat Transfer For Internally Grooved Tubes. Appl. Therm. Eng., 29 (4): 753-761.

BILEN, K., YAPICI, S., 2002. Heat Transfer From A Surface Fitted With Rectangular Blocks At Different Orientation Angle, Heat Mass Transfer, 38: 649–655.

BLANCHER, S., CREFF, R., QUERE, P.L., 1998. Effect Of Tollmien Schlichting Wave On Convective Heat Transfer In A Wavy Channel. Part I: Linear Analysis. International Journal of Heat and Fluid Flow, 19: 39–48.

BURNS, J.C., PARKS, T., 1967. Peristaltic Motion. J. Fluid Mech, 29: 405–416.

CEYLAN, K., KELBALIYEV, G. , 2003. The Roughness Effects On Friction And Heat Transfer In The Fully Developed Turbulent Flow In Pipes. Appl. Thermal Eng, 23 (5): 557–570.

CHANG, SW., JAN,YJ., LIOU, JS., 2007. Turbulent Heat Transfer And Pressure Drop In Tube Fitted With Serrated Twisted Tape. Int J Therm Sci, 46:506–18.

CHAUBE, A., SAHOO, P.K., SOLANKI, S.C., 2006. Analysis Of Heat Transfer Augmentation And Flow Characteristics Due To Rib Roughness Over Absorber Plate Of A Solar Air Heater. Renewable Energy, 31: 317–331.

COMINI, G., NONINO, C., SAVINO, S., 2003. Effect Of Aspect Ratio On Convection Enhancement In Wavy Channels, Numerical Heat Transfer, Part A, 44: 21–37.

DUAN, Z., MUZYCHKA, Y.S., 2010. Effects Of Axial Corrugated Roughness On Low Reynolds Number Slip Flow And Continuum Flow In Microtubes. J. Heat Transfer, 132: 1–8.

DURMUS, A., BENLI, H., KURTBAS, I., GUL, H., 2009. Investigation Of Heat Transfer And Pressure Drop In Plate Heat Exchangers Having Different Surface Profiles. International Journal of Heat and Mass Transfer, 52: 1451–1457.

EIAMSA-ARD, S., PROMVONGE, P., 2003. Numerical Study On Heat Transfer Of Turbulent Channel Flow Over Periodic Grooves. Heat and Mass Transfer, 35: 844-852.

EIAMSA-ARD, S., THIANPONG, C., PROMVONGE, P., 2006. Experimental Investigation Of Heat Transfer And Flow Friction In A Circular Tube Fitted With Regularly Spaced Twisted Tape Elements. International Communication in Heat Mass Transfer, 33: 1225–33.

EIMSA-ARD, S., PROMVONGE, P., 2009. Thermal characteristics of turbulent rib-grooved channel flows. International Communications in Heat and Mass Transfer, 36: 705–711.

ELSHAFEI, E.A.M., AWAD, M.M., EL-NEGIRY, E., ALI, A.G., 2008. Heat Transfer And Pressure Loss In Narrow Channels With Corrugated Walls, Thermal Issues in Emerging Technologies, Egypt, Dec 17–29th 2008.

FABBRI, G., 2000. Heat Transfer Optimization In Corrugated Wall Channels. International Journal of Heat and Mass Transfer, 43: 4299–4310.

FABBRI, G., ROSSI, R., 2005. Analysis Of The Heat Transfer In The Entrance Region Of Optimized Corrugated Wall Channel. International Communications in Heat and Mass Transfer, 32: 902–912.

FAIZAL, M., AHMED, M.R., 2012. Experimental Studies On A Corrugated Plate Heat Exchanger For Small Temperature Difference Applications. Experimental Thermal and Fluid Science, 36: 242–248.

FERNANDES, C.S., DIAS, R.P., NOBREGA, J.M., MAIA, J.M., 2007. Laminar Flow In Chevron-Type Plate Heat Exchangers: CFD Analysis Of Tortuosity, Shape Factor And Friction Factor. Chemical Engineering and Processing, 46: 825–833.

FERNANDES, C.S., DIAS, R.P., NOBREGA, J.M., MAIA, J.M., 2008. Friction Factors Of Power-Law Fluids In Chevron-Type Plate Heat Exchangers. Journal of Food Engineering, 89: 441–447.

FERNANDES, C.S., DIAS, R.P., NOBREGA, J.M., MAIA, J.M., 2011. Investigation Of New Corrugation Pattern For Low Pressure Plate Condensers. Applied Thermal Engineering, 31: 2146–2152.

FRANKE, K., 2008.Http://www.Oobgolf.com/content/columns/know+the+game/1-1675-Why_Does_A_Golf_Ball_Have_Dimples.Html,".

FUSEGI, T., Numerical Study Of Convective Heat Transfer From Periodic Open Cavities İn A Channel With Oscillatory Through Flow. International Journal of Heat and Fluid Flow, 18: 376–383.

GARG, V.K., MAJI, P.K., 1988. Flow and Heat Transfer in a Sinusoidally Curved Channel. Int J Engineering Fluid Mechanics, 1: 293-319.

GOLDSTEIN, J.L., SPARROW, E.M., 1977. Heat Mass Transfer Characteristic For Flow In A Corrugated Wall Channel. ASME J. Heat Transfer,99: 187-195.

GOLDSTEIN, L., SPARROW, EM., 1997 Heat/Mass Transfer Characteristics For Flow In A Corrugated Wall Channel. Transaction of the ASME, Journal of Heat Transfer, 99:187–95.

GRADECK, M., HOAREAU, B., LEBOUCHE, M., 2002. Local Analysis Of Heat Transfer Inside Corrugated Channel, International Journal of Heat and Mass Transfer, 48:2587–2595.

GRADECK, M., HOAREAU, B., LEBOUCHÉ, M., 2005. Local Analysis Of Heat Transfer Inside Corrugated Channel. International Journal of Heat and Mass Transfer, 48: 1909–1915.

GSCHWIND, P., REGELE, A., KOTTKE, V., 1995. Sinusoidal Wavy Channels With Taylor–Goertler Vortices. Experimental Thermal and Fluid Science, 11: 270–275.

GUPTA, A., IOSR, M., 2012. Review of Heat Transfer Augmentation Through Different Passive Intensifier Methods. Journal of Mechanical and Civil Engineering, 1: 14-21.

GUT, J.A.W., PINTO, J.M., Modeling Of Plate Heat Exchangers With Generalized Configurations. International Journal of Heat and Mass Transfer, 46: 2571–2585.

HAN, H., LI, B.,YU, B., HE, Y., LI, F., 2012. Numerical Study Of Flow And Heat Transfer Characteristics In Outward Convex Corrugated Tubes. International Journal of Heat and Mass Transfer, 55: 7782–7802.

HAN, J.C., PARK, J.S., LEI, C.K., 1989. Augmented Heat Transfer in Rectangular Channel of Narrow Aspect Ratios with Rib Turbulators, International Journal of Heat and Mass Transfer 32:1619–1630.

HASANUZZAMAN, M., R. SAIDUR, ALI, M., MASJUKI, H.H., 2007. Effect Of Variables On Natural Convective Heat Transfer Through V-Corrugated Vertical Plates, International Journal of Mechanical and Materials Engineering, 2 (2): 109–117.

HERMAN, C., KANG, E., 2002. Heat Transfer Enhancement In A Grooved Channel With Curved Vanes. Int. J. Heat Mass Transfer, 45: 3741–3757.

HEWITT, G.F., SHIRES, G.L. AND BOTT, T.R., 1994. Process Heat Transfer, Boca Raton, Florida.

HONG, Z.-C., ZHEN, C.-E., YANG, C.-Y., 2008. Fluid Dynamics and Heat Transfer Analysis Of Three Dimensional Microchannel Flows With Microstructures. Numerical Heat Transfer, Part A, 54: 293–314.

INCROPERA, F.P., DEWITT, D.P., BERGMAN, T.L., LAVINE, A.S., 2011. Fundamentals o f Heat And Mass Transfer. John Wiley & Sons, Inc.

ISLAMOGLU, Y., KURT, A., 2004. Heat Transfer Analysis Using Ann's With Experimental Data For Air Flowing In Corrugated Channels, International Journal of Heat and Mass Transfer, 47:1361–1365.

ISLAMOGLU, Y., PARMAKSIZOGLU, C., 2003. The Effect Of Channel Height On The Enhanced Heat Transfer Characteristics In A Corrugated Heat Exchanger Channel, Applied Thermal Engineering, 23:979–987.

ISMAIL, L.S., VELRAJ, R., Studies On Fanning Friction (f) And Colburn (j) Factors Of Offset And Wavy Fins Compact Plate Fin Heat Exchanger – a CFD Approach. Numerical Heat Transfer, Part A, 56: 987–1005.

JAURKER, A.R., SAINI, J.S., GANDHI, B.K., 2006. Heat Transfer and Friction Characteristics Of Rectangular Solar Air Heater Duct Using Rib–Grooved Artificial Roughness, Solar Energy, 80:895–907.

KAEWKOHKIAT, Y., KONGKAITPAIBOON, V., EIAMSA-ARD, S., PIMSARN, M., 2010. Heat Transfer Enhancement In A Channel With Rib-Groove Turbulators. AIP Conf. Proc., 1207 (1), 313-316.

KANARIS, A.G., MOUZA, A.A., PARA, S.V., 2009. Optimal Design of A Plate Heat Exchanger with Undulated Surfaces. International Journal of Thermal Sciences, 48: 1184–1195.

KANARIS, G., MOUZA, A.A., PARAS, S.V., Flow And Heat Transfer In Narrow Channels With Corrugated Walls A CFD Code Application. Chemical Engineering Research and Design, 83: 460–468.

KARAKUS, C., 2007. Investigation Of Tip Vortex Formation, Development And Merging Using Particle Image Velocimetry (PIV) Technique. Çukurova University Institute of Natural and Applied Sciences, ADANA, Ph.D. Thesis.

KIM, K.Y., LEE, Y.M., 2007. Design Optimization Of Internal Cooling Passage With V-Shaped Ribs. Numerical Heat Transfer, Part A: Applications, 51 (11): 1103–1118.

KIM, M., BAIK, Y.J., PARK, S.R., SANG RA, H., LIM, H., 2010. Experimental Study On Corrugated Cross-Flow Air-Cooled Plate Heat Exchangers. Experimental Thermal and Fluid Science, 34: 1265–1272.

KIM, S.K., 2001. An Experimental Study Of Developing And Fully Developed Flows In A Wavy Channel By PIV. KSME International Journal 15: 1853–1859.

KIML, R., MAGDA, A., MOCHIZUKI, S., MURATA, A., 2004. Rib-Induced Secondary Flow Effects On Local Circumferential Heat Transfer Distribution Inside A Circular Rib Roughened Tube, International Journal of Heat and Mass, 47 (6–7): 403–412.

KORICHI, A., OUFER, L., 2007. Heat Transfer Enhancement In Oscillatory Flow In Channel With Periodically Upper And Lower Walls Mounted Obstacles. International Journal of Heat and Fluid Flow, 28: 1003–1012.

KWON, H.G., HWANG, S.D., CHO, H.H., 2008. Flow And Heat/Mass Transfer In A Wavy Duct With Various Corrugation Angles In Two Dimensional Flow Regimes. Heat Mass Transfer, 45: 157–165.

LAOHALERTDECHA, S., WONGWISES, S., 2010. The Effects Of Corrugation Pitch On The Condensation Heat Transfer Coefficient And Pressure Drop Of R-134a Inside Horizontal Corrugated Tube. International Journal of Heat and Mass Transfer, 53: 2924–2931.

LAYEK, A., SAINI, J.S., SOLANKI, S.C., 2006. Heat Transfer And Friction Characteristics Of Solar Air Heater Having Compound Turbulator On Absorber Plate, Advanced Energy Resource Technology. 188–194.

LAYEK, A., SAINI, J.S., SOLANKI, S.C., 2009. Effect Of Chamfering On Heat Transfer And Friction Characteristics Of Solar Air Heater Having Absorber Plate Roughened With Compound Turbulators, Renew. Energy, 34 (5): 1292-1298.

LAYEK, A., SAINI, J.S., SOLANKI, S.C.,. 2007 Second Law Optimization Of A Solar Air Heater Having Chamfered Rib-Groove Roughness On Absorber Plate, Renewable Energy,32: 1967–1980.

LEE, B.S., KANG, I.S., LIM, H.C., 1999. Chaotic Mixing And Mass Transfer Enhancement By Pulsatile Laminar In An Axisymmetric Wavy Channel. International Journal of Heat and Mass Transfer, 42: 2571–2581.

LIN, D.T.W., CHI, H.T.X., CHANG, C.C., WANG, C.C., HUANG, C.N., 2010. The Optimal Design Process Of The Plate Heat Exchanger. IEEE in: 2010 International Symposium on Computer, Communication, Control and Automation, 2010.

LIN, J.H., HUANG, C.Y., SU, C.C., 2007. Dimensional Analysis For The Heat Transfer Characteristic In The Corrugated Channels Of Plate Heat Exchangers, International Communications in Heat and Mass Transfer, 34:304–312.

LIU, X., JENSEN, M.K., 2001. Geometry Effects On Turbulent Flow and Heat Transfer In Internally Finned Tubes. J. Heat Transfer, 123: 1035–1044.

LORENZ, S., MUKOMILOW, D., LEINER, W., 1995. Distribution Of The Heat Transfer Coefficient In A Channel With Periodic Transverse Grooves, Experimental Thermal and Fluid Science, 11: 234–242.

LORENZ, S., MUKOMILOW, D., LEINER, W., 1995. Distribution Of The Heat Transfer Coefficient In A Channel With Periodic Transverse Grooves, Exp. Therm. Fluid Science, 11: 234–242.

LUO, D.D., LEUNG, C.W., CHAN, T.L., WONG, W.O., 2005. Flow and Forced-Convection Characteristics of Turbulent Flow Through Parallel Plates With Periodic Transverse Ribs. Numerical Heat Transfer, Part A: Applications, 48 (1): 43–58.

MAHMUD, S., ISLAM, S.A.K.M., MAMUN, M.A.H., 2002. Separation Characteristics Of Fluid Flow Inside Two Parallel Plates With Wavy Surface. International Journal of Engineering Science, 40: 1495–1509.

MAHUREAND, A., and KRIPLANI, V., 2012. Review of Heat Transfer Enhancement Techniques. International Journal of Engineering, 5: 241-249.

MARTIN, S.R., BATES, C.J., 1992. Small-Probe-Volume Laser Doppler Anemometry Measurements Of Turbulent Flow Near The Wall Of A Rib-Roughened Channel, Flow Measurement and Instrumentation, 3: 81–88.

MELLING, A., 1997. Tracer particles and seeding for particle image Velocimetry. Measurement Science Technology, 8:1406-1416.

MENDES, P., SPARROW, EM., 1984. Periodically Converging–Diverging Tubes And Their Turbulent Heat Transfer, Pressure Drop, Fluid Flow, And Enhancement Characteristics. Journal of Heat Transfer, 106: 55–63.

METWALLY, H.M., MANGLIK, R.M., 2004. Enhanced Heat Transfer Due To Curvature-Induced Lateral Vortices In Laminar Flows In Sinusoidal Corrugated-Plate Channels, International Journal of Heat and Mass Transfer, 47:2283–2292.

MOHAMED, N., KHEDİDJA, B., BELKACEM, Z., MICHEL, D., 2008. Numerical Study Of Laminar Forced Convection In Entrance Region Of A Wavy Wall Channel. Numerical Heat Transfer, Part A, 53: 35–52.

MOHAMMED, H.A., AZHER, M., WAHID, M.A., 2013. The Effects Of Geometrical Parameters Of A Corrugated Channel With In Out Of Phase Arrangement. International Communications in Heat and Mass Transfer, 40:47–57.

MOHAMMED, H.A., GUNNASEGARAN, P., SHUAIB, N.H., 2011. Numerical Simulation Of Heat Transfer Enhancement In Wavy Microchannel Heat Sink. International Communication in Heat and Mass Transfer, 38: 63–68.

MOHAMMED, N., KHEDIDJAB IS, B., ABDELKADERA, AZ., 2007. Heat Transfer And Flow Field In The Entrance Region Of A Symmetric Wavy-Channel With Constant Wall Heat Flux Density, International Journal of Dynamics of Fluids, 3:63–79.

NAPHON ,P., 2008.Effect Of Corrugated Plates In An In-Phase Arrange On The Heat Transfer And Flow Developments. International Journal of Heat and Mass Transfer, 51: 3963–3971.

NAPHON ,P.,SUCHANA, T., 2011. Heat Transfer Enhancement And Pressure Drop Of The Horizontal Concentric Tube With Twisted Wires Brush Inserts. International Communications in Heat and Mass Transfer, 38:236–241.

NAPHON, P., 2006. Effect Of Coil-Wire Insert On Heat Transfer Enhancement And Pressure Drop Of The Horizontal Concentric Tubes, International Communication in Heat Mass Transfer, 33 (6): 753–763.

NAPHON, P., 2007. Heat Transfer Characteristics And Pressure Drop In Channel With V-Corrugated Upper And Lower Plates. Energy Conversion and Management, 48(5): 1516–24.

NAPHON, P., 2007. Laminar Convective Heat Transfer And Pressure Drop In The Corrugated Channels. International Communications in Heat and Mass Transfer, 34: 62–71.

NAPHON, P., 2009. Effect Of Wavy Plate Geometry Configurations On The Temperature And Flow Distribution. International Communication in Heat and Mass Transfer, 36: 942–946.

NAPHON, P., KORNKUMJAYRIT, K., 2007. Numerical Analysis On The Fluid Flow And Heat Transfer In The Channel With V-Shaped Wavy Lower Plate. Int. Communication Heat Mass Transfer, 34: 62–71.

NAPHON, P., NUCHJAPO, M., KURUJAREON, J., 2006. Tube Side Heat Transfer Coefficient And Friction Factor Characteristics Of Horizontal Tubes With Helical Rib, Energy Conversion and Management, 47: 3031–3044.

NAPHON, P., SRIROMRULN, P., 2006. Single-Phase Heat Transfer And Pressure Drop In The Micro-Fin Tubes With Coiled Wire Insert, International Communication in Heat Mass Transfer, 33:176–183.

NASIRUDDIN, M.H., SIDDIQUI, K., 2007. Heat Transfer Augmentation in a Heat Exchanger Tube Using a Baffle. International Journal of Heat and Fluid Flow ,2: 318–328.

NICENO, B., NOBILE, E., 2001. Numerical analysis of fluid flow and heat transfer in periodic wavy channels. International Journal of Heat and Fluid Flow, 22:156– 167.

NISHIMURA,T., MATHUR, S., 1996. Mass Transfer Enhancement in a Sinusoidal Wavy Channel for Pulsatile Flow Heat and Mass Transfer, 32(1-2): 65-72.

O'BRIAN, JE., SPARROW, EM., 1982. Corrugated-Duct Heat Transfer, Pressure Drop, And Flow Visualization. Transaction of the ASME, Journal of Heat Transfer, 104:410–416.

OKAMOTO, S., NAKASO, K., 1991. Turbulent Shear Flow Over Rows Of Two-Dimensional Square Ribs On Ground Plane, Eight Symposium Turbulent Shear Flows, Technical University of Munich, Sept. 9–11

OZALP, C., 2006. Large and small scale instabilities for shear layer along a Perforated surface, Çukurova University Institute of Natural and Applied Sciences, ADANA, Ph.D. Thesis.

OZALP, C., PINARBASI, A., SAHIN, B., 2010. Experimental Measurement Of Flow Past Cavities Of Different Shapes. Experimental Thermal and Fluid Science, 34: 505–515.

OZKAN, G., ORUC, V., AKILLI, H., SAHIN, B., 2012. Flow Around A Cylinder Surrounded By A Permeable Cylinder In Shallow Water. Experiments In Fluids, 53: 1751-1763.

OZTURK N. A., AKKOCA A. and SAHIN, B., 2008. Flow details of a circular cylinder mounted on a flat plate. Journal of Hydraulic Research, 46: 334-355.

OZTURK, N.A. 2006 ,Investigation of flow characteristics in heat exchangers of various geometries, Çukurova University Institute of Natural and Applied Sciences, ADANA, Ph.D. Thesis.

PATANKAR, S.V., 1980. Numerical Heat Transfer And Fluid Flow, NY: Taylor & Francis. New York

PENG, L., ZHAO, L.,PING, Z., 2008. Comparison Study of Flow and Heat Transfer Characteristics in Two Kinds of Wavy Channels. Journal of Engineering Thermophysics, 29(10):1755-1758.

PETKHOOL, S., EIAMSA-ARD, S., KWANKAOMENG, S., PROMVONGE, P., 2011. Turbulent Heat Transfer Enhancement In A Heat Exchanger Using Helically Corrugated Tube. International Communications in Heat and Mass Transfer, 38: 340–347.

PINAR, E., 2013.Flow control of a cylinder in shallow water using perforated cylinder. Çukurova University Institute of Natural and Applied Sciences, Turkey, PhD Thesis.

PROMVONGE, P., THIANPONG, C., 2008. Thermal Performance Assessment Of Turbulent Channel Flows Over Different Shaped Ribs. International Communication in Heat and Mass Transfer, 35: 1327–1334.

RUSH, T.A., NEWELL, T.A., JACOBI,A.M., 1999. An Experimental Study of Flow and Heat Transfer in Sinusoidal Wavy Passages[J]. International Journal of Heat and Mass Transfer, 42(9): 1541-1553.

SAHIN, B., AKKOCA, A., ÖZTÜRK, N.A., and AKILLI, H., 2006. Investigations of flow characteristics in a plate fin and tube heat exchanger model composed of single cylinder. International Journal of Heat and Fluid Flow, 27:522-530.

SAHIN, B., OZTURK N. A., and AKKOCA A., 2008. PIV measurements of flow past a confined cylinder. Experiments in Fluids, 44: 1001-1014, 2008.

SAHIN, B., OZTURK, N.A., 2009. Behaviors of flow at the junction of cylinder and base plate in deep water. Measurement, 42:225–240.

SAIDI, A., SUNDEN, B., 2006. Numerical Simulation Of Turbulent Convective Heat Transfer In Square Ribbed Ducts, Numerical Heat Transfer, Part A: Applications, 38: 67–88.

SAN, J.Y., HUANG, W.C., 2006. Heat Transfer Enhancement Of Transverse Ribs İn Circular Tubes With Consideration Of Entrance Effect, International Journal of Heat Mass Transfer, 49 (17–18): 2965–2971.

SANIEI, N., DINI, S., 1993. Heat Transfer Characteristics in a Wavy-Walled Channel, Journal of. Heat Transfer, 6.115-788.

SAVINO, S., COMINI, G., NONINO, C., 2004. Three-Dimensional Analysis Of Convection In Two-Dimensional Wavy Channels. Numerical Heat Transfer Part A – Applications, 46: 869–890.

SAWYER, D., SEN, M., CHANG, H.C., 1998. Heat Transfer Enhancement In Three Dimensional Corrugated Channel Flow. International Journal of Heat and Mass Transfer, 41: 3559–3573.

SHAH, R.K, 2002. Fundamentals of Heat Exchanger Design. Wiley, J. and Sons, Inc. New York.

SHAIKH, N., SIDDIQUI, MHK., 2007. Heat Transfer Augmentation In A Heat Exchanger Tube Using A Baffle. Int J Heat Fluid Flow, 28: 318–28.

SONG, W.M., MENG, J.A., LI, Z.X., 2010. Numerical Study Of Air-Side Performance Of A Finned Flat Tube Heat Exchanger With Crossed Discrete Double Inclined Ribs. Appl. Therm. Eng., 30 (13): 1797-1804.

SPARROW, E.M., KORAM, K.K., CHARMCHI, M., 1980. Heat Transfer And Pressure Drop Characteristics Induced By A Slat Blockage In A Circular Tube. ASME J. Heat Transfer, 102: 64–70.

SPARROW, EM., COMB, JW., 1983. Effect Of Interval Spacing And Fluid Flow Inlet Conditions On A Corrugated Wall Heat Exchanger. International Journal of Heat and Mass Transfer, 26(7):993–1005.

STASIEK, J.A., 1998. Experimental Studies Of Heat Transfer And Fluid Flow Across Corrugate Undulated Heat Exchanger Surfaces, International Journal of Heat and Mass Transfer, 41 (6–7): 899–914.

STASIEK, J.A., COLLINS, M.W., CIOFALO, M., CHEW, P.E., 1996. Investigation Of Flow And Heat Transfer In Corrugated Passages-I. Experimental Results. International Journal of Heat and Mass Transfer, 39 (l):149–164.

STONE, K., VANKA, S.P., 1999. Numerical Study Of Developing Flow And Heat Transfer In A Wavy Passage. Journal of Fluids Engineering, 121: 713–719.

SUI, Y., TEO, C.J., LEE, P.S., CHEW, Y.T., SHU, C., 2010. Fluid Flow And Heat Transfer In Wavy Microchannels. Int. J. Heat Mass Transfer, 53: 2760–2772

SUN, Z., JALURIA, Y., 2010. Unsteady Two-Dimensional Nitrogen Flow In Long Microchannels With Uniform Wall Heat Flux. Numerical Heat Transfer, Part A, 57: 625–641.

TANDA, T., 2004. Heat Transfer In Rectangular Channels With Transverse And V-Shaped Broken Ribs, International Journal of Heat and Mass, 47 (2):229–243.

TATSUMI, K., IWAI, H., INAOKA, K., SUZUKI, K., 2003. Numerical Analysis For Heat Transfer Characteristics Of An Oblique Discrete Rib Mounted In A Square Duct. Numerical Heat Transfer, Part A: Applications, 44 (8): 811–831.

TIJING LD, PAK BC, BAEK BJ, LEE DH., 2006. A Study On Heat Transfer Enhancement Using Straight And Twisted Internal Fins. International Communication in Heat Mass Transfer, 33:719–26.

TSAL, S.F., SHEU, T.H.W., LEE, S.M., MITRA, N.K., 1999. Heat Transfer In A Conjugate Heat Exchanger With A Wavy Fin Surface. International Journal of Heat and Mass Transfer, 42: 1735–1745.

TURGAY, M.B., YAZICIOGLU, A.G., 2009. Effect Of Surface Roughness In Parallel-Plate Microchannels On Heat Transfer. Numerical Heat Transfer, Part A, 56: 497–514.

VASUDEVIAH, M., BALAMURUGAN, K., 2001. On Forcer Convective Heat Transfer For A Stokes Flow In A Wavy Channel. International Communications in Heat and Mass Transfer, 28: 289–297.

VICENTE, P.G., GARCIA, A., VIEDMA, A., 2004. Mixed Convection Heat Transfer And Isothermal Pressure Drop In Corrugated Tubes For Laminar And Transition Flow, International Communications in Heat and Mass Transfer, 31: 651–662.

WAHIDI, R., CHAKROUN, W., AL-FAHED, S., 2005. The Behavior Of The Skin-Friction Coefficient Of A Turbulent Boundary Layer Flow Over A Flat Plate With Differently Configured Transverse Square Grooves, Experimental Thermal Fluid Science, 30: 141–152.

WANG, C.C., CHEN, C.K., 2002. Forced Convection In A Wavy-Wall Channel. International Journal of Heat and Mass Transfer, 45: 2587–2595.

WANG, C.C., JANG, J.Y., CHIOU, N.F., 1999. A Heat Transfer And Friction Correlation For Wavy Fin-And-Tube Heat Exchangers International Journal of Heat and Mass Transfer, 42: 1919–1924.

WANG, G., VANKA, S. P., Convective Heat Transfer in Periodic Wavy Passages. Int J Heat Mass Transfer, 38(17): 3219- 3230.

WANG, L., SUNDEN, B., 2007. Experimental Investigation Of Local Heat Transfer In A Square Duct With Various-Shaped Ribs. Heat and Mass Transfer, 43: 759–766.

WEBB, R.L., 1987. Enhancement of Single-Phase Convective Heat Transfer. in S. Kakaç, R.K. Shah, and W.Aung, eds, Handbook of single-Phase Convective Heat Transfer, John Wiley and Sons, New York .

WEBB, R.L., ECKERT, E.R.G, GOLDSTEIN,R.J., 1971. Heat Transfer and Friction In Tubes with Repeated-Rib Roughness, International Journal of Heat and Mass Transfer, 14:601–617.

XIANG,Y., JUN,L., PING, F., 2005. Numerical Investigation Of Effects Of Plate Spacing On Flow And Heat Transfer In Sinusoidal Channels. Journal of Thermal Science and Technology, 4(2):123-129.

XIN, R.C., TAO, W.Q., 1988. Numerical Prediction Of Laminar Flow And Heat Transfer In Wavy Channels Of Uniform Cross-Sectional Area. Numerical Heat transfer, 14: 465–481.

YAKUT, K., SAHIN, B., 2004. The Effects Of Vortex Characteristics On Performance Of Coiled Wire Turbulators Used For Heat Transfer Augmentation, Applied Thermal Engineering, 24 (16): 2427–2438.

YANG, K.S., Large Eddy Simulation Of Turbulent Flows In Periodically Grooved Channel. Journal of Wind Engineering and Industrial Aerodynamics, 84: 47–64.

YANG, Y.T., HWANG, C.W., Numerical Calculations Of Heat Transfer And Friction Characteristics In Rectangular Ducts With Slit And Solid Ribs Mounted On One Wall. Numerical Heat Transfer, Part A: Applications, 45 (4): 363–375.

YIN, J.,YANG, G., LI, Y., 2012 The Effects of Wavy Plate Phase Shift on Flow and Heat Transfer Characteristics in Corrugated Channel. Energy Procedia, 14: 1566-1573.

ZHANG, J., KUNDU, J., MANGLIK, R.M., 2004. Effect Of Finn Waviness And Spacing On The Lateral Vortex Structure And Laminar Heat Transfer In Wavy-Plate–Fin Cores. International Journal of Heat and Mass Transfer, 47: 1719–1730.

ZHANG, L., CHE, D., 2011. Influence Of Corrugation Profile On The Thermal hydraulic Performance Of Cross-Corrugated Plates. Numerical Heat Transfer, Part A, 59: 267–296.

CIRRICULUM VITAE

Nehir TOKGÖZ was born on 1982 in Erzurum, Turkey. She graduated from Erzurum Anatolian İmam-Hatip High School, and enrolled in Mechanical Engineering Department of Erciyes Universty in 2000. She began his MSc education at the Department of Mechanical Engineering of Erciyes University in 2005. She completed her Master of Science education in 2008. She began his PhD education at the Department of Mechanical Engineering of Çukurova University in 2010. She completed her Doctor of Philosophy education in 2014.